

REPORT NO.
UCB/EERC-89/06
JULY 1989

EARTHQUAKE ENGINEERING RESEARCH CENTER

EFFECTS OF SPATIAL VARIATION OF GROUND MOTIONS ON LARGE MULTIPLY-SUPPORTED STRUCTURES

by

HONG HAO

PREFACE

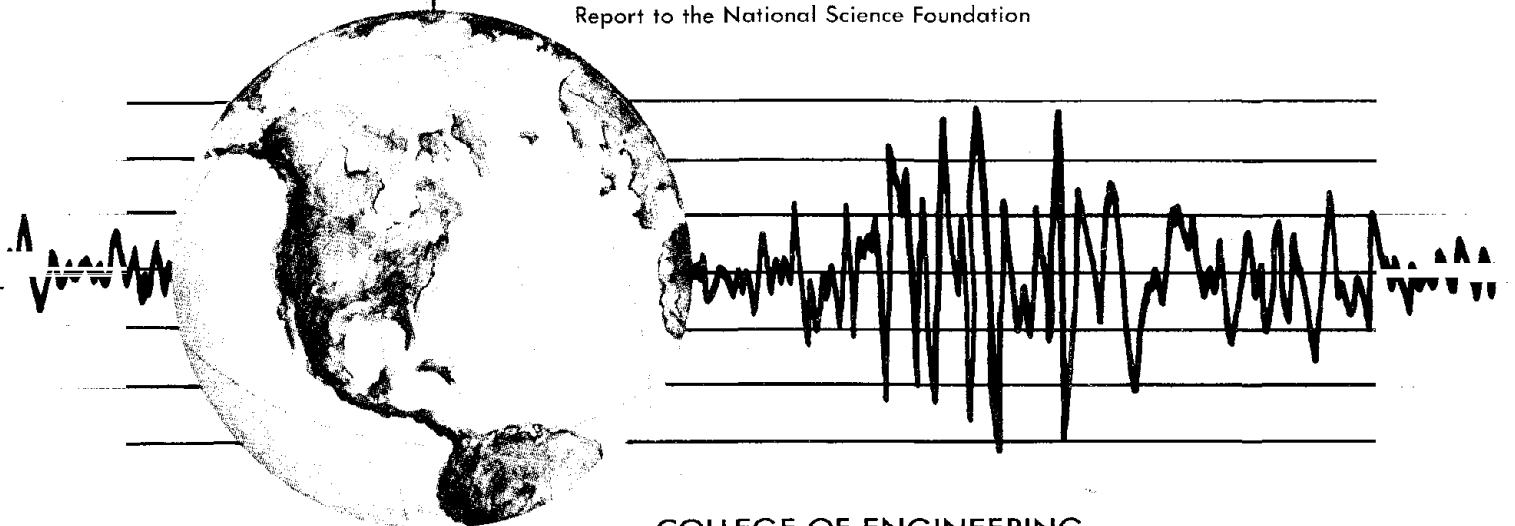
by

BRUCE A. BOLT

and

JOSEPH PENZIEN

Report to the National Science Foundation



COLLEGE OF ENGINEERING

UNIVERSITY OF CALIFORNIA AT BERKELEY

REPRODUCED BY
U.S. DEPARTMENT OF COMMERCE

NATIONAL TECHNICAL
INFORMATION SERVICE
SPRINGFIELD, VA 22161

i.b

For sale by the National Technical Information
Service, U.S. Department of Commerce,
Springfield, Virginia 22161

See back of report for up to date listing of
EERC reports.

DISCLAIMER

Any opinions, findings, and conclusions or
recommendations expressed in this publica-
tion are those of the authors and do not nec-
essarily reflect the views of the National Sci-
ence Foundation or the Earthquake Engineer-
ing Research Center, University of California
at Berkeley.

**EFFECTS OF SPATIAL VARIATION OF GROUND MOTIONS
ON LARGE MULTIPLY-SUPPORTED STRUCTURES**

by

Hong Hao

PREFACE

by

Bruce A. Bolt
and
Joseph Penzien

Report to the National Science Foundation

Report No. UCB/EERC-89/06
Earthquake Engineering Research Center
University of California
Berkeley, California

July 1989

j.a

PREFACE

This is the fourth report in a research series which is based on measurements made of seismic strong ground motion by the large-scale digital array of accelerometers in Taiwan, called SMART-1. The array was installed and is operated by the Institute of Earth Sciences and National Science Council, Taiwan, R.O.C.. The uniformly diligent work carried out by scientists at the Institute has provided high-quality data for many studies. SMART-1 began operation in September 1980 and through June 1989 recorded strong ground motions (with some accelerations exceeding 0.3g) from over 50 local earthquakes. The first two reports in the series are: UCB/EERC-82/18 by B. A. Bolt, C. H. Loh, J. Penzien, Y. B. Tsai and Y. T. Yeh and UCB/EERC-85/82 by N. A. Abrahamson. In 1988, R. B. Darragh published "Analysis of Near Source Waves: Separation of Wave Types Using Strong Motion Array Recordings" in Report UCB/EERC-88/08. A research Summary through 1986 was published in "Earthquake Spectra", 3, 263-287, 1987 by N. A. Abrahamson, B. A. Bolt, R. B. Darragh, J. Penzien and Y. B. Tsai.

From its inception, the SMART-1 research program has had as a major goal the accumulation of ground motion data which were useful in exploring the effect of seismic inputs on multiply-supported large structures. For theoretical reasons, it was expected that multiple-input effects could not be represented adequately by a single base excitation because of phase differences and loss of wave coherency. For dynamical analysis of large structures for earthquake resistance, inclusion of multiple-inputs might well be envisaged in certain circumstances. Over the last several years, earthquake engineers around the world have made use of SMART-1 data to explore aspects of this problem, particularly that related to incoherency in strong ground motion over distances of order 100 meters. This work has led, among other results, to the construction of various coherency models of wave propagation as functions of separation distance of the supports and of the frequency.

The present report by Dr. Hong Hao advances the study of the effects of the spatial variation of ground motions on large multiply-supported structures. He has applied random processes to develop particular simulation techniques that generate multiple-support inputs which allow more realistic assessment of structural response than the usual present practice. His main conclusions bear on two aspects of the problem. The first is the simulation of realistic ground motion for spatially-correlated, quasi-stationary multiple ground motions and the second is the development of an appropriate computer program which would simulate structural response itself, including soil-structure interaction effects. He has suggested a model for coherency with four parameters and has explored the nonlinear interaction between the parameters. The models have been tested using earthquakes recorded by SMART-1. In his second main contribution, Dr. Hong Hao has developed ways to interpolate multiple-motion

time histories to preserve the properties of the prescribed ground motion and response spectra. His newly-written computer program demonstrates that often there is a general reduction in structural response when multiple inputs are used and that response modes such as rocking and rotation are significant when different phasing is allowed at each input.

The report uses methods of array analysis not ordinarily available in the engineering literature. For a basic explanation of these methods, readers are referred to "Seismic Strong Motion Synthetics," B. A. Bolt (Editor), Academic Press, 1987.

B. A. Bolt

J. Penzien

ABSTRACT

The spatial variability of ground motions recorded during 17 earthquakes by a strong motion accelerograph array in Taiwan (SMART-1) is analyzed. The power spectral density functions and envelope functions of the ground motion are calculated and compared with previous results. A coherency function is suggested for pairs of stations as a function of both frequency and also the projected separation distances between the stations in the wave propagation and transverse directions, respectively. The apparent velocities of the seismic waves are studied in different time windows as a function of frequency. A method is developed to simulate and interpolate multiple ground motions that are spatially correlated, quasi-stationary, and response spectrum compatible. Also, the equations that describe structural response under multiple ground motion excitations are formulated in the cases both with and without soil-structure interaction effects. Numerical methods for solving these equations in the frequency domain are presented.

A computer program SSIAM is developed. It can simulate and interpolate spatially correlated, stationary or quasi-stationary multiple ground motions compatible with the prescribed ground motion properties and the given response spectrum. It then uses these simulated ground motions as the multiple inputs to solve the structural responses. By using program SSIAM, some examples of ground motion simulation and interpolation are calculated. The results are presented and compared with the prescribed ground motion properties; also, some examples of structural responses under the simulated multiple ground motion excitations are calculated with soil-structure interaction effects. The results show that it is important to consider the ground motion wave propagation effects in seismic response analysis of large dimensional structures.

ACKNOWLEDGEMENTS

I am grateful to Professors Joseph Penzien and Bruce A. Bolt, who kindly guided me throughout the course of this work, and offered encouragement and many valuable suggestions and insights.

Thanks also go to Dr. Carlos S. Oliveira, Earthquake Engineering Instituto Superior Tecnico, Lisbon, Portugal, for valuable discussions during his periodical visits to Berkeley, and to Mr. S. J. Chiou for providing me with the recorded earthquake data. Also, thanks to Dr. Beverley Bolt for editing this report.

Part of my study and research at Berkeley was supported by the Ministry of Education of the People's Republic of China and National Science Foundation of the U. S. A., and this support is also acknowledged.

Finally, I would like to extend my deepest gratitude to my family for their continued support.

TABLE OF CONTENTS

	Page
Preface	i
Abstract	iii
Acknowledgements	iv
Table of Contents	v
1 INTRODUCTION	1
2 NUMERICAL PROCESSING METHODS FOR RANDOM PROCESSES	3
2.1 Estimation of Covariance	3
2.2 Estimation of Spectra, Coherency and Phase Spectrum	4
2.3 Estimation of Envelope Function	5
2.4 Computational Procedures and Examples	6
3 MULTIPLE STATION GROUND MOTION PROCESSING	14
3.1 The SMART-1 Array	14
3.2 Information Recorded by the SMART-1 Array	15
3.3 Power Spectral Density Function	15
3.4 Shape Function	17
3.5 Apparent Velocity	18
3.6 Coherency	18
4 MULTIPLE STATION GROUND MOTION SIMULATION	57
4.1 Review of Previous Methods	57
4.2 Ground Motion Simulation Criteria	57
4.3 Spatially Correlated Stationary Ground Motion Simulation	58
4.4 Spatially Correlated Quasi-Stationary Ground Motion Simulation	60
4.5 Simulated Ground Motion Correction	61
4.6 Ground Motion Time-History Interpolation	62
4.7 Examples	64
5 RESPONSE OF LARGE STRUCTURES WITH MULTIPLE SUPPORTS	97
5.1 SDOF Structure without Soil-Structure Interaction Effects	97
5.2 MDOF Structure without Soil-Structure Interaction Effects	98
5.3 SDOF Structure with Soil-Structure Interaction Effects	99
5.4 MDOF Structure with Soil-Structure Interaction Effects	100
5.5 Impedance Matrix	103
5.6 Numerical Methods	105
5.7 Numerical Procedure	107

6 EXAMPLES	113
6.1 Description of SSIAM Program	113
6.2 Verification of the SSIAM Program	114
6.3 Example I, A Long Span Arch Beam	114
6.4 Example II, A Long Span Continuous Beam	116
6.5 Conclusions	118
7 CONCLUSIONS AND RECOMMENDATIONS	147
REFERENCES	150

CHAPTER 1 INTRODUCTION

During an earthquake, the ground motions produced at the multiple support points of large structures, such as dams, pipelines, bridges, and nuclear power plants, can differ considerably. Therefore, realistic assessments of structural response must consider spatial variations of free-field ground motions. The seismic inputs at the structure's multiple support points must not only possess realistic characteristics individually but they must also be properly cross-correlated with each other.

Simulation techniques can be used to generate such multiple support inputs provided the appropriate cross-correlation functions can be defined. Strong ground motion array data are now available for this purpose, including data from the SMART-1 (Strong Motion Array, Taiwan-1) array, located in Lotung, Taiwan, see Bolt et al. (1982), Darragh (1987).

In the research investigation reported herein, extensive use has been made of the SMART-1 data to establish free-field ground motion models in terms of random processes, with time and spatial coordinates as the independent variables. Simulation procedures are developed for generating time-histories of ground motions consistent with these models. The time-histories can be used as the multiple inputs to large structures. These procedures have been implemented into a computer program SSIAM which can also generate structural response, including soil-structure interaction effects.

Chapter 2 of this report introduces the pertinent numerical methods developed for processing properly cross-correlated time series. The techniques used include Fourier and Hilbert transforms, various forms of wave filtering, and truncation techniques. Random process properties such as covariance, correlation, spectral density, coherency, and phase spectra are also discussed. Processing steps used in the research are listed and an example solution is obtained.

Chapter 3 presents the results of wave analyses using the SMART-1 data, including power spectral density functions, shape functions, apparent velocities, and coherency functions. The power spectral density functions were generated for all components of ground motion measured at the inner ring stations (see Figure 3.2) during earthquake Events 24 and 45. These results are compared with previously published results by Tajimi (1960), Bolotin (1960), Barstein (1960), Toki (1968), and Iyengar and Iyengar (1969). It is found that most of the generated power spectral density functions are similar to the Tajimi-Kanai form. The exceptions are the power spectral density functions for the vertical components of motion measured during Event 24 which have forms similar to those for banded white noise.

Shape functions were also generated for all of the above mentioned components of

motion measured during Events 24 and 45. They were compared with previously proposed shape functions of Bolotin (1960), Bogdanoff et al. (1961), Amin and Ang (1966), Shinozuka (1967), Toki (1968), Jennings et al. (1968), and Iyengar and Iyengar (1969). Most of the generated shape functions are quite similar to the Bogdanoff form except for those generated for the vertical components of motion measured during Event 24. These latter shape functions are more similar to the Amin and Ang form.

Apparent wave velocity is one of the most important properties associated with spectral variations in the ground motions. Unfortunately, it is a difficult parameter to evaluate from field test data due to the complexities caused by wave reflections and refractions and noise effects. In the past, it has been evaluated by several different methods, e.g. the aligned motion method by Harichandran and Vanmarcke (1984) and the cross-correlation method used by Loh (1985), Oliveira (1985), and Loh and Yeh (1988). In the investigation reported herein, all apparent velocities were calculated by the frequency-wave number (F-K) method used by Abrahamson and Bolt (1987).

Using SMART-1 data, many researchers have developed ground motion coherency models, including Harichandran and Vanmarcke (1984), Loh (1985), Tsai (1988), Abrahamson (1988), and Loh and Yeh (1988). In this research, coherency functions were intensively investigated using the data from 17 SMART-1 events. This analysis leads to the definition of a new coherency model.

In Chapter 4, previous ground motion simulation methods are reviewed, including those reported by Ruiz and Penzien (1969), Penzien and Watabe (1975), Kubo and Penzien (1976), Penzien (1988), Hoshiya et al. (1976), Samaras et al. (1987), and Watabe (1987). A new method of simulating spatially correlated motions is then developed based on random process assumptions, including that of quasi-stationarity. In addition, an interpolation method is developed that reduces computational effort when many spatially correlated components of ground motion are required. Examples of spatially correlated motions are generated and compared with the prescribed random characteristics.

Structural seismic response equations of motion are formulated in Chapter 5 to accommodate single or multiple support inputs and to include soil-structure interaction effects, if desired. Foundation impedance functions are used to account for such effects. Solutions of the equations of motion are obtained through the frequency domain. Example solutions are presented and discussed in Chapter 6 which illustrate the importance of considering the spatial variations of ground motion when assessing the seismic response of large structures.

General conclusions and recommendations are presented in Chapter 7.

CHAPTER 2 NUMERICAL PROCESSING METHODS FOR RANDOM PROCESSES

The basis for probability modelling, processing and simulation of spatial variations of ground motion is the theory of random processes. The pertinent numerical processing methods of such processes are presented in the following sections.

2.1 Estimation of Covariances

Assume that $x_1(t)$ and $x_2(t)$, $0 \leq t \leq T$, are two joint stationary random processes having zero mean values. An estimation of the autocovariance function for $x_1(t)$ is

$$B_{x_1x_1}(\tau) = \begin{cases} \frac{1}{T} \int_0^{T-|\tau|} x_1(t)x_1(t+|\tau|)dt & 0 \leq |\tau| \leq T \\ 0 & |\tau| > T \end{cases} \quad (2.1)$$

For discrete data series having N data points at intervals Δt , so that $N\Delta t = T$, the autocovariance function is estimated using

$$B_{x_1x_1}(l) = \begin{cases} \frac{1}{N} \sum_{n=1}^{N-l} x_1(n+l)x_1(n) & 0 \leq l \leq N \\ 0 & l > N \end{cases} \quad (2.2)$$

It can be shown that both $B_{x_1x_1}(\tau)$ and $B_{x_1x_1}(l)$ are biased estimators of the autocovariance function for finite T and N , i.e., they are asymptotically unbiased only as $T \rightarrow \infty$ and $N \rightarrow \infty$, respectively. However, they do satisfy the positive definite property and their mean square errors are small. Therefore, $B_{x_1x_1}(\tau)$ and $B_{x_1x_1}(l)$ can be used as proper estimators of the autocovariance function for continuous and discrete time series, respectively.

The estimator of the cross covariance function for processes $x_1(t)$ and $x_2(t)$ is

$$B_{x_1x_2}(\tau) = \begin{cases} \frac{1}{T} \int_0^{T-\tau} x_1(t)x_2(t+\tau)dt & 0 \leq \tau \leq T \\ \frac{1}{T} \int_{\tau}^T x_1(t)x_2(t+\tau)dt & -T \leq \tau \leq 0 \\ 0 & |\tau| > T \end{cases} \quad (2.3)$$

For a discrete data series, Eq.(2.3) becomes

$$B_{x_1x_2}(l) = \begin{cases} \frac{1}{N} \sum_{n=1}^{N-l} x_1(n)x_2(n+l) & 0 \leq l \leq N \\ \frac{1}{N} \sum_{n=1}^N x_1(n)x_2(n+l) & -N \leq l \leq 0 \\ 0 & |l| > N \end{cases} \quad (2.4)$$

It can be shown that both $B_{x_1x_2}(\tau)$ and $B_{x_1x_2}(l)$ are also biased estimators of the cross covariance. They become unbiased only when $T \rightarrow \infty$ and $N \rightarrow \infty$.

The autocorrelation coefficient and cross correlation coefficient functions of the discrete time series $x_1(t)$ and $x_2(t)$ can be easily calculated using

$$\rho_{x_1x_1}(l) = \frac{B_{x_1x_1}(l)}{B_{x_1x_1}(0)} \quad (2.5)$$

$$\rho_{x_1x_2}(l) = \frac{B_{x_1x_2}(l)}{\sqrt{B_{x_1x_1}(0)B_{x_2x_2}(0)}} \quad (2.6)$$

2.2 Estimation of Spectra, Coherency and Phase Spectrum

Assume $x_1(t)$ is a series in $0 \leq t \leq T$ having sample increment Δt ; thus, the total number of data points is $N = \frac{T}{\Delta t}$. The power spectral density function of $x_1(t)$ can be estimated by first tapering $x_1(t)$ (Hao, 1989), and then evaluating its Fourier transform

$$X_1(\omega_m) = \sum_{n=-\infty}^{+\infty} x_1(t_n) e^{-i\omega_m t_n} \quad (2.7)$$

The power spectral density function is then obtained using

$$S_{x_1x_1}(\omega) = \frac{1}{T} \sum_{m=-M}^M W_m X_1(\omega + \frac{2\pi m}{T}) X_1^*(\omega + \frac{2\pi m}{T}) \quad (2.8)$$

where W_m is a weight function used in the frequency domain to smooth the spectrum, and $2M + 1$ is the window width defining the number of consecutive discrete frequencies to be smoothed. The smoothing spectral window W_m is normalized so that its values at all $2M + 1$ points sum to unity. Function $X^*(\omega_m)$ is the complex conjugate of $X(\omega_m)$, and T is the period of the series $x(t)$ resulting from the FFT procedure.

Equation (2.8) is equivalent to the Fourier transform of the convolution of $W(l)$ with the autocovariance as shown by

$$S_{x_1x_1}(\omega) = \frac{1}{T} \int_{-\infty}^{+\infty} \left[\int_{-\infty}^{+\infty} W(l) B_{x_1x_1}(\tau - l) dl \right] e^{-i\omega \tau} d\tau \quad (2.9)$$

Abrahamson and Darragh (1987) have used the triangular shape window in the frequency domain. The inverse Fourier transform of this window is given by

$$W(l) = A \frac{\sin^2(\omega_0 \pi l)}{(\pi l)^2} \quad (2.10)$$

which can be used to smooth the covariance function.

To compute the cross power spectral density function between $x_1(t)$ and $x_2(t)$, both $x_1(t)$ and $x_2(t)$ need to be tapered. Then after transforming $x_1(t)$ and $x_2(t)$ to the frequency domain, the cross power spectral density function can be obtained using

$$S_{x_1x_2}(i\omega) = \frac{1}{T} \sum_{m=-M}^M W_m X_1(\omega + \frac{2\pi m}{T}) X_2^*(\omega + \frac{2\pi m}{T}) \quad (2.11)$$

where $X_2^*(\omega)$ is the complex conjugate of $X_2(\omega)$, the Fourier transform of $x_2(t)$. The coherency function can now be calculated in accordance with

$$\gamma_{x_1x_2}(i\omega) = \frac{S_{x_1x_2}(i\omega)}{[S_{x_1x_1}(\omega)S_{x_2x_2}(\omega)]^{\frac{1}{2}}} \quad (2.12)$$

If uncorrelated noise is present in each of $x_1(t)$ and $x_2(t)$, it should be eliminated to the extent possible by smoothing the power spectra before evaluating the coherency function; otherwise, significant error will be introduced.

The phase spectrum can be calculated by the following expression

$$\begin{aligned} \phi_{x_1x_2}(\omega) &= \tan^{-1} \left(\frac{Im[S_{x_1x_2}(i\omega)]}{Re[S_{x_1x_2}(i\omega)]} \right) \\ &= \tan^{-1} \left(\frac{Im[\gamma_{x_1x_2}(i\omega)]}{Re[\gamma_{x_1x_2}(i\omega)]} \right) \end{aligned} \quad (2.13)$$

It can be shown that the variance of the smoothed coherency and the phase estimators depend not only on the type and band width of the spectral window employed, but also on the coherency. The variances of these estimators are small when the coherency is high, but increase as the coherency decreases. Noise in the series will tend to dominate when the coherency values are low; thus, for weakly correlated series, smoothing to remove the noise is very important. Some researchers also set up confidence levels for coherency by calculating the numerical coherency values of the noise. Abrahamson (1985) reported 0.4 as a reasonable coherency confidence level. In the present investigation, the confidence level was found to be approximately 0.35 at low frequencies, increasing to 0.45 at 10Hz. These are the numerical coherency values of the white noise after smoothing with a triangular shaped window of width 0.97Hz.

2.3 Estimation of Envelope Function

The envelope function of a time series can be calculated using the Hilbert transform technique. The envelope function $f_c(t)$ of $x(t)$ is defined as

$$f_c(t) = x(t) - if_h(t) \quad (2.14)$$

where $f_h(t)$ is the Hilbert transform, which introduces a 90° phase shift with respect to $x(t)$ so that the envelope of the real time function can be obtained. The function $f_h(t)$ can be calculated by the formula,

$$f_h(t) = \frac{i}{2\pi} \int_0^{+\infty} [X(i\omega)e^{i\omega t} - X(-i\omega)e^{-i\omega t}]d\omega \quad (2.15)$$

and its Fourier transform by

$$F_h(\omega) = iX(i\omega)Sgn(\omega) \quad (2.16)$$

where

$$Sgn(\omega) = \begin{cases} 1, & \omega > 0 \\ 0, & \omega = 0 \\ -1, & \omega < 0 \end{cases} \quad (2.17)$$

Function $f_h(t)$ can now be obtained by applying the inverse FFT to $F_h(\omega)$; that is

$$f_h(t) = \int_{-\infty}^{+\infty} F_h(\omega)e^{i\omega t}d\omega \quad (2.18)$$

Hence the envelope of the time series $x(t)$ can be obtained by the following formula

$$E(t) = |f_c(t)| = [x^2(t) + f_h^2(t)]^{\frac{1}{2}} \quad (2.19)$$

A more detailed description of the Hilbert transform theory and its applications can be seen in Kanasewich (1981).

2.4 Computational Procedures and Examples

The practical procedure of calculating the functions introduced above will now be outlined and some examples given:

Let us consider the two time series $x(t)$ and $y(t)$ shown in Fig. 2.1, which are accelerograms recorded in the same direction in discrete form at two stations in the SMART-1 array having 400m separation. The recording time increment is $\Delta t = 0.01sec$. Assume that they are samples of stationary processes within the time window 7 – 27sec having zero mean values. Using $\Delta t = 0.01sec$, $N = 2^{11} = 2048$, and $T = N\Delta t = 20.48sec$, each wave form can be transformed using the FFT technique. The following steps are followed in calculating the desired functions:

(a) Covariances, correlations, and envelope functions

1. Reduce each series by its mean value to satisfy the assumption of zero mean processes.

2. Taper the series to make the series compatible with the periodic property of the FFT requiring that the beginning and the ending values of the series be continuous.
3. Use Eq.(2.2) to calculate the autocovariance function and Eq.(2.4) to calculate the cross covariance function. Then, normalize the autocovariance function by its value at zero time lag, which yields the autocorrelation coefficient function as given by Eq.(2.5). Normalize the cross covariance function by the product of $B_{xx}(0)$ and $B_{yy}(0)$, which gives the cross correlation coefficient function of Eq.(2.6). Note that the time lag τ only needs to be calculated up to 10 or 20 percent of T . Larger lags will result in unreliable results since, by shifting the two series away in the convolution process, a lot of information will be lost.
4. Using the Hilbert transformation technique, the envelope function can be calculated.

Figure 2.2 shows the autocorrelation coefficient function of $x(t)$. Since this function is an even function, it need be evaluated for positive time lags only. Figure 2.3 shows the cross correlation coefficient function of $x(t)$ and $y(t)$. Unlike the autocorrelation coefficient function, its peak value equals 0.769, which does not occur at zero lag but at $\tau = 0.07sec$. For the wave propagation problem, this means that the dominant waves travel from the point of measuring $x(t)$ to the point of measuring $y(t)$ in $0.07sec$. This information which is very important in studying the spatial variation of ground motion, can be used to calculate the apparent wave velocity. This velocity is calculated by dividing the projected distance along the main wave propagation direction by τ . Figures 2.4 and 2.5 show envelope functions of $x(t)$ and $y(t)$, respectively.

(b) Power spectrum, coherency and phase spectrum

1. Remove the mean and taper of the sample wave forms.
2. Compute the Fourier transform of each wave form
3. Filter the wave forms in the frequency domain. If the wave forms are represented by frequencies higher than the Nyquist frequency $f_n = 1/(2\Delta t)$, the power spectrum will be aliased into a power spectrum represented only in the principal range $[-f_n, f_n]$. In this case, the wave forms should be filtered to remove the power at frequencies above f_n . Also, for practical reasons, the power below a selected frequency should be removed.

4. Choose the proper smoothing window shape and width. The bigger the window width, the smoother the spectrum will be; however the resolution of the calculated spectrum will be low. The window width should be chosen so that it not only results in a satisfactory smoothing spectrum, but also keeps the resolution as high as possible.
5. Use Eq.(2.8) to calculate the power spectral density function. Figure 2.6 shows the power spectral density function of $x(t)$ obtained using a triangular smoothing window with a band width equal to $0.4Hz$.
6. Use Eq.(2.11) to calculate the cross power spectral density function. Figure 2.7 shows the absolute value of the cross power spectral density function of $x(t)$ and $y(t)$ using a triangular smoothing window of band width $0.4Hz$
7. Use the results obtained in Step 5 and Step 6 to calculate coherency through Eq.(2.12). Be sure that the power spectrum has been smoothed so that the calculated absolute coherency values will not equal unity. Figure 2.8 shows the absolute-value coherency function between $x(t)$ and $y(t)$.
8. Use the cross power spectral density function or the coherency function to calculate the phase spectrum for $x(t)$ and $y(t)$ as shown in Fig. 2.9.

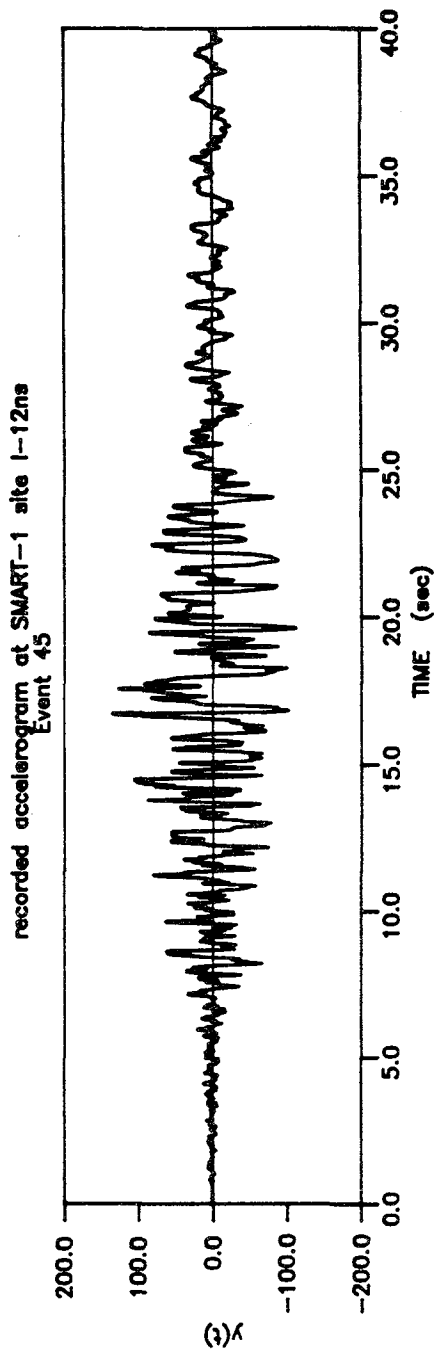
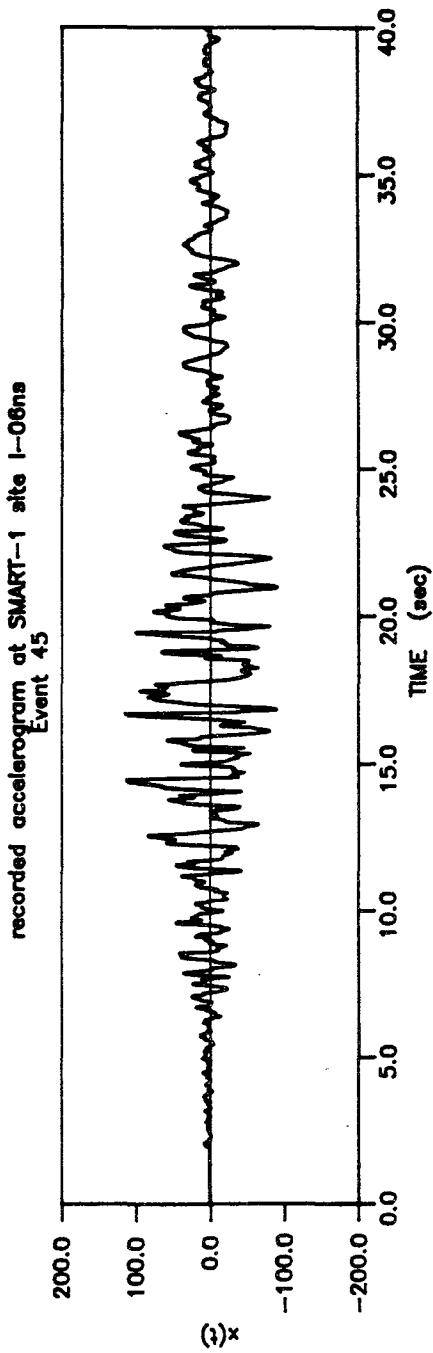


Fig.2.1 Ground Motion Time-Histories Recorded in the
Same Direction at SMART-1 Site during Event
45

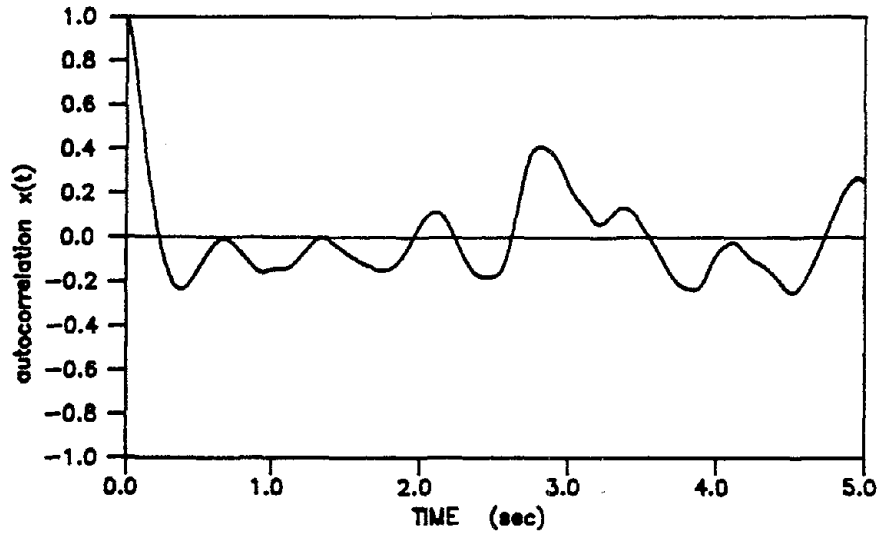


Fig.2.2 Autocorrelation Coefficient Function of $x(t)$

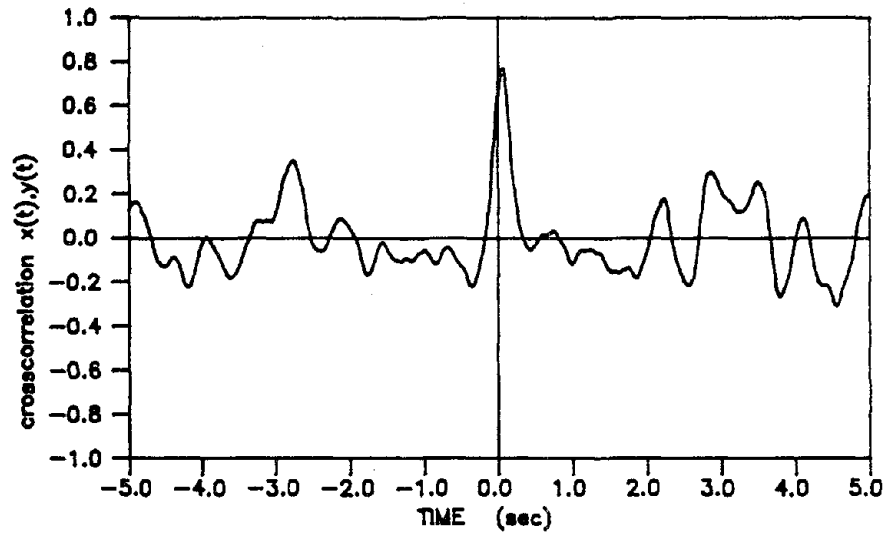


Fig.2.3 Cross Correlation Coefficient Function of $x(t)$ and $y(t)$

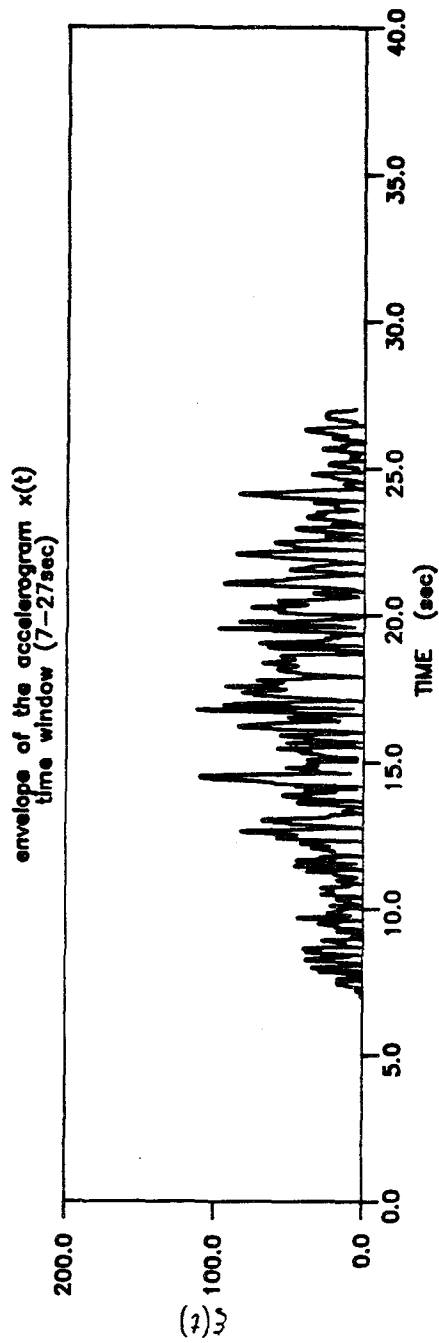


Fig.2.4 Envelope Function of Time-History $x(t)$

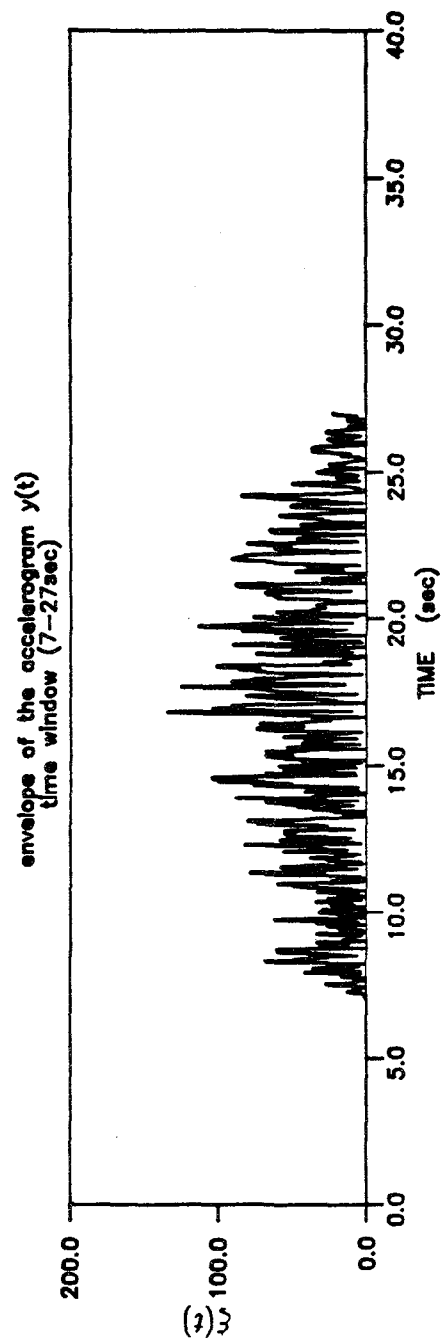


Fig.2.5 Envelope Function of Time-History $y(t)$

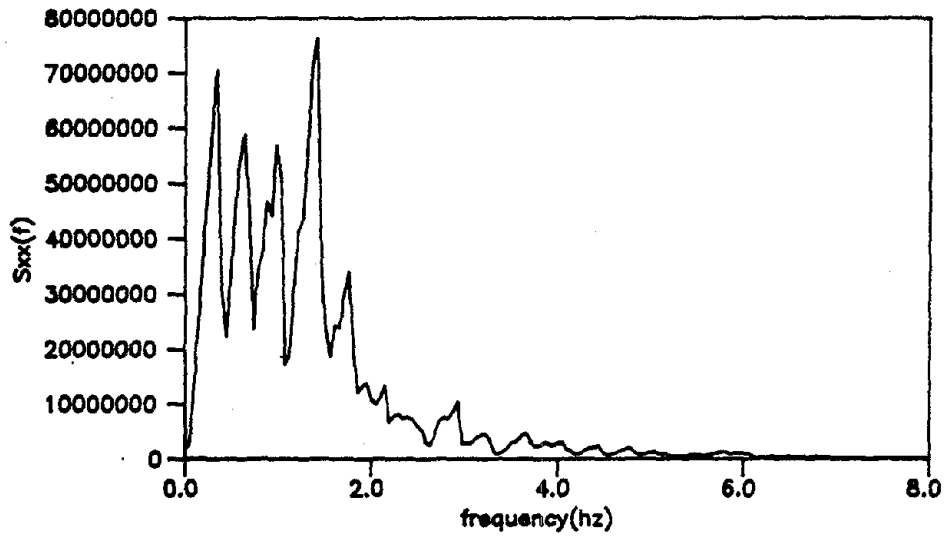


Fig.2.6 Power Spectral Density Function of $x(t)$ Obtained Using Smoothing Window of Width $0.4Hz$

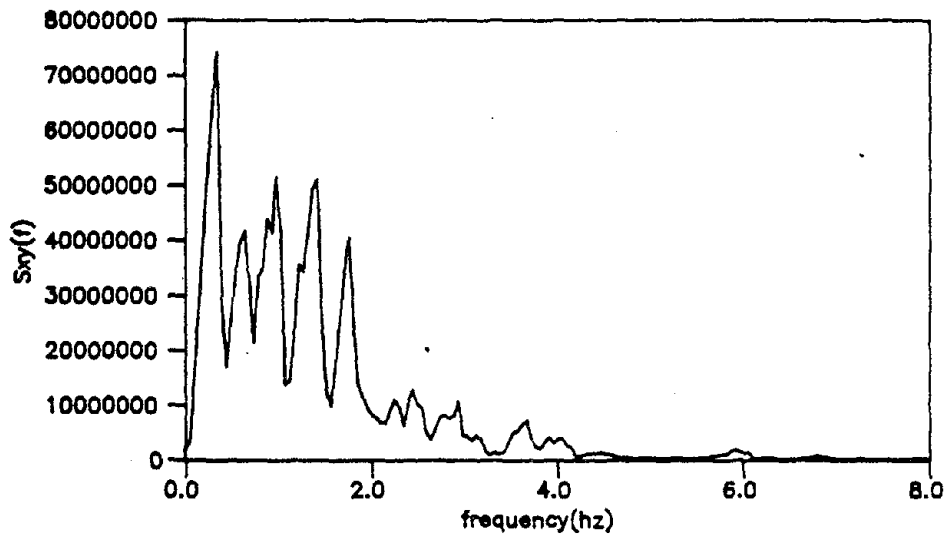


Fig.2.7 Absolute Values of the Cross Power Spectral Density Function of $x(t)$ and $y(t)$

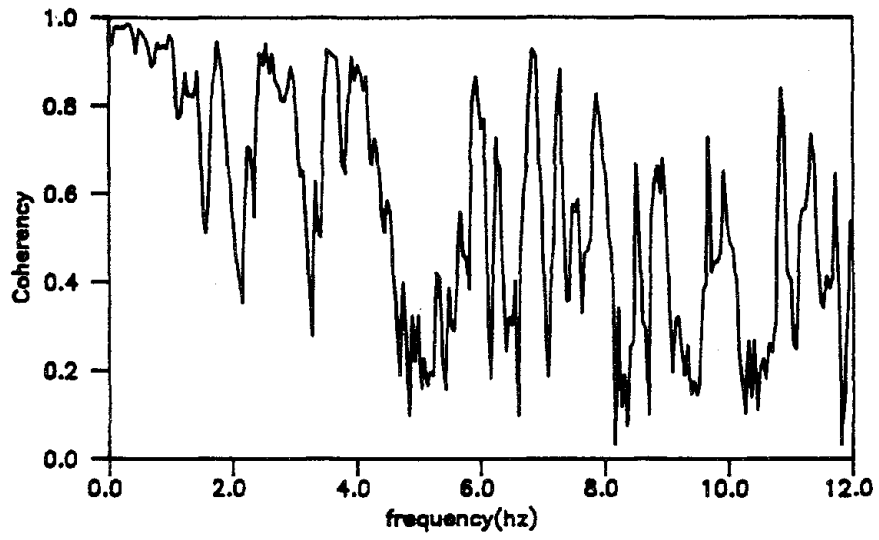


Fig.2.8 Absolute Values of Coherency of $x(t)$ and $y(t)$

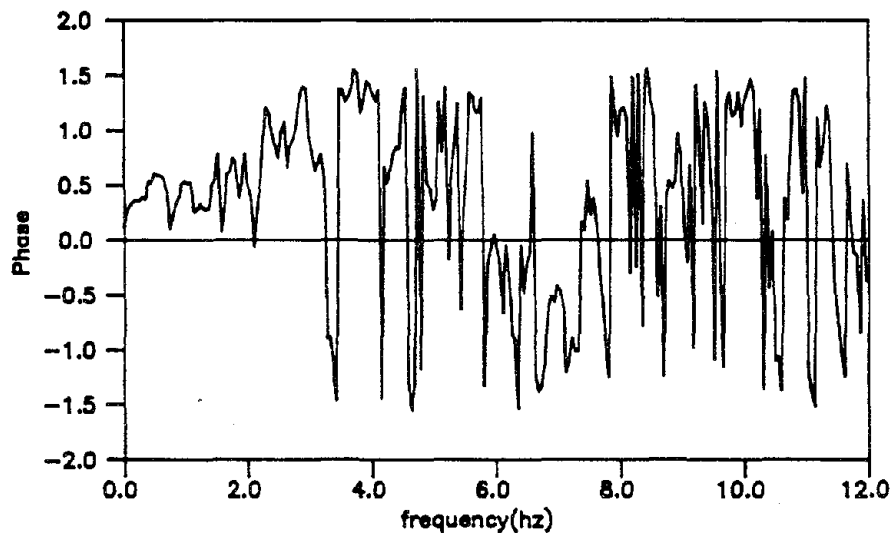


Fig.2.9 Phase Spectrum of $x(t)$ and $y(t)$

CHAPTER 3 MULTIPLE STATION GROUND MOTION PROCESSING

When ground motions are simulated for engineering design purposes, they should be realistic representations of the seismic motions expected at the site under consideration. Hence, it is necessary to know such properties of the expected ground motion as duration, peak, shape function, power spectral density function, coherency, and apparent velocity. Knowing these ground motion properties, one can generate realistic inputs to be used in dynamic analyses; and thus, contribute to the design of economical and safe structures. In this chapter, the recorded SMART-1 ground motions of two earthquake events are analyzed to establish shape functions, power spectral density functions, and apparent wave velocities with respect to different frequencies. Also, the ground motions are analyzed to establish a coherency function which can be used in simulating spatial variation of the ground motions. While these functions are site specific for the SMART-1 site, they can also be used for sites with similar properties.

3.1 The SMART-1 Array

The SMART-1 array, see Bolt, et al. (1982) and Darragh (1987), is the first high density array developed that permits the study of spatial variation of ground motion in a small area. The array is located in the northeast corner of Taiwan near the city of Lotung on the Lan-yang plain; see Fig. 3.1. The array consists of 37 force-balanced triaxial accelerometers configured in three circular concentric rings of radii 200m, 1000m, and 2000m. The three rings are named I(inner), M(middle), and O(outer), respectively. There are 12 stations in each ring named from 1 to 12, and one center station named C-00. The distance between station pairs varies from a minimum of approximately 105m to a maximum of 4000m. In June 1983, two additional stations, E-01 and E-02, were added to the array at 2.8km and 4.8km south of the center station. The configuration of the array is shown in Fig. 3.2.

The SMART-1 array is located on recent alluvium. The ground water level is almost at ground surface. The area is very flat having surface elevations which vary from 2.4m to 18.1m. All stations are located on soil sites, except for station E-02 which is located on rock. Two north-south cross sections are shown in Fig. 3.3. The soils beneath the main array consist of 4-12 meters of clays and muds over recent alluvium of depths up to 50m. Below the alluvium layer are gravels having pebble sizes which increase with depth. The bedrock below the gravels is slate. The depth of the bedrock varies from 170m at the southern end of the outer ring to 600m at the northern end of the outer ring. The foundation properties and the P and S wave velocities are given in Table 3.1. These data were obtained by the HCK Geophysical Company by drilling seven holes and using crosshole and uphole seismic

methods.

3.2 Information Recorded by the SMART-1 Array

This array recorded its first earthquake on October 18, 1980. Up to January, 1988, 50 events had been recorded by some or all stations in the array. Figure 3.4 shows the epicentral positions of the seventeen recorded events used in this study. Among all these events, Events 24 and 45 were chosen to be studied thoroughly for power spectral density functions, envelope functions, apparent velocities, and coherency because of their long epicentral distances and high magnitudes. Figure 3.5 shows some of the recorded accelerograms of Event 24. Besides completely processing the recorded accelerograms of Events 24 and 45, a total of seventeen events were chosen to be studied intensively for coherency effects. Special study is needed since coherency is the most important function characterizing spatial variations of ground motion. The seventeen earthquakes chosen were selected on the basis of having epicentral distances larger than 30km, magnitudes larger than 5, and having triggered at least seven of the inner ring stations. Table 3.2 gives information on each of these events.

3.3 Power Spectral Density Function

The power spectral density function is a measure of the frequency content in a stationary random process. Earthquake ground motions are actually nonstationary in both the time and frequency domains. It is found, however, that a satisfactory and practical way of treating ground motion nonstationarity, is to assume the ground motions to be piecewise stationary or quasi-stationary. This assumption is made on the basis that ground motions propagating in the earth usually consist of three different types of wave; the primary P-wave, the secondary S-wave, and surface waves (Rayleigh and Love waves). The motions of each wave type can be modelled as a stationary process better than the combined motions of all the wave types. The piecewise stationary assumption is applied in the subsequent treatment.

Power spectral density functions were calculated for all components of ground motion recorded at the inner ring stations for Events 24 and 45 using the frequency domain method given in the previous chapter, Eq.(2.8). Triangular smoothing windows were used for all the calculations using the data of Events 24 and 45. The window width and M-value were chosen such that the resulting power spectral density functions were smooth enough while their standard deviations were not too large. It was found that the vertical components of ground motion have higher frequency content and less energy than the horizontal components for both Events 24 and 45; see Hao (1989). Also, the power spectral density functions for a particular component are almost the same at all the inner ring stations for each of the two events, and that the frequency content of the ground motion decreases as the time window moves to later times.

On the basis of the results presented and discussed in Hao (1989) for Events 24 and 45, the following conclusions have been drawn.

1. Attenuation of the ground motion wave propagation can be neglected across the SMART-1 array, i.e. the intensities of corresponding components of motion are nearly constant for all stations in the array.
2. The quasi-stationary frequency content assumption can be used to model the nonstationarity of the ground motion.
3. A power spectral density function of the Tajimi-Kanai form can be satisfactorily used for simulation purposes.

Thus, power spectral density functions representing the entire site can be obtained by averaging those for corresponding components of motion recorded throughout the array. This averaging procedure will greatly reduce the contributions from noise in the resulting power spectral density functions. Such average results for each component, each time window, and each event were obtained. The results for the EW components of motion for each of the two events are shown in Figs. 3.6 through 3.11. These results were used to establish the Tajimi-Kanai model in each case; the expression for the Tajimi-Kanai form is given by

$$S(\bar{\omega}) = \frac{1 + 4\xi_g^2 \frac{\bar{\omega}^2}{\omega_g^2}}{(1 - \frac{\bar{\omega}^2}{\omega_g^2})^2 + 4\xi_g^2 \frac{\bar{\omega}^2}{\omega_g^2}} S_0 \quad (3.1)$$

the corresponding values of ω_g , ξ_g , and S_0 were obtained for Events 24 and 45; see Table 3.3.

The results for the vertical components of motion for Event 24 are missing in Table 3.3, since it was found that the Tajimi-Kanai model was inadequate. Figure 3.12 shows an example of the averaged power spectral density function for the vertical component of motion in the first window as recorded during Event 24. It is seen that the banded white noise model fits better than the Tajimi-Kanai model in this case. It can be seen that the central frequency ω_g decreases with time for all cases except the EW component for Event 24, where ω_g actually increases from 1.0Hz to 1.2Hz. The damping ratio ξ_g of the first time window is much higher than that of the second window. In the first window, $\xi_g = 0.95$, which corresponds to a very broad band window. In the second window, $\xi_g = 0.3$ which represents a much narrower band.

The above power spectral density function results can be used to simulate ground motions in consecutive time windows separately. The stationarity assumption can be used in each time window consistent with the corresponding power spectral density function. The ground motion mean square intensity in each window can be calculated by integration of the

power spectral density function as

$$\sigma_0^2 = \int_0^{\infty} S(\bar{\omega}) d\bar{\omega} \quad (3.2)$$

Substituting the Tajimi-Kanai power spectral density function of Eq.(3.1) into Eq.(3.2) and integrating gives the covariance of motion in the approximate form

$$\sigma_0^2 = \int_0^{\infty} S(\bar{\omega}) d\bar{\omega} = \omega_g \frac{1 + 4\xi_g^2}{4\xi_g} \quad (3.3)$$

see Ruiz and Penzien (1969). By using Eq.(3.3) and the parameters in Table 3.3, the normalized scale factors for the power spectral density function in each time window are obtained giving the results presented in Table 3.4. These scale factors for the power spectral density functions are used to maintain uniform intensity of ground motion within each time window before applying the time-dependent shape function.

3.4 Shape Function

The shape function is used to characterize ground motion nonstationarity in the time domain. It is the normalized envelope function of ground motion. Shape functions of all accelerograms recorded during Events 24 and 45 at the inner ring stations were evaluated using the Hilbert transform approach described in Chapter 2; see Eq.(2.19). Since there is no significant attenuation of the ground motions across the array, the shape functions of the corresponding accelerograms recorded at all inner ring stations can be assumed the same. Thus, a representative ground motion accelerogram shape function for each component of motion can be obtained by averaging the shape functions for corresponding accelerograms. These averaged shape functions for all three components were calculated and plotted. Figures 3.13 and 3.14 show the averaged shape function for the EW component using data from Events 24 and 45.

It is seen that, except for those generated using the vertical components of motion recorded during Event 24, all the calculated shape functions of accelerograms are similar to the Bogdanoff type having the form

$$\xi(t) = \begin{cases} 0 & t \leq 0 \\ ate^{-bt} & t > 0 \end{cases} \quad (3.4)$$

where a and b are parameters to be determined consistent with observed ground motion nonstationarity. Figure 3.15 shows the averaged envelope functions for motions recorded in the vertical direction during Event 24. These shape functions fit better the Amin and Ang form given by

$$\xi(t) = \begin{cases} I_0 \left(\frac{t}{t_1}\right)^2 & 0 \leq t \leq t_1 \\ I_0 & t_1 \leq t \leq t_2 \\ I_0 e^{-c(t-t_2)} & t_2 \leq t \end{cases} \quad (3.5)$$

where I_0 represents ground motion intensity. The normalized shape function is obtained by setting $I_0 = 1$. Quantities t_1 , t_2 are values of time that separate the shape function into its parabolic, constant, and exponential decay forms. Constant c controls the rate of decay at the end of the motion.

To fit the Bogdanoff shape function given by Eq.(3.4), two parameters a and b can be determined by the condition that at a certain time $t = t_p$, $\xi(t)$ reaches its peak value which is normalized to be one. Then, by differentiating Eq.(3.4) with respect to t , one obtains

$$t_p = \sqrt{\frac{1}{2b}} \quad (3.6)$$

and

$$a = \sqrt{2be} \quad (3.7)$$

By solving these two equations for a and b , the shape functions can be determined in terms of t_p and e (the base of the natural logarithm) for all three components motion.

The results for a , b , and t_p of Events 24 and 45 are shown in Table 3.5. Since the results of the vertical component for Event 24 do not fit this type of shape function properly, values for the above constants are not given in Table 3.5.

3.5 Apparent Velocity

Apparent velocity is one of the most difficult parameters to assess due to the fact that the waves are of different types moving in different directions experiencing multiple reflections and refractions.

Some example apparent velocities calculated for Event 45 by the frequency-wave-number (F-K) method (Abrahamson, 1985) are shown in Fig. 3.16. In this report, the apparent velocities are assumed to be frequency independent. Thus, by approximately fitting many F-K results, the apparent velocities of Event 24 are obtained as $3km/s$, and $4km/s$ for the horizontal and vertical components, respectively, and $4km/s$ and $6km/s$ for the apparent velocity values of Event 45. Two F-K diagrams of the approaching wave field are shown in Fig. 3.17. From this figure, it is seen that the approaching wave directions are very diverse.

3.6 Coherency

As previously mentioned, coherency is one of the most important and effective quantities used to describe the spatial variations of ground motion. Using the SMART-1 data, several authors have studied the coherency relation given as

$$\gamma_{ij}(i\bar{\omega}, d_{ij}) = |\gamma_{ij}(i\bar{\omega}, d_{ij})| \exp\left[i\bar{\omega} \frac{x_{ij}}{v_a}\right] \quad (3.8)$$

where subscripts i and j represent the two different stations, x_{ij} is the projected distance in the wave propagating direction between stations i and j , v_a is apparent velocity, $\bar{\omega}$ is circular frequency, and $|\gamma_{ij}(i\bar{\omega}, d_{ij})|$ is the loss of coherency with separation due to unknown effects. All the loss of coherency models, that have been proposed, are dependent only on the absolute distance between the the two stations; see Loh (1985), Harrichandran and Vanmarcke (1984), Abrahamson (1988), Tsai (1988), and Loh and Yeh (1988). It has been found that the loss of coherency is dependent on both the projected distance in the direction of wave propagation (d_{ij}^l), and the projected distance transverse to it (d_{ij}^t) (Hao, 1989).

To develop a new two-dimensional coherency model, the loss of coherency between all station pairs for all components of ground motion recorded during Events 24 and 45 was calculated. It has been found that the values of loss of coherency were almost the same for the ground motions recorded in the two horizontal directions, but were different for those in the vertical direction (Hao, 1989). On the basis of the calculated losses of coherency for Events 24 and 45, it was found that the coherency model of Eq.(3.8) can still be used provided it is expressed in the two dimensional form given by

$$|\gamma(f, d_{ij}^l, d_{ij}^t)| = \exp(-\beta_1 d_{ij}^l - \beta_2 d_{ij}^t) \exp[-(\alpha_1(f)\sqrt{d_{ij}^l} + \alpha_2(f)\sqrt{d_{ij}^t})f^2] \quad (3.9)$$

where f is frequency and where d_{ij}^l and d_{ij}^t are the projected longitudinal and transverse distances defined above. Parameters β_1 and β_2 are constants which control the coherency values at zero frequency while $\alpha_1(f)$ and $\alpha_2(f)$ are two frequency dependent parameters which control the loss of coherency with respect to frequency. All parameters β_1 , β_2 , $\alpha_1(f)$ and $\alpha_2(f)$ were determined by fitting Eq.(3.9) to the coherency data using the least squares method.

In order to investigate coherency, ground motions recorded during the 17 events shown in Table 3.2 were used to evaluate β_1 , β_2 , $\alpha_1(f)$ and $\alpha_2(f)$. Since the loss of coherency with distance can be assumed the same for the two horizontal components of motion, only the NS components were analyzed. The coherencies of the vertical components were studied for Events 24 and 45 only.

Loss of coherency values were calculated for all components of motion recorded at the inner ring station pairs. To aid in interpreting the results, the inner ring station pairs were divided into 9 groups with respect to the distances d_{ij}^l and d_{ij}^t falling in the ranges 0-100m, 100-200m, and 200-400m. All loss of coherency values for station pairs in the same group were averaged. These average values were then considered to represent the loss of coherency for d_{ij}^l and d_{ij}^t at distances of 50m, 150m, and 300m.

The two constant parameters β_1 and β_2 were determined using the loss of coherency

values at zero frequency for each of the 9 distance groups for each event. The detailed procedure can be seen in Hao (1989); the results are presented in Table 3.6 for all 17 events.

To calculate the two frequency parameter functions $\alpha_1(f)$ and $\alpha_2(f)$ for each event, the least squares method was used. It was found that two nonlinear functions

$$\begin{aligned}\alpha_1(f) &= \frac{a}{f} + bf + c \\ \alpha_2(f) &= \frac{d}{f} + ef + g\end{aligned}\tag{3.10}$$

best fit the raw data, where a , b , c , d , e , and g are six constants, which were obtained by weighted least squares fitting. The values of the six constants obtained for all 17 events, which are valid for $0.05Hz \leq f \leq 10Hz$ and $0 \leq d_{i,j}^l, d_{i,j}^r \leq 400m$, are presented in Table 3.7. When $f > 10Hz$, the loss of coherency values can be assumed to be constant at the $f = 10Hz$ value. The detailed procedure can be found in Hao (1989).

Figures 3.18 through 3.21 show comparisons between the loss of coherency values calculated by Eq.(3.9) and the generated values using the raw data for Events 24, 31, 45, and 46. Similar comparisons were found using the data for all 17 events. From these figures, it can be noticed that, at the lower frequencies, the analytical model values are always smaller than those generated directly from the raw data. Also notice that the analytical model decays as e^{-f} while the raw data loss of coherency decays more closely to e^{-f^2} at short distances. This latter incompatibility results from a lack of raw data for short distances. A more sophisticated model, that would properly control the loss of coherency in the short distance range, could be obtained for $\alpha_1(f)$ and $\alpha_2(f)$, if more raw data were available. Figures 3.22 through 3.24 show the model errors in loss of coherency for Event 45 calculated for all the available distances. The model $\alpha_1(f)$ and $\alpha_2(f)$ functions for all 17 events were determined. The results for Events 20, 22, 23, 24, 41, 45, 46, 47 are shown in Figs. 3.25 and 3.26.

From Table 3.6, and the calculated loss of coherency values, it is observed that the β values are dependent on peak ground acceleration. Figures 3.27 and 3.28 show the β_1 and β_2 relations, respectively, with respect to PGA. The β values are seen to decrease with increasing PGA which corresponds to an increase in loss of coherency values. This is because the ground motion energy dissipation from wave propagation through the same distance, is the same. A ground motion having a higher PGA usually contains a higher amount of energy. Consider two waves travelling along the same path between points P and Q, with energy content E_1 and E_2 at the point P. If δ is the amount of energy dissipated by the waves between P and Q, then the proportional energy dissipation is defined to be $\frac{\delta}{E_1}$ and $\frac{\delta}{E_2}$, respectively.

$$\text{If } E_1 > E_2, \quad \text{then} \quad \delta/E_1 < \delta/E_2$$

That is, the proportional energy dissipation of a ground motion with a higher PGA is smaller

than the proportional energy dissipation of a ground motion with a lower PGA, along the same path. It follows that the ground motion, that has the higher proportional energy dissipation, has smaller loss of coherency values along the same path. Another property that can be noticed is that β_1 is larger than β_2 for the events with azimuths between 90° and 180° , except for Event 33, and β_1 is smaller than β_2 for the events with azimuths in the range $0^\circ - 90^\circ$ and $180^\circ - 270^\circ$. This phenomenon takes place because of the presence of a mountain to the north-west of the SMART-1 site while the terrain is flat in all other directions. This mountain will certainly disturb the propagation of plane waves.

The same methods of processing were used for the ground motions recorded in the vertical component of Events 24 and 45. The β values obtained were $\beta_1 = 1.795 \times 10^{-3}$ and $\beta_2 = 1.442 \times 10^{-3}$ for Event 24, and $\beta_1 = 2.014 \times 10^{-4}$ and $\beta_2 = 1.066 \times 10^{-4}$ for Event 45. The 6 constants in the α functions (a , b , c , d , e , and g) are 5.331×10^{-4} , -4.740×10^{-6} , 6.507×10^{-5} , -3.891×10^{-3} , -7.571×10^{-5} and 1.025×10^{-3} , respectively, for Event 24 and 1.455×10^{-2} , 1.711×10^{-4} , -3.024×10^{-3} , -1.255×10^{-2} , -1.255×10^{-4} and 2.327×10^{-3} , respectively, for Event 45. The α functions for the vertical components of the two events are shown in Fig. 3.29.

Table 3.1 Velocity and Moduli Values

depth (m)	V_p (m/s)	V_s (m/s)	ν	G(kg/cm ²)	E(kg/cm ²)
0-5	370	120	0.441	264	761
5-8	810	140	0.485	360	1069
8-13	1270	190	0.488	663	1973
13-31	1330	220	0.486	889	2642
31-34	1330	280	0.477	1440	4254
34-48	1250	250	0.479	1148	3396
48-60	1220	270	0.474	1339	3947
60-80	1470	320	0.475	1881	5549
80-150	1540	480	0.398	4232	11833

V_p = P wave velocity

V_s = S wave velocity

ρ = Bulk density = 1.8gm/cc

ν = Poisson ratio

G = Shear modulus = ρV_s^2

E = Young's modulus = $2G(1+\nu)$

Table 3.2 Characteristics of the 17 Recorded Events

event	M _L	Depth (km)	Epicentral Distance	Azimuth (Deg)	Stations Triggered	Maximum Accelerations (gal)		
						V	EW	NS
20	6.4	87	81	96	36	31.8	62.8	86.1
22	6.4	28	35	217	35	36.7	71.1	64.0
23	6.6	37	85	128	23	12.4	26.1	36.1
24	6.9	44	85	130	31	15.4	51.1	64.9
25	6.8	28	75	148	35	11.0	35.6	38.5
29	6.0	9	35	69	30	23.5	83.3	65.0
30	6.3	61	29	63	32	34.9	66.2	78.7
31	5.9	4	48	79	37	36.8	101.0	69.2
33	6.5	3	45	104	36	38.2	148.6	97.2
36	6.3	6	47	110	36	55.4	113.4	82.8
37	5.3	2	30	167	33	41.0	63.0	73.4
40	6.5	16	67	195	37	72.5	210.5	251.1
41	6.2	22	71	192	37	28.5	62.5	99.8
45	7.0	7	79	175	36	110.3	178.0	251.0
46			79	175				
47			79	175				
48			79	175				

Table 3.3 Parameters of the Power Spectral Density Functions

window number	Event 24						Event 45								
	NS			EW			NS			EW			DN		
	ξ_g	ω_g	S_o	ξ_g	ω_g	S_o	ξ_g	ω_g	S_o	ξ_g	ω_g	S_o	ξ_g	ω_g	S_o
1	.30	1.9	8.0×10^4	.95	1.0	2.3×10^5	.33	2.0	3.0×10^5	.84	1.7	5.0×10^5	.80	4.5	2×10^5
2	.26	1.0	4.0×10^5	.30	1.2	1.0×10^6	.83	.90	1.2×10^7	.80	1.2	1.2×10^7	.80	4.5	8×10^5
3	.58	.80	7.3×10^5	.71	1.0	8.1×10^5	.60	.50	4.5×10^6	.95	.50	9.5×10^6	.41	.60	3×10^5

Table 3.4 Scale Factors for the Power Spectral Density Functions

Window number	Event 24			Event 45		
	NS	EW	DN	NS	EW	DN
1	1.0	1.0		1.0	1.0	1.0
2	1.34	0.94		1.49	1.24	1.0
3	1.65	1.06		2.07	1.80	2.82

Table 3.5 Parameters for the Shape Functions

	Event 24			Event 45		
	NS	EW	DN	NS	EW	DN
$t_{max}(s)$	8	11		12	12	8
a	0.206	0.15		0.1347	0.1347	0.206
b	0.0078	0.00413		0.00347	0.00347	0.0078

Table 3.6 Calculated β Values

Event	20	22	23	24	25	29
β_1	5.350×10^{-4}	1.130×10^{-4}	5.290×10^{-4}	2.622×10^{-4}	2.390×10^{-4}	3.550×10^{-4}
β_2	3.670×10^{-4}	3.710×10^{-4}	1.860×10^{-4}	1.211×10^{-4}	1.820×10^{-4}	6.310×10^{-4}
Event	30	31	33	36	37	40
β_1	2.250×10^{-4}	4.620×10^{-4}	2.810×10^{-4}	3.530×10^{-4}	7.910×10^{-4}	9.323×10^{-5}
β_2	5.100×10^{-4}	4.820×10^{-4}	3.710×10^{-4}	2.830×10^{-4}	6.830×10^{-4}	1.421×10^{-4}
Event	41	45	46	47	48	
β_1	3.062×10^{-4}	1.109×10^{-4}	1.193×10^{-3}	7.420×10^{-4}	1.391×10^{-3}	
β_2	6.894×10^{-4}	6.730×10^{-5}	9.010×10^{-4}	1.202×10^{-3}	4.723×10^{-4}	

Table 3.7 Constants in the α Functions

Event	a	b	c	d	e	g
20	1.356×10^{-2}	8.590×10^{-5}	-1.933×10^{-3}	4.554×10^{-3}	1.697×10^{-5}	-4.339×10^{-4}
22	8.639×10^{-3}	6.219×10^{-5}	-1.251×10^{-3}	2.644×10^{-3}	-5.264×10^{-5}	5.261×10^{-4}
23	9.003×10^{-3}	7.243×10^{-5}	-1.445×10^{-3}	7.016×10^{-3}	2.420×10^{-5}	-6.489×10^{-4}
24	3.113×10^{-3}	-6.635×10^{-6}	2.042×10^{-5}	3.286×10^{-3}	2.590×10^{-6}	-1.050×10^{-4}
25	7.016×10^{-3}	2.640×10^{-5}	-6.749×10^{-4}	1.583×10^{-2}	1.903×10^{-4}	-3.528×10^{-3}
29	-4.177×10^{-4}	-9.938×10^{-5}	1.223×10^{-3}	8.767×10^{-3}	1.203×10^{-4}	-2.007×10^{-3}
30	1.066×10^{-2}	2.651×10^{-5}	-9.988×10^{-4}	6.655×10^{-3}	5.883×10^{-5}	-1.118×10^{-3}
31	7.483×10^{-3}	7.660×10^{-5}	-1.375×10^{-3}	7.062×10^{-3}	5.553×10^{-5}	-1.168×10^{-3}
33	3.624×10^{-3}	-1.705×10^{-5}	3.678×10^{-5}	5.815×10^{-3}	5.687×10^{-5}	-1.005×10^{-3}
36	8.240×10^{-4}	1.267×10^{-5}	-1.476×10^{-4}	7.468×10^{-3}	1.943×10^{-5}	-6.911×10^{-4}
37	1.186×10^{-2}	1.451×10^{-4}	-2.498×10^{-3}	-1.124×10^{-2}	-1.966×10^{-4}	3.297×10^{-3}
40	1.037×10^{-2}	9.330×10^{-5}	-1.821×10^{-3}	8.090×10^{-3}	4.083×10^{-5}	-1.007×10^{-3}
41	1.279×10^{-3}	-9.656×10^{-6}	1.225×10^{-4}	4.355×10^{-3}	4.282×10^{-5}	-7.403×10^{-4}
45	3.853×10^{-3}	-1.811×10^{-5}	1.177×10^{-4}	5.163×10^{-3}	-7.583×10^{-6}	-1.905×10^{-4}
46	2.025×10^{-3}	1.802×10^{-5}	-2.668×10^{-4}	1.110×10^{-3}	-4.701×10^{-5}	5.659×10^{-4}
47	1.883×10^{-3}	5.172×10^{-6}	-1.395×10^{-4}	-1.872×10^{-3}	-1.020×10^{-5}	3.005×10^{-4}
48	5.210×10^{-3}	6.383×10^{-5}	-1.036×10^{-3}	-2.339×10^{-4}	-6.473×10^{-5}	9.687×10^{-4}

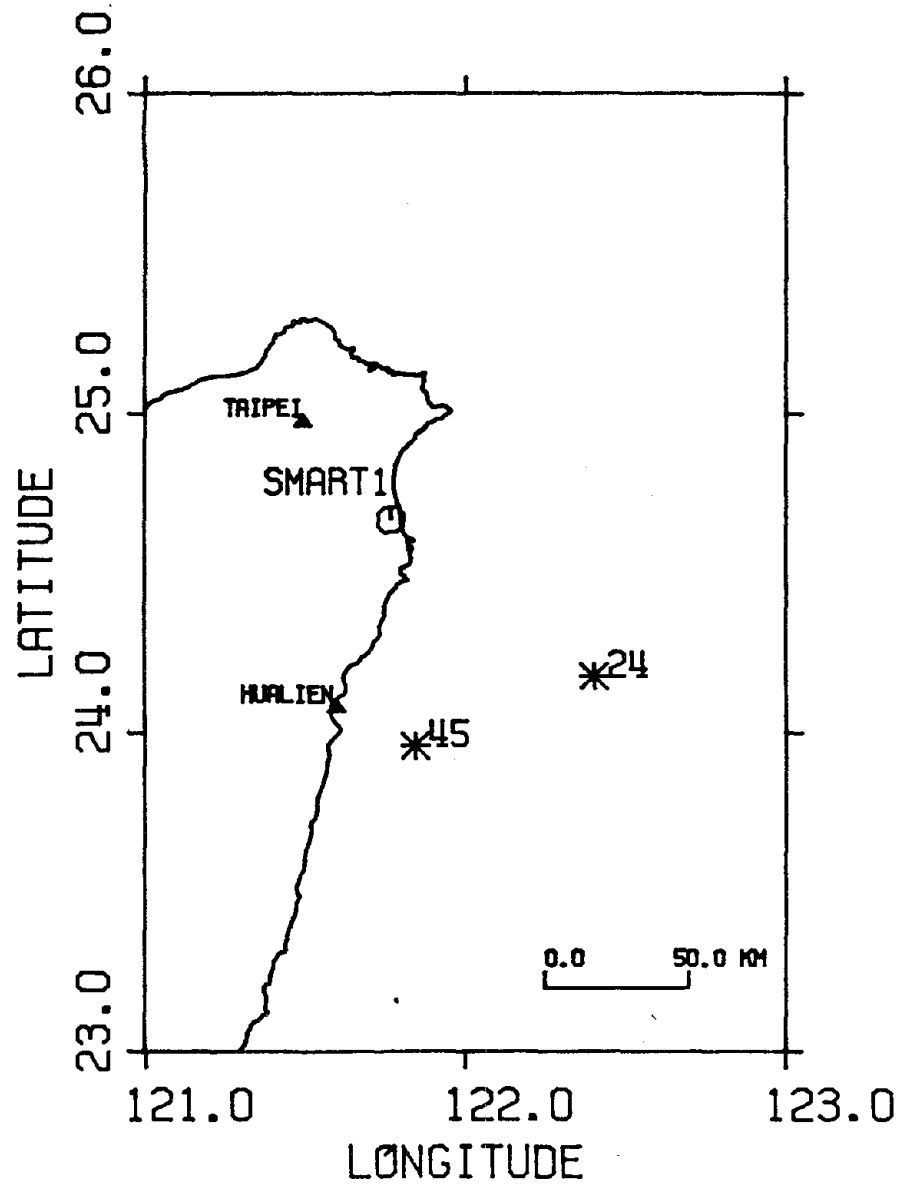


Fig.3.1 Map of the SMART-1 Location

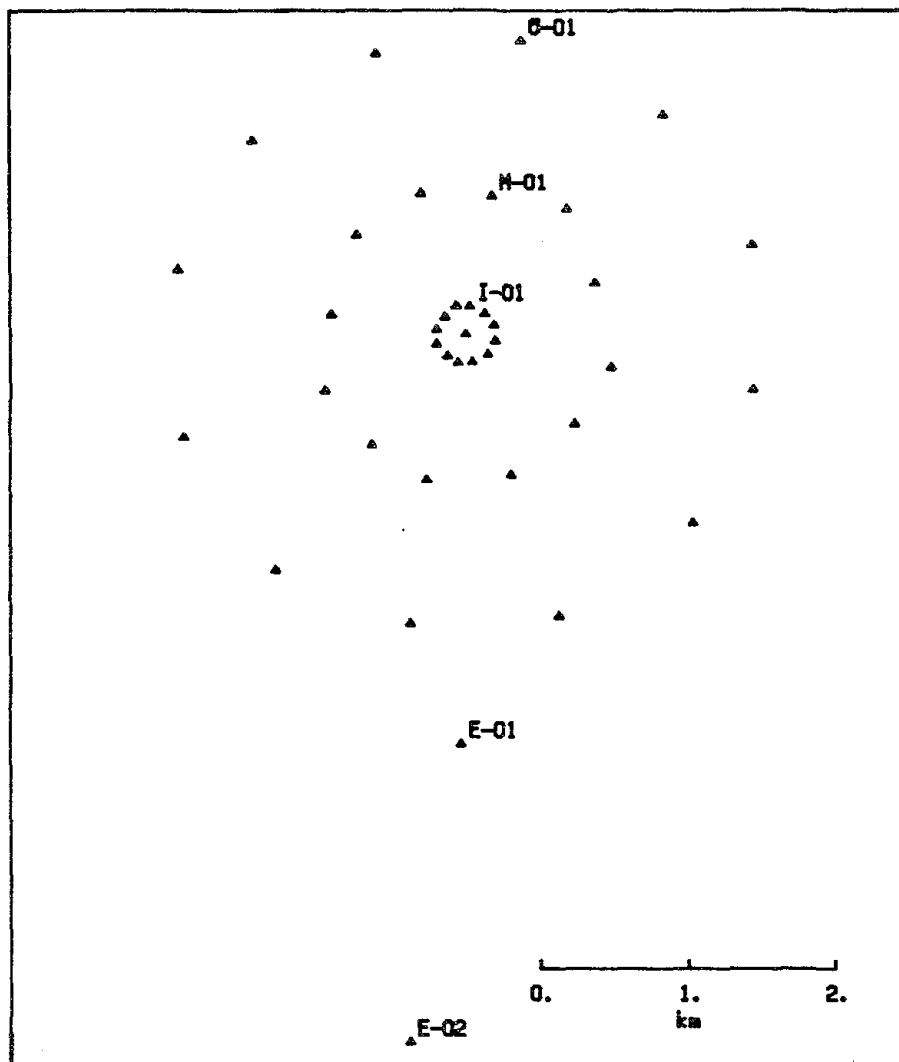


Fig.3.2 The Configuration of the SMART-1 Array

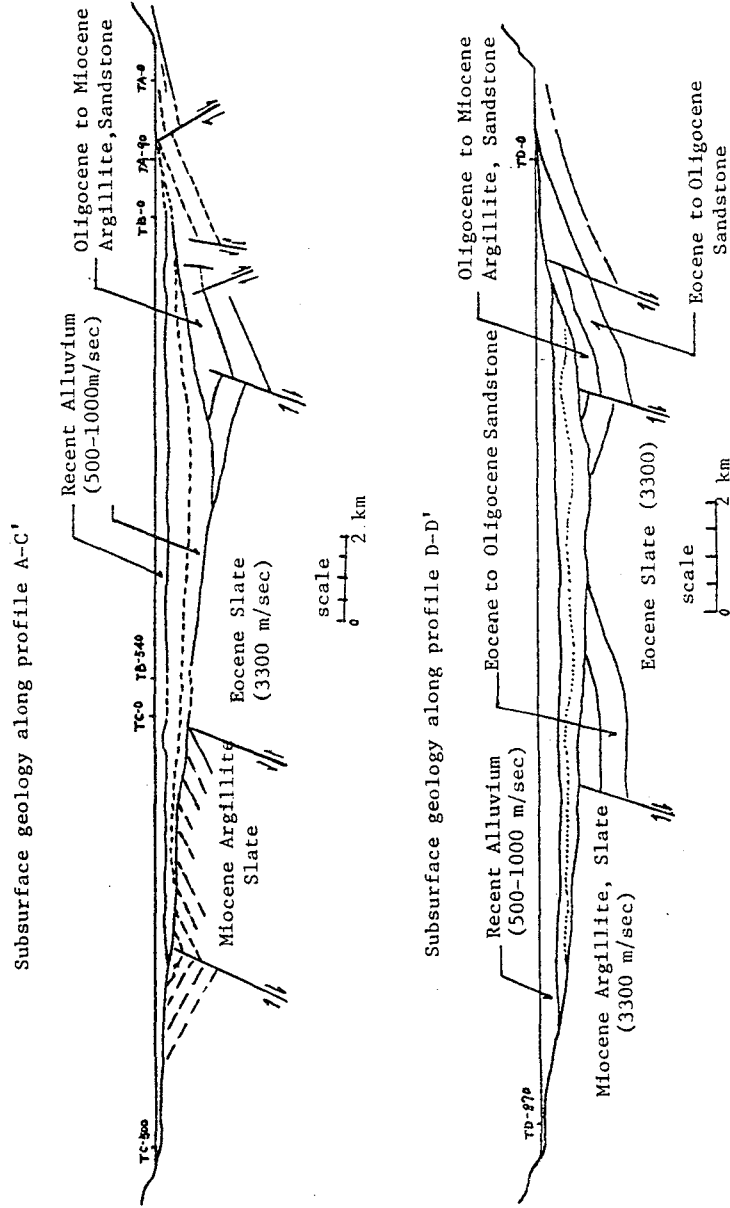


Fig.3.3 Two North-South Cross Sections of the SMART-1 Array

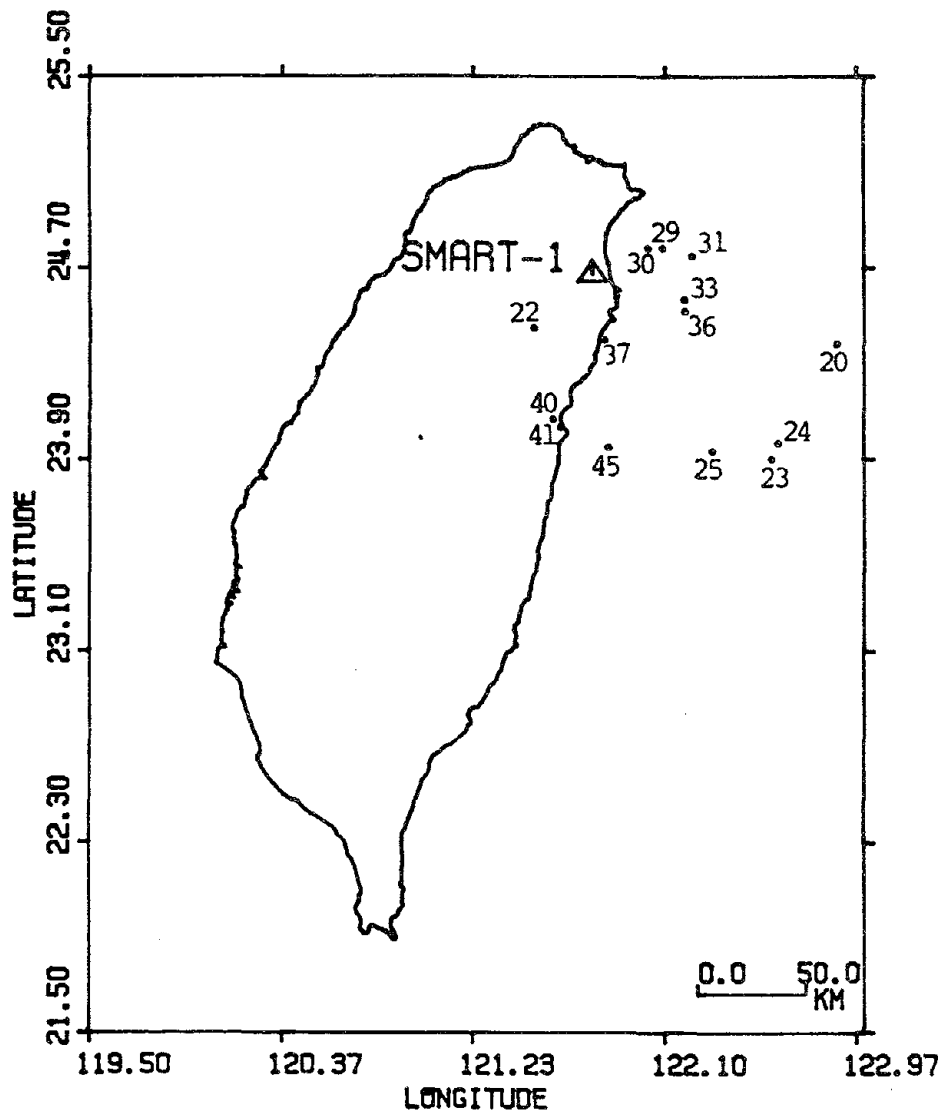


Fig.3.4 Epicentral Positions of the 17 Recorded Events

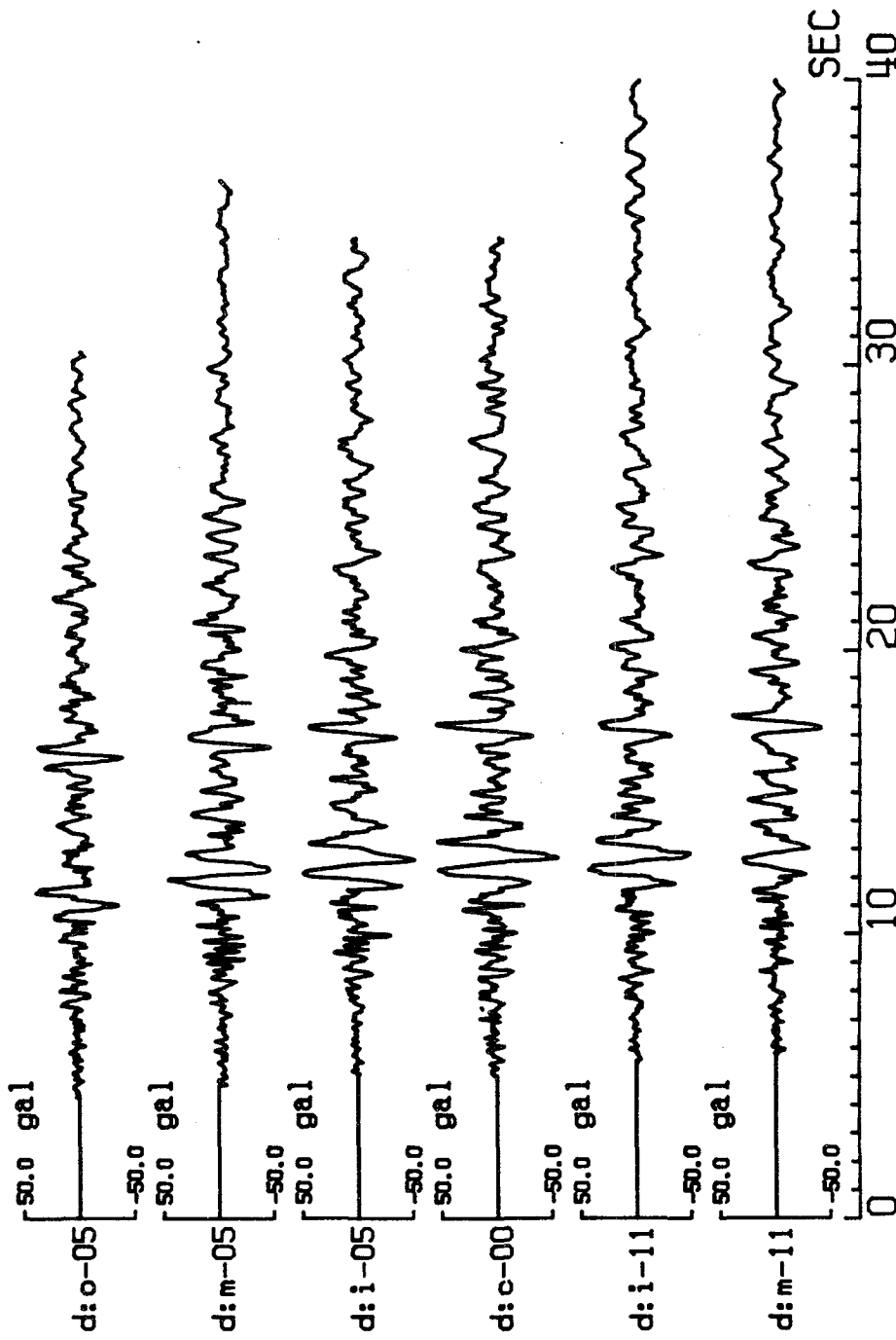


Fig.3.5 Recorded Accelerograms in NS Direction during Event 24

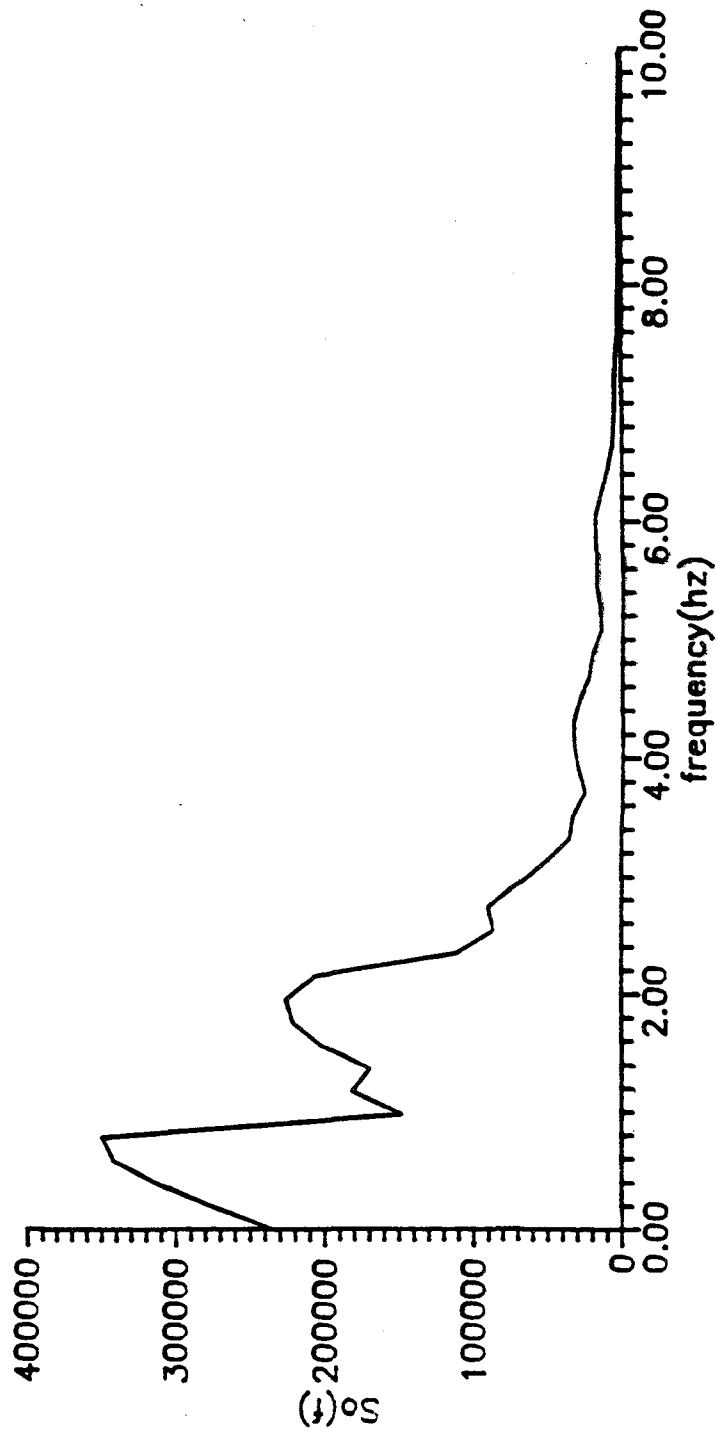


Fig.3.6 Averaged Power Spectral Density Function for Accelerations Recorded in EW Direction during Event 24 (Time Window 5-10sec)

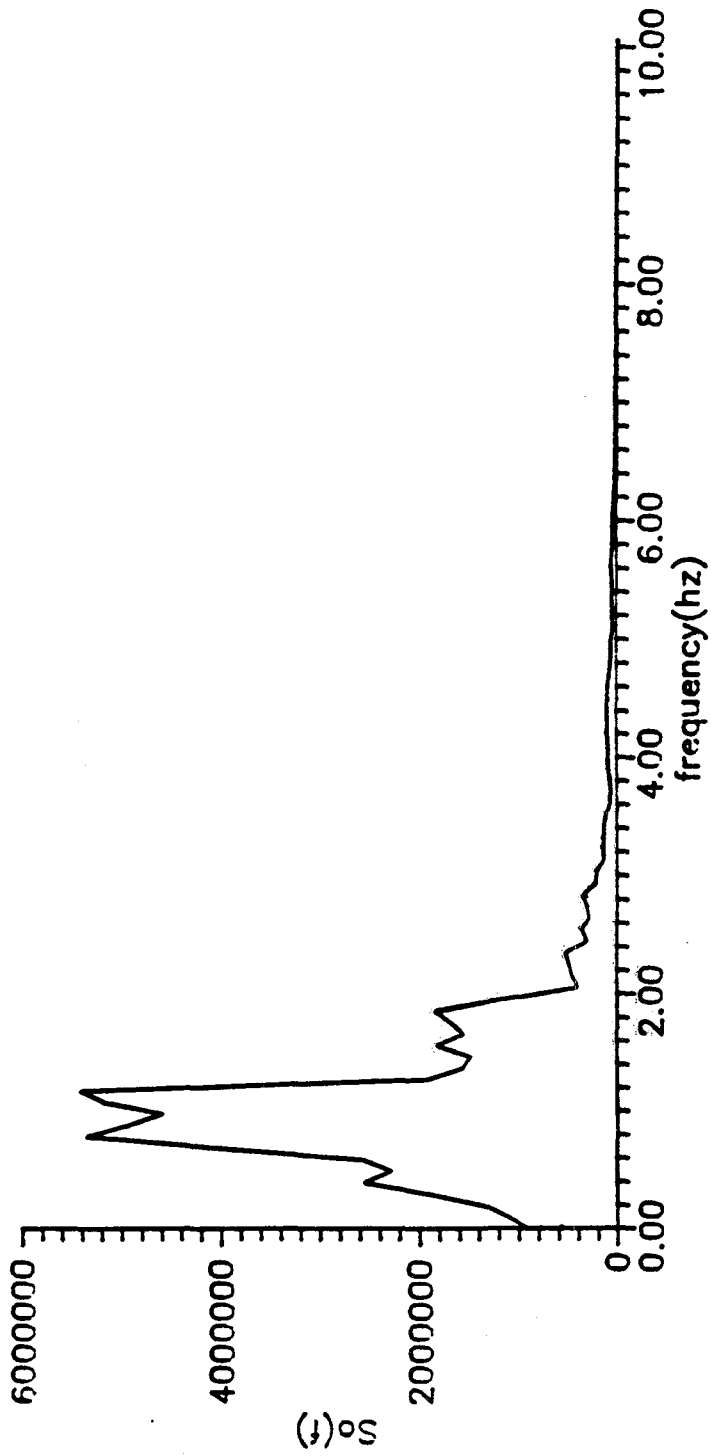


Fig.3.7 Averaged Power Spectral Density Function for Accelerations Recorded in EW Direction during Event 24 (Time Window 9-19sec)

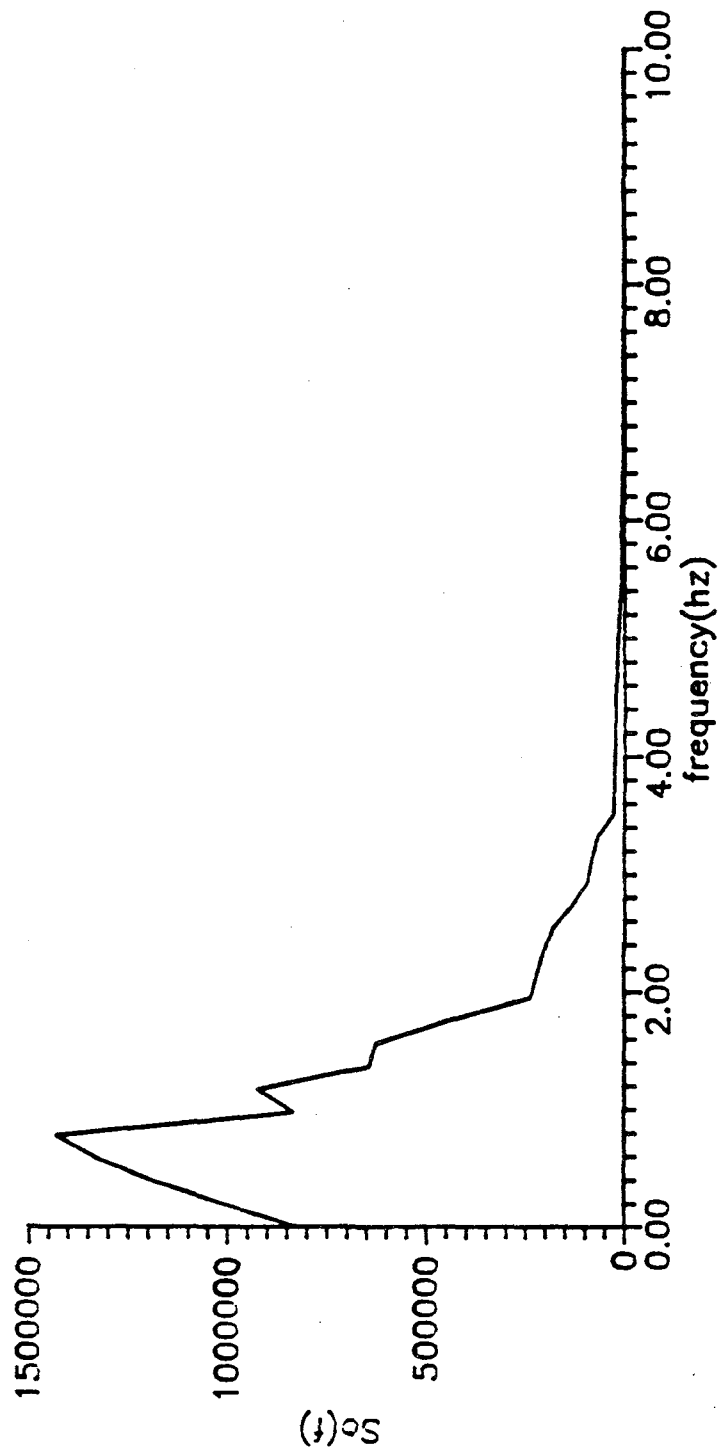


Fig.3.8 Averaged Power Spectral Density Function for Accelerations Recorded in EW Direction during Event 24 (Time Window 18-23sec)

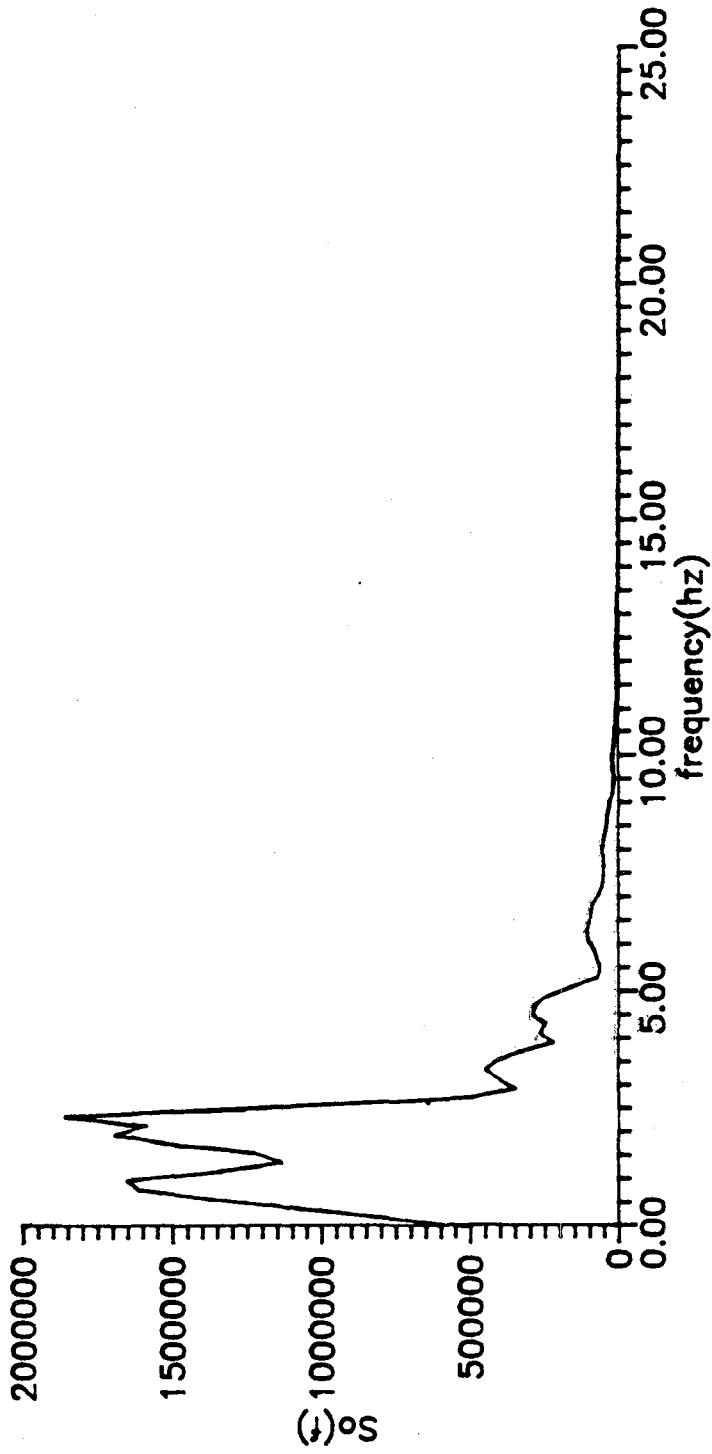


Fig.3.9 Averaged Power Spectral Density Function for Accelerations Recorded in EW Direction during Event 45 (Time Window 5-10sec)

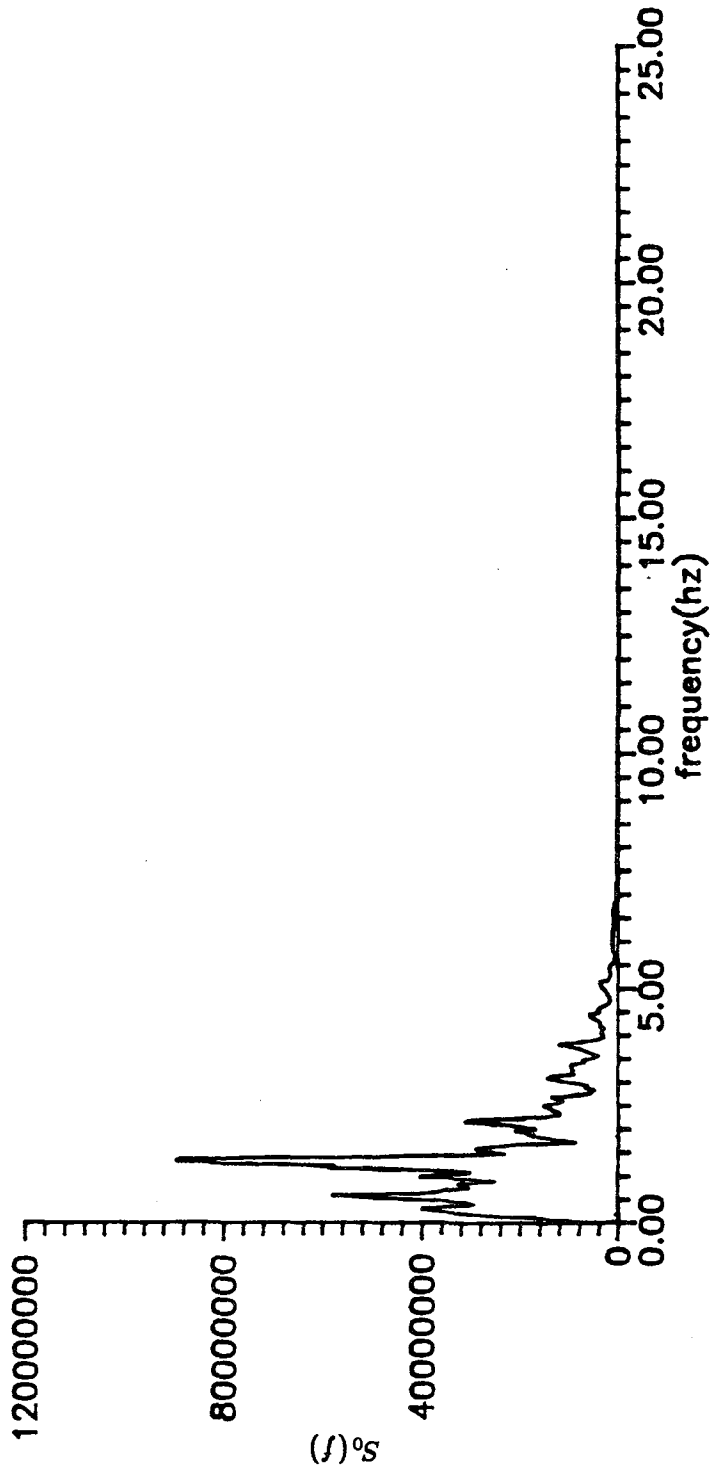


Fig.3.10 Averaged Power Spectral Density Function for Accelerations Recorded in EW Direction during Event 45 (Time Window 9-29sec)

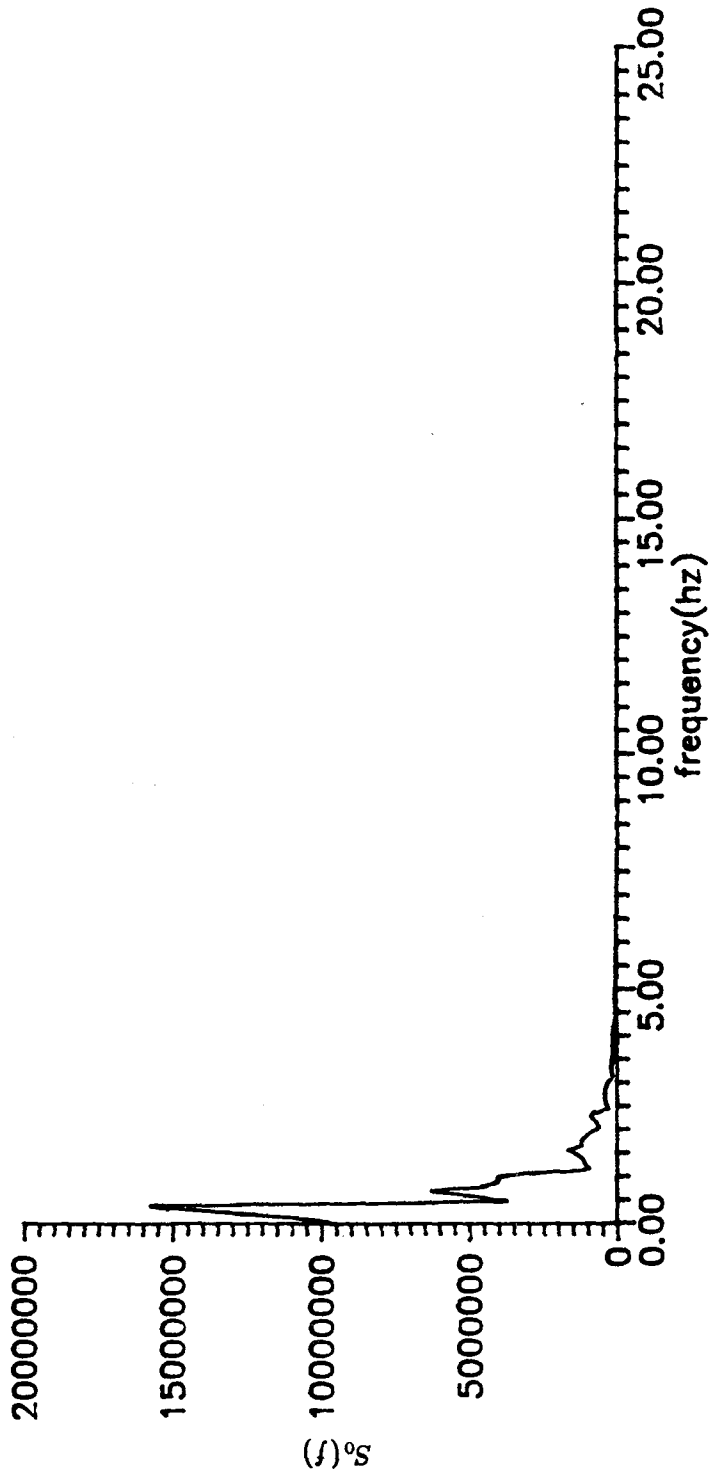


Fig.3.11 Averaged Power Spectral Density Function for Accelerations Recorded in EW Direction during Event 45 (Time Window 28-38sec)

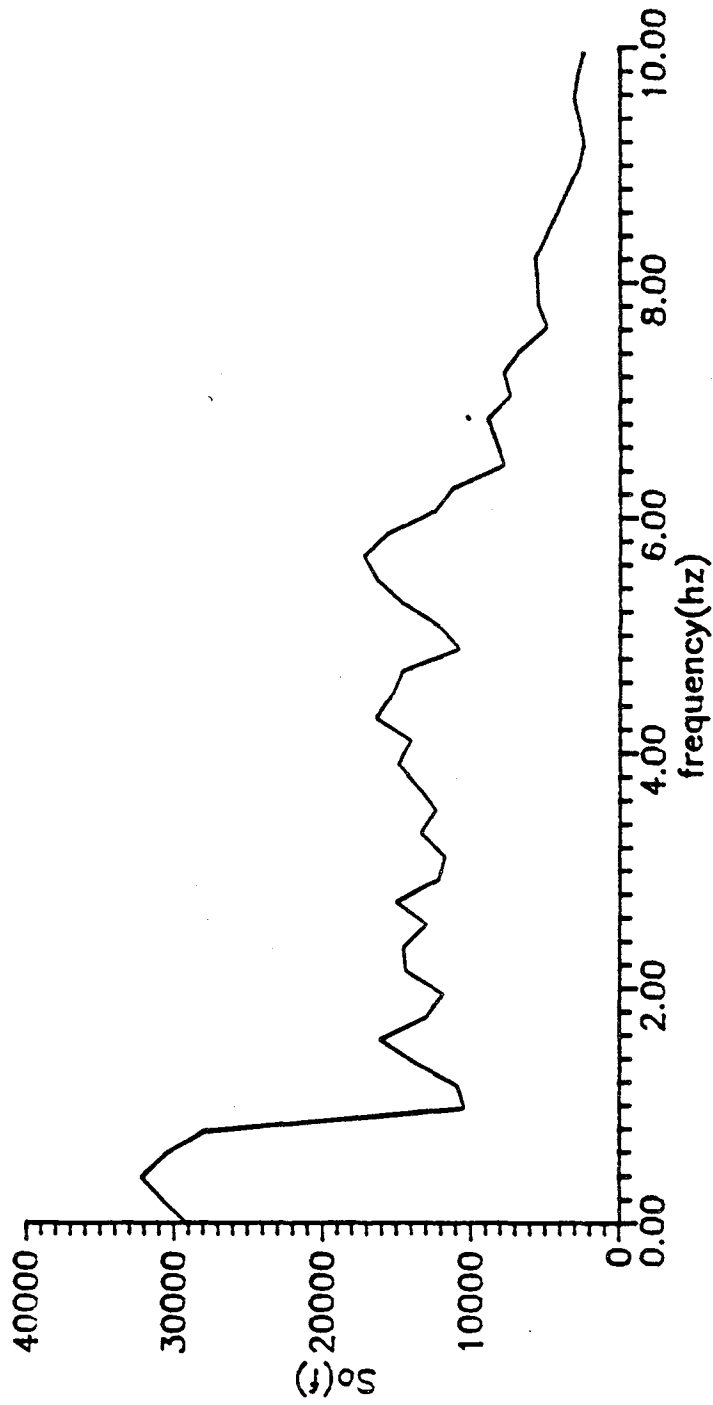


Fig.3.12 Averaged Power Spectral Density Function for Accelerations Recorded in Vertical Direction during Event 24 (Time Window 5-10sec)

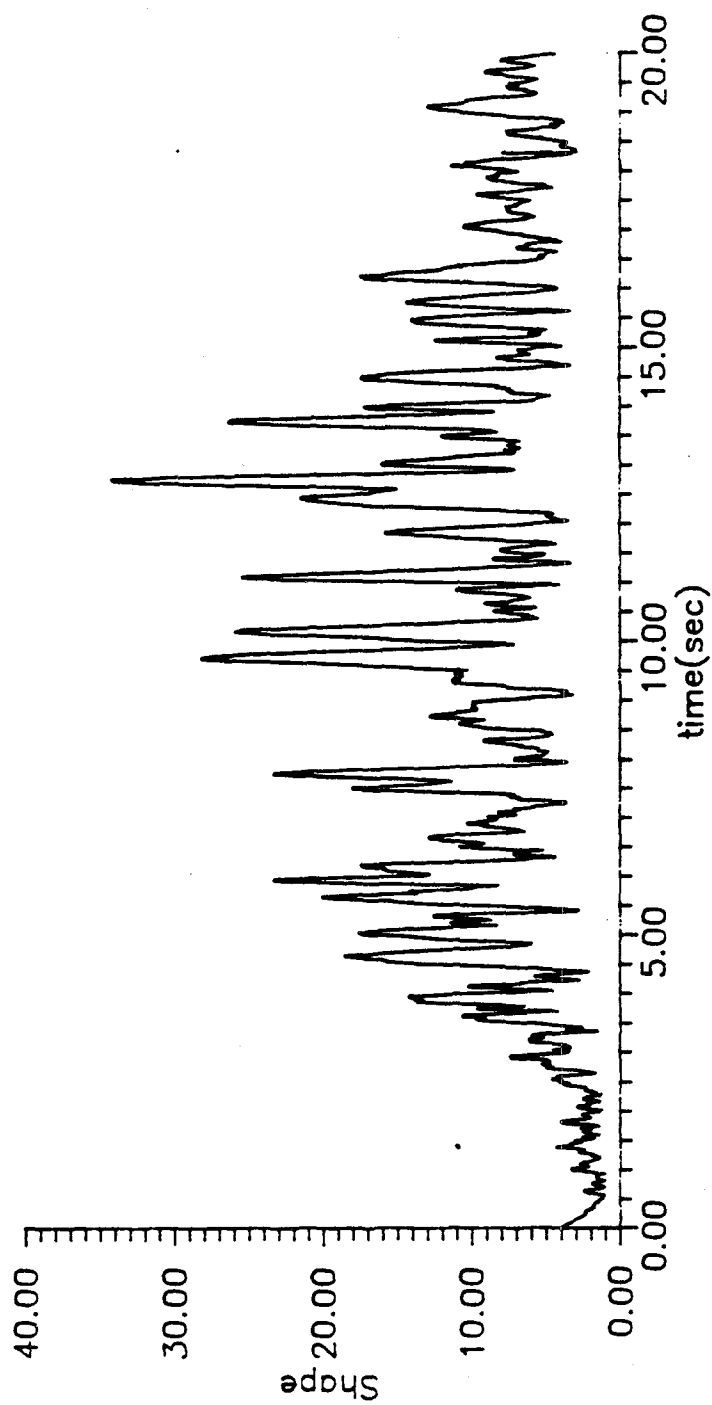


Fig.3.13 Averaged Envelope Function for Ground Motions
Recorded in EW Direction during Event 24

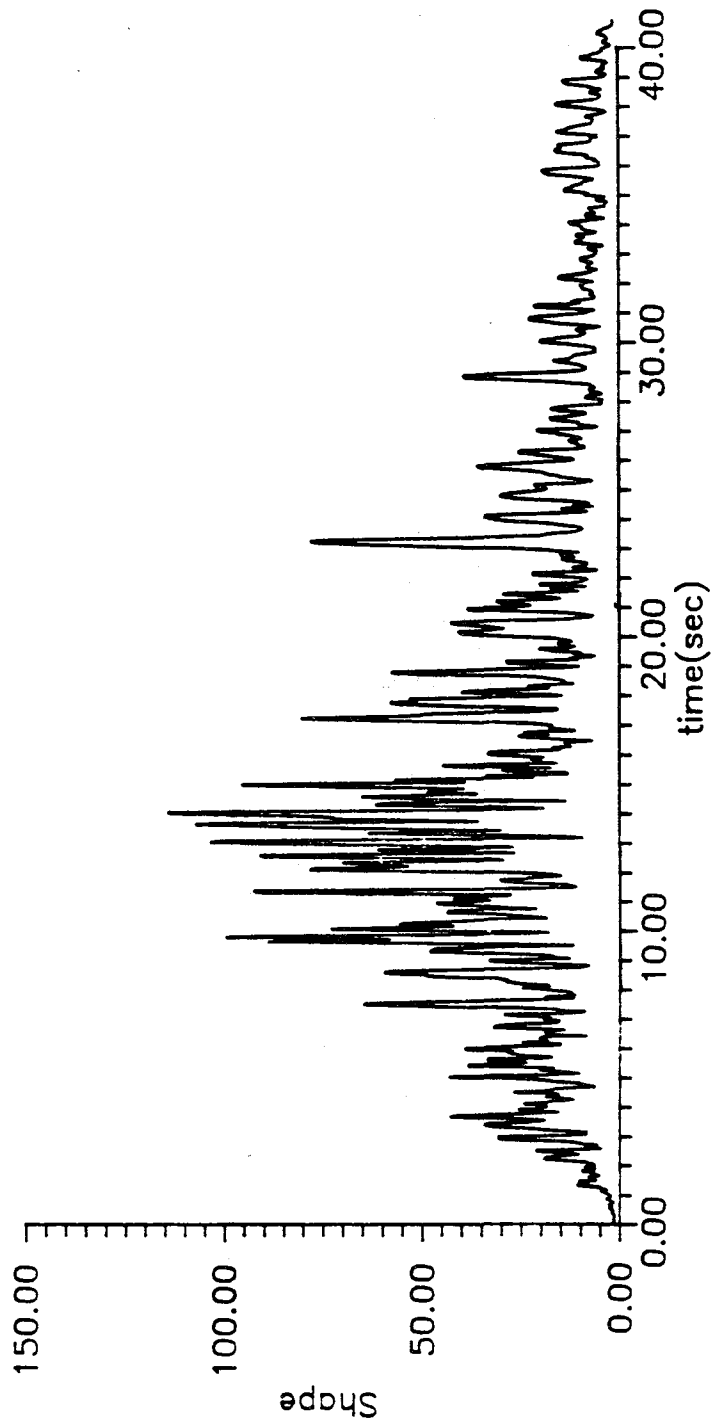


Fig.3.14 Averaged Envelope Function for Ground Motions
Recorded in EW Direction during Event 45

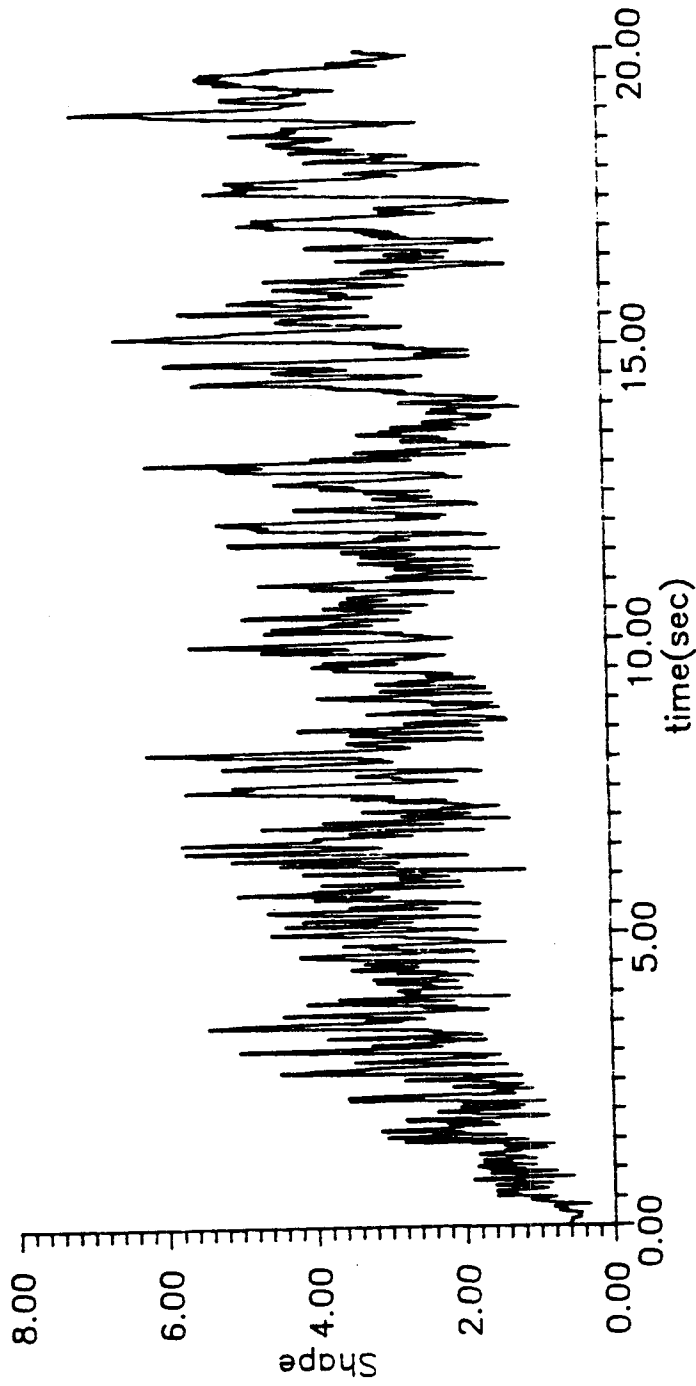


Fig.3.15 Averaged Envelope Function for Ground Motions
Recorded in Vertical Direction during Event 24

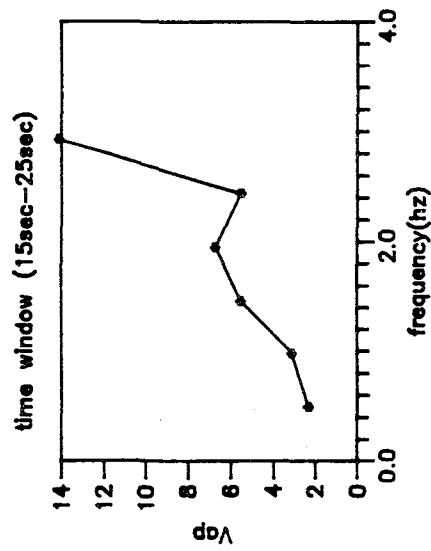
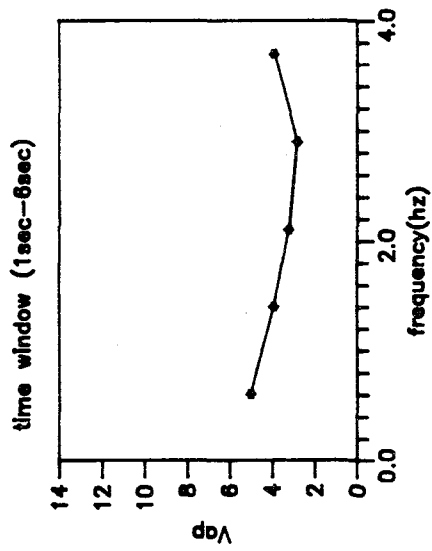
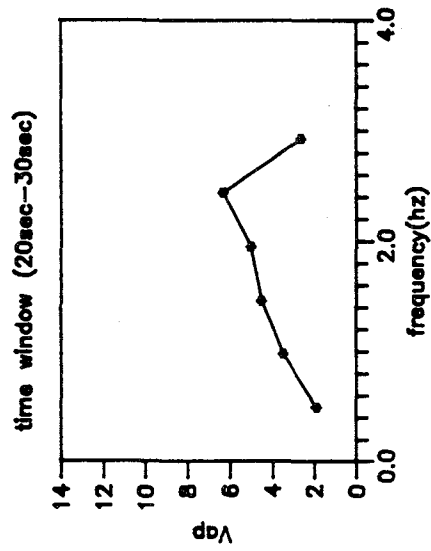
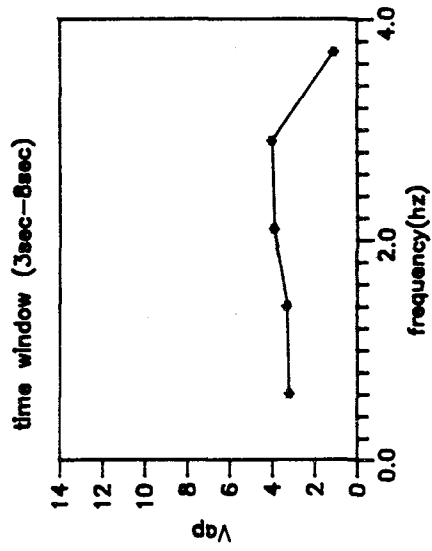
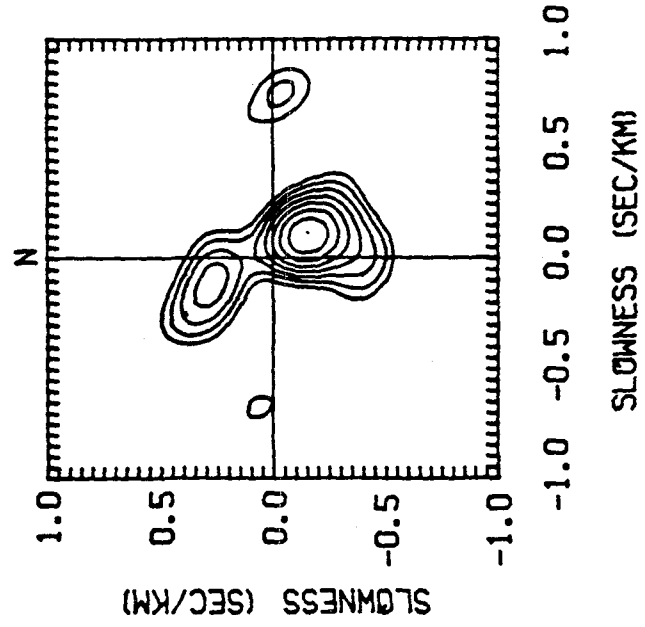


Fig.3.16 Example Apparent Velocities Calculated by F-K Method for Event 45

45 N 15-25 SEC 1.46 HZ
 AZIMUTH OF PEAK = 146
 APPARENT VELOCITY (km/sec) = 5.5
 MAXIMUM POWER (cm/sec)² = 2535



45 N 15-25 SEC 1.95 HZ
 AZIMUTH OF PEAK = 180
 APPARENT VELOCITY (km/sec) = 6.7
 MAXIMUM POWER (cm/sec)² = 2167

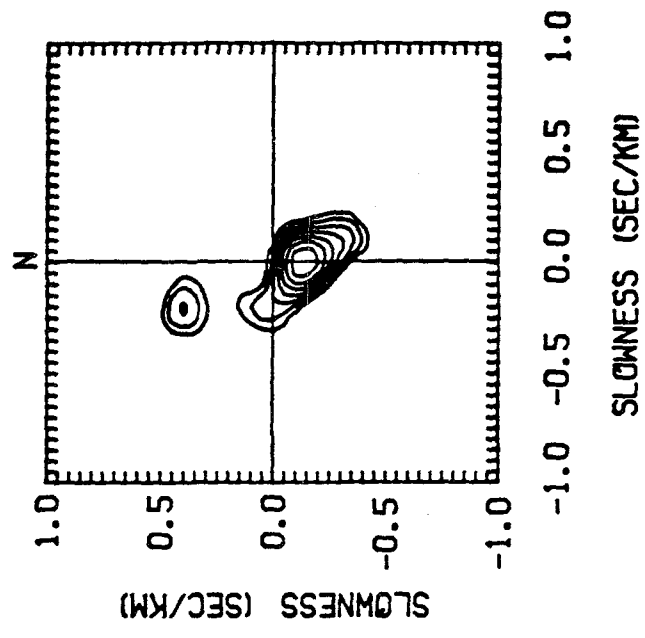


Fig.3.17 Example F-K Diagram for Accelerations Recorded during Event 45

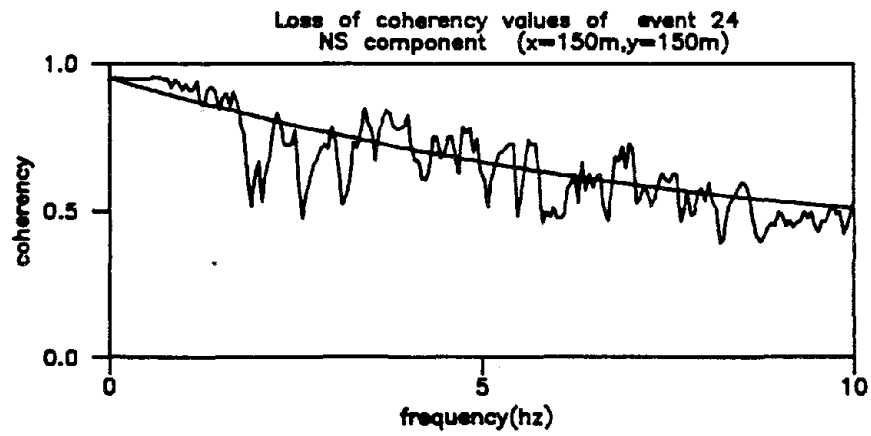
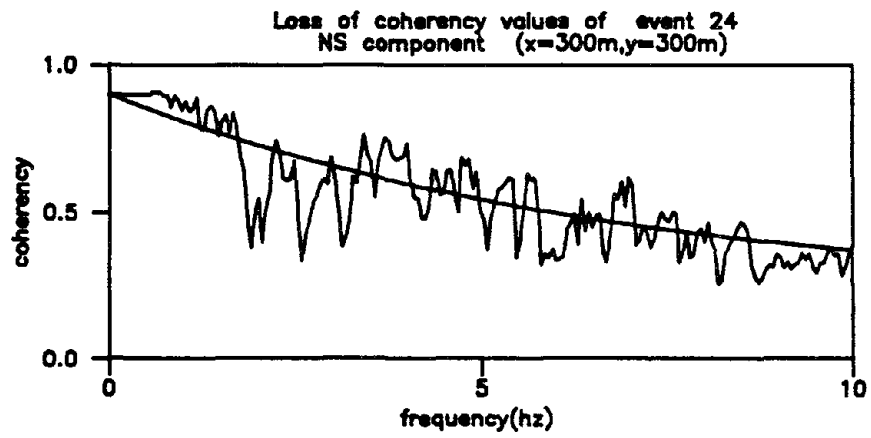
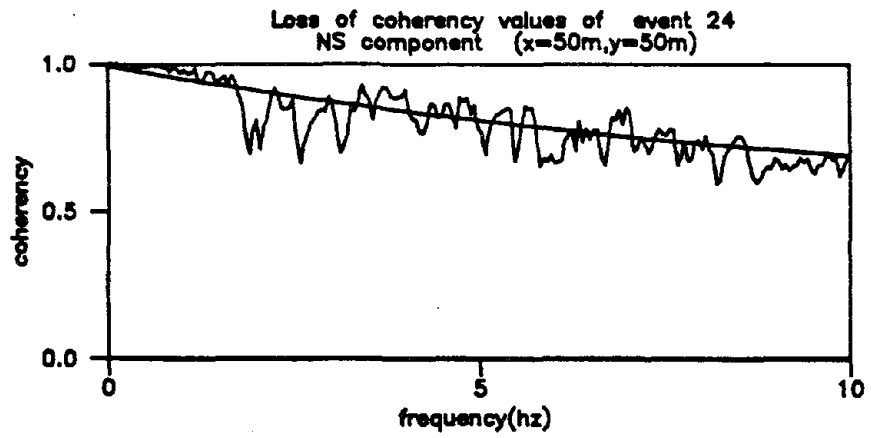


Fig.3.18 Comparison the Model Coherency Values with the Raw Data for Event 24

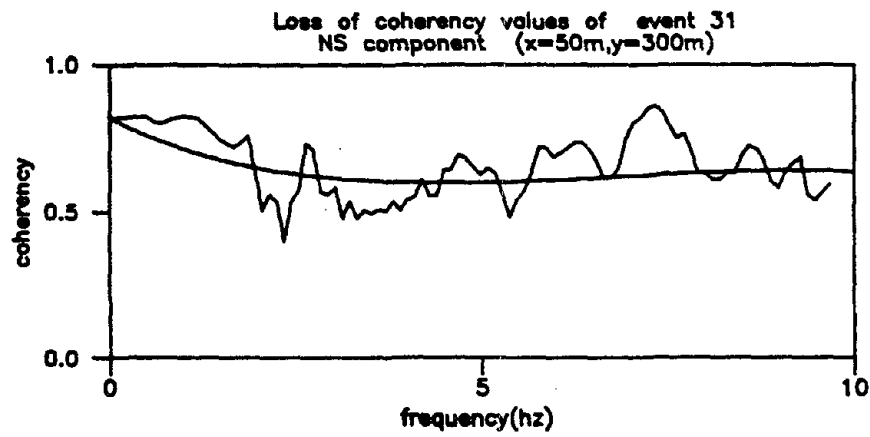
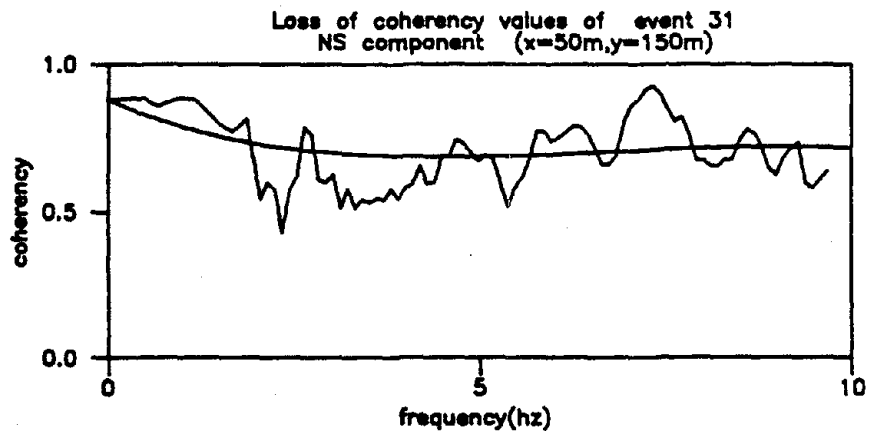
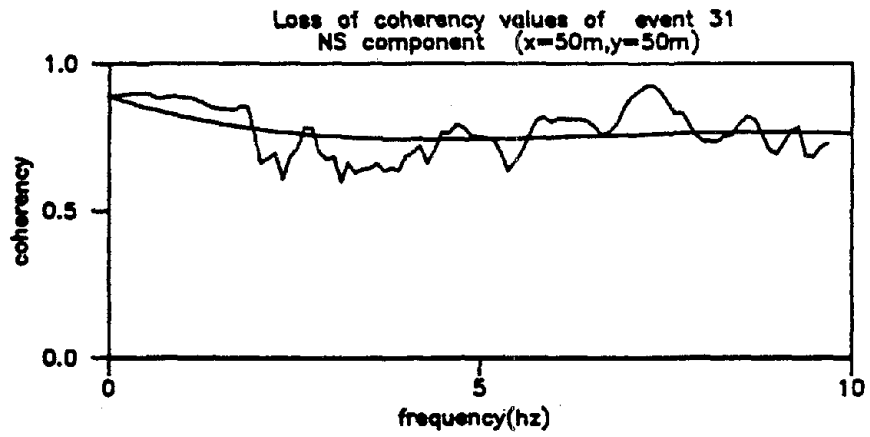


Fig.3.19 Comparison the Model Coherency Values with the Raw Data for Event 31

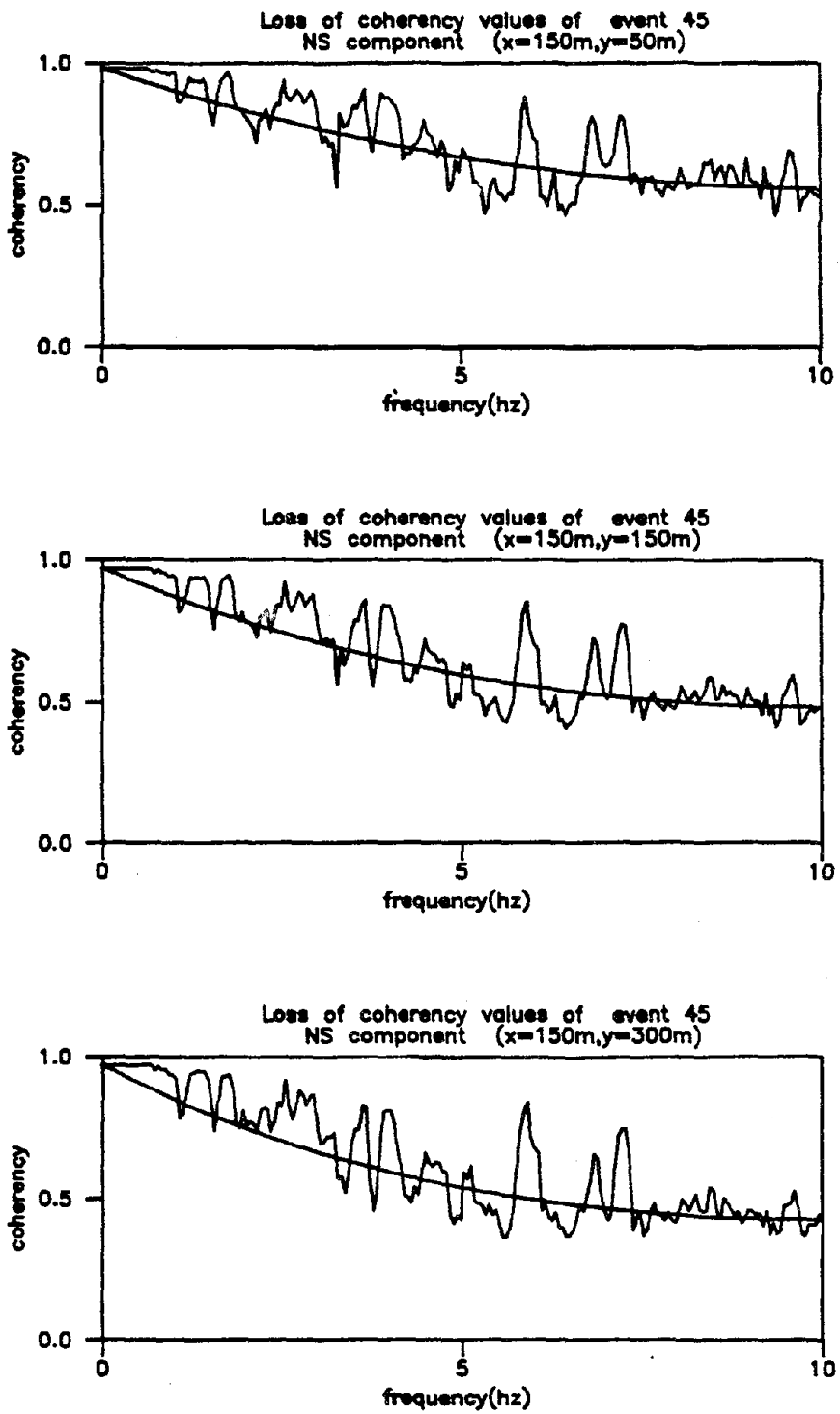


Fig.3.20 Comparison the Model Coherency Values with the Raw Data for Event 45

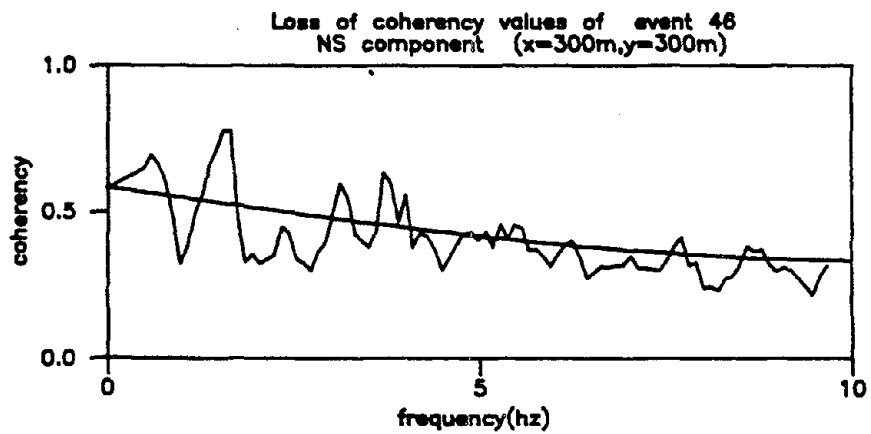
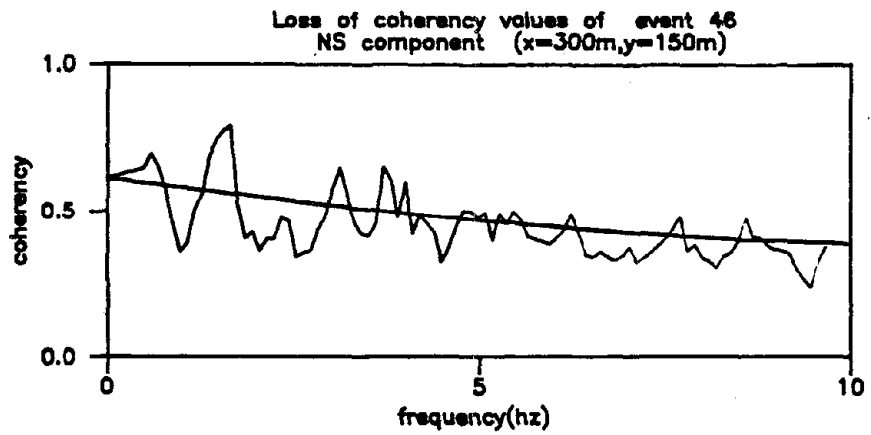
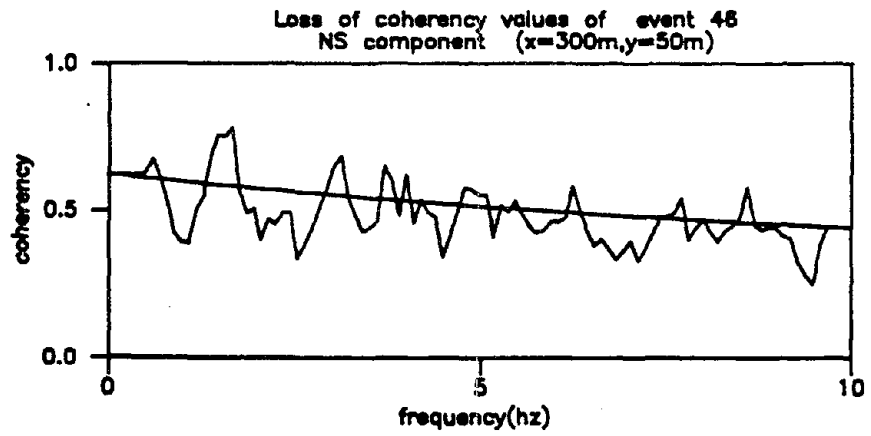


Fig.3.21 Comparison the Model Coherency Values with the Raw Data for Event 46

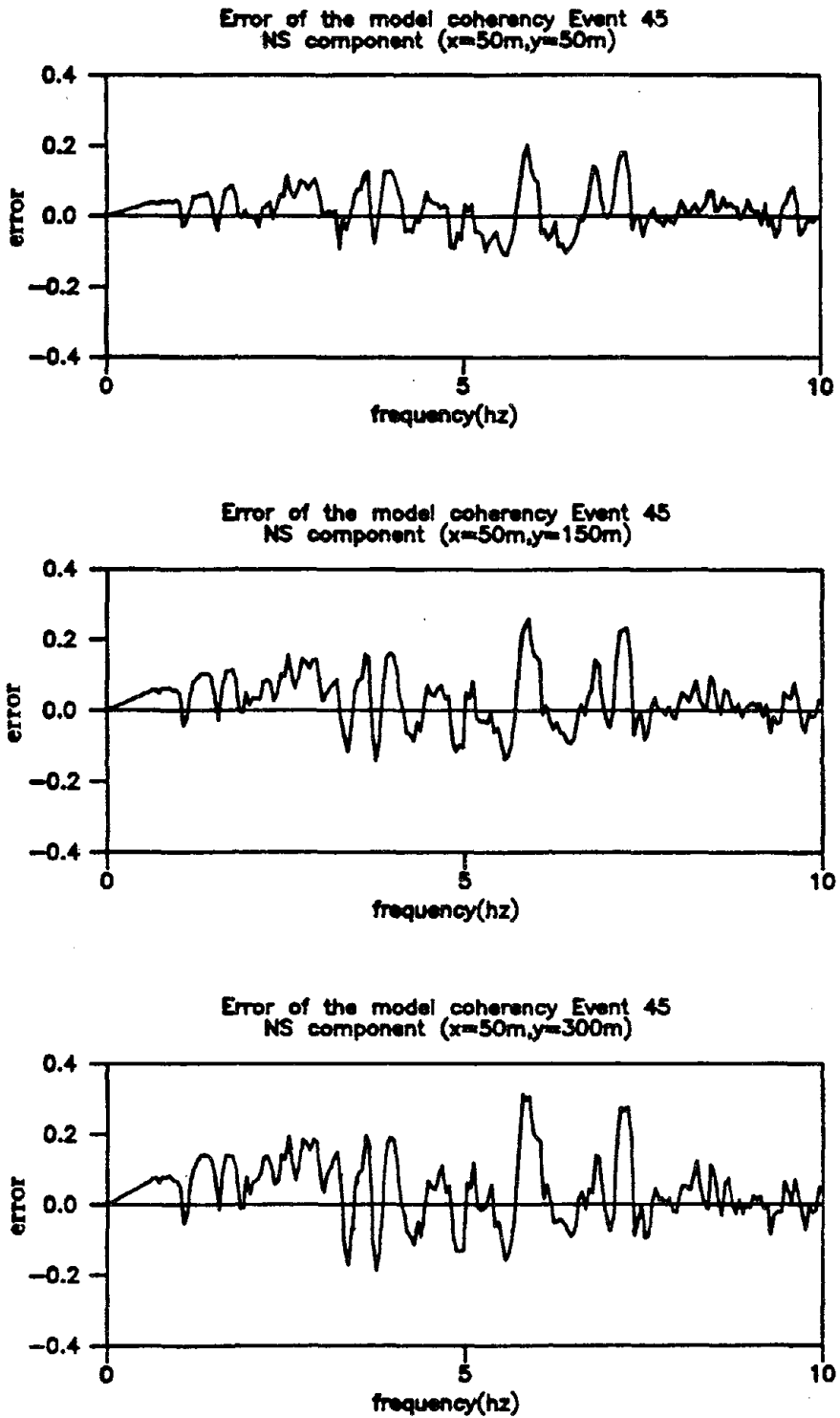


Fig.3.22 Errors of the Model Coherency Values with respect to the Raw Data of Event 45 for Different Distance Groups

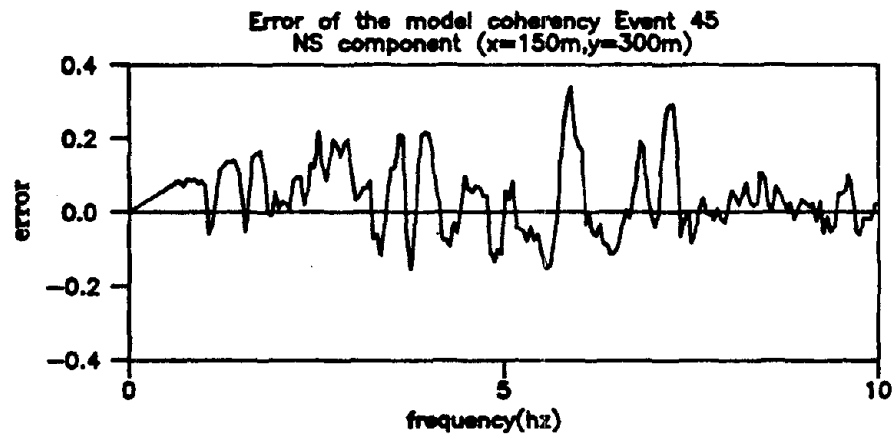
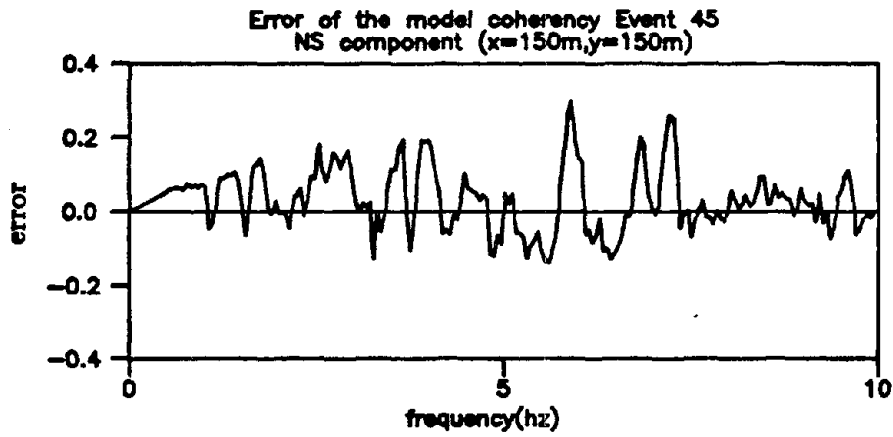
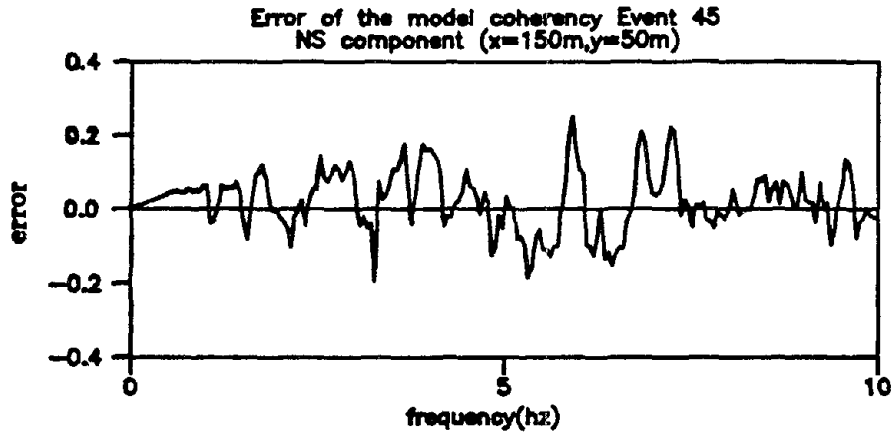


Fig.3.23 Errors of the Model Coherency Values with respect to the Raw Data of Event 45 for Different Distance Groups

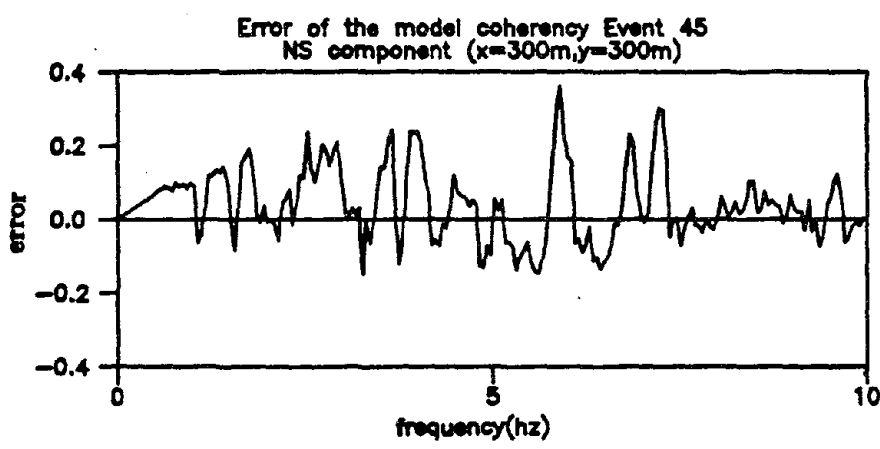
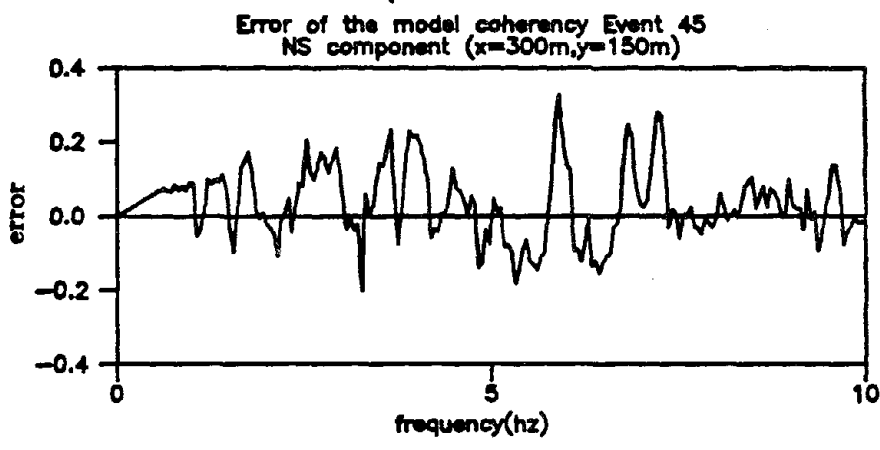
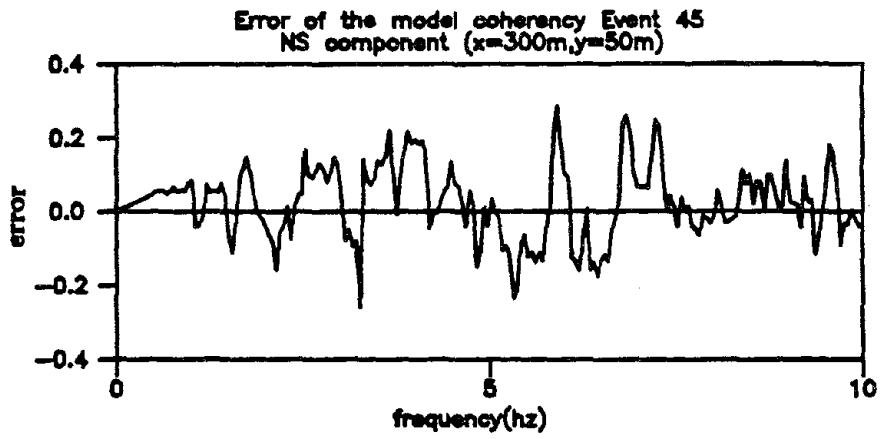


Fig.3.24 Errors of the Model Coherency Values with respect to the Raw Data of Event 45 for Different Distance Groups

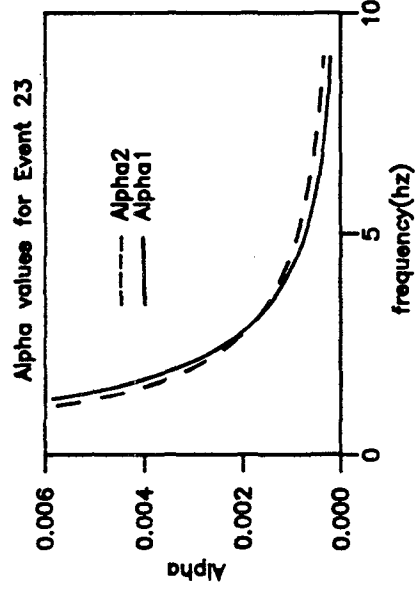
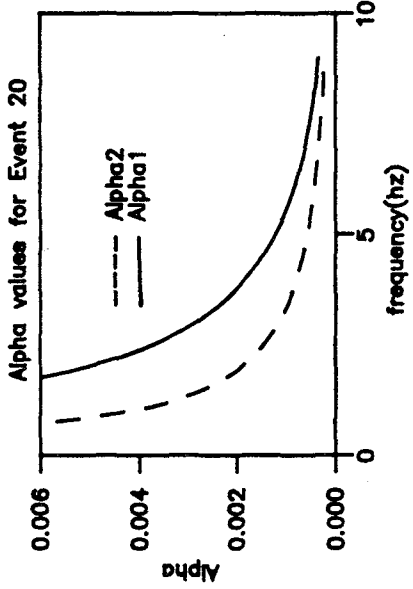
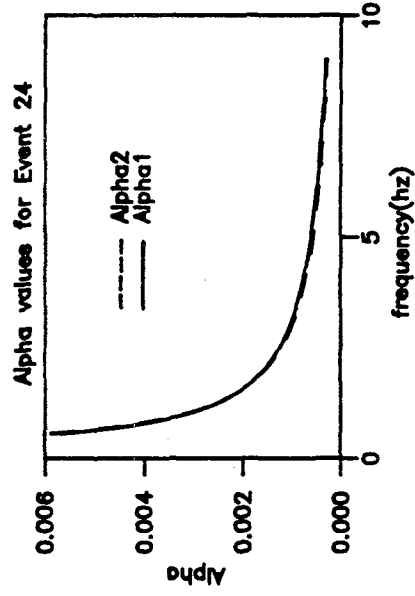
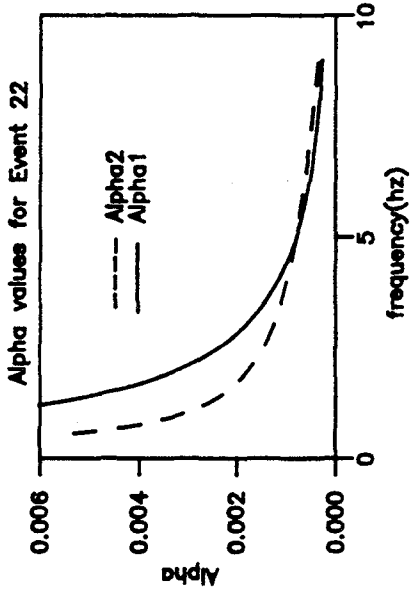


Fig.3.25 Model Values of the α Function in the Coherency Model for Different Events

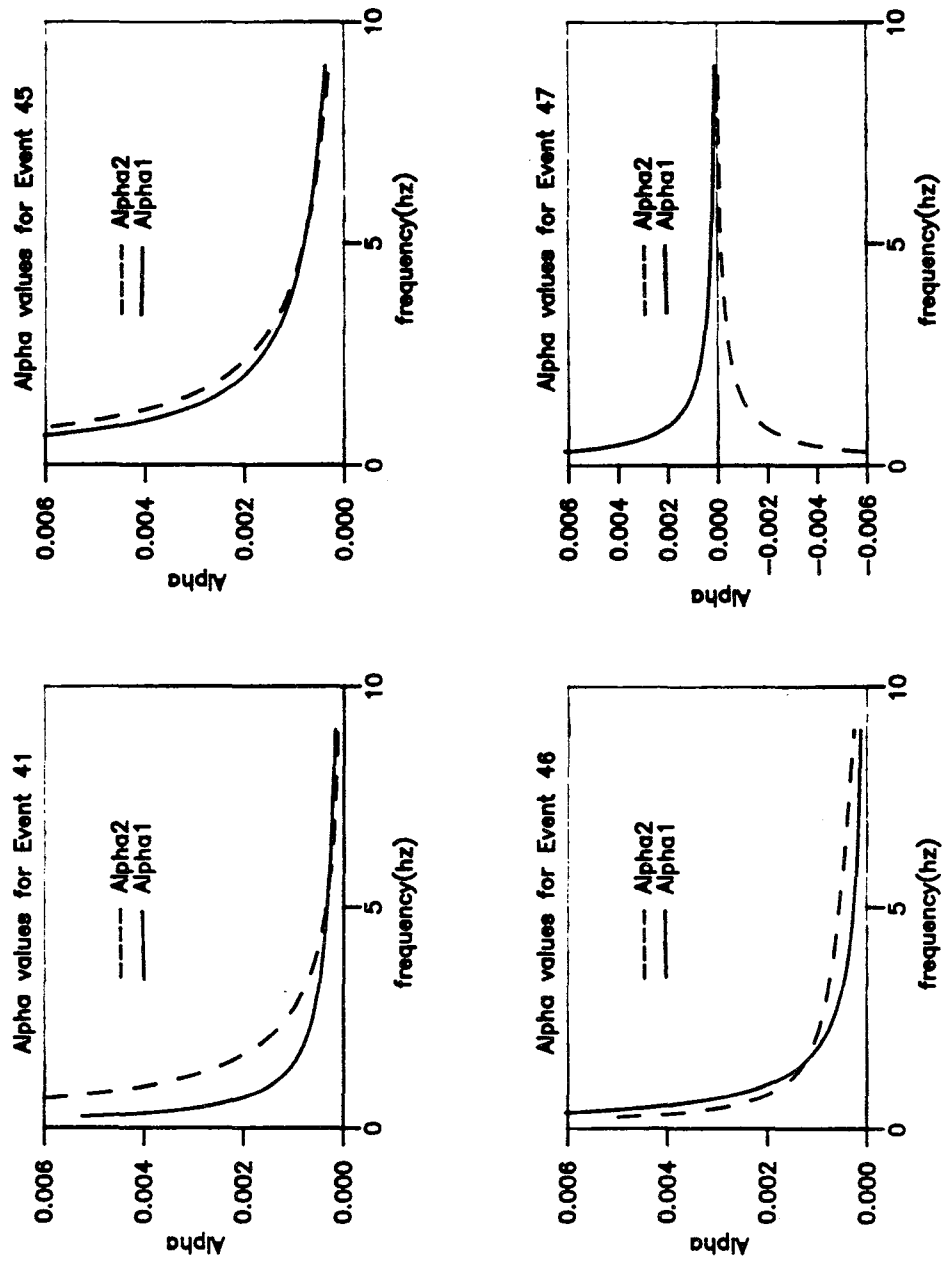


Fig.3.26 Model Values of the α Functions in the Coherency Model for Different Events

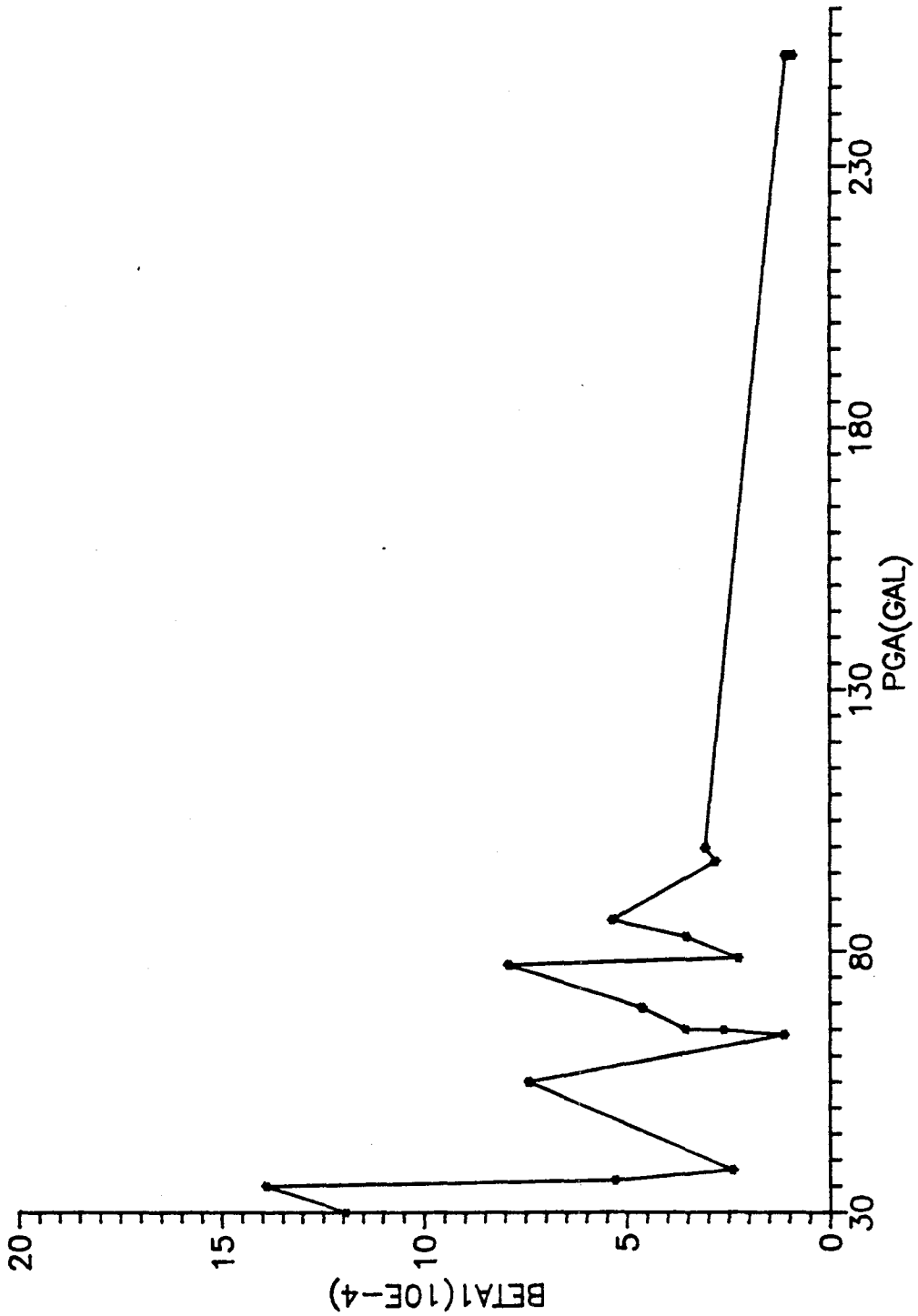


Fig.3.27 Calculated β_1 Values with respect to the PGA for the 17 Events

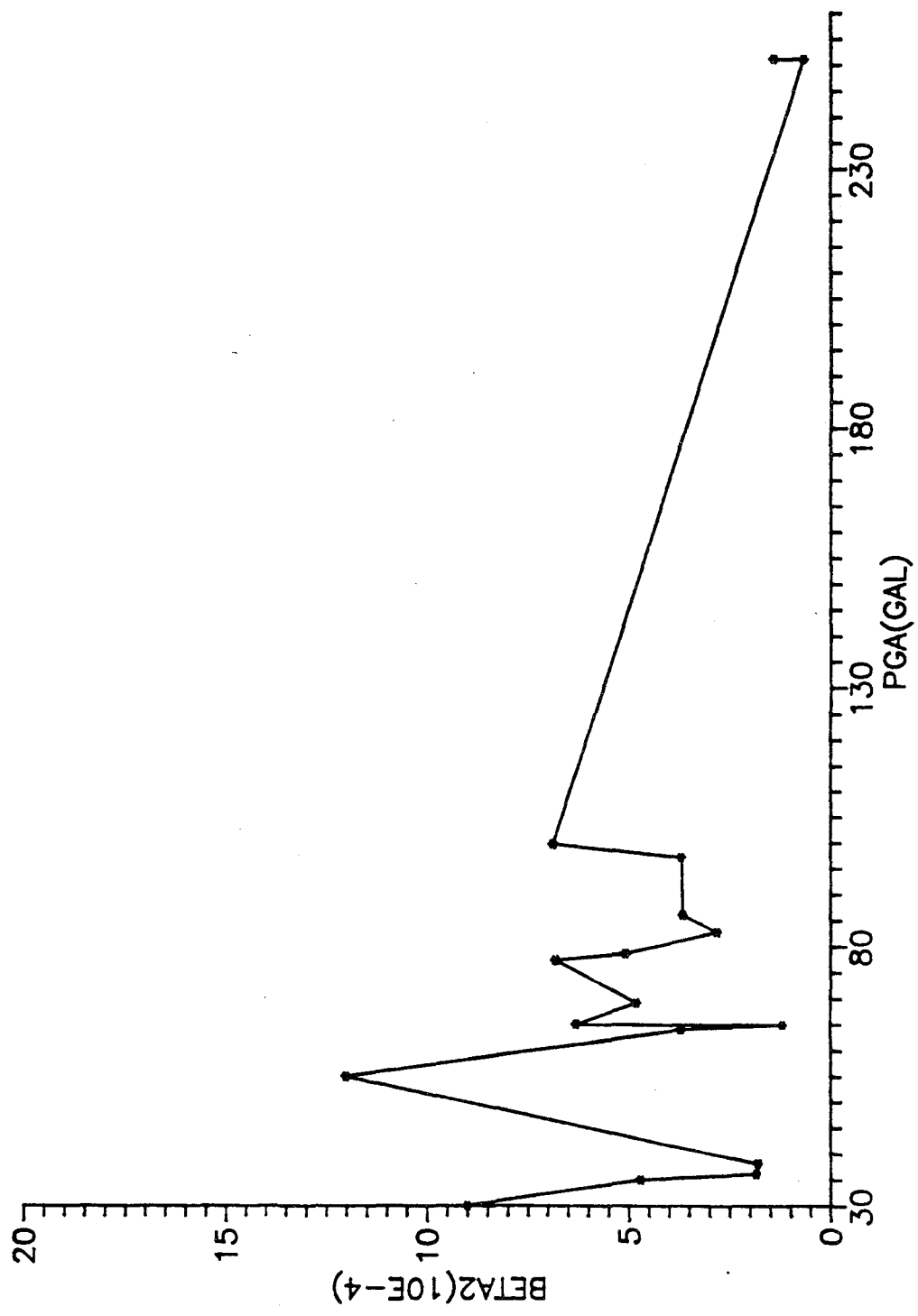


Fig.3.28 Calculated β_2 Values with respect to the PGA for the 17 Events

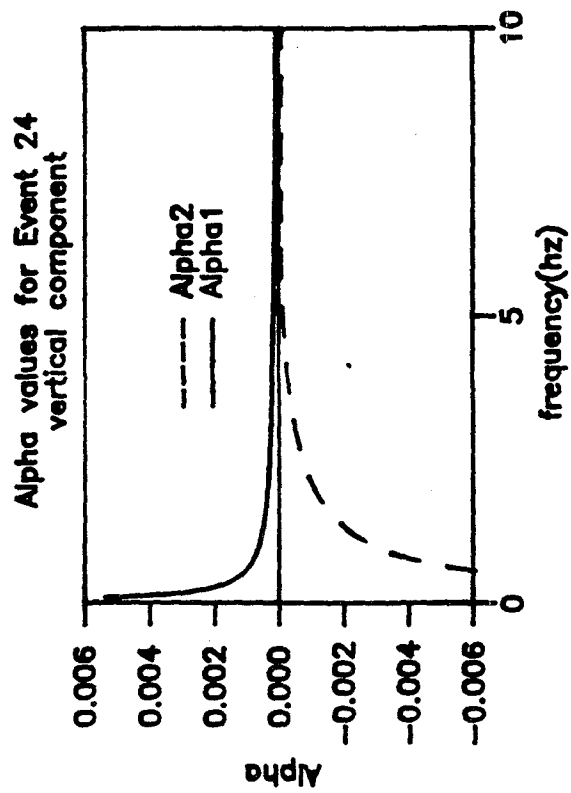
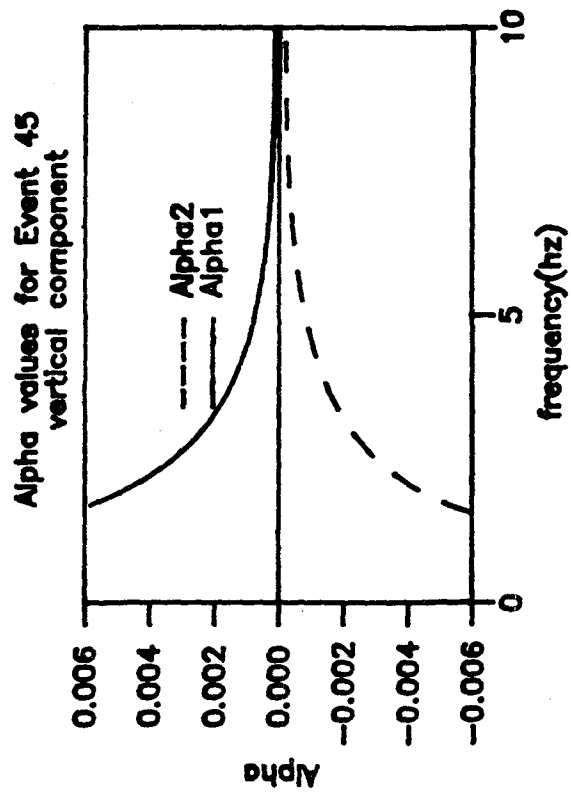


Fig.3.29 Model α Values for Ground Motions Recorded in the Vertical Direction during Events 24 and 45

CHAPTER 4 MULTIPLE STATION GROUND MOTION SIMULATION

In this chapter, some previously used methods of simulating earthquake ground motions are discussed, and a new method of simulating stationary or quasi-stationary motions, which are spatially correlated and response spectrum compatible, is presented.

4.1 Review of Previous Methods

Amin and Ang (1968), Ruiz and Penzien (1969), Penzien and Watabe (1975), Kubo and Penzien (1976) and many others have simulated components of ground acceleration using the non-stationary model

$$a_g(t) = \xi(t)x(t) \quad (4.1)$$

where $\xi(t)$ is an envelope function and $x(t)$ is a stationary random process having a specified power spectral density function. Both the envelope function and the power spectral density function were discussed previously in Chapter 3. The stationary process $x(t)$ can be obtained either in the time domain or in the frequency domain from the power spectral density functions (Hao, 1989).

Another way to simulate ground motions is to generate stationary motions using

$$x(t) = \sum_{i=1}^n A_i \cos(\bar{\omega}_i t + \phi_i) \quad (4.2)$$

where the A_i are specified amplitudes and the ϕ_i are random phase angles uniformly distributed over the range $[0, 2\pi]$. The A_i can be generated from a specified power spectral density function $S(\bar{\omega})$ using

$$A_i = \sqrt{4S(\bar{\omega}_i)\Delta\bar{\omega}} \quad (4.3)$$

where $\Delta\bar{\omega}$ is the frequency interval.

4.2 Ground Motion Simulation Criteria

When a ground motion time series is to be simulated for a given site, one should (Penzien, 1988), (1) investigate all possible active faults or tectonic regions in the area, (2) study the geological, seismological and geophysical conditions, (3) estimate the shortest source-to-site distance and probabilistically predict the maximum possible earthquake event, (4) set up an appropriate empirical attenuation law in order to determine the peak ground motions or response spectra at the site, and (5) establish an empirical ground motion duration law.

Ground motion accelerograms can be simulated only after their durations, peak values and response spectra have been specified. The peak values of ground motion are usually

determined by deterministic methods with least squares fitting of available data. Since the available data at different sites are different, the attenuation laws obtained by many authors vary from site to site; see Estera and Rosenblueth (1964), Milne and Davenport (1969), Joyner et al. (1981), Bolt and Abrahamson (1982), Peng et al. (1985), Watabe (1988).

Duration of ground motion also is a very important parameter since the overall response of lightly damped linear systems and yielding nonlinear systems depends significantly on the duration of shaking. Based on the different definitions and data studied, some empirical relations for duration have been obtained by different authors, such as Housner (1965), Estera and Rosenblueth (1964), Bolt (1973), Trifunac and Westermo (1976), Watabe and Tohdo (1982).

The response spectrum of the expected ground motion is another very important function to be specified. Newmark and Hall (1969) presented the idea of a design response spectrum which is now commonly used in aseismic design. Many empirical relations for the response spectrum have been obtained by different authors from studies of different data; see, for example, Wong and Trifunac (1979), Trifunac (1979), Kobayashi and Nagahashi (1977), and Watabe (1988).

4.3 Spatially Correlated Stationary Ground Motion Simulation

For structures having plan dimensions which are large compared with the wave length of significant earthquake ground motion, the out-of-phase effects in the multiple input motions play an important role in their overall dynamic response. Hence, realistic spatially correlated ground motions should be simulated for use as inputs to multiple supports.

Ground motions, obtained from the SMART-1 array, have been intensively studied for their correlation and coherency structures, see previous chapter. Using these models, spatially correlated multiple ground motion time-histories can be simulated using multiple random process theory. Every simulated time-history should be compatible with the prescribed power spectral density function, and each pair should have coherency values compatible with the prescribed cross coherency function. Assuming that earthquake ground motions are stationary random processes having zero mean values and known power spectral density functions and coherency functions, a series of spatially correlated ground motions can be simulated by means of the following method (Samaras et al. 1987):

Assume the ground motion time series has the same power spectral density function $S(\bar{\omega})$ ($-\bar{\omega}_N \leq \bar{\omega} \leq \bar{\omega}_N$, where $\bar{\omega}_N$ is the Nyquist frequency) at every station. This is a reasonable assumption when the epicentral distance is large compared with the site dimensions, as discussed in the previous chapter. The power spectral density function matrix in

the range $-\bar{\omega}_N \leq \bar{\omega} \leq \bar{\omega}_N$ can be expressed in terms of $S(\bar{\omega})$ and the coherency functions $\gamma_{ij}(i\bar{\omega}, d_{ij}^l, d_{ij}^t)$;

$$\hat{S}(\bar{\omega}) = \begin{pmatrix} 1 & \gamma_{12}(i\bar{\omega}, d_{12}^l, d_{12}^t) & \dots & \gamma_{1n}(i\bar{\omega}, d_{1n}^l, d_{1n}^t) \\ \gamma_{21}(i\bar{\omega}, d_{21}^l, d_{21}^t) & 1 & \dots & \gamma_{2n}(i\bar{\omega}, d_{2n}^l, d_{2n}^t) \\ \vdots & \vdots & \ddots & \vdots \\ \gamma_{n1}(i\bar{\omega}, d_{n1}^l, d_{n1}^t) & \gamma_{n2}(i\bar{\omega}, d_{n2}^l, d_{n2}^t) & \dots & 1 \end{pmatrix} S(\bar{\omega}) \quad (4.4)$$

where $\bar{\omega}$ is the circular frequency and n is the total number of points of input to the structure.

To simulate spatially correlated ground motions, samples of stationary random processes $x_1(t), x_2(t), \dots, x_n(t)$, which are compatible with the individual specified functions in $\hat{S}(\bar{\omega})$, are generated first. To do this, let

$$x_i(t) = \sum_{k=1}^i \sum_{l=1}^N A_{ik}(\bar{\omega}_l) \cos[\bar{\omega}_l t + \beta_{ik}(\bar{\omega}_l) + \phi_{kl}] \quad i = 1, 2, \dots, n \quad (4.5)$$

where amplitudes $A_{ik}(\bar{\omega}_l)$ and phase angles $\beta_{ik}(\bar{\omega}_l)$ are determined so that $x_i(t)$ is consistent with the given power spectral density function and coherency functions, ϕ_{kl} is a random phase angle uniformly distributed over the range 0 to 2π , N is the number corresponding to the Nyquist frequency $\bar{\omega}_N$. Note that ϕ_{kl} and ϕ_{rs} should be statistically independent unless $k = r$ and $l = s$.

Since the matrix $\hat{S}(\bar{\omega})$, given by Eq.(4.4), is Hermitian and positive definite, it can always be factored into a complex lower triangular matrix $\underline{L}(i\bar{\omega}_k)$ and its Hermitian matrix $\underline{L}^H(i\bar{\omega}_k)$ (see Gantmacher, 1977), as shown by

$$\hat{S}(\bar{\omega}) = \underline{L}(i\bar{\omega})\underline{L}^H(i\bar{\omega})S(\bar{\omega}) \quad (4.6)$$

where

$$\underline{L}(i\bar{\omega}) = \begin{pmatrix} l_{11}(i\bar{\omega}) & 0 & \dots & 0 \\ l_{21}(i\bar{\omega}) & l_{22}(i\bar{\omega}) & \dots & 0 \\ \vdots & \vdots & \ddots & \vdots \\ l_{n1}(i\bar{\omega}) & l_{n2}(i\bar{\omega}) & \dots & l_{nn}(i\bar{\omega}) \end{pmatrix} \quad (4.7)$$

and where l_{ij} ($i = 1, 2, \dots, n; j = 1, 2, \dots, i$) can be calculated by the Cholesky decomposition method (Atkinson, 1979), as given by

$$l_{ii}(\bar{\omega}) = [1 - \sum_{k=1}^{i-1} l_{ik}(i\bar{\omega})l_{ik}^*(i\bar{\omega})]^{1/2} \quad i = 1, 2, \dots, n \quad (4.8)$$

$$l_{ij}(i\bar{\omega}) = \frac{\gamma_{ij}(i\bar{\omega}) - \sum_{k=1}^{j-1} l_{ik}(i\bar{\omega})l_{jk}^*(i\bar{\omega})}{l_{jj}(\bar{\omega})} \quad j = 1, 2, \dots, i \quad (4.9)$$

For the case of $i \geq j$, the individual function in $\hat{S}(\bar{\omega})$ can be written as

$$\hat{S}_{ij}(i\bar{\omega}_k)\Delta\bar{\omega} = S(\bar{\omega}_k) \sum_{m=1}^j L_{im}(i\bar{\omega}_k)L_{jm}^*(i\bar{\omega}_k)\Delta\bar{\omega} \quad k = 1, 2, \dots, N \quad (4.10)$$

It can be shown that, see Hao (1989),

$$A_{ij}(\bar{\omega}_k) = \sqrt{4S(\bar{\omega}_k)\Delta\bar{\omega}} |l_{ij}(i\bar{\omega}_k)| \quad 0 \leq \bar{\omega}_k \leq \bar{\omega}_N \quad (4.11)$$

$$\beta_{ij}(\bar{\omega}_k) = \tan^{-1}\left(\frac{\text{Im}[l_{ij}(i\bar{\omega}_k)]}{\text{Re}[l_{ij}(i\bar{\omega}_k)]}\right) \quad 0 \leq \bar{\omega}_k \leq \bar{\omega}_N \quad (4.12)$$

Using Eqs.(4.5), (4.11), and (4.12), a set of spatially correlated time-histories $x_i(t)$ ($i = 1, 2, \dots, n$) can be simulated, and the corresponding ground motions $a_i(t)$ ($i = 1, 2, \dots, n$) can be obtained by multiplying each time-history by a proper shape function $\xi(t)$. By this procedure, one first simulates a time-history of motion for support point 1, and then, simulates a time-history for support point 2 by summing up wave contributions that are properly correlated with the simulated motion for point 1. Similarly, the simulated time-history for the motions of support point 3 will be correlated with those previously simulated for points 1 and 2, etc.. The first time-history of motion can be either a synthetic motion or a real motion provided that it is compatible with the prescribed spectral density matrix $\hat{S}(\bar{\omega})$.

Instead of using Eq.(4.5) to simulate $x_i(t)$, it also can be simulated more easily in the frequency domain. To proceed with this new approach, express the Fourier transform of $x_i(t)$ in the form

$$X_i(i\bar{\omega}_k) = \sum_{m=1}^i B_{im}(\bar{\omega}_k)[\cos\alpha_{im}(\bar{\omega}_k) + i\sin\alpha_{im}(\bar{\omega}_k)] \quad k = 1, 2, \dots, N \quad (4.13)$$

where $B_{im}(\bar{\omega}_k)$ is the amplitude at frequency $\bar{\omega}_k$, and $\alpha_{im}(\bar{\omega}_k)$ is the corresponding phase angle which is to be determined. By transforming Eq.(4.5) into the frequency domain, it can be shown that

$$B_{im}(\bar{\omega}_k) = \frac{1}{2}A_{im}(\bar{\omega}_k) \quad (4.14)$$

$$\alpha_{im}(\bar{\omega}_k) = \beta_{im}(\bar{\omega}_k) + \phi_{mk} \quad (4.15)$$

Then, by using Eqs.(4.13), (4.14), and (4.15), the Fourier transform $X_i(i\bar{\omega}_k)$ of $x_i(t)$ can be determined. The time-history $x_i(t)$ is then obtained by transforming $X_i(i\bar{\omega}_k)$ back to the time domain.

4.4 Spatially Correlated Quasi-Stationary Ground Motion Simulation

The simulation method presented above is based on stationarity assumptions of the ground motions even though the ground motions are actually nonstationary in both the time

and frequency domains. The ground motion nonstationary property in the frequency domain can be simulated by the quasi-stationary method. This method is based on a quasi-stationary assumption for the ground motion P-waves, S-waves and surface waves, as discussed in the previous chapter. The total ground motion time-history is divided into three time windows for different types of waves and the time-history in each window is assumed stationary and simulated independently. The total ground motion time-history is obtained by combining the time-histories in the three windows.

Combined with the method discussed above to simulate quasi-stationary ground motions, the simulation method for stationary ground motions is still applicable. The only new feature that needs to be studied is the combination. To combine the time-histories simulated by different power spectral density functions in the different time windows, certain overlapping of the different types of motion is needed; The transient part of the overlapping should be made as smooth as possible in order to reduce the false energy and overshooting that will be introduced by time-window cutting. The sum of the transient functions in the overlapping part should be equal to one in order to keep the proper ground motion intensity in that part. Several types of windows with different transient functions were tried for this purpose; e.g., the triangular, cosine bell, and exponential types shown in Fig. 4.1. It was found that, among the types tried, the exponential type produced the best results. As shown in Fig. 4.1, with the four times t_1 , t_2 , t_3 , and t_4 specified, the exponential window transient part used is $1 - e^{-(t-t_1)^2}$ on the left side and $e^{-(t-t_3)^2}$ on the right side.

4.5 Simulated Ground Motion Correction

Because of uncertainties regarding the initial conditions for the ground motion and the position of the zero acceleration axis in the recorded accelerogram, predictions of the corresponding velocity and displacement time-histories are unreliable unless realistic adjustments are made to account for these effects through baseline corrections to the accelerograms. The adjustments can be made in either the time domain or the frequency domain. Many criteria have been used to control the adjustments. The most common of these are: (1) zero mean acceleration, which implies the initial and ending velocity values are the same, (2) zero initial velocity, (3) zero initial displacement, (4) minimum mean square velocity, which implies minimizing the ground motion energy content, and (5) zero mean velocity which implies no permanent ground motion displacement.

Berg and Housner (1961) suggested the following method, based on the above criteria, for adjustments in the time domain. The acceleration null line is assumed to have the shape of a parabola which is determined by the method of least squares. The constants of the parabolic equation should minimize the computed mean square of the velocity. After this correction, both the acceleration and velocity terminate at the end of the motion. Using

the same criteria and the same second order parabolic null line assumption for acceleration, Kausel and Ushijima (1979) suggested a method of making adjustments in the frequency domain.

Another correction for the simulated ground motions is their response spectrum. Once a response spectrum has been specified for a given site, ground motion time-histories can be adjusted to be compatible with the specified spectrum. A method by Scanlan and Sachs (1974), that can be used for this purpose, is based on the fact that the Fourier spectrum of the ground acceleration time-history is equal to the velocity response spectrum for zero damping. The procedure is (1) to calculate the velocity response spectrum \hat{S}_v , (2) to calculate the ratio of \hat{S}_v to the specified response spectrum S_v , $\alpha = \frac{\hat{S}_v}{S_v}$, (3) to multiply the Fourier series of the time-history by α , and (4) to inverse FFT the result back to the time domain. The velocity response spectrum for this corrected motion can be evaluated and the above procedure repeated. Through this iterative procedure, an accelerogram compatible with the spectrum is obtained. Usually, only 3 iterations are needed to make \hat{S}_v converge to a satisfactory result.

4.6 Ground Motion Time-History Interpolation

When multiple inputs are specified for large structures, spatially correlated ground motion time-histories at all structure-foundation contact points are needed. If the number of contact points is large, the simulation of these motions becomes expensive. Therefore, an interpolation method is suggested here to reduce costs. By this method, ground motion time-histories are simulated at a limited number of support points, and at all other points, the ground motion time-histories are interpolated in the frequency domain by adjusting phase angles and amplitudes to provide the proper cross correlations and power spectral contents.

The interpolation function used is derived using the shape function idea. Consider the one-dimensional case shown in Fig. 4.2, where x_1 , x_2 and x_3 are the points where the ground motion time-histories are to be simulated, and x_k is an arbitrary point where the ground motion time-history is to be interpolated. The interpolation function for the one-dimensional case is

$$f_{jk} = \frac{\prod_{\substack{i=1 \\ i \neq j}}^n (x_k - x_i)}{\prod_{\substack{i=1 \\ i \neq j}}^n (x_j - x_i)} \quad j = 1, 2, \dots, m \quad (4.16)$$

where m is the total number of points at which the ground motion time-histories are simulated, n is the total number of structure-foundation contact points, x_i , x_j and x_k are the corresponding coordinates, f_{jk} is the interpolation function representing the contribution to the ground motion at point k from the ground motion at point j . For the two-dimensional

case, see Fig. 4.2, the interpolation function is

$$f_{jk} = \frac{\prod_{\substack{i=1 \\ i \neq j}}^n [y_k - f_k(i, i+1)]}{\prod_{\substack{i=1 \\ i \neq j}}^n [y_j - f_j(i, i+1)]} \quad j = 1, 2, \dots, m \quad (4.17)$$

where y_j, y_k are the corresponding coordinates, and $f_k(i, i+1)$ is the value on the line connecting points i and $i+1$ at x_k ; in general;

$$f_k(i, i+1) = \frac{y_{i+1} - y_i}{x_{i+1} - x_i} (x_k - x_i) + y_i \quad (4.18)$$

If $x_i = x_{i+1}$ or $y_i = y_{i+1}$, Eq.(4.18) becomes $f_k(i, i+1) = x_i$ or $f_k(i, i+1) = y_i$, respectively.

Using the above interpolation functions, the ground motion time-history at any support point can be interpolated using the time-histories simulated at the control points. The ground motion time-history at point k is interpolated in the frequency domain using

$$\bar{A}_k(i\bar{\omega}) = \sum_{j=1}^n f_{jk} A_j(i\bar{\omega}) \left[\cos\left(\phi_j - \frac{d_{jk}^i \bar{\omega}}{v(\bar{\omega})}\right) + i \sin\left(\phi_j - \frac{d_{jk}^i \bar{\omega}}{v(\bar{\omega})}\right) \right] \quad (4.19)$$

where $\bar{A}_k(i\bar{\omega})$ is the Fourier transform of $a_k(t)$ at frequency $\bar{\omega}$; $A_j(i\bar{\omega})$ is the amplitude of the time-history $a_j(t)$ at point j at frequency $\bar{\omega}$; ϕ_j is the phase angle of $a_j(t)$ at $\bar{\omega}$; d_{jk}^i is the projected distance between points j and k in the wave propagation direction, and $v(\bar{\omega})$ is the apparent velocity at $\bar{\omega}$. It can be shown that the interpolated time-history $a_k(t)$ will have the correct phase differences and cross correlations.

An example interpolation for the one-dimensional case was calculated using three stations located 25m apart in the direction of wave propagation. The ground motion time-histories at the two end points, 0m and 50m, were simulated by using the coherency model, Eq.(3.9), three segments of quasi-stationary motion having power spectral densities of the Tajimi-Kanai type. All coherency and power spectral density function parameters were based on those obtained for the NS components recorded during Event 45; see chapter 3. The apparent velocity was arbitrarily assigned the low value of 35m/sec in order to see the cross correlation values more clearly. Figure 4.3 shows the simulated acceleration time-histories after iteration to be compatible with the Newmark and Hall (1969) response spectrum normalized to 0.3g PGA, where a_1 and a_2 are simulated at 0m and 50m, respectively, and a_3 is interpolated at 25m. Figures 4.4 and 4.5 show the cross correlations of the three time-histories before and after the response spectrum compatible iterations. It is obvious that the cross correlation values are compatible with the prescribed wave propagation property. Also it can be seen that the cross correlation values remain almost the same, and the phase difference

exactly the same before and after the iterations. This is because the iteration procedure only works on the Fourier amplitudes, not on the phase angles. Figures 4.6 through 4.8 show the loss of coherency values between the three time histories. Figures 4.9 and 4.10 show the power spectral density functions of the three time histories. From these results, it can be seen that the interpolated time-history satisfies the prescribed cross correlation structure and the power spectral density function.

4.7 Examples

Using the method discussed above and the coherency model presented in the previous chapter, realistic examples of spatially correlated ground motion time-histories were simulated giving the following results:

Spatially correlated stationary ground motion time-histories were simulated at four stations along an epicentral direction separated 100m from one another ($x=0; 100; 200; 300m$). These time-histories with 20sec duration and $\Delta t = 0.02sec$ were simulated using the following specifications:

- (a) The stationarity assumption was used with the Tajimi-Kanai (1960) power spectral density function, Eq.(3.1) having parameters $\xi_g = 0.6$ and $\omega_g = 5\pi rad/sec$, and with $S_0 = 1.0$.
- (b) The Harichandran and Vanmarcke (1984) coherency model was used with parameters $A = 0.736$, $\alpha = 0.147$, and a spatial scale of fluctuation $\theta(\bar{\omega}) = 3300[1 + (\frac{\bar{\omega}}{1.5\pi})^2]^{-\frac{1}{2}}$. The apparent wave velocity used was $v = 2.5km/sec$.
- (c) The shape function, Eq.(3.5), suggested by Amin and Ang (1968) was used with $t_1 = 2sec$, $t_2 = 10sec$ and $I_0 = 1.0$.
- (d) The baseline correction was carried out by first filtering out the energy for $f \leq 0.5hz$, and then using the time domain baseline correction method.
- (e) The Newmark and Hall (1969) 5% damped design response spectrum, normalized to a 0.5g PGA, was used.

The four simulated ground motion time-histories are shown in Figs. 4.11 through 4.13, expressed in terms of acceleration, velocity, and displacement, respectively. Figures 4.14 and 4.15 show the auto and cross correlation coefficients of the four time-histories, respectively. From the cross correlation coefficients, it can be noticed that the proper phase differences occur between the four simulated time-histories. Figure 4.16 shows comparisons between the power spectral density functions of the simulated ground motions before the iterations to be compatible with the response spectrum and the prescribed Tajimi-Kanai power spectral density function. It can be seen that they match well, except for the apparent discrepancy

of high values in the low frequency portion of the spectrum at $x = 300m$, which can be attributed to the random nature of the process. Figure 4.17 compares the loss of coherency values with the prescribed model. It can be seen that at $\Delta x = 300m$, as the frequency increases, the compatibility is not very good. This is because the calculated loss of coherency values were not smoothed, and as the distance increases, the coherency values will be lower, so that the noise will tend to be more dominant in the calculated values since the noise level is increasing with frequency; the level is 0.35 at 1Hz and 0.45 at 10Hz; see chapter 3. Figure 4.18 shows the calculated response spectra after two iterations compared with the prescribed Newmark and Hall design response spectrum.

Another example considered was the simulation of spatially correlated ground motions at each corner of a 20m rectangular foundation. The ground motions were simulated for the x , y and z directions. Suppose a wave propagates in a 45° direction to the foundation. Then, in terms of the distances d_{ij}^t and d_{ij}^b as defined before, the coordinates of the corner points are $(0, 0)$, $(14.14, 14.14)$, $(28.28, 0)$, and $(14.14, -14.14)$, respectively. The ground motions were first simulated in the wave propagating direction, transverse to the wave propagating direction, and the vertical direction, independently. Because the wave propagating direction generally coincides with the principal direction, the ground motions in that direction are uncorrelated with the ground motions in its transverse direction, likewise, the vertical component of ground motion is independent of the ground motions in the horizontal directions. The ground motions in the x and y components were obtained by rotating the horizontal ground motions to these directions. The simulated ground motions satisfy the following specifications:

- (a) A quasi-stationarity assumption was used for all three components. The time window width and the parameters used for the Tajimi-Kanai power spectral density functions were those obtained by processing SMART-1 data for Event 45; see Tables 3.3 and 3.4. The power spectral density functions were all normalized using $S_0 = 1.0$. The corresponding scaling factors in Table 3.4 were then applied.
- (b) The suggested coherency model, Eq.(3.9), was used with the results obtained for Event 45 as shown in Table 3.6 and Table 3.7.
- (c) The same shape function, Eq.(3.4), with the results obtained for Event 45, was used with the parameters in Table 3.5.
- (d) The same baseline correction procedure was used as in the previous example. The Newmark and Hall design response spectra with damping ratio 0.05 normalized to 0.5g PGA for horizontal components and 0.3g PGA for the vertical component were used as the target response spectra.

Figures 4.19 through 4.21 show the simulated accelerations for x , y , and z components, respectively. Figures 4.22 through 4.24 show the corresponding displacements. From these results, it can be noticed that the cross correlations of the components were well controlled. The two horizontal components are independent of the vertical component which has the highest frequency content and lowest intensity. These results all coincide with the observed ground motion records. Figures 4.25 through 4.27 show the comparisons between the calculated response spectra and the target response spectrum. Good results were obtained after two iterations. It can be seen that the convergence is very good.

A final example was generated to illustrate the interpolation problem. Assume there is a 50m rectangular foundation. The ground motion time-histories were simulated at the four corner points with coordinates (0,0), (50,0), (50,50), (0,50). Five ground motion time-histories at (25,0), (50,25), (25,50), (0,25), and (25,25) were obtained by interpolation. Suppose the wave comes in the x direction. The four simulated ground motions all satisfy the specifications of Event 45 as given in the previous example for power spectral density functions, coherency, and shape functions. The baseline correction procedure used was the same as in the previous example. The Newmark and Hall design response spectrum for 5% damping ratio normalized to the 0.3g PGA level was used again as the target spectrum. Note that, in order to save computing time, the interpolation procedure should be carried out after the iterations. Following this procedure, the response spectra can be interpolated the same way as the time histories. If the response spectra are the same for all interpolated time histories, the response spectrum of the interpolated time-history will still be compatible with the target response spectrum since the interpolating procedure actually works on the amplitudes and phase angles independently while the response spectrum is controlled by the amplitudes. Figure 4.28 shows the accelerograms in the x direction before iterations. Figure 4.29 shows the accelerograms after 3 iterations. Figure 4.30 shows the displacements after 3 iterations. From these figures, it can be concluded that the ground motion properties are properly controlled by the simulation and interpolation procedures.

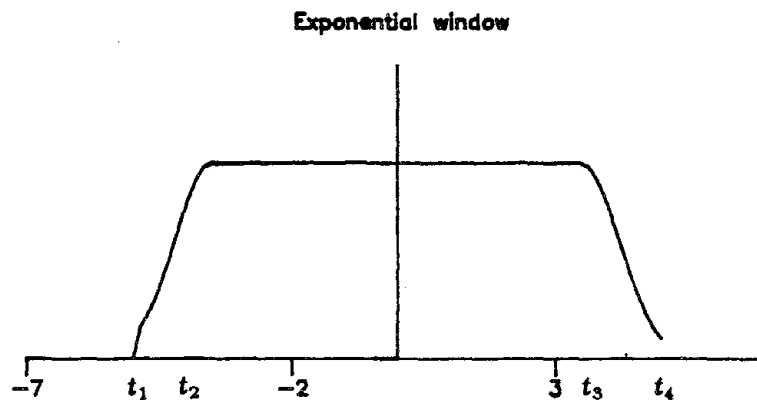
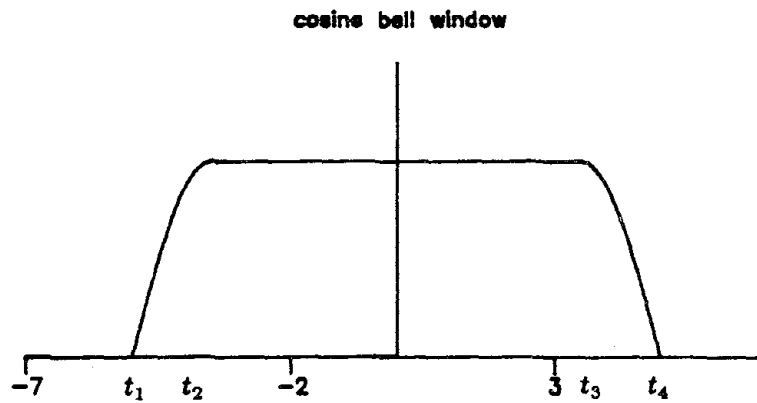
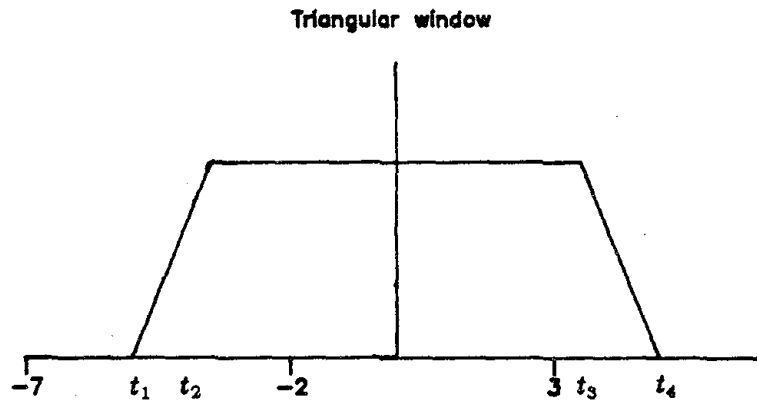
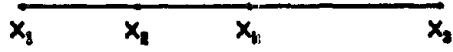
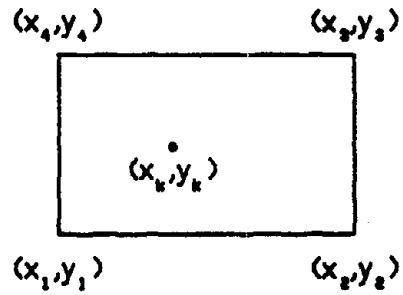


Fig.4.1 Different Types of Transient Functions for Combining the Ground Motions Simulated in Consecutive Time Windows

One-Dimensional case



Two-Dimensional Rectangular



Two-Dimensional Arbitrary

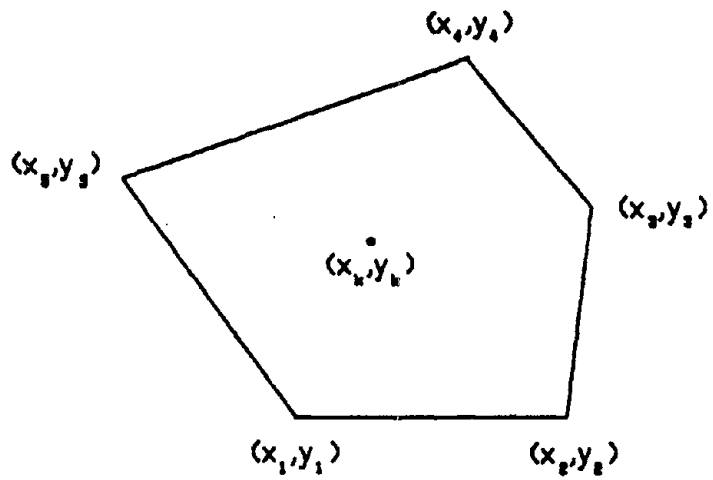


Fig.4.2 The Points for the Ground Motion Interpolation

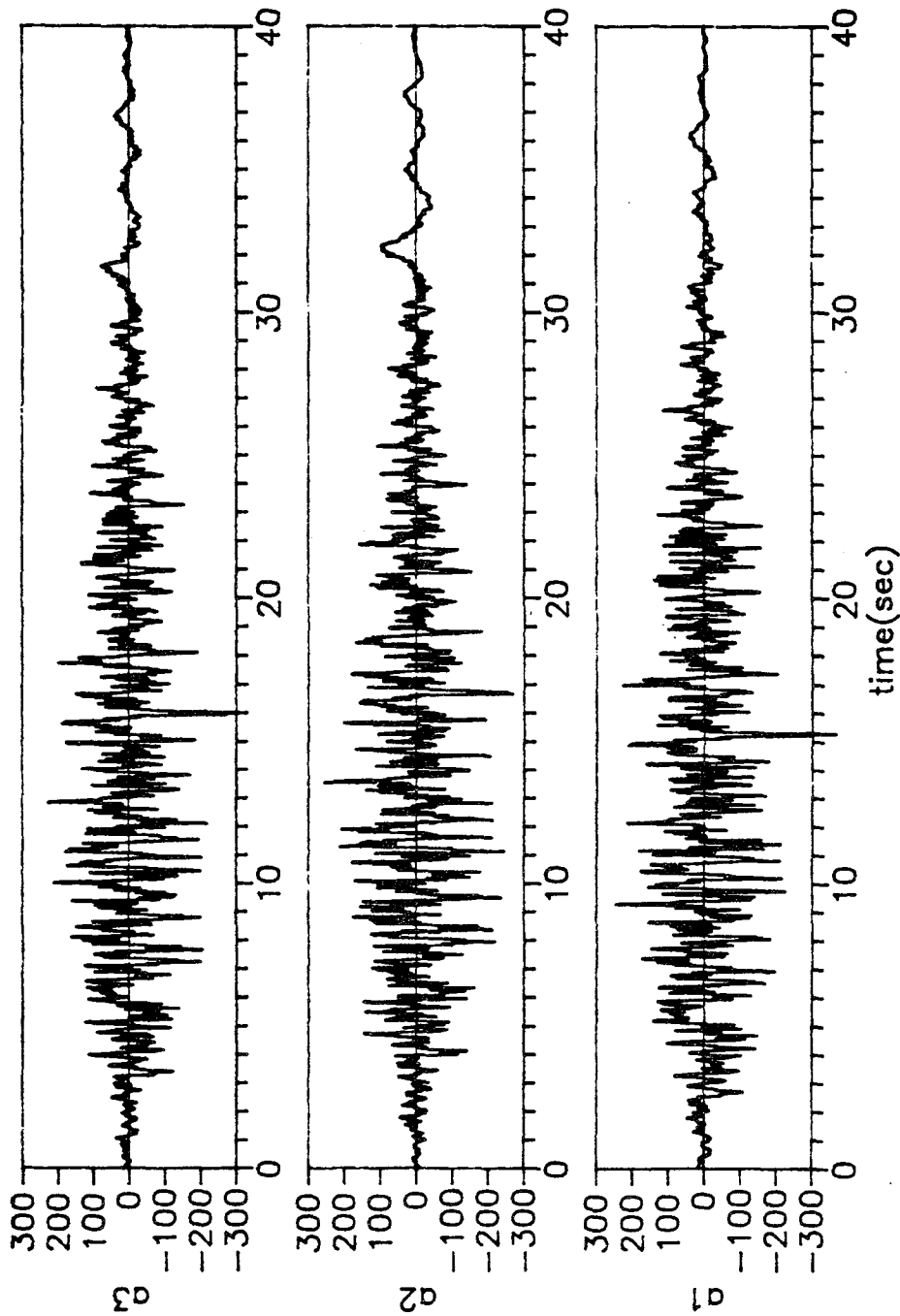


Fig.4.3 Example of Simulated Ground Motion Accelerations Compatible with Newmark and Hall Design Response Spectrum of 5% Damping Normalized to $0.3g$ (a_1 and a_3 are Simulated, and a_2 is Interpolated)

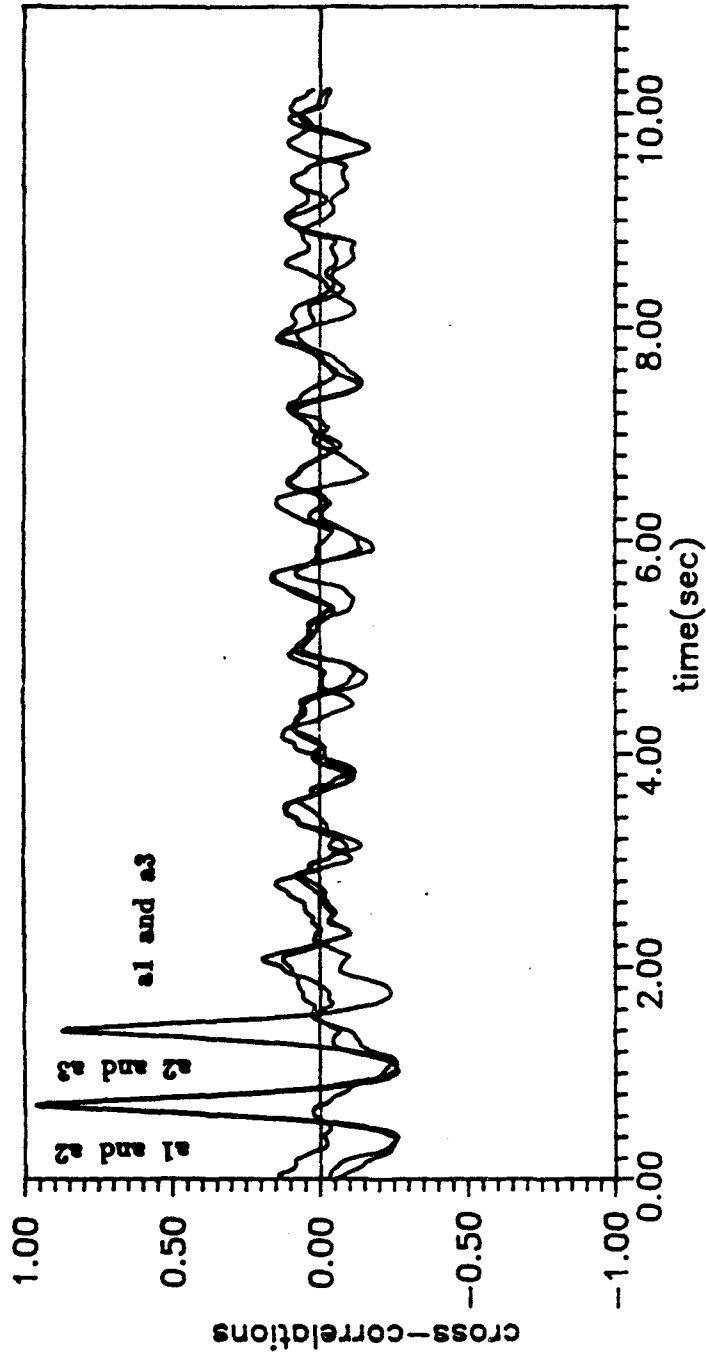


Fig.4.4 Cross Correlation Coefficients of the Simulated and Interpolated Ground Accelerations before Iterations

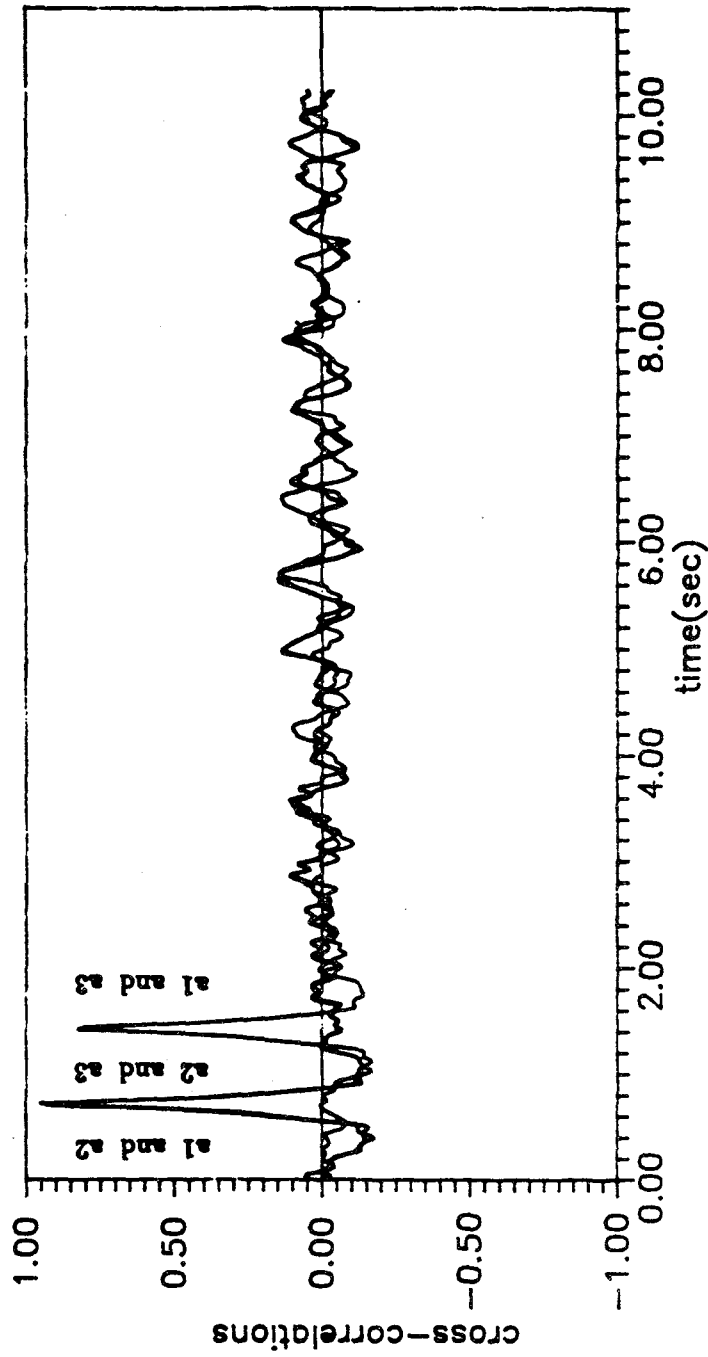


Fig.4.5 Cross Correlation Coefficients of the Simulated and Interpolated Ground Accelerations after Iterations

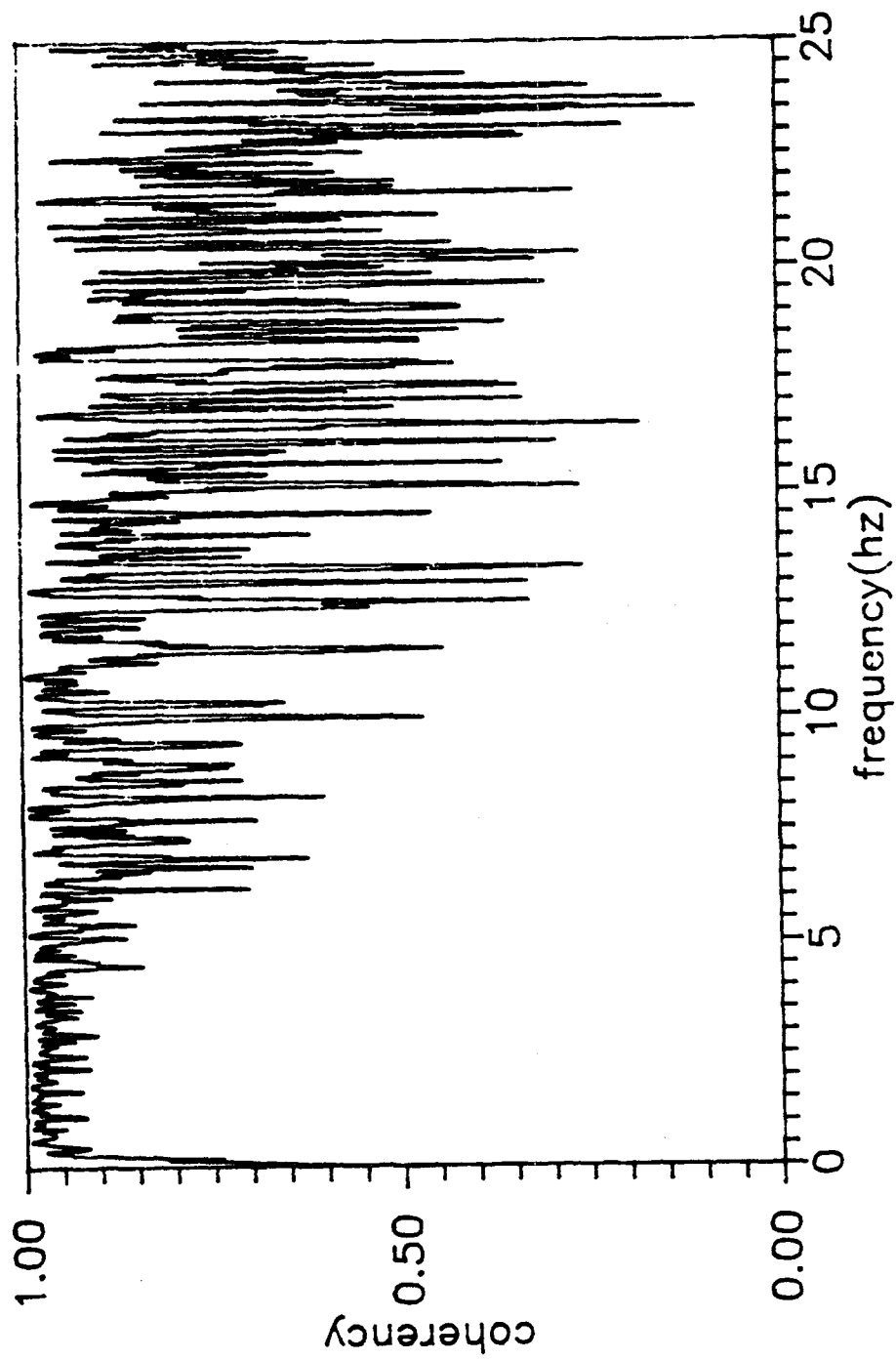


Fig.4.6 Coherency Values between a1 and a2 (x=0m, and X=25m)

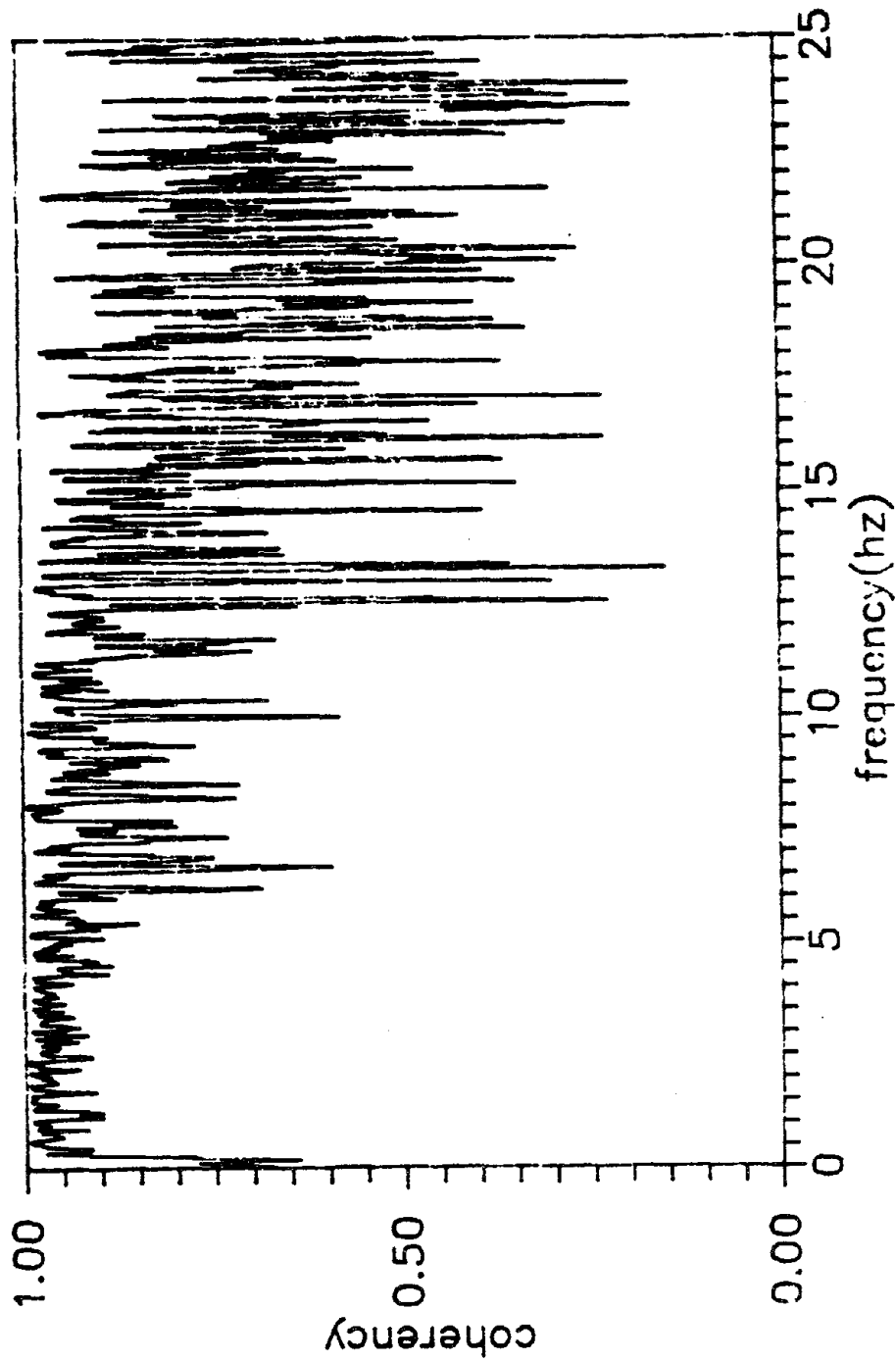


Fig.4.7 Coherency Values between a2 and a3 (x=25m, and X=50m)

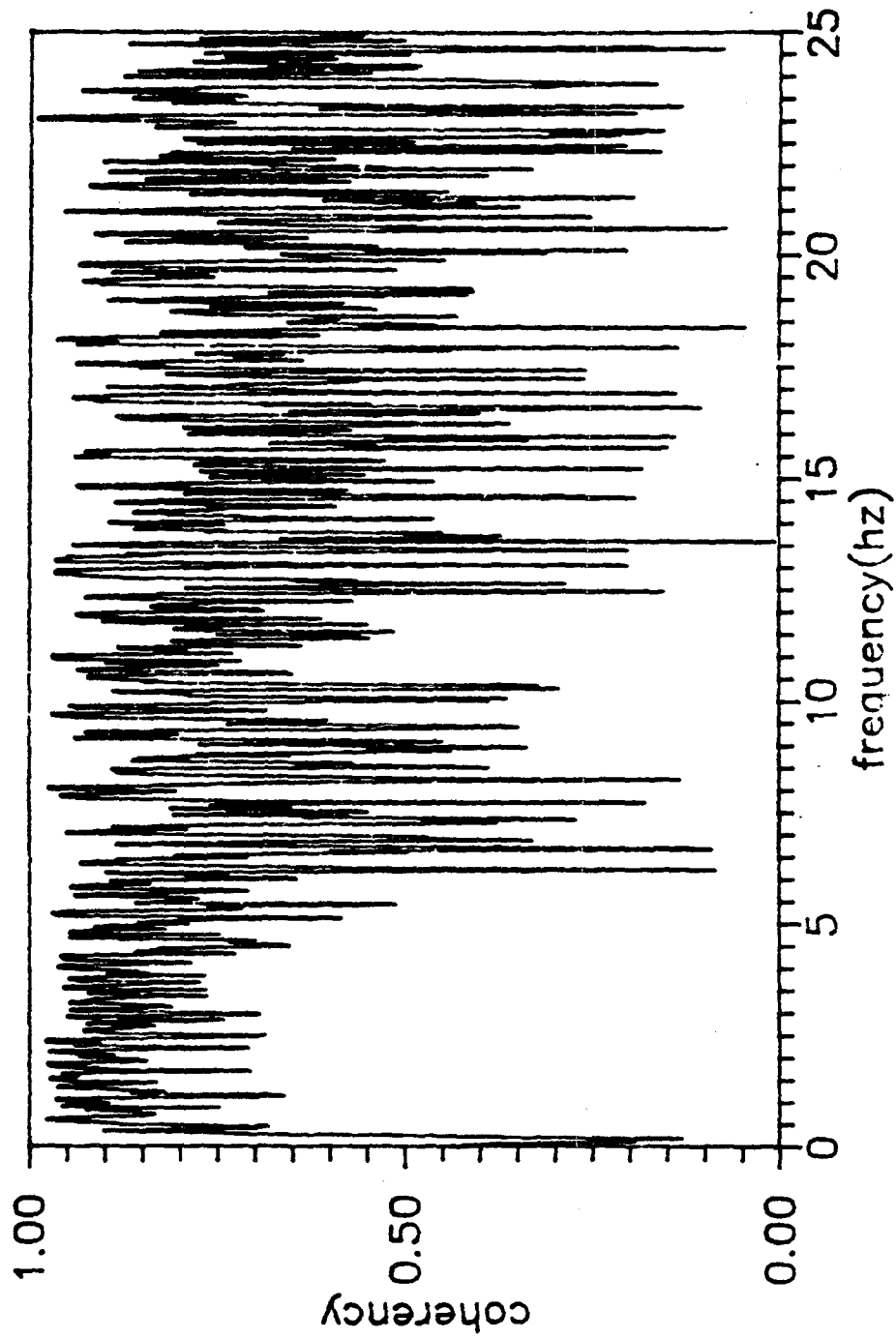


Fig.4.8 Coherency Values between a1 and a3 ($x=0m$, and $X=50m$)

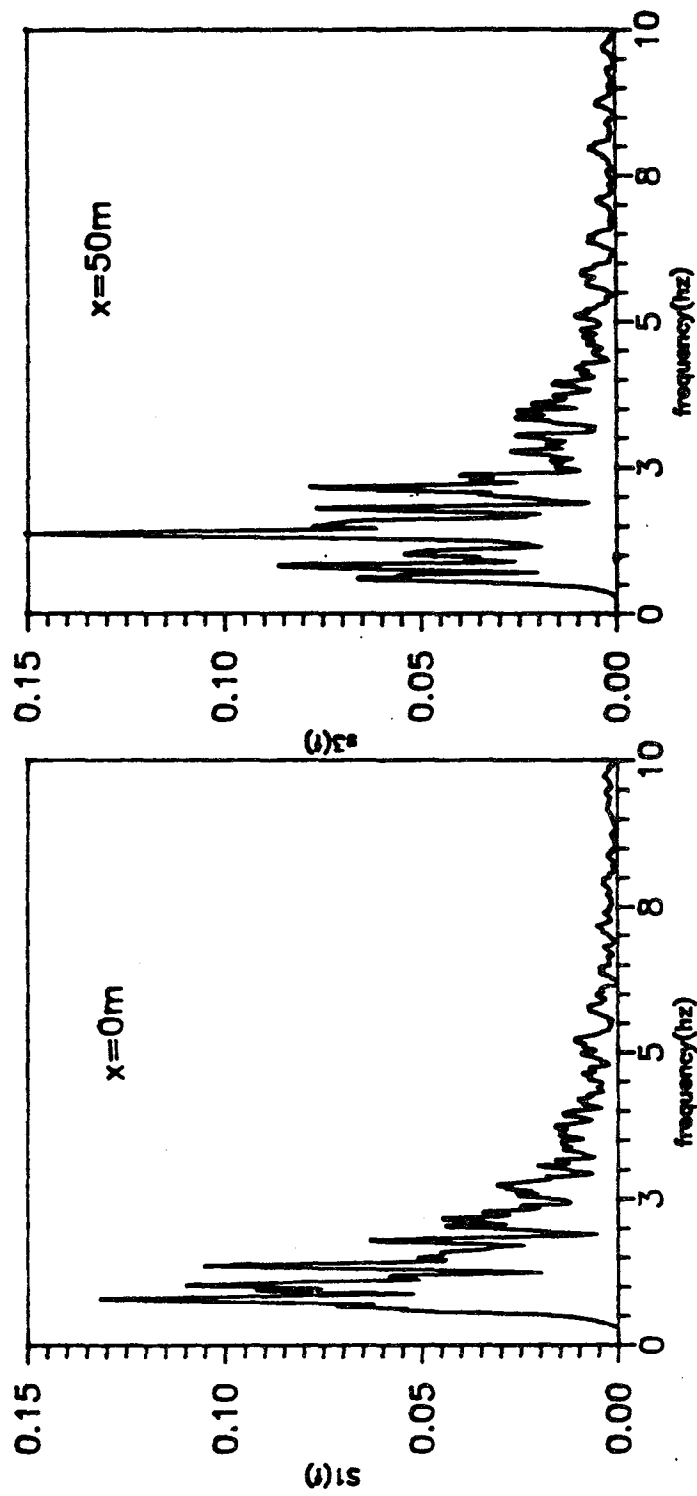


Fig.4.9 Power Spectral Density Functions for a_1 and a_3

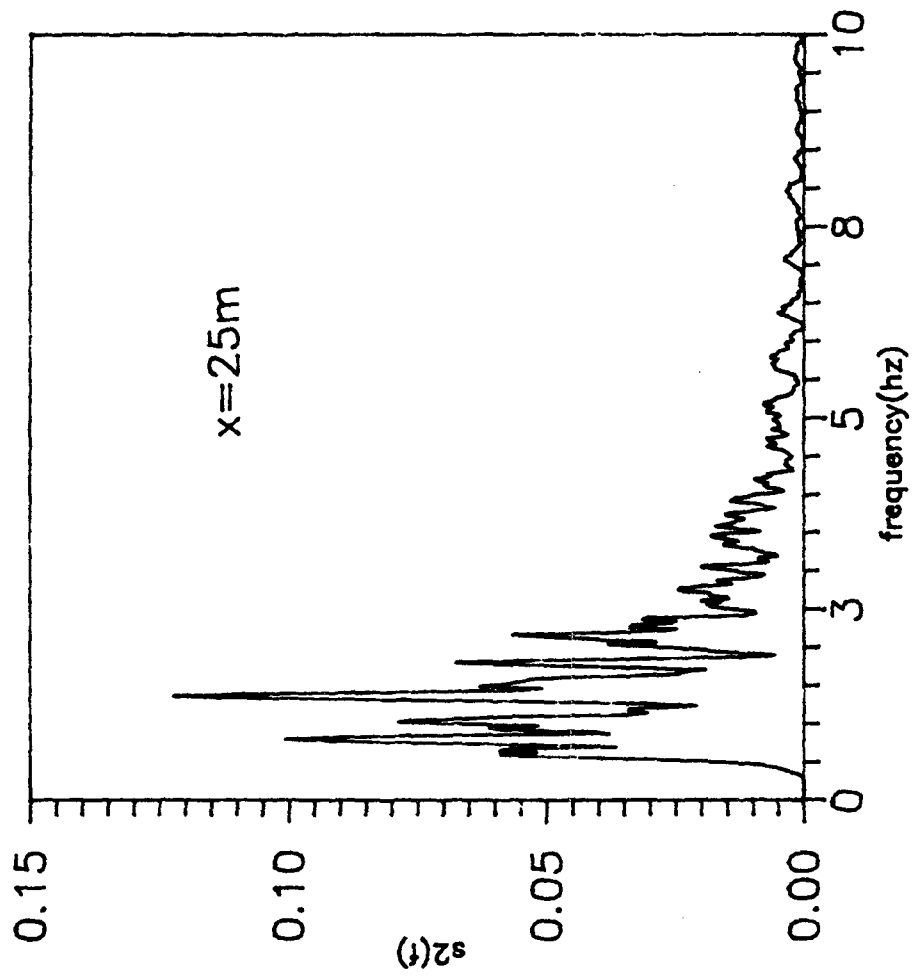


Fig.4.10 Power Spectral Density Functions for a2

generated response spectral compatible ground motion acceleration at $x=0$ m (peak acc=0.5g)

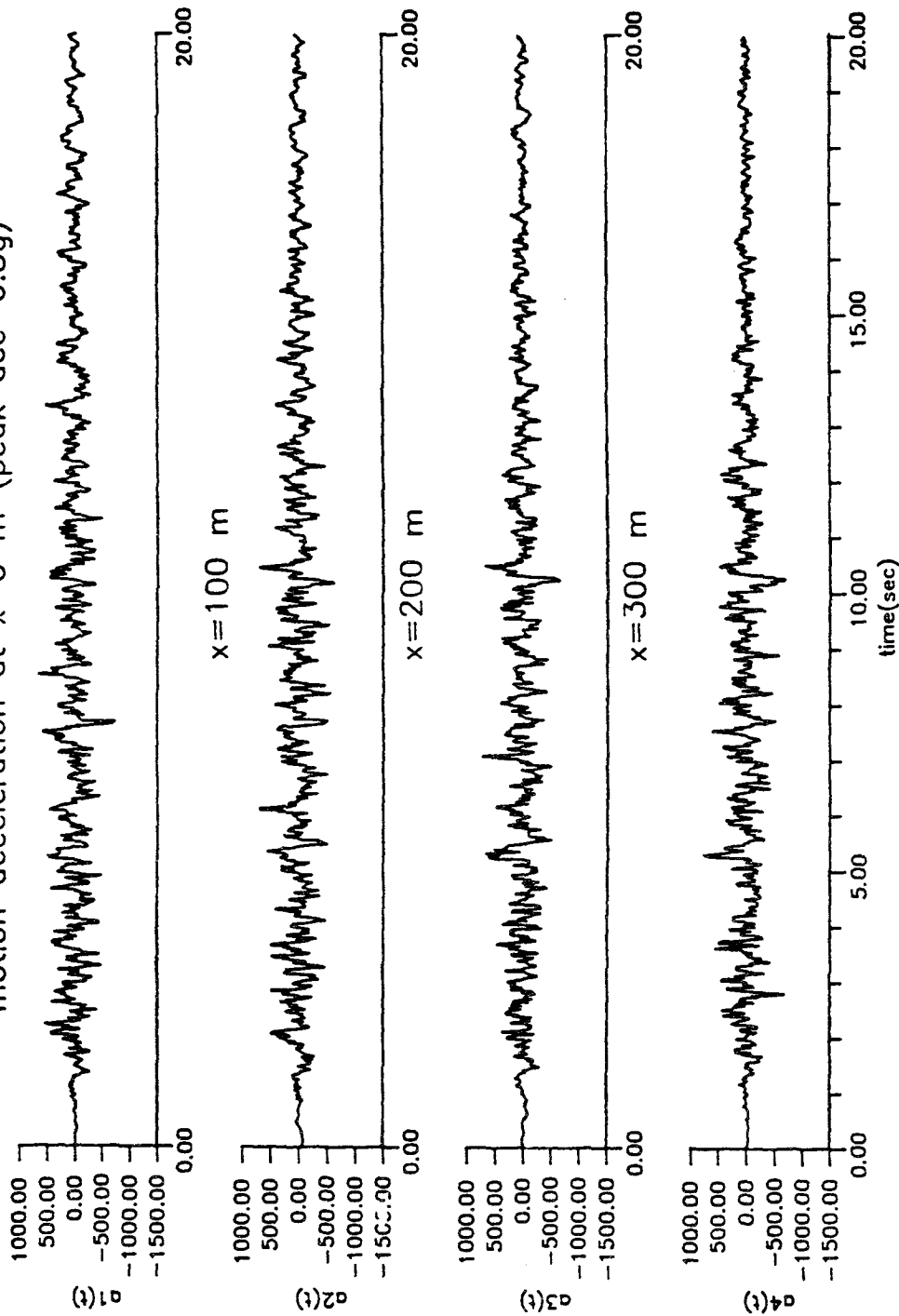


Fig.4.11 Simulated Response Spectral Compatible Ground Accelerations at Different Locations; Specifications: PGA=0.5g, $\xi = 0.05$, $v_{app} = 2500\text{m/s}$, Harichandran and Vanmarck Coherency Model

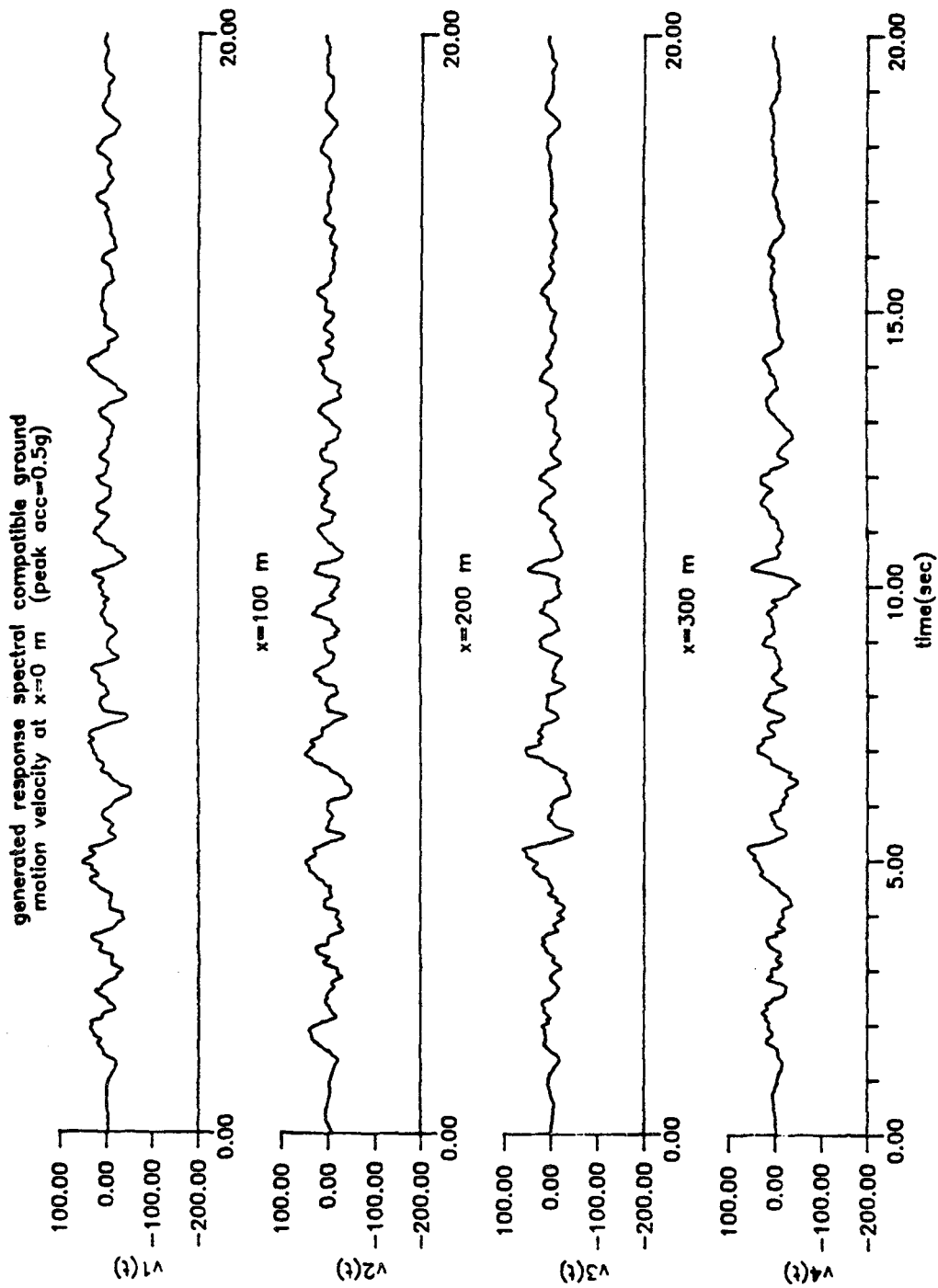


Fig.4.12 Simulated Response Spectral Compatible Ground Velocities at Different Locations; Specifications: $PGA=0.5g$, $\xi = 0.05$, $v_{app} = 2500m/s$, Harichandran and Vanmarck Coherency Model

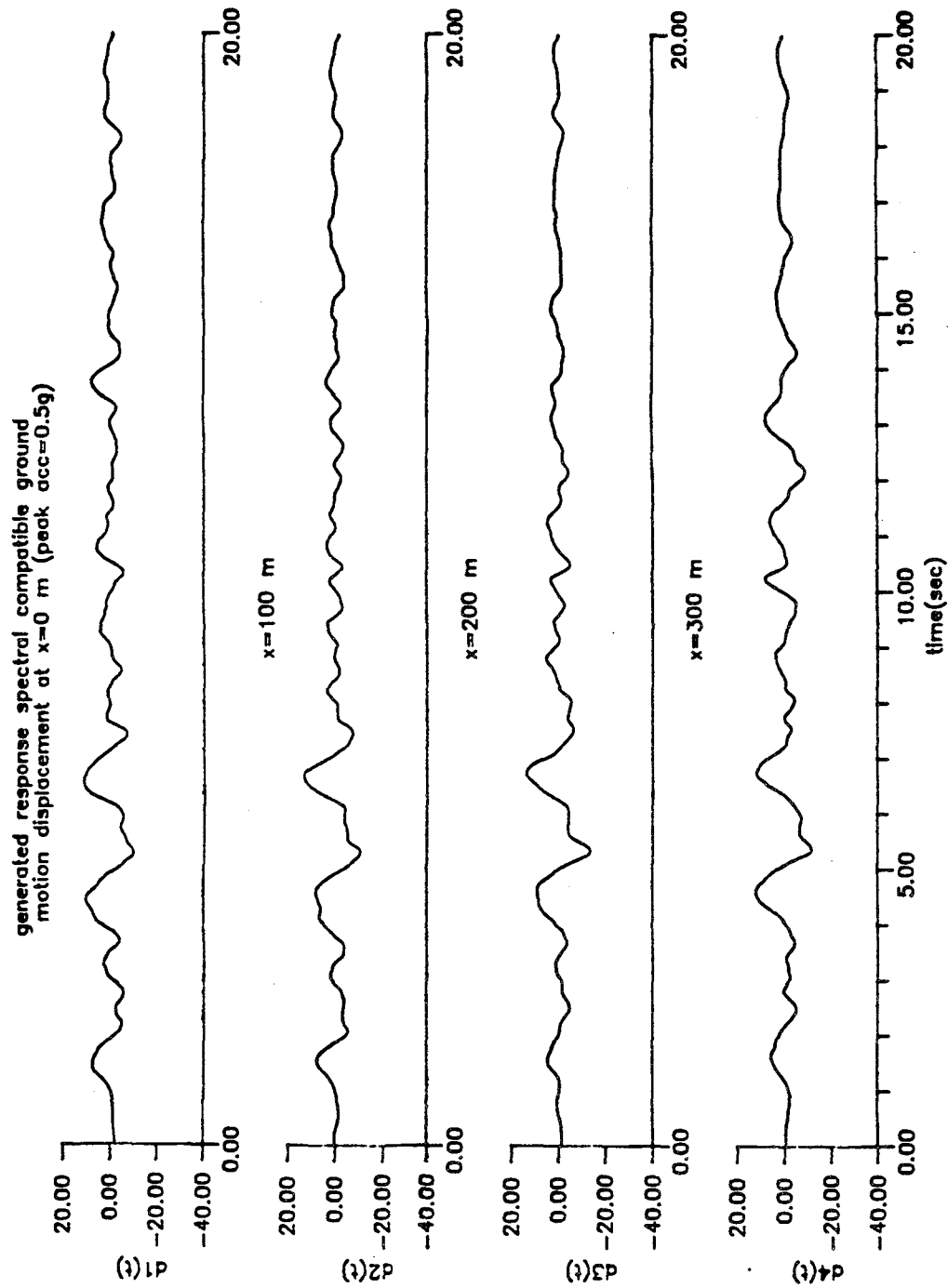


Fig.4.13 Simulated Response Spectral Compatible Ground Displacements at Different Locations; Specifications: $PGA=0.5g$, $\xi = 0.05$, $v_{app} = 2500m/s$, Harichandran and Vanmarck Coherency Model

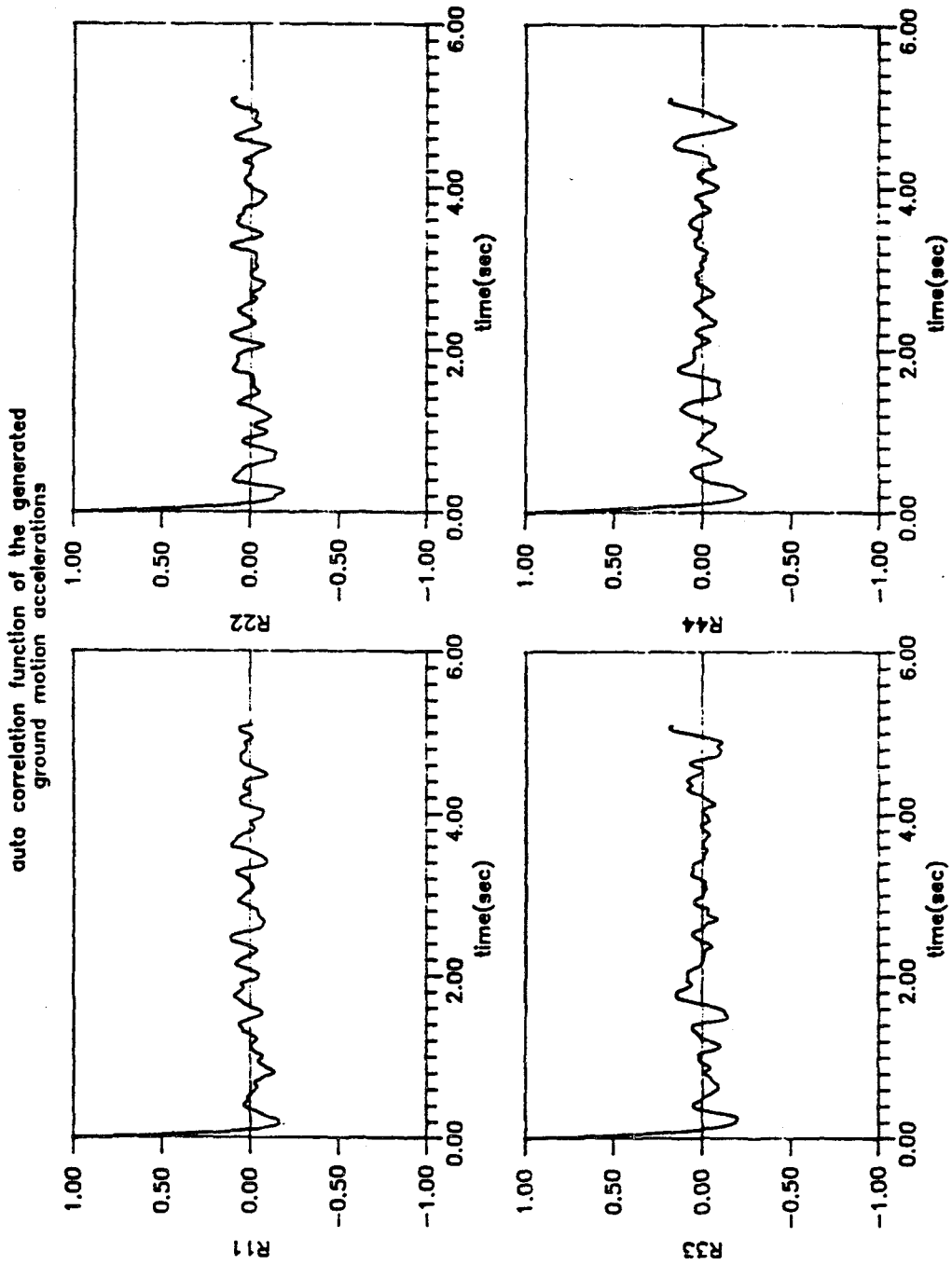


Fig.4.14 Autocorrelation Coefficient Functions of the Four Simulated
Ground Accelerations

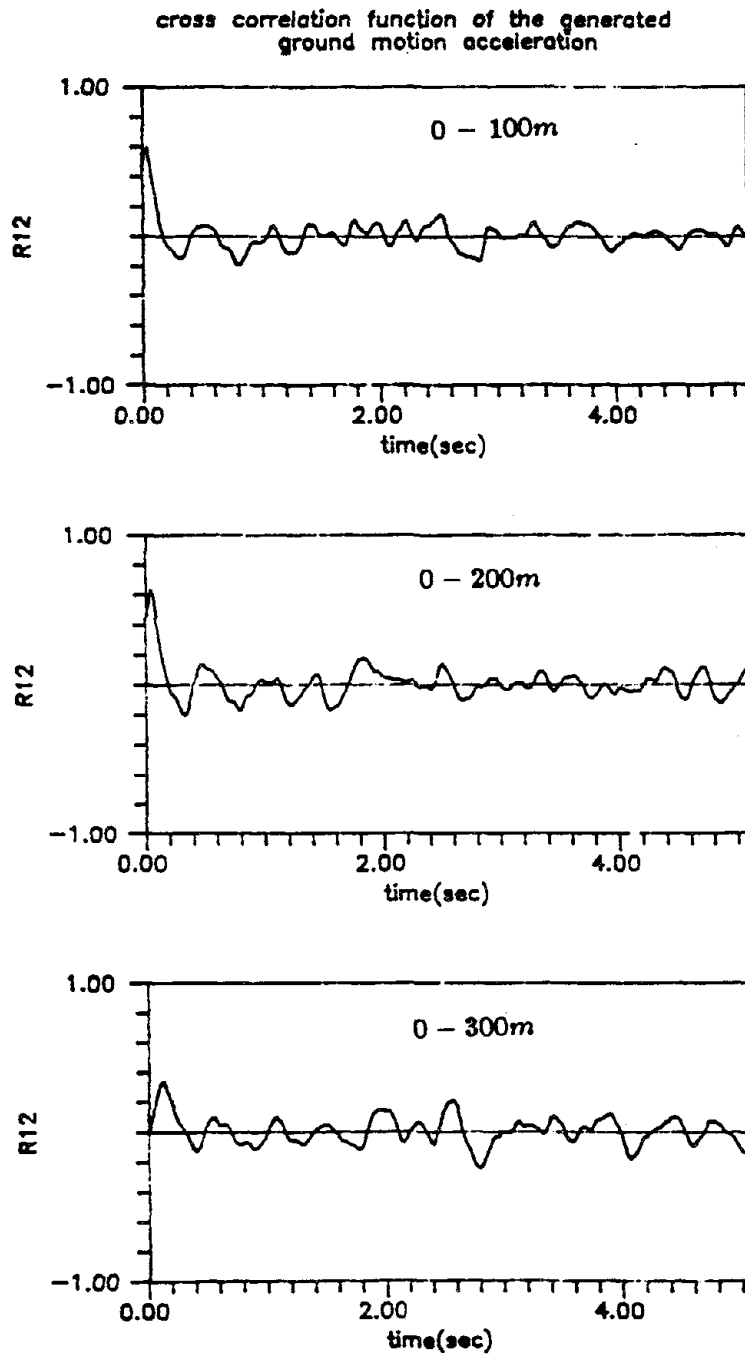


Fig.4.15 Cross Correlation Coefficient Functions between the Simulated Ground Accelerations

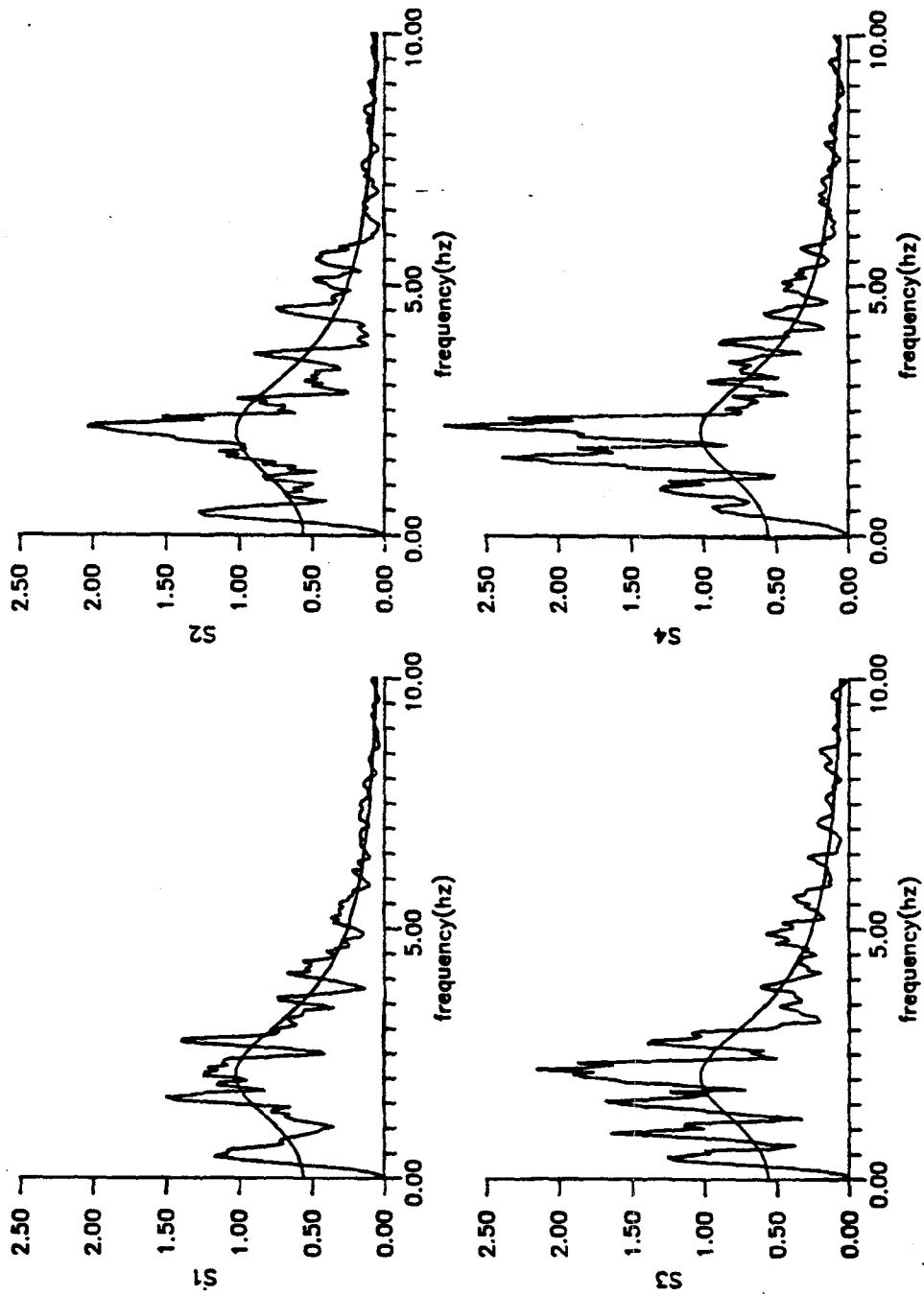


Fig.4.16 Comparison of the Power Spectral Density Functions of the Simulated Ground Accelerations with the Model Values

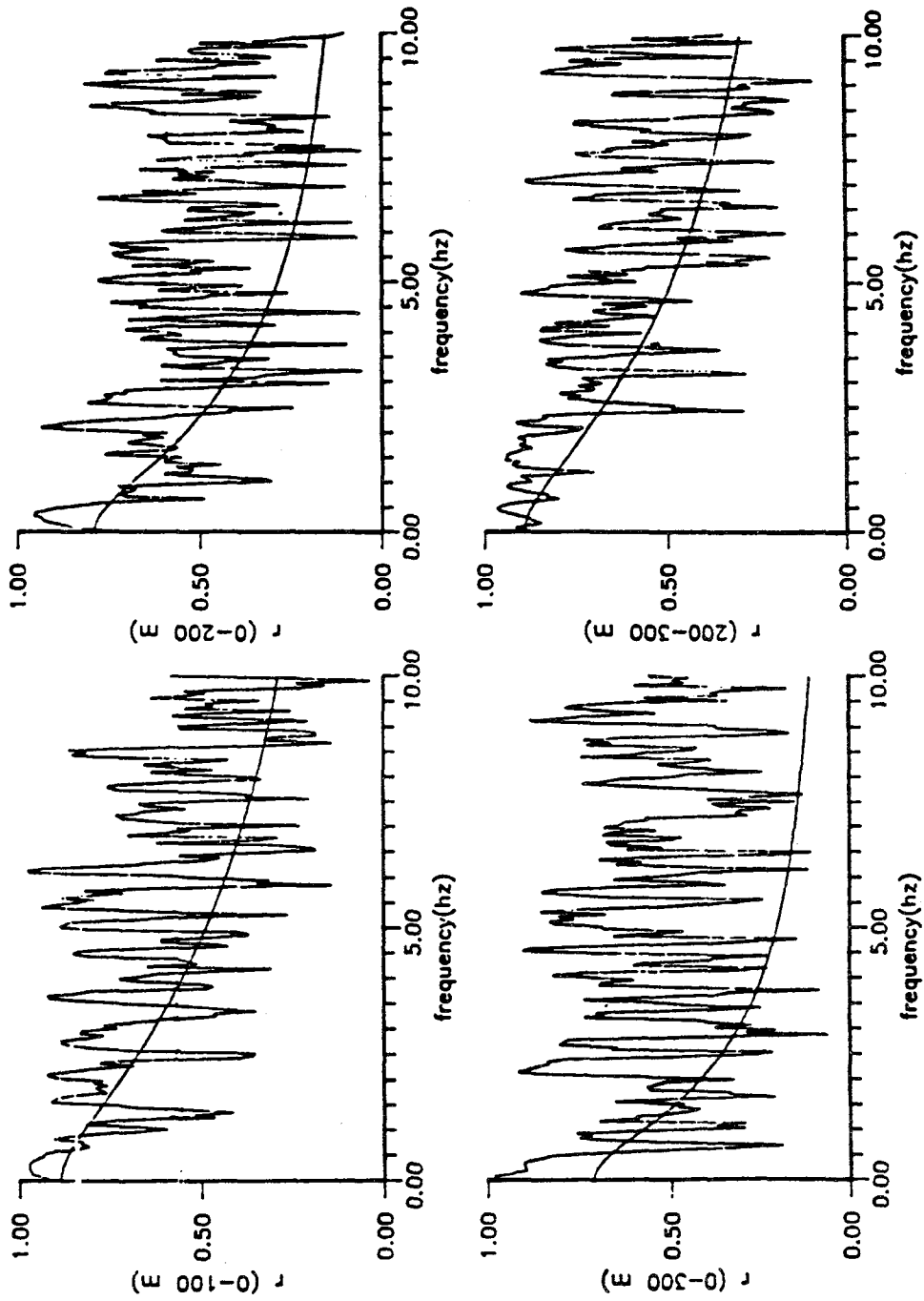


Fig.4.17 Comparison of the Coherency Functions of the Simulated Ground Accelerations with the Model Values

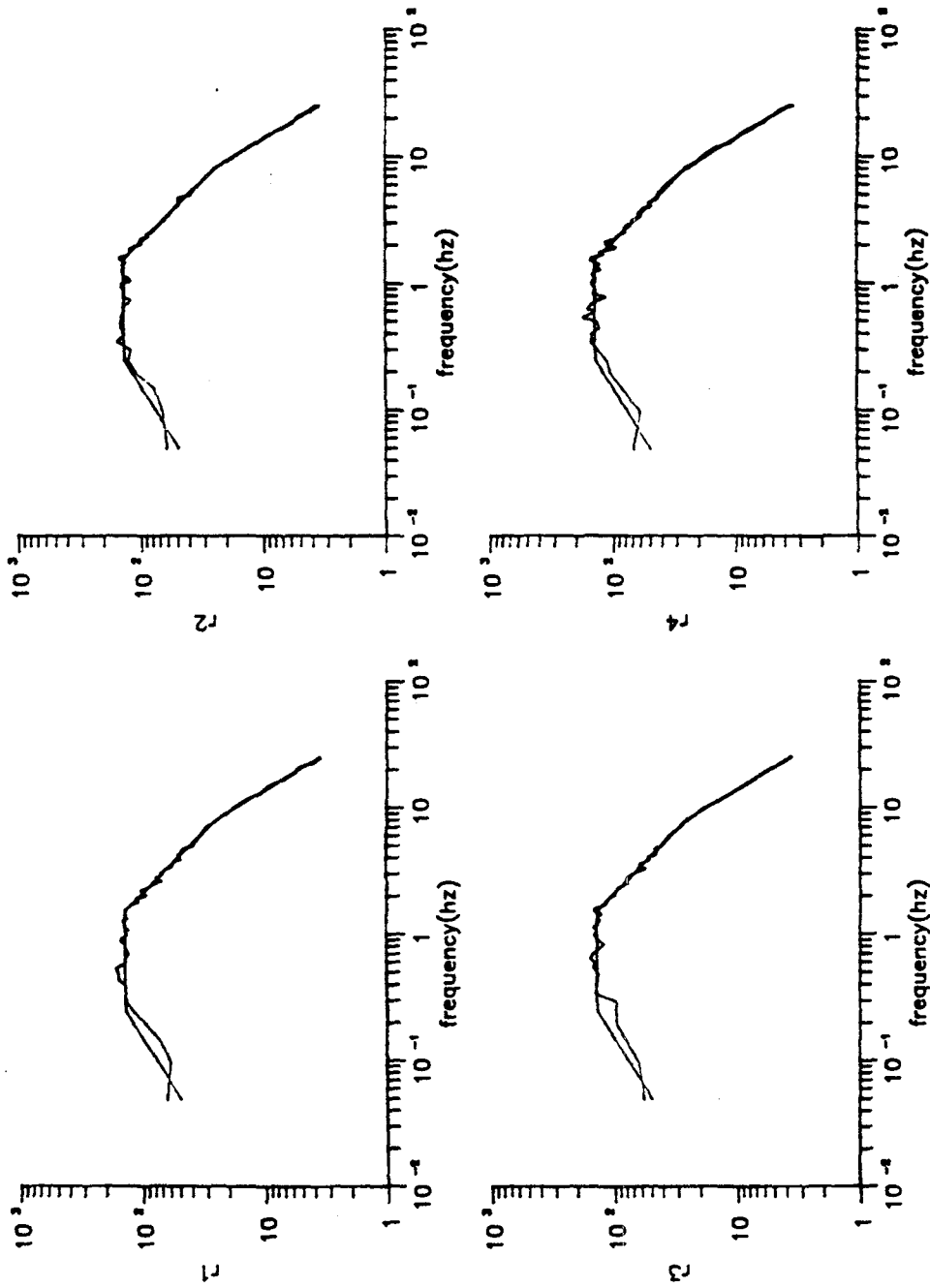


Fig.4.18 Comparison of the Response Spectra of the Simulated Ground Motions with the Target Spectrum

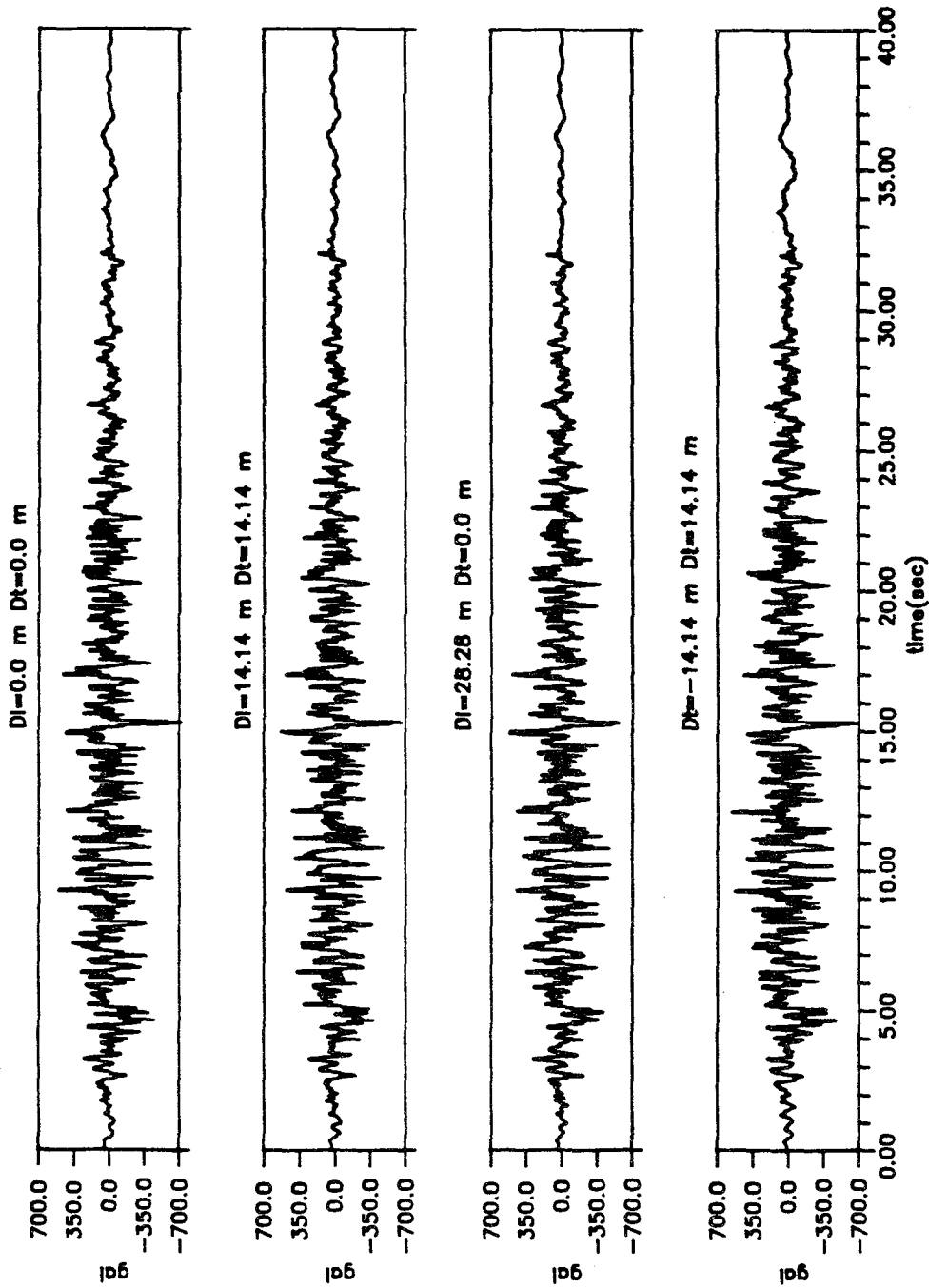


Fig.4.19 Simulated Ground Motion Accelerations (x Component); Response Spectrum Compatible (PGA=0.5g)

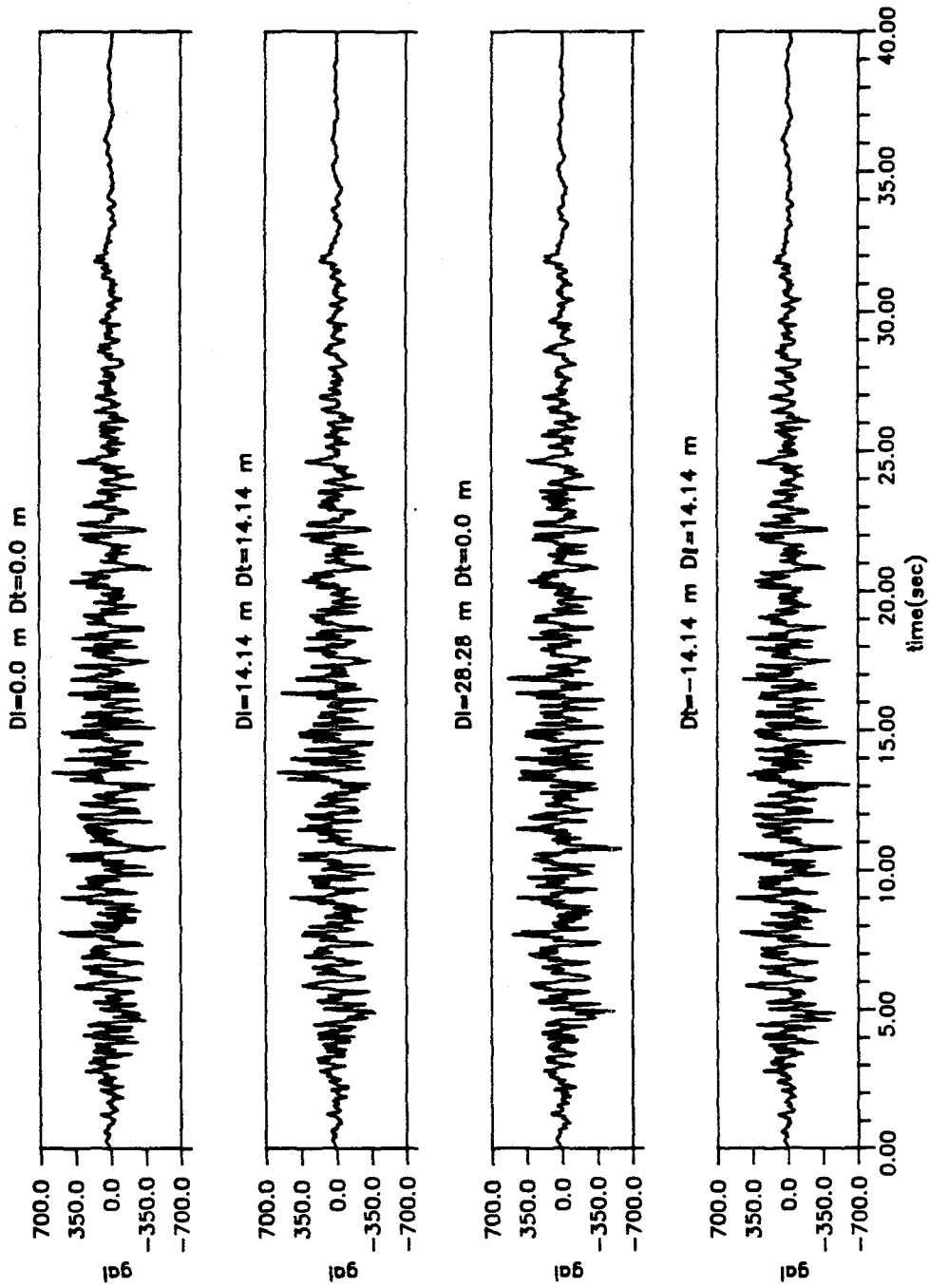


Fig.4.20 Simulated Ground Motion Accelerations (y Component); Response Spectrum Compatible (PGA=0.5g)

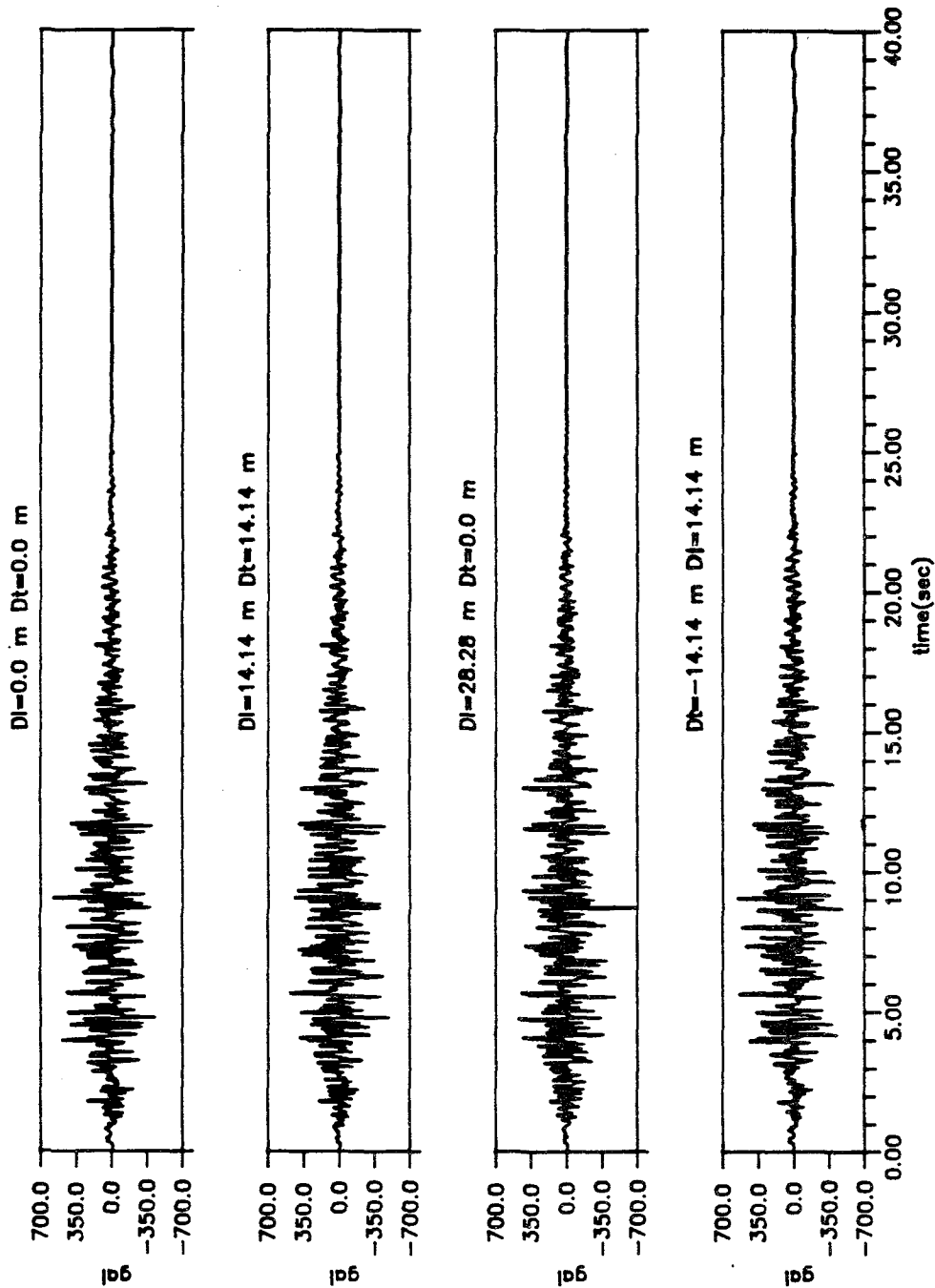


Fig.4.21 Simulated Ground Motion Accelerations (z Component); Response Spectrum Compatible (PGA=0.3g)

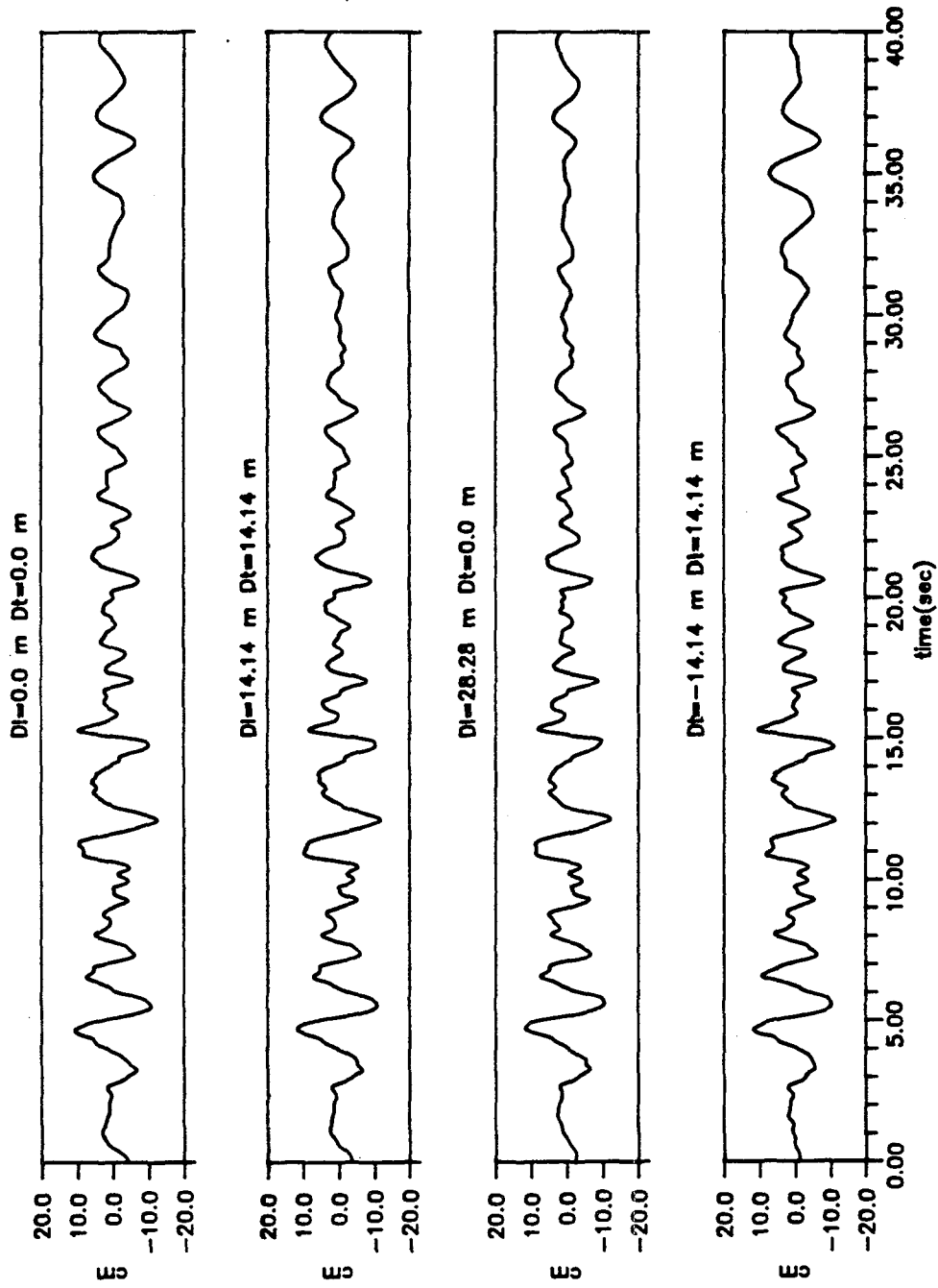


Fig.4.22 Simulated Ground Motion Displacements (x Component);
 Response Spectrum Compatible (PGA=0.5g)

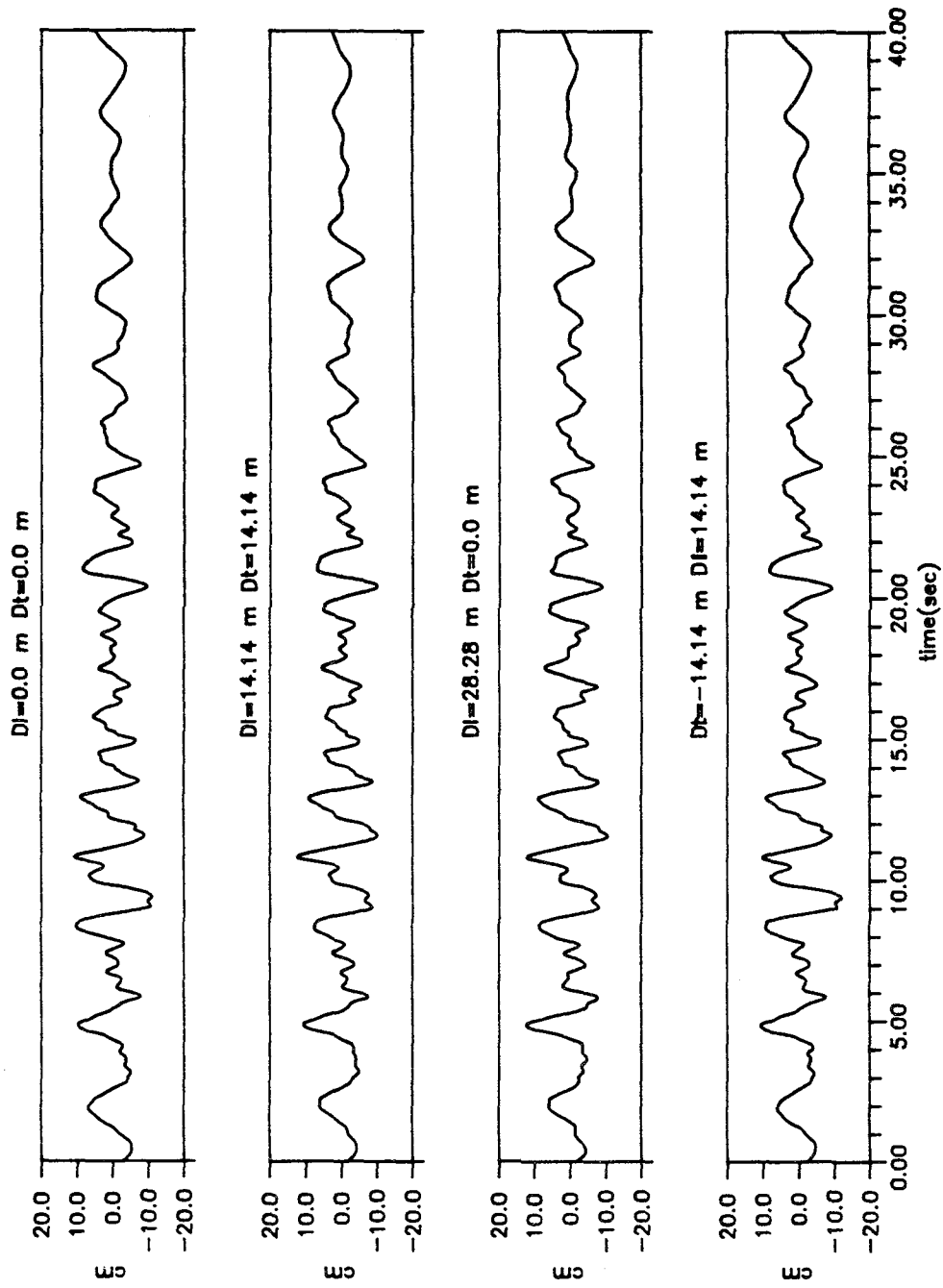


Fig.4.23 Simulated Ground Motion Displacements (y Component);
Response Spectrum Compatible (PGA=0.5g)

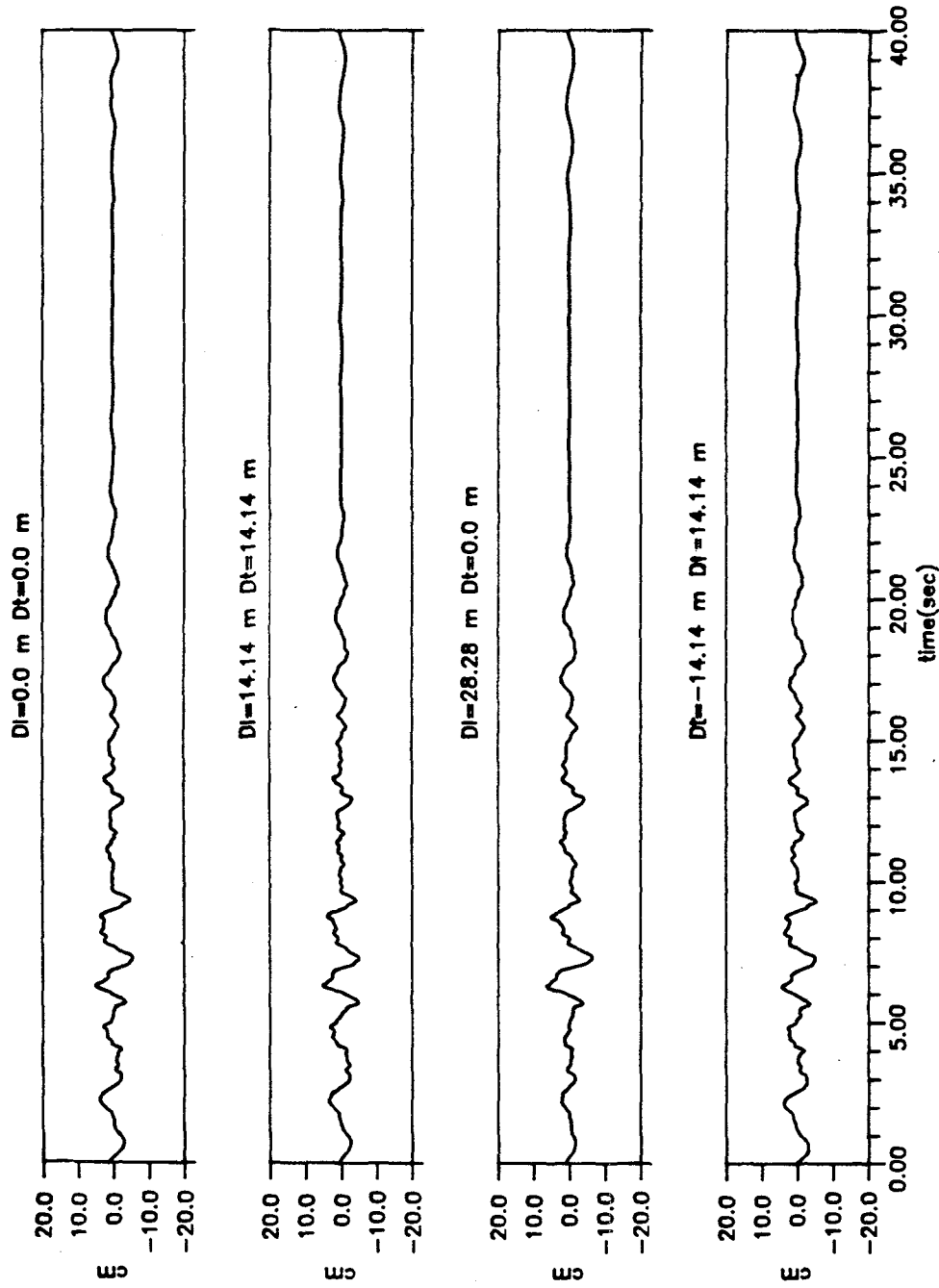


Fig.4.24 Simulated Ground Motion Displacements (z Component);
Response Spectrum Compatible (PGA=0.3g)

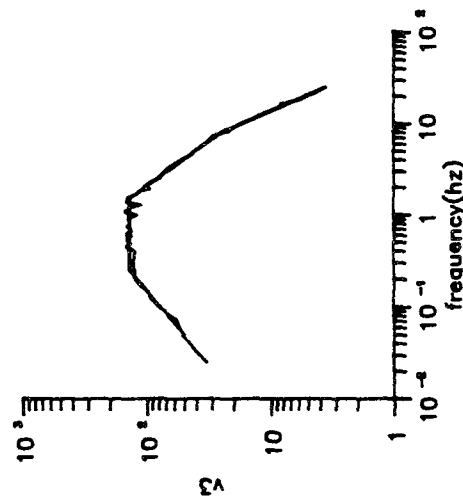
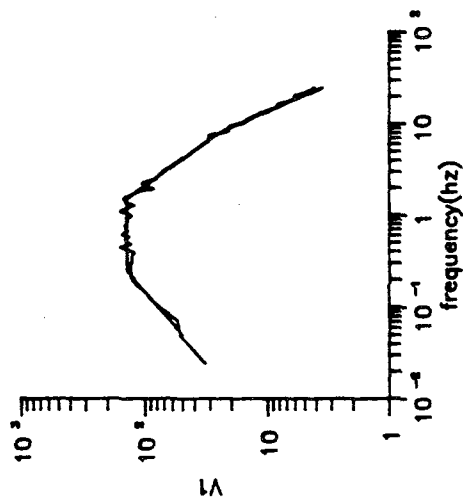
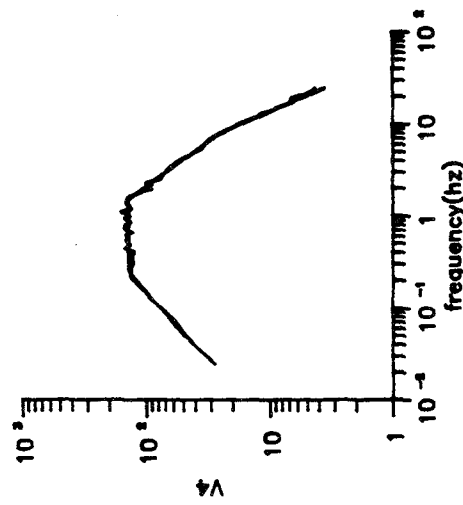
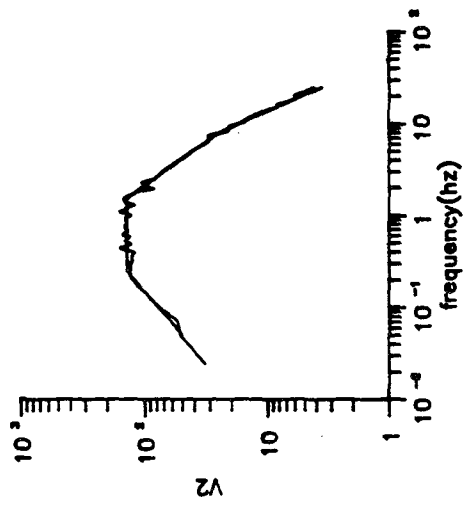


Fig.4.25 Comparison of the Response Spectra of the Simulated Ground Motions with the Target Spectrum (x component)

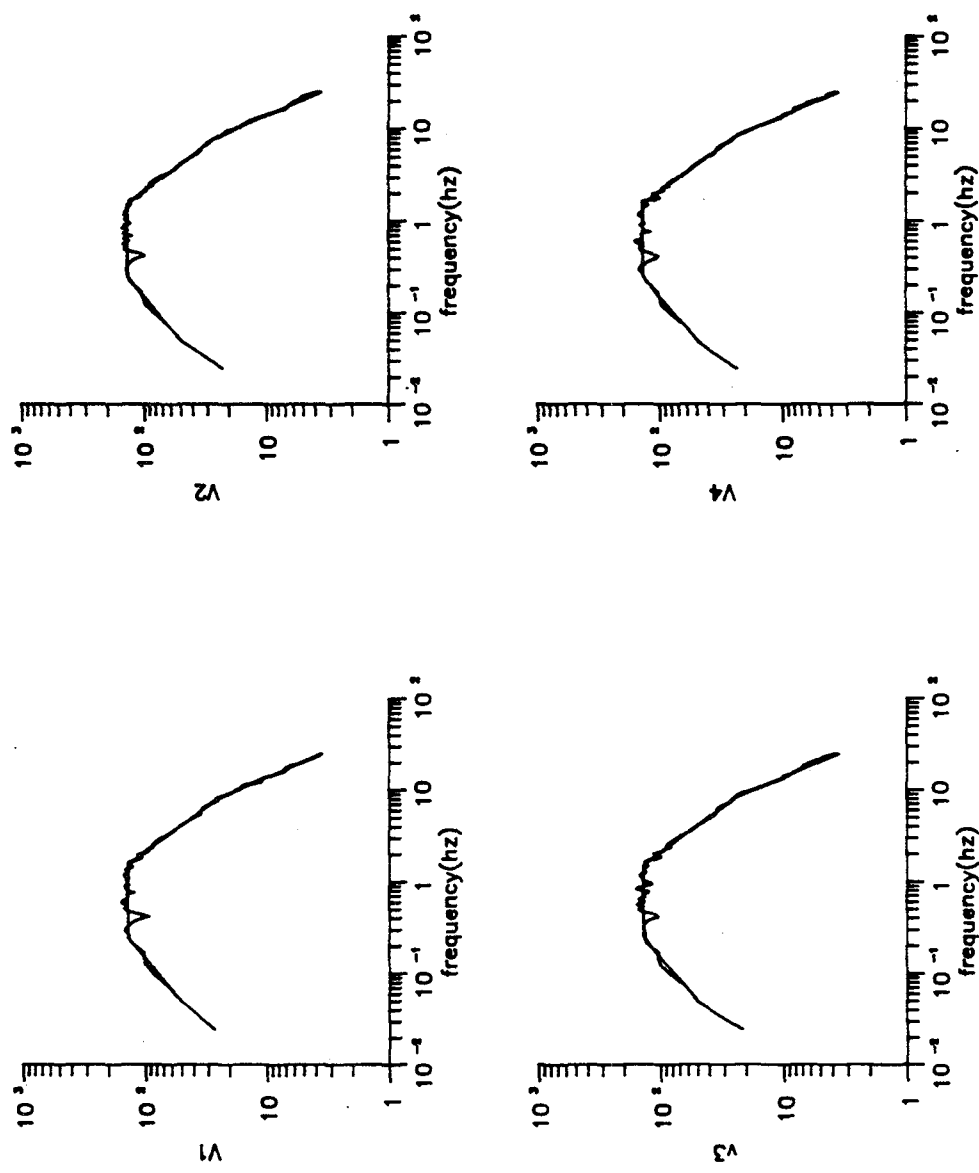


Fig.4.26 Comparison of the Response Spectra of the Simulated Ground Motions with the Target Spectrum (y component)

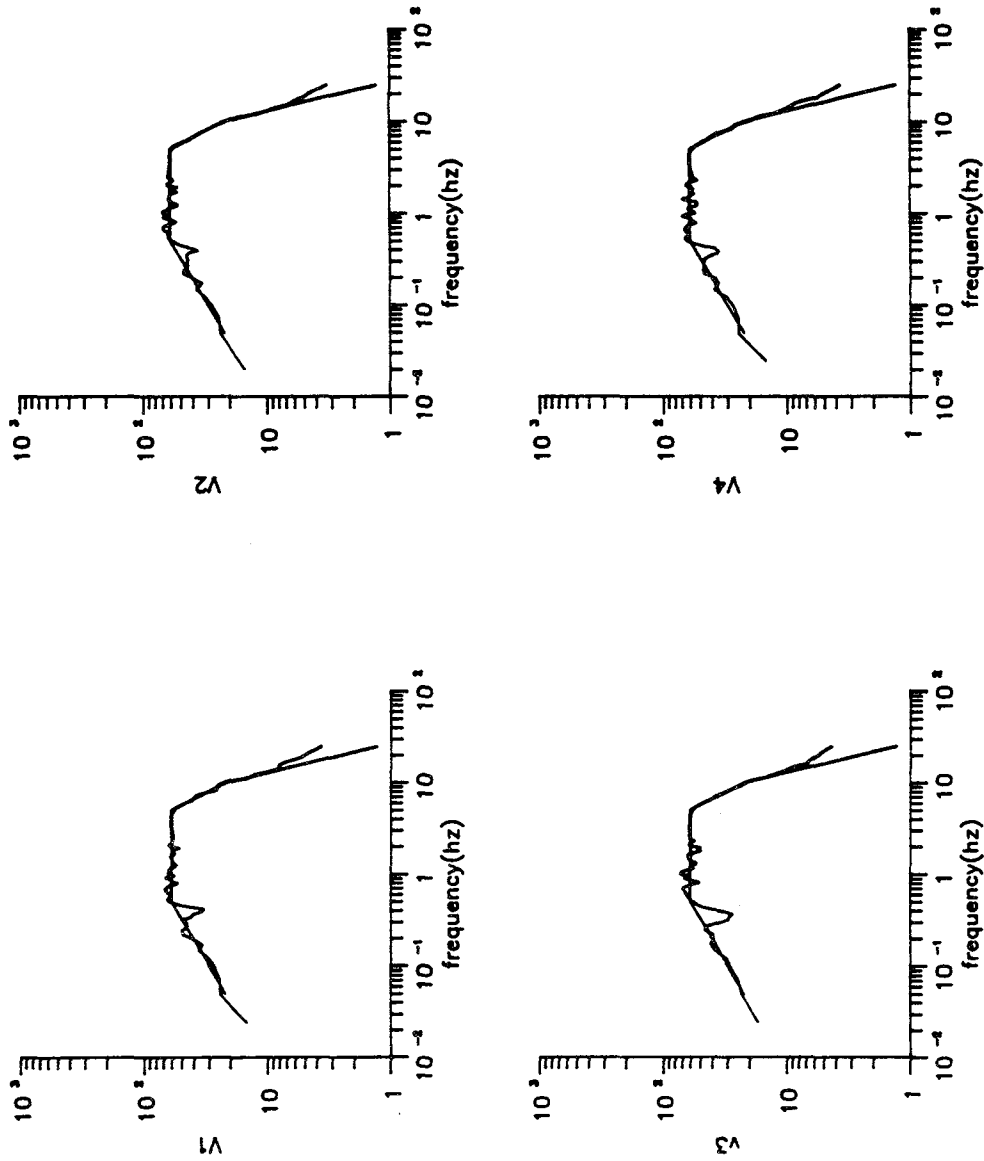


Fig.4.27 Comparison of the Response Spectra of the Simulated Ground Motions with the Target Spectrum (z component)

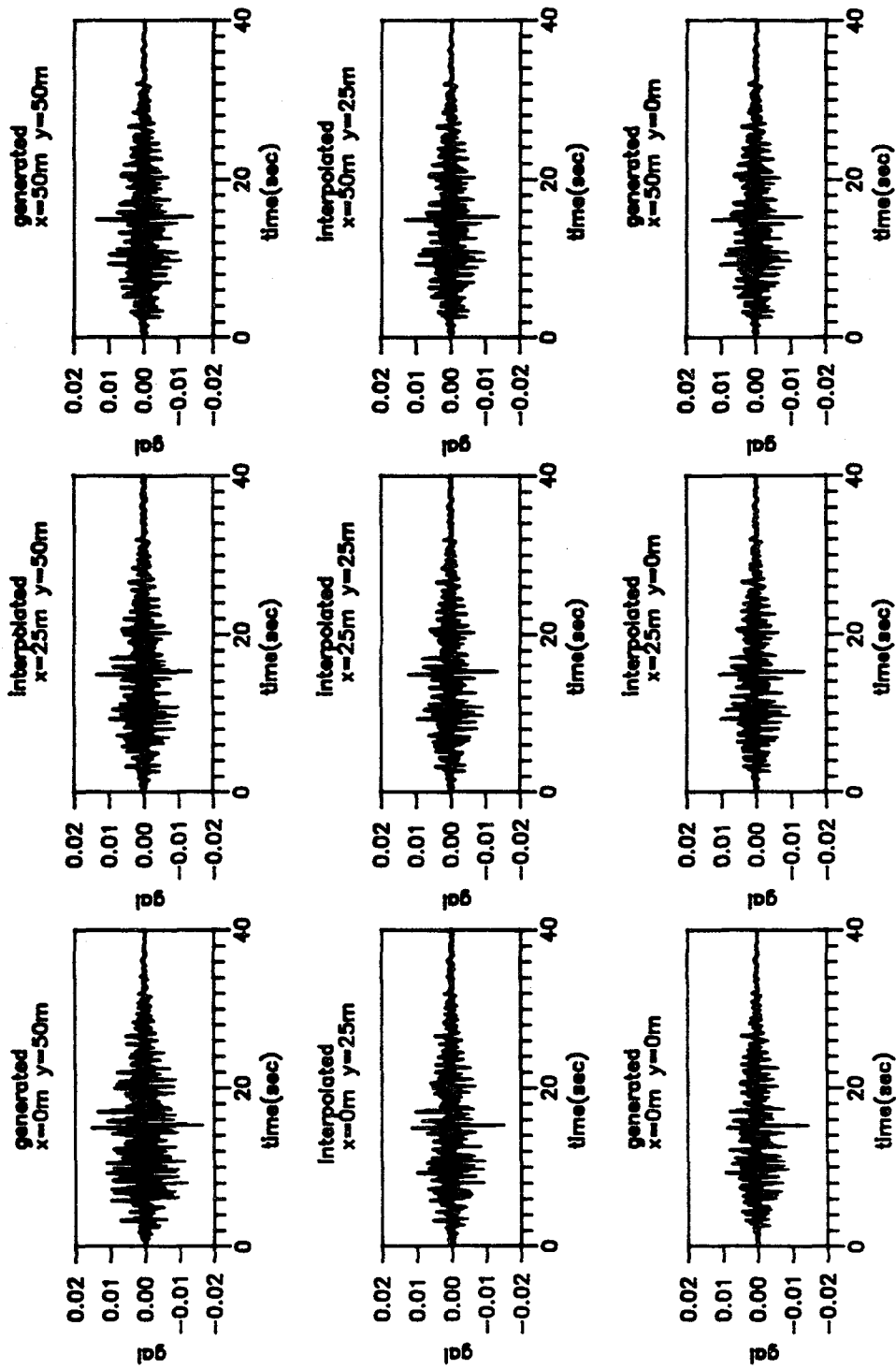


Fig.4.28 Simulated and Interpolated Quasi-Stationary Ground Motion Accelerations before Iterations

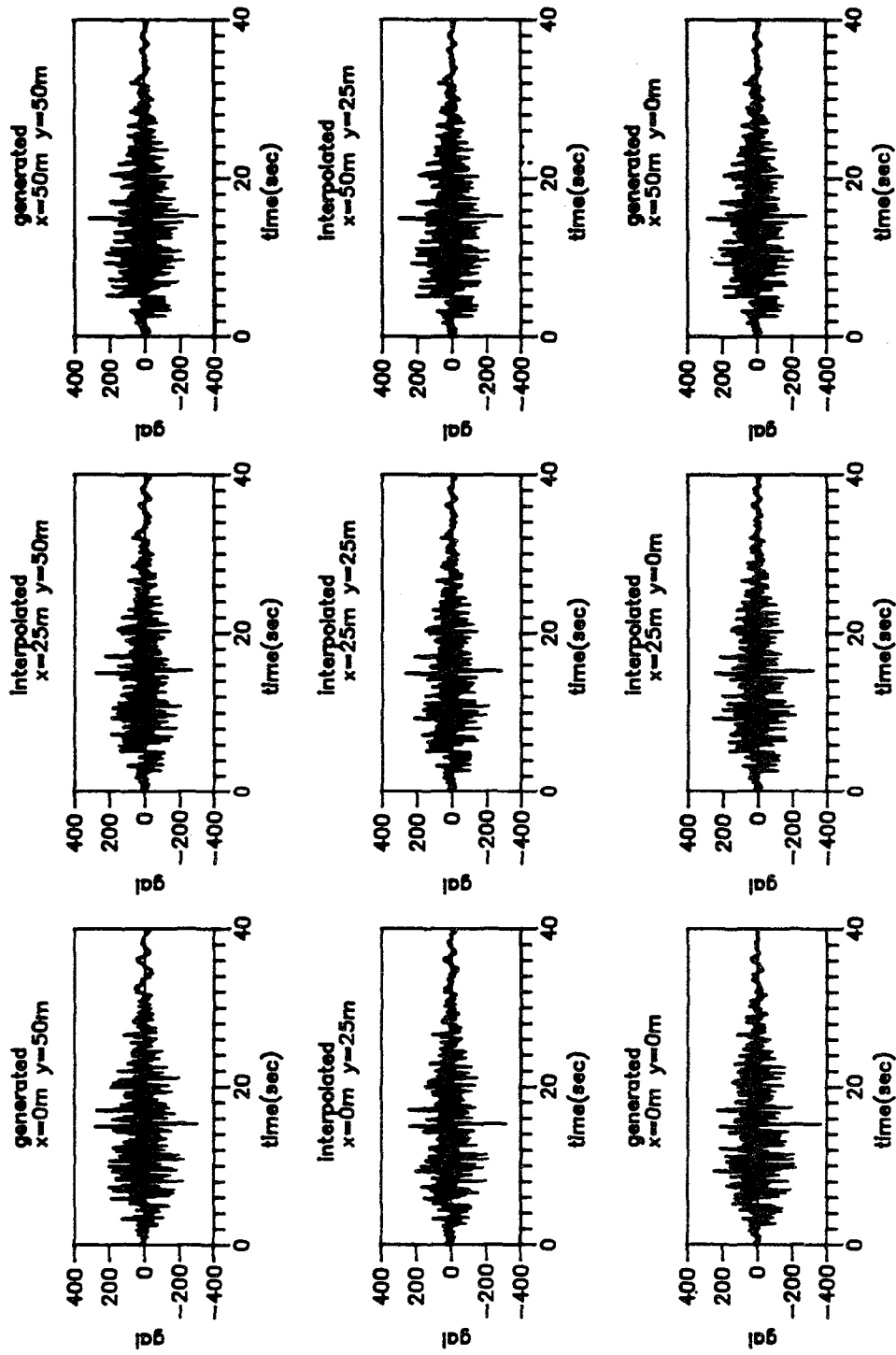


Fig.4.29 Simulated and Interpolated Quasi-Stationary Ground Motion Accelerations after Iterations

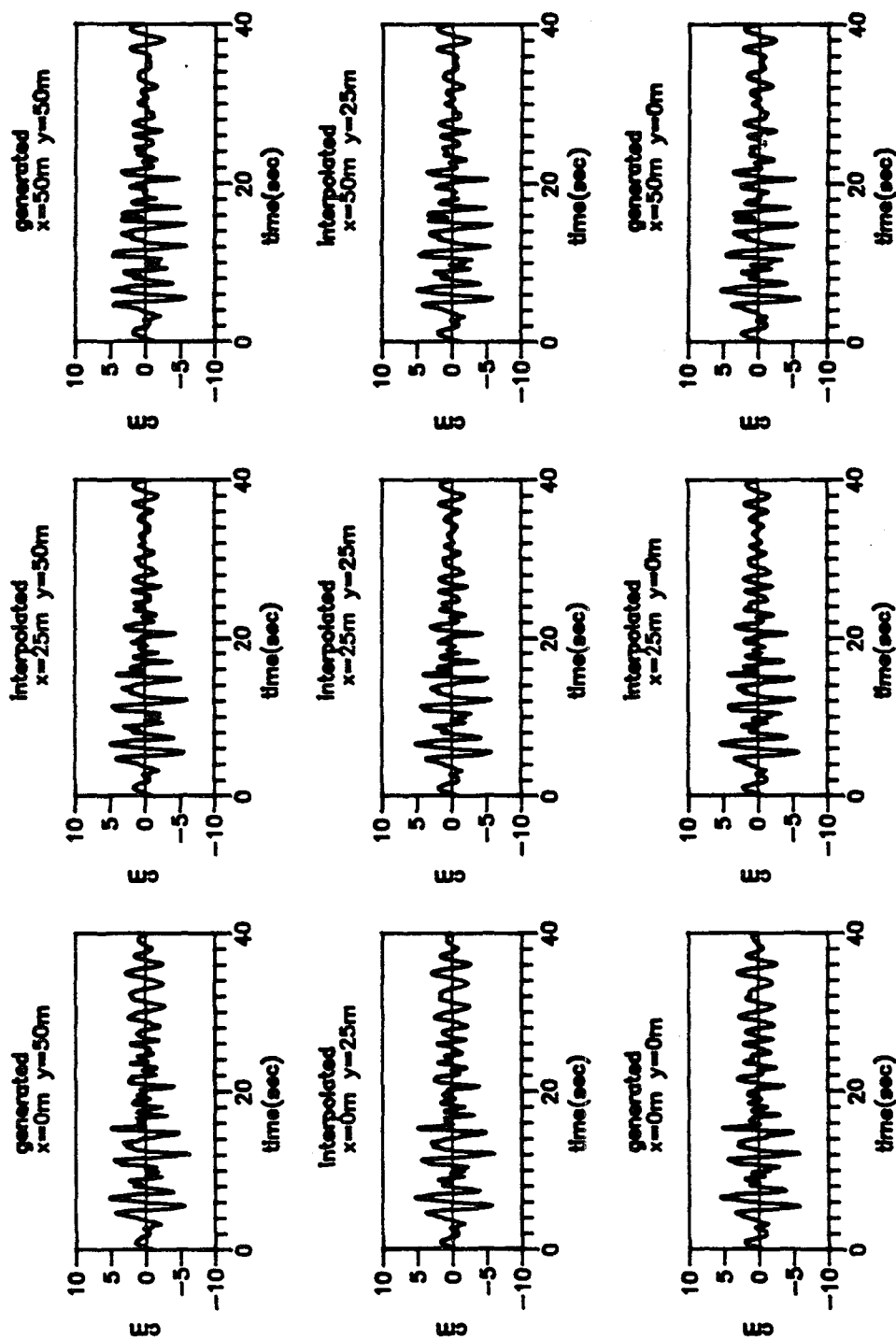


Fig.4.30 Simulated and Interpolated Quasi-Stationary Ground Motion Displacements after Iterations

CHAPTER 5 RESPONSE OF LARGE STRUCTURES WITH MULTIPLE SUPPORTS

This chapter presents (1) the equations of structural response for multiple inputs for cases with and without soil-structure interaction effects, (2) the method of solving these equations in the frequency domain, and (3) selected foundation impedances for treating soil-structure interaction.

5.1 SDOF Structure without Soil-Structure Interaction Effects

Assume a SDOF structure supported at points A and B as shown in Fig. 5.1. The structural system has mass m , stiffness $\frac{k}{2}$ at each support, and damping c . The differential ground motion inputs are \ddot{v}_{gA} and \ddot{v}_{gB} at points A and B , respectively. If the two support points are considered as two degrees of freedom with the prescribed ground displacements, the structural system has 3 degrees of freedom. The general equilibrium equations of the total structural system can be written as,

$$\underline{m} \ddot{\underline{r}}^t + \underline{c} \dot{\underline{r}}^t + \underline{k} \underline{r}^t = \underline{0} \quad (5.1)$$

where \underline{r}^t is the total displacement vector with respect to a fixed reference containing 3 components; \underline{m} , \underline{c} , and \underline{k} are 3×3 mass, damping and stiffness matrices, respectively. These equations of motion can be rewritten in the form

$$\begin{pmatrix} m & 0 & 0 \\ 0 & 0 & 0 \\ 0 & 0 & 0 \end{pmatrix} \begin{pmatrix} \ddot{\underline{y}}^t \\ \ddot{v}_{gA} \\ \ddot{v}_{gB} \end{pmatrix} + \begin{pmatrix} c & 0 & 0 \\ 0 & 0 & 0 \\ 0 & 0 & 0 \end{pmatrix} \begin{pmatrix} \dot{\underline{y}}^t \\ \dot{v}_{gA} \\ \dot{v}_{gB} \end{pmatrix} + \begin{pmatrix} k & \frac{-k}{2} & \frac{-k}{2} \\ \frac{-k}{2} & \frac{k}{2} & 0 \\ \frac{-k}{2} & 0 & \frac{k}{2} \end{pmatrix} \begin{pmatrix} \underline{y}^t \\ v_{gA} \\ v_{gB} \end{pmatrix} = \underline{0} \quad (5.2)$$

where the total displacement vector \underline{r}^t can be partitioned as,

$$\underline{r}^t = \begin{pmatrix} \underline{y}^t \\ v_{gA} \\ v_{gB} \end{pmatrix} = \begin{pmatrix} \underline{y}^d \\ 0 \\ 0 \end{pmatrix} + \begin{pmatrix} \underline{y}^{qs} \\ v_{gA} \\ v_{gB} \end{pmatrix} \quad (5.3)$$

where \underline{y}^{qs} is the quasi-static displacement, \underline{y}^d is the dynamic displacement. To obtain the quasi-static displacement, substitute Eq.(5.3) into Eq.(5.2), and let the dynamic terms be zero; then

$$\underline{y}^{qs} = \frac{1}{2}(v_{gA} + v_{gB}) \quad (5.4)$$

The final equation of motion for the SDOF structure with 2 points of input is

$$\ddot{y}^d + 2\xi\omega\dot{y}^d + \omega^2 y^d = \frac{-1}{2}(\ddot{v}_{gA} + \ddot{v}_{gB}) \quad (5.5)$$

where $\omega = \sqrt{\frac{k}{m}}$ is the natural frequency of the structure, $\xi = \frac{c}{2m\omega}$ is the damping ratio. The total response \underline{y}^t can be calculated by Eq.(5.3) using Eqs.(5.5) and (5.4).

5.2 MDOF Structure without Soil-Structure Interaction Effects

Consider a general MDOF structural system having a total of n degrees of freedom where $n = n_s + n_b$; n_s is the number of degrees of freedom associated with the structure alone, and n_b is the number of degrees of freedom associated with the structure-soil contact points; see Fig. 5.2. The equations of motion can be written in the same form as Eq.(5.1) and are given by

$$\begin{pmatrix} \underline{M}_{ss} & \underline{M}_{sb} \\ \underline{M}_{bs} & \underline{M}_{bb} \end{pmatrix} \begin{pmatrix} \underline{\dot{r}}_s^t \\ \underline{\dot{r}}_b^t \end{pmatrix} + \begin{pmatrix} \underline{C}_{ss} & \underline{C}_{sb} \\ \underline{C}_{bs} & \underline{C}_{bb} \end{pmatrix} \begin{pmatrix} \underline{\dot{r}}_s^t \\ \underline{\dot{r}}_b^t \end{pmatrix} + \begin{pmatrix} \underline{K}_{ss} & \underline{K}_{sb} \\ \underline{K}_{bs} & \underline{K}_{bb} \end{pmatrix} \begin{pmatrix} \underline{r}_s^t \\ \underline{r}_b^t \end{pmatrix} = \underline{0} \quad (5.6)$$

where \underline{M}_{ss} , \underline{M}_{sb} , \underline{M}_{bs} , and \underline{M}_{bb} are the corresponding mass matrices for the structure and soil elements, respectively. The total response can be separated into quasi-static and dynamic responses as

$$\underline{r}^t = \begin{pmatrix} \underline{r}_s^{qs} \\ \underline{v}_g \end{pmatrix} + \begin{pmatrix} \underline{r}_s^d \\ \underline{0} \end{pmatrix} \quad (5.7)$$

where \underline{r}_s^{qs} is the quasi-static displacement vector, \underline{r}_s^d is the dynamic response vector and \underline{v}_g is the prescribed free field ground motion displacement vector for input at multiple structure-soil contact points.

The quasi-static displacement vector \underline{r}_s^{qs} can be obtained by setting all the dynamic terms in Eq.(5.6) to zero, from which

$$\underline{r}_s^{qs} = -\underline{K}_{ss}^{-1} \underline{K}_{sb} \underline{v}_g \quad (5.8)$$

Substituting Eqs.(5.8) and (5.7) into Eq.(5.6), one obtains

$$\underline{M}_{ss} \ddot{\underline{r}}_s^d + \underline{M}_{ss} \ddot{\underline{r}}_s^{qs} + \underline{M}_{sb} \ddot{\underline{v}}_g + \underline{C}_{ss} \dot{\underline{r}}_s^d + \underline{C}_{ss} \dot{\underline{r}}_s^{qs} + \underline{C}_{sb} \dot{\underline{v}}_g + \underline{K}_{ss} \underline{r}_s^d + \underline{K}_{ss} \underline{r}_s^{qs} + \underline{K}_{sb} \underline{v}_g = \underline{0} \quad (5.9)$$

It can be seen from Eq.(5.8) that $\underline{K}_{ss} \underline{r}_s^{qs} + \underline{K}_{sb} \underline{v}_g = \underline{0}$; Eq.(5.9) reduces to

$$\underline{M}_{ss} \ddot{\underline{r}}_s^d + \underline{C}_{ss} \dot{\underline{r}}_s^d + \underline{K}_{ss} \underline{r}_s^d = [\underline{M}_{ss} \underline{K}_{ss}^{-1} \underline{K}_{sb} - \underline{M}_{sb}] \ddot{\underline{v}}_g + [\underline{C}_{ss} \underline{K}_{ss}^{-1} \underline{K}_{sb} - \underline{c}_{sb}] \dot{\underline{v}}_g \quad (5.10)$$

For stiffness proportional damping, the second term on the right hand side is zero, and it is negligible for other types of damping. Also, $\underline{M}_{sb} = \underline{0}$ if the lumped mass is used. Then, the final equations of motion are

$$\underline{M}_{ss} \ddot{\underline{r}}_s^d + \underline{C}_{ss} \dot{\underline{r}}_s^d + \underline{K}_{ss} \underline{r}_s^d = \underline{M}_{ss} \underline{K}_{ss}^{-1} \underline{K}_{sb} \ddot{\underline{v}}_g \quad (5.11)$$

By solving this system of linear equations for \underline{r}_s^d , and calculating \underline{r}_s^{qs} by Eq.(5.8), the total structural response can be obtained. The equations of motion can be solved either in the

time domain by mode decomposition analysis or in the frequency domain. In the frequency domain, Eq.(5.11) becomes

$$[-\bar{\omega}^2 \underline{M}_{s,s} + i\bar{\omega} \underline{C}_{s,s} + \underline{K}_{s,s}] \underline{r}_s^d(i\bar{\omega}) = \underline{M}_{s,s} \underline{K}_{s,s}^{-1} \underline{K}_{s,b} \ddot{\underline{v}}_g(i\bar{\omega}) \quad (5.12)$$

where $\underline{r}_s^d(i\bar{\omega})$ and $\ddot{\underline{v}}_g(i\bar{\omega})$ are the dynamic displacement vector and the ground motion acceleration vector, respectively.

5.3 SDOF Structure with Soil-Structure Interaction Effects

Assume a SDOF rigid bar with mass m , supported by two massless frames with property EI on two different foundations at points A and B ; the foundation A has mass m_A and moment of inertia J_A , and the foundation B has mass m_b and moment of inertia J_B ; the structural system has damping c ; the system is excited by two spatially correlated ground motions \ddot{v}_{gA} and \ddot{v}_{gB} at points A and B , respectively; see Fig. 5.3. The total system has 5 degrees of freedom, as shown in Fig. 5.3, which are $y(t)$, $v_A(t)$, $v_B(t)$, $\theta_A(t)$, $\theta_B(t)$. If there is no soil-structure interaction effect, $v_A(t)$ and $v_B(t)$ will be equal to the corresponding ground motions v_{gA} and v_{gB} , respectively, and $\theta_A(t)$ and $\theta_B(t)$ will be zero. The general equilibrium equations for the structural system can be written as

$$\underline{M} \ddot{\underline{r}}^t + \underline{C} \dot{\underline{r}}^t + \underline{K} \underline{r}^t = \underline{p}(t) \quad (5.13)$$

where $\underline{p}(t)$ is the interaction force vector which will be discussed later. Equation (5.13) can be rewritten in the matrix form

$$\begin{pmatrix} m & 0 & 0 & 0 & 0 \\ 0 & m_A & 0 & 0 & 0 \\ 0 & 0 & m_B & 0 & 0 \\ 0 & 0 & 0 & J_A & 0 \\ 0 & 0 & 0 & 0 & J_B \end{pmatrix} \begin{pmatrix} \ddot{y}^t \\ \ddot{v}_A \\ \ddot{v}_B \\ \ddot{\theta}_A \\ \ddot{\theta}_B \end{pmatrix} + \begin{pmatrix} c & 0 & 0 & 0 & 0 \\ 0 & 0 & 0 & 0 & 0 \\ 0 & 0 & 0 & 0 & 0 \\ 0 & 0 & 0 & 0 & 0 \\ 0 & 0 & 0 & 0 & 0 \end{pmatrix} \begin{pmatrix} \dot{y}^t \\ \dot{v}_A \\ \dot{v}_B \\ \dot{\theta}_A \\ \dot{\theta}_B \end{pmatrix} + \begin{pmatrix} \frac{24EI}{L^3} & \frac{-12EI}{L^3} & \frac{-12EI}{L^3} & \frac{6EI}{L^2} & \frac{6EI}{L^2} \\ \frac{-12EI}{L^3} & \frac{12EI}{L^3} & 0 & \frac{6EI}{L^2} & 0 \\ \frac{-12EI}{L^3} & 0 & \frac{12EI}{L^3} & 0 & \frac{6EI}{L^2} \\ \frac{6EI}{L^2} & \frac{6EI}{L^2} & 0 & \frac{4EI}{L} & 0 \\ \frac{6EI}{L^2} & 0 & \frac{6EI}{L^2} & 0 & \frac{4EI}{L} \end{pmatrix} \begin{pmatrix} y^t \\ v_A \\ v_B \\ \theta_A \\ \theta_B \end{pmatrix} = \begin{pmatrix} 0 \\ V_A \\ V_B \\ M_A \\ M_b \end{pmatrix} \quad (5.14)$$

where V_A , V_B , M_A , and M_B are the corresponding interaction shear forces and moments.

The total displacement vector \underline{r}^t can be partitioned into the dynamic displacement vector \underline{r}^d and the quasi-static displacement vector \underline{r}^{qs} as

$$\underline{r}^t = \begin{pmatrix} y^{qs} \\ v_{gA} \\ v_{gB} \\ 0 \\ 0 \end{pmatrix} + \begin{pmatrix} r^d \\ v_A^d \\ v_B^d \\ \theta_A \\ \theta_B \end{pmatrix} = \underline{r}^{qs} + \underline{r}^d \quad (5.15)$$

where v_A^d and v_B^d are the dynamic interaction displacements at the foundations A and B , and θ_A and θ_B are the interaction rotations at foundations A and B . The quasi-static displacement y^{qs} can be determined by substituting Eq.(5.15) into Eq.(5.14), and setting all the dynamic terms to zero, then

$$y^{qs} = \frac{1}{2}(v_{gA} + v_{gB}) \quad (5.16)$$

It can be noted that this equation is the same as Eq.(5.4) for the case of no soil-structure interaction effect.

By substituting Eq.(5.15) into Eq.(5.14), Eq.(5.14) becomes

$$\underline{M} \ddot{r}^d(t) + \underline{C} \dot{r}^d(t) + \underline{K} r^d(t) = -\underline{M} \ddot{r}^{qs}(t) - \underline{C} \dot{r}^{qs}(t) - \underline{K} r^{qs}(t) + \underline{p}(t) \quad (5.17)$$

where $\underline{K} r^{qs}(t) = \underline{0}$; $\underline{C} \dot{r}^{qs}(t) = \underline{0}$, if stiffness proportional damping is used, and it is negligible for other types of damping. The final equation of motion reduces to

$$\underline{M} \ddot{r}^d(t) + \underline{C} \dot{r}^d(t) + \underline{K} r^d(t) = -\underline{M} \ddot{r}^{qs}(t) + \underline{p}(t) \quad (5.18)$$

Equation (5.18) can be solved either in the time domain or in the frequency domain. The equation in the frequency domain can be obtained from the Fourier transform of Eq.(5.18),

$$[-\bar{\omega}^2 \underline{M} + i\bar{\omega} \underline{C} + \underline{K}] \bar{r}^d(i\bar{\omega}) = -\underline{M} \ddot{\bar{r}}^{qs}(i\bar{\omega}) + \bar{p}(i\bar{\omega}) \quad (5.19)$$

where $\bar{r}^d(i\bar{\omega})$ is the dynamic response displacement vector; $\ddot{\bar{r}}^{qs}(i\bar{\omega})$ is the quasi-static displacement vector and $\bar{p}(i\bar{\omega})$ is the interaction force vector.

5.4 MDOF Structure with Soil-Structure Interaction Effects

The most commonly used method of treating soil-structure interaction is the substructure method, see Gutierrez and Chopra (1976), Kausel (1974), which partitions the total soil-structure system into two substructures: the structural system and the soil system. The equilibrium equations are formed separately for the two substructures; the equilibrium equations are solved for the upper structure with the soil-structure interaction effects being considered by the interaction forces which can be represented through a foundation impedance matrix. The foundation impedances are usually calculated independently of the upper structure. Another commonly used method is the hybrid method of Gupta, Lin, Penzien and Yeh (1980), which separates the soil volume into a near field and a far field; the far-field soil volume is modelled with an impedance matrix, in the same manner as in the substructure method, and the near-field soil volume is combined with the structural system. This method, which is a modification of the substructure method, has been proposed to eliminate the difficulties in calculating the impedance matrix for embedded structures required by the

direct substructure method. Detailed formulations of these methods, and their advantages and disadvantages can be found in the corresponding references. Only the substructure method formulation is presented here.

Assume there are n_s degrees of freedom for the upper structure, n_b degrees of freedom for the structure-foundation contact points, and n_f degrees of freedom for the soil volume of interest. The equations of motion for the upper structure are of the same form as given by Eq.(5.6), except that an interaction force vector \underline{p}_b is included. In this case, the equilibrium equations are given by

$$\begin{pmatrix} \underline{M}_s & \underline{0} \\ \underline{0} & \underline{M}_b \end{pmatrix} \begin{pmatrix} \ddot{\underline{r}}_s^t \\ \ddot{\underline{r}}_b^t \end{pmatrix} + \begin{pmatrix} \underline{C}_{ss} & \underline{C}_{sb} \\ \underline{C}_{bs} & \underline{C}_{bb} \end{pmatrix} \begin{pmatrix} \dot{\underline{r}}_s^t \\ \dot{\underline{r}}_b^t \end{pmatrix} + \begin{pmatrix} \underline{K}_{ss} & \underline{K}_{sb} \\ \underline{K}_{bs} & \underline{K}_{bb} \end{pmatrix} \begin{pmatrix} \underline{r}_s^t \\ \underline{r}_b^t \end{pmatrix} = \begin{pmatrix} \underline{0} \\ \underline{p}_b \end{pmatrix} \quad (5.20)$$

The total displacement response vector can again be partitioned into the dynamic response displacement and quasi-static displacement vectors

$$\begin{pmatrix} \underline{r}_s^t \\ \underline{r}_b^t \end{pmatrix} = \begin{pmatrix} \underline{r}_s^d \\ \underline{r}_b^d \end{pmatrix} + \begin{pmatrix} \underline{r}_s^{qs} \\ \underline{v}_g \end{pmatrix} \quad (5.21)$$

where \underline{r}_b^d is the interaction displacement vector at the structure-foundation contact points, and \underline{v}_g is the corresponding spatially correlated free-field ground motion vector.

The quasi-static displacements can be obtained by substituting Eq.(5.21) into Eq.(5.20) and setting all the dynamic terms to zero, so that

$$\underline{r}_s^{qs} = -\underline{K}_{ss}^{-1} \underline{K}_{sb} \underline{v}_g \quad (5.22)$$

The equations of motion can now be written in terms of the dynamic response displacements as

$$\begin{aligned} & \begin{pmatrix} \underline{M}_s & \underline{0} \\ \underline{0} & \underline{M}_b \end{pmatrix} \begin{pmatrix} \ddot{\underline{r}}_s^d \\ \ddot{\underline{r}}_b^d \end{pmatrix} + \begin{pmatrix} \underline{C}_{ss} & \underline{C}_{sb} \\ \underline{C}_{bs} & \underline{C}_{bb} \end{pmatrix} \begin{pmatrix} \dot{\underline{r}}_s^d \\ \dot{\underline{r}}_b^d \end{pmatrix} \\ & + \begin{pmatrix} \underline{K}_{ss} & \underline{K}_{sb} \\ \underline{K}_{bs} & \underline{K}_{bb} \end{pmatrix} \begin{pmatrix} \underline{r}_s^d \\ \underline{r}_b^d \end{pmatrix} = - \begin{pmatrix} \underline{M}_s & \underline{0} \\ \underline{0} & \underline{M}_b \end{pmatrix} \begin{pmatrix} -\underline{K}_{ss}^{-1} \underline{K}_{sb} \ddot{\underline{v}}_g \\ \ddot{\underline{v}}_g \end{pmatrix} \\ & - \begin{pmatrix} \underline{C}_{ss} & \underline{C}_{sb} \\ \underline{C}_{bs} & \underline{C}_{bb} \end{pmatrix} \begin{pmatrix} -\underline{K}_{ss}^{-1} \underline{K}_{sb} \dot{\underline{v}}_g \\ \dot{\underline{v}}_g \end{pmatrix} - \begin{pmatrix} \underline{K}_{ss} & \underline{K}_{sb} \\ \underline{K}_{bs} & \underline{K}_{bb} \end{pmatrix} \begin{pmatrix} -\underline{K}_{ss}^{-1} \underline{K}_{sb} \underline{v}_g \\ \underline{v}_g \end{pmatrix} + \begin{pmatrix} \underline{0} \\ \underline{p}_b \end{pmatrix} \end{aligned} \quad (5.23)$$

The damping term at the right hand side of this equation is zero when stiffness proportional damping is used, and it can be dropped for other forms of damping as it has a negligible effect on the response. Further, the stiffness term on the right hand side is zero since the stiffness matrix is singular. Therefore, Eq.(5.23) can be reduced to

$$\begin{pmatrix} \underline{M}_s & \underline{0} \\ \underline{0} & \underline{M}_b \end{pmatrix} \begin{pmatrix} \ddot{\underline{r}}_s^d \\ \ddot{\underline{r}}_b^d \end{pmatrix} + \begin{pmatrix} \underline{C}_{ss} & \underline{C}_{sb} \\ \underline{C}_{bs} & \underline{C}_{bb} \end{pmatrix} \begin{pmatrix} \dot{\underline{r}}_s^d \\ \dot{\underline{r}}_b^d \end{pmatrix} + \begin{pmatrix} \underline{K}_{ss} & \underline{K}_{sb} \\ \underline{K}_{bs} & \underline{K}_{bb} \end{pmatrix} \begin{pmatrix} \underline{r}_s^d \\ \underline{r}_b^d \end{pmatrix}$$

$$= \begin{pmatrix} \underline{M}_s \underline{K}_{ss}^{-1} \underline{K}_{sb} \ddot{\underline{v}}_g \\ -\underline{M}_b \ddot{\underline{v}}_g \end{pmatrix} + \begin{pmatrix} \underline{0} \\ \underline{p}_b \end{pmatrix} \quad (5.24)$$

Transforming Eq.(5.24) into the frequency domain, it becomes

$$\begin{aligned} & \{-\bar{\omega}^2 \begin{pmatrix} \underline{M}_s & \underline{0} \\ \underline{0} & \underline{M}_b \end{pmatrix} + i\bar{\omega} \begin{pmatrix} \underline{C}_{ss} & \underline{C}_{sb} \\ \underline{C}_{bs} & \underline{C}_{bb} \end{pmatrix} + \begin{pmatrix} \underline{K}_{ss} & \underline{K}_{sb} \\ \underline{K}_{bs} & \underline{K}_{bb} \end{pmatrix}\} \begin{pmatrix} \underline{r}_s^d(i\bar{\omega}) \\ \underline{r}_b^d(i\bar{\omega}) \end{pmatrix} \\ & = \begin{pmatrix} \underline{M}_s \underline{K}_{ss}^{-1} \underline{K}_{sb} \ddot{\underline{v}}_g(i\bar{\omega}) \\ -\underline{M}_b \ddot{\underline{v}}_g(i\bar{\omega}) \end{pmatrix} + \begin{pmatrix} \underline{0} \\ \underline{p}_b(i\bar{\omega}) \end{pmatrix} \end{aligned} \quad (5.25)$$

where interaction forces can be expressed in terms of the impedance matrix, $\underline{S}_I(i\bar{\omega})$. Suppose there is only one three-dimensional rigid mat foundation with 6 degrees of freedom, then the resultant interaction forces are

$$\begin{aligned} -\underline{p}_b(i\bar{\omega}) &= \begin{pmatrix} -V_x(i\bar{\omega}) \\ -M_y(i\bar{\omega}) \\ -V_y(i\bar{\omega}) \\ -M_x(i\bar{\omega}) \\ -P_z(i\bar{\omega}) \\ -M_z(i\bar{\omega}) \end{pmatrix} \\ &= \begin{pmatrix} S_{uu}(i\bar{\omega}) & S_{u\theta_y}(i\bar{\omega}) & 0 & 0 & 0 & 0 \\ S_{\theta_y u}(i\bar{\omega}) & S_{\theta_y \theta_y}(i\bar{\omega}) & 0 & 0 & 0 & 0 \\ 0 & 0 & S_{vv}(i\bar{\omega}) & S_{v\theta_x}(i\bar{\omega}) & 0 & 0 \\ 0 & 0 & S_{\theta_x v}(i\bar{\omega}) & S_{\theta_x \theta_x}(i\bar{\omega}) & 0 & 0 \\ 0 & 0 & 0 & 0 & S_{ww}(i\bar{\omega}) & 0 \\ 0 & 0 & 0 & 0 & 0 & S_{\theta_x \theta_x}(i\bar{\omega}) \end{pmatrix} \begin{pmatrix} \bar{u} \\ \bar{\theta}_y \\ \bar{v} \\ \bar{\theta}_x \\ \bar{w} \\ \bar{\theta}_z \end{pmatrix} \end{aligned} \quad (5.26)$$

or

$$-\underline{p}_b(i\bar{\omega}) = \underline{S}_I(i\bar{\omega}) \underline{r}_b^d(i\bar{\omega}) \quad (5.27)$$

If there are m such foundations, and it is assumed that they are independent of each other, the total foundation impedance matrix becomes

$$\underline{S}_I(i\bar{\omega}) = \begin{pmatrix} \underline{S}_{I1} & \underline{0} & \dots & \underline{0} \\ \underline{0} & \underline{S}_{I2} & \dots & \underline{0} \\ \vdots & \vdots & \ddots & \vdots \\ \underline{0} & \underline{0} & \dots & \underline{S}_{Im} \end{pmatrix} \quad (5.28)$$

Substituting Eq.(5.27) into Eq.(5.25), one obtains

$$\begin{aligned} & \{-\bar{\omega}^2 \begin{pmatrix} \underline{M}_s & \underline{0} \\ \underline{0} & \underline{M}_b \end{pmatrix} + i\bar{\omega} \begin{pmatrix} \underline{C}_{ss} & \underline{C}_{sb} \\ \underline{C}_{bs} & \underline{C}_{bb} \end{pmatrix} + \begin{pmatrix} \underline{K}_{ss} & \underline{K}_{sb} \\ \underline{K}_{bs} & \underline{K}_{bb} + \underline{S}_I \end{pmatrix}\} \begin{pmatrix} \underline{r}_s^d(i\bar{\omega}) \\ \underline{r}_b^d(i\bar{\omega}) \end{pmatrix} \\ & = \begin{pmatrix} \underline{M}_s \underline{K}_{ss}^{-1} \underline{K}_{sb} \ddot{\underline{v}}_g(i\bar{\omega}) \\ -\underline{M}_b \ddot{\underline{v}}_g(i\bar{\omega}) \end{pmatrix} \end{aligned} \quad (5.29)$$

The above formulations are based on the viscous damping assumption. If the hysteretic damping assumption is used, then, the stiffness matrix is modified to

$$\underline{K}^* = (1 + iG)\underline{K} \quad (5.30)$$

and the viscous damping term is dropped; thus, Eq.(5.29) becomes

$$\{-\bar{\omega}^2 \begin{pmatrix} \underline{M}_s & \underline{0} \\ \underline{0} & \underline{M}_b \end{pmatrix} + \begin{pmatrix} \underline{K}_{ss}^* & \underline{K}_{sb}^* \\ \underline{K}_{bs}^* & \underline{K}_{bb}^* + \underline{S}_I \end{pmatrix}\} \begin{pmatrix} \bar{r}_s^d(i\bar{\omega}) \\ \bar{r}_b^d(i\bar{\omega}) \end{pmatrix} = \begin{pmatrix} \underline{M}_s \underline{K}_{ss}^{-1} \underline{K}_{sb} \ddot{\bar{v}}_g(i\bar{\omega}) \\ -\underline{M}_b \ddot{\bar{v}}_g(i\bar{\omega}) \end{pmatrix} \quad (5.31)$$

where the coefficient G can be determined by assuming the stress-strain relationship for viscoelastic material. $G = 2\xi$ for small damping ratios and $G = 2i\xi^2 + 2\xi\sqrt{1 + \xi^2}$ for large damping ratios, see Lysmer et al. (1975).

By summing the matrices on the left hand side of Eq.(5.29) or Eq.(5.31), the equation of motion for the upper structure in the substructure method can be written as

$$\begin{pmatrix} I_{ss}(i\bar{\omega}) & I_{sb}(i\bar{\omega}) \\ I_{bs}(i\bar{\omega}) & I_{bb}(i\bar{\omega}) + S_I(i\bar{\omega}) \end{pmatrix} \begin{pmatrix} \bar{r}_s^d(i\bar{\omega}) \\ \bar{r}_b^d(i\bar{\omega}) \end{pmatrix} = \begin{pmatrix} \underline{M}_s \underline{K}_{ss}^{-1} \underline{K}_{sb} \ddot{\bar{v}}_g(i\bar{\omega}) \\ -\underline{M}_b \ddot{\bar{v}}_g(i\bar{\omega}) \end{pmatrix} \quad (5.32)$$

where $I_{ij}(i\bar{\omega})$ is the corresponding sub-matrix obtained by summing up the mass, damping and stiffness matrices.

5.5 Impedance Matrix

Determining the foundation impedance matrix is one of the key elements in the formulation of the substructure method of treating soil-structure interaction effects. For a single rigid mat foundation sitting on soil, the 6×6 impedance matrix relates the interaction forces that the foundation exerts on the soil to the interaction displacements at the foundation. The impedance matrix depends on the geometry of the foundation, on the soil characteristics, on the nature of the contact between the foundation and the soil, and on the excitation frequencies (Luco, 1982).

Evaluation of the impedance matrix for a rigid foundation is a mixed boundary value problem, in which the displacements between the foundation and soil are prescribed and the tractions on the free soil surface outside the mat foundation are zero. Usually, the problem can be reduced to Fredholm integral equations of the second type. Veletsos and Wei (1971) and Luco and Westmann (1971) evaluated the impedances for a rigid circular plate resting on a uniform half space. Wong (1975), and Wong and Luco (1976) evaluated the impedances for a rigid foundation of an arbitrary shape resting on the surface of the half space. Luco (1976) evaluated the impedances of a rigid circular foundation on a multilayered viscoelastic half space. Wong and Luco (1985) presented tables of impedances for a square plate resting on layered soil. The impedances for various types of embedded foundations have also been

calculated. Liou (1988) developed a method to obtain closed form solutions for embedded foundations on layered soil.

The impedances obtained by previous authors can be used as follows:

Each impedance function is of the form

$$S_f(i\bar{\omega}) = G^R(a_o) + iG^I(a_o) \quad (5.33)$$

where $a_o = \frac{R_p \bar{\omega}}{c_s}$ is a dimensionless frequency parameter. R_p is related to the dimensions of the foundation plate: for a circular plate foundation, R_p is the radius of the plate, and for a rectangular plate foundation for $a \doteq b$, $R_p = \sqrt{4ab/\pi}$, where a and b are the dimensions of the foundation. C_s is the shear wave velocity in the soil;

$$c_s = \sqrt{\frac{G}{\rho}} \quad (5.34)$$

where G is the shear modulus and ρ is the density of the soil.

The impedance values are usually given in terms of α and β , as shown in Fig. 5.4; see Penzien (1976). These results were obtained by Veletsos and Wei (1971) for a circular rigid foundation on an elastic half space. The impedance values can be obtained using

$$G^R(a_o) = \frac{4GR_p\alpha_v}{1-\nu} \quad (5.35)$$

$$G^I(a_o) = \frac{4GR_p a_o \beta_v}{1-\nu} \quad (5.36)$$

for the vertical translational degrees of freedom;

$$G^R(a_o) = \frac{8GR_p\alpha_t}{2-\nu} \quad (5.37)$$

$$G^I(a_o) = \frac{8GR_p a_o \beta_t}{2-\nu} \quad (5.38)$$

for the lateral translational degrees of freedom;

$$G^R(a_o) = \frac{8GR_p^3\alpha_m}{3(1-\nu)} \quad (5.39)$$

$$G^I(a_o) = \frac{8GR_p^3 a_o \beta_m}{3(1-\nu)} \quad (5.40)$$

for the rocking degrees of freedom;

$$G^R(a_o) = \frac{8GR_p^2\alpha_{tm}}{2-\nu} \quad (5.41)$$

$$G^I(a_o) = \frac{8GR_p^2 a_o \beta_{tm}}{2 - \nu} \quad (5.42)$$

for the rocking and lateral translational coupling terms; and

$$G^R(a_o) = \frac{16GR_p^3 \alpha_{to}}{3} \quad (5.43)$$

$$G^I(a_o) = \frac{16GR_p^3 a_o \beta_{to}}{3} \quad (5.44)$$

for the torsional degrees of freedom. Where ν is the Poisson ratio of the soil for a homogeneous half space, or the Poisson ratio in the first layer of the layered foundation.

5.6 Numerical Methods

Since the interaction forces depend on the excitation frequencies and the impedances are expressed in terms of the frequency, the substructure formulation is solved in the frequency domain.

In order to obtain the response time-history $\mathbf{r}^d(t)$, Eq.(5.32) should be solved at every discrete frequency inside the range of interest. It is very time consuming to solve the equation at all the frequency points. Fortunately, Tajirian (1981) has suggested an approximate interpolation function, based on the response function of a two DOF structure, given by

$$y(i\bar{\omega}) = \frac{c_{1j}\bar{\omega}^4 + c_{2j}\bar{\omega}^2 + c_{3j}}{\bar{\omega}^4 + c_{4j}\bar{\omega}^2 + c_{5j}} \quad (5.45)$$

where $y(i\bar{\omega})$ is the interpolated response value, c_{ij} are complex coefficients to be determined, and j refers to the subdivided frequency range.

With this interpolation function, the response function only needs to be solved at fewer selected frequency points, then its values at other points can be obtained by the interpolation method. Since the interpolation function was based on the response function of a two DOF structure, the interpolation range should be chosen assuming that only two modes contribute significantly to the response in that range, and that the contributions from other modes are negligible. In each range j , five discrete frequencies $\bar{\omega}_i$, $i = 1, 2, 3, 4, 5$, are selected; at these five selected frequencies, Eq.(5.32) is solved in order to determine the coefficients c_{ij} . The selection of these five frequencies in each range j depends on the rapidity with which the responses vary with the excitation frequency. The frequency points should be closely spaced in the range where the responses vary sharply, and widely spaced in the range where the responses vary slowly. This can be achieved by imposing a control constant b (Fok and Chopra, 1985). Suppose $\bar{\mathbf{r}}_{ij}^d(i\bar{\omega}_i)$ is the response vector solved at the frequency $\bar{\omega}_i$ for the range j , and $\bar{\mathbf{r}}_{(i-1)j}^d(i\bar{\omega}_{i-1})$ is solved at the frequency $\bar{\omega}_{i-1}$, then the frequency interval can

be determined as

$$\Delta\bar{\omega}_i = \Delta\bar{\omega}_{i-1} \frac{b}{\max\left(\frac{\bar{r}_{ij}^d(i\bar{\omega}_i) - \bar{r}_{(i-1)j}^d(i\bar{\omega}_{i-1})}{\bar{r}_{ij}^d(i\bar{\omega}_i)}\right)} \quad (5.46)$$

where $\max\left(\frac{\bar{r}_{ij}^d(i\bar{\omega}_i) - \bar{r}_{(i-1)j}^d(i\bar{\omega}_{i-1})}{\bar{r}_{ij}^d(i\bar{\omega}_i)}\right)$ is the maximum absolute value calculated by using all the possible component in vectors \bar{r}_{ij}^d and $\bar{r}_{(i-1)j}^d$. With $\Delta\bar{\omega}_i$, the next discrete frequency value can be obtained:

$$\bar{\omega}_{i+1} = \bar{\omega}_i + \Delta\bar{\omega}_i \quad (5.47)$$

Sometimes, an impractically small or large value of $\Delta\bar{\omega}_i$ is obtained depending on the calculated vectors \bar{r}_{ij}^d and $\bar{r}_{(i-1)j}^d$, so that it is necessary to set $\Delta\bar{\omega}_{max}$ and $\Delta\bar{\omega}_{min}$ values.

After five discrete frequency points have been selected in each range j , Eq.(5.32) can be solved, and the five constants c_{ij} for each DOF k can be determined as

$$\begin{pmatrix} \bar{\omega}_1^4 & \bar{\omega}_1^2 & 1 & -\bar{r}_{1j}^d \bar{\omega}_1^2 & -\bar{r}_{1j}^d \\ \bar{\omega}_2^4 & \bar{\omega}_2^2 & 1 & -\bar{r}_{2j}^d \bar{\omega}_2^2 & -\bar{r}_{2j}^d \\ \bar{\omega}_3^4 & \bar{\omega}_3^2 & 1 & -\bar{r}_{3j}^d \bar{\omega}_3^2 & -\bar{r}_{3j}^d \\ \bar{\omega}_4^4 & \bar{\omega}_4^2 & 1 & -\bar{r}_{4j}^d \bar{\omega}_4^2 & -\bar{r}_{4j}^d \\ \bar{\omega}_5^4 & \bar{\omega}_5^2 & 1 & -\bar{r}_{5j}^d \bar{\omega}_5^2 & -\bar{r}_{5j}^d \end{pmatrix}_k \begin{pmatrix} c_{1j} \\ c_{2j} \\ c_{3j} \\ c_{4j} \\ c_{5j} \end{pmatrix}_k = \begin{pmatrix} \bar{r}_{1j}^d \bar{\omega}_1^4 \\ \bar{r}_{2j}^d \bar{\omega}_2^4 \\ \bar{r}_{3j}^d \bar{\omega}_3^4 \\ \bar{r}_{4j}^d \bar{\omega}_4^4 \\ \bar{r}_{5j}^d \bar{\omega}_5^4 \end{pmatrix}_k \quad k = 1, 2, \dots, n \quad (5.48)$$

where $n = n_s + n_b$ is the total number of degrees of freedom. Using the coefficients determined, the frequency response values at all other discrete frequency points in that range can be determined by the interpolation function.

If n_s is very large, solving Eq.(5.32) directly becomes very expensive. A good improvement can be achieved using the normal modes of vibration to modify the equation before solving it. For the structure only, the vibration modes can be obtained as

$$[\underline{K}_{s,s} - \omega^2 \underline{M}_s] \underline{\Phi}_s = 0 \quad (5.49)$$

where $\underline{K}_{s,s}$ and \underline{M}_s are the stiffness and lumped mass matrices of the upper structure as given before. By solving this eigenvalue problem, l ($l \ll n_s$) natural frequencies $\omega_1, \omega_2, \dots, \omega_l$ and the corresponding vibration mode shapes $\underline{\phi}_1, \underline{\phi}_2, \dots, \underline{\phi}_l$ can be obtained. By forming an $n_s \times l$ mode shape matrix $\underline{\Phi}$,

$$\underline{\Phi} = (\underline{\phi}_1 \quad \underline{\phi}_2 \quad \dots \quad \underline{\phi}_l) \quad (5.50)$$

The dynamic response \bar{r}^d can be approximated as

$$\begin{pmatrix} \bar{r}_s^d \\ \bar{r}_b^d \end{pmatrix} = \begin{pmatrix} \underline{\Phi} & \underline{\gamma} \\ \underline{0} & \underline{I} \end{pmatrix} \begin{pmatrix} \underline{v}_s \\ \underline{v}_b \end{pmatrix} = \underline{QY} \quad (5.51)$$

where \underline{I} is a $n_b \times n_b$ identity matrix, and $\underline{\gamma} = -\underline{K}_{s,s}^{-1} \underline{K}_{s,b}$ is the influence coefficient matrix.

Substituting Eq.(5.51) into Eq.(5.24), and premultiplying both sides of Eq.(5.24) by \underline{Q}^T results in

$$\begin{aligned}
& \left(\begin{array}{cccc} m_1 & 0 & \dots & 0 \\ 0 & m_2 & \dots & 0 \\ \vdots & \vdots & \ddots & \vdots \\ 0 & 0 & \dots & m_l \end{array} \right) \begin{array}{c} \underline{\Phi}^T \underline{M}_s \underline{\gamma} \\ \underline{\gamma}^T \underline{M}_s \underline{\Phi} \\ \underline{\gamma}^T \underline{M}_s \underline{\gamma} + \underline{M}_b \end{array} \begin{pmatrix} \ddot{\underline{v}}_s \\ \ddot{\underline{v}}_b \end{pmatrix} \\
& + \left(\begin{array}{cccc} 2\xi_1 \omega_1 m_1 & 0 & \dots & 0 \\ 0 & 2\xi_2 \omega_2 m_2 & \dots & 0 \\ \vdots & \vdots & \ddots & \vdots \\ 0 & 0 & \dots & 2\xi_l \omega_l m_l \end{array} \right) \begin{array}{c} \underline{0} \\ \underline{0} \end{array} \begin{pmatrix} \dot{\underline{v}}_s \\ \dot{\underline{v}}_b \end{pmatrix} \\
& + \left(\begin{array}{cccc} \omega_1^2 m_1 & 0 & \dots & 0 \\ 0 & \omega_2^2 m_2 & \dots & 0 \\ \vdots & \vdots & \ddots & \vdots \\ 0 & 0 & \dots & \omega_l^2 m_l \end{array} \right) \begin{array}{c} \underline{0} \\ \underline{0} \end{array} \begin{pmatrix} \underline{v}_s \\ \underline{v}_b \end{pmatrix} \\
& = -\underline{Q}^T \begin{pmatrix} \underline{M}_s & \underline{0} \\ \underline{0} & \underline{M}_b \end{pmatrix} \begin{pmatrix} -\underline{K}_{s,s}^{-1} \underline{K}_{s,b} \ddot{\underline{v}}_g \\ \ddot{\underline{v}}_g \end{pmatrix} + \underline{Q}^T \begin{pmatrix} \underline{0} \\ \underline{p}_b \end{pmatrix} \quad (5.52)
\end{aligned}$$

Transforming the above equation to the frequency domain gives

$$\begin{aligned}
& [-\bar{\omega}^2 \left(\begin{array}{cccc} m_1 & 0 & \dots & 0 \\ 0 & m_2 & \dots & 0 \\ \vdots & \vdots & \ddots & \vdots \\ 0 & 0 & \dots & m_l \end{array} \right) \begin{array}{c} \underline{\Phi}^T \underline{M}_s \underline{\gamma} \\ \underline{\gamma}^T \underline{M}_s \underline{\Phi} \\ \underline{\gamma}^T \underline{M}_s \underline{\gamma} + \underline{M}_b \end{array} \begin{pmatrix} \ddot{\underline{v}}_s(i\bar{\omega}) \\ \ddot{\underline{v}}_b(i\bar{\omega}) \end{pmatrix} + \\
& \left(\begin{array}{cccc} \omega_1^2 + i2\xi_1 \omega_1 \bar{\omega} m_1 & \dots & \dots & 0 \\ \vdots & \vdots & \ddots & \vdots \\ 0 & \dots & \omega_l^2 m_l + i2\xi_l \omega_l \bar{\omega} m_l & \dots \end{array} \right) \begin{array}{c} \underline{0} \\ \underline{0} \end{array} \begin{pmatrix} \underline{v}_s(i\bar{\omega}) \\ \underline{v}_b(i\bar{\omega}) \end{pmatrix} \Big| \underline{S}_I(i\bar{\omega}) \\
& = \underline{Q}^T \begin{pmatrix} \underline{M}_s \underline{K}_{s,s}^{-1} \underline{K}_{s,b} \\ -\underline{M}_b \end{pmatrix} \ddot{\underline{v}}_g(i\bar{\omega}) \quad (5.53)
\end{aligned}$$

The equation is now reduced to $l + n_b$ degrees of freedom for the upper structure.

5.7 Numerical Procedure

The procedure for solving the general structural system with soil-structure interaction effects excited by multiple inputs is given in the following:

1. Form the stiffness, damping and mass matrices for the structure-foundation system. Calculate the influence coefficient matrix $\gamma = -\underline{K}_{ss}^{-1} \underline{K}_{sb}$.
2. Form the impedance matrix $S_I(i\bar{\omega})$, taking into account the foundation and soil properties, and using the impedance results obtained previously such as those shown in Fig. 5.4 by Veletsos and Wei (1971), and Eqs.(5.35) through (5.44).
3. Form Eq.(5.24), and transform it to the frequency domain, and incorporate the impedance matrix $S_I(i\bar{\omega})$ to the equation to obtain Eq.(5.32).
4. If the structural system is very large, the mode decomposition method is applied first to the structural system as shown in the previous section.
5. Use the interpolation method to solve Eq.(5.32) or Eq.(5.53) in the range of 0 to $\bar{\omega}_{max}$, where $\bar{\omega}_{max}$ is the Nyquist frequency.
6. The control constant b , $\Delta\bar{\omega}_{min}$, and $\Delta\bar{\omega}_{max}$ should be determined first if the interpolation method is used.
7. The equation is solved starting at zero frequency, and $\Delta\bar{\omega}_1 = \Delta\bar{\omega}_{min}$. The next frequency point can be determined by Eqs.(5.46) and (5.47). Continue to solve the equation at the frequency points selected by this procedure. The last frequency point should be $\bar{\omega}_{max}$.
8. Subdivide the frequency points into ranges with the five points selected above as one range. $\bar{\omega}_{max}$ should be the last frequency point in the last range. If $\bar{\omega}_{max}$ is not, it can be forced to be by including the necessary points from the previous range.
9. In each range, the coefficients c_{ij} are determined by Eq.(5.48) for each vibration DOF. The frequency response values for this DOF in that range can be calculated by the interpolation function Eq.(5.45).
10. Calculate all the frequency responses for each DOF from 0 to $\bar{\omega}_{max}$.
11. Transform the calculated frequency responses back to the time domain to obtain the response time-histories.

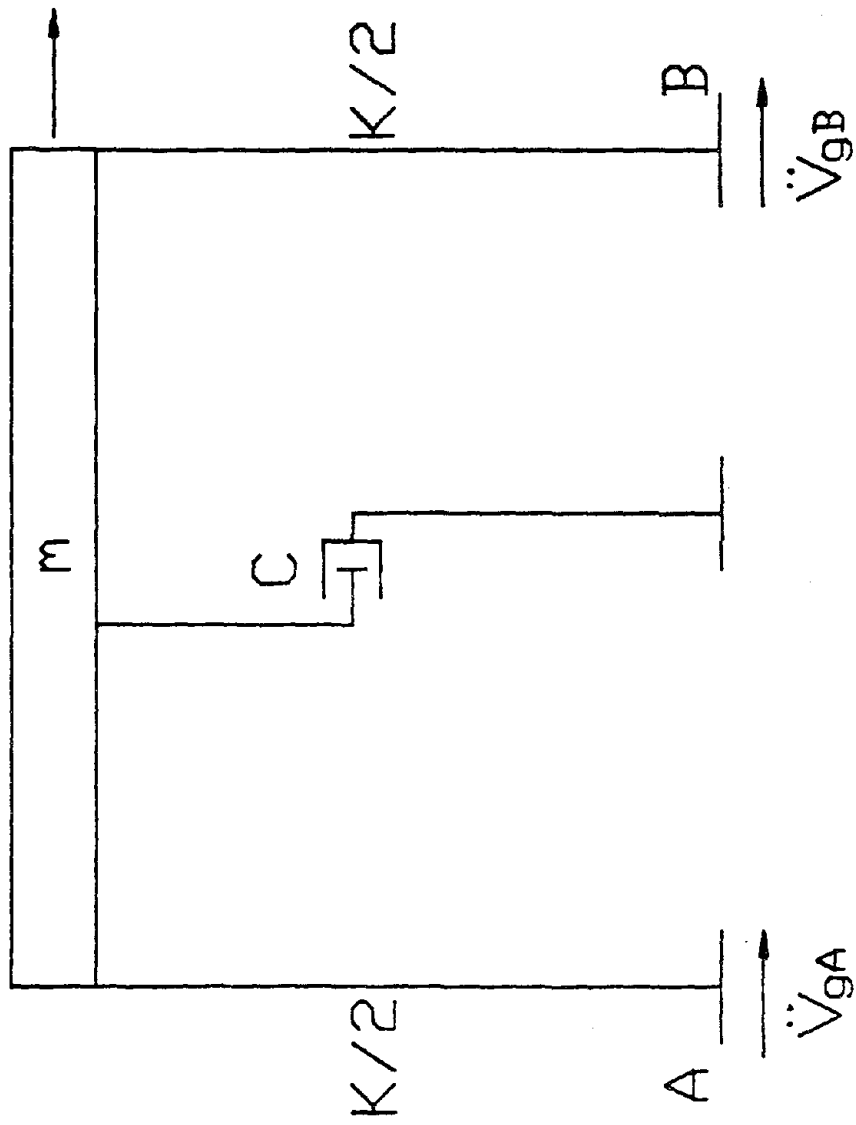


Fig.5.1 Simple SDOF Structure Supported at Points A and B

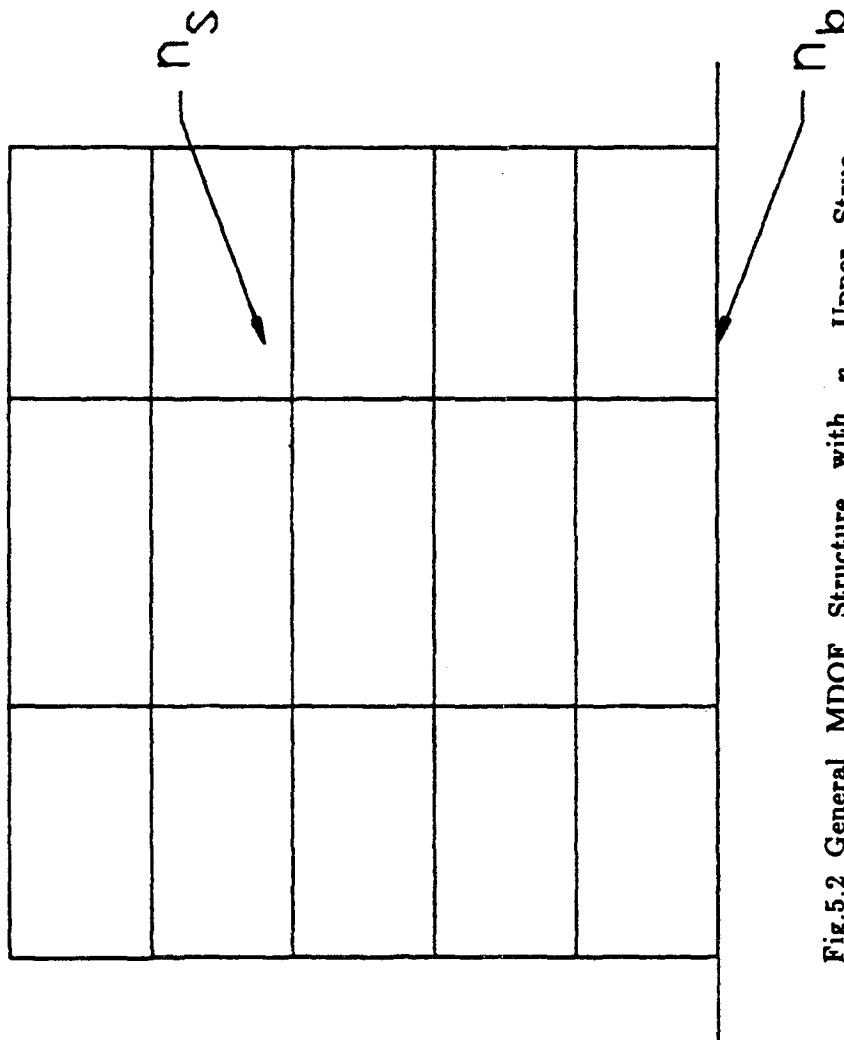


Fig.5.2 General MDOF Structure with n_s Upper Structure Degrees of Freedom and n_b Structure-Foundation Contact Degrees of Freedom

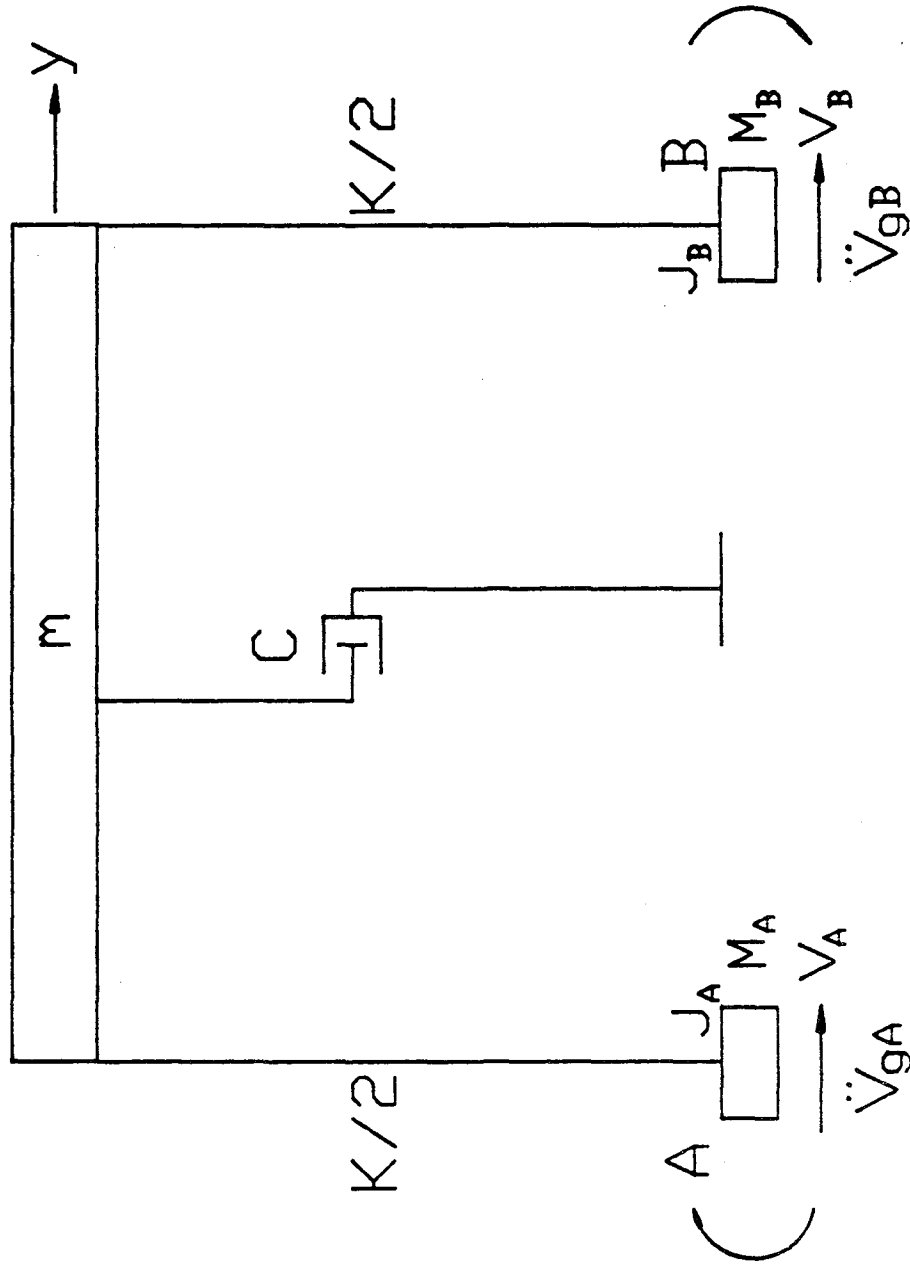
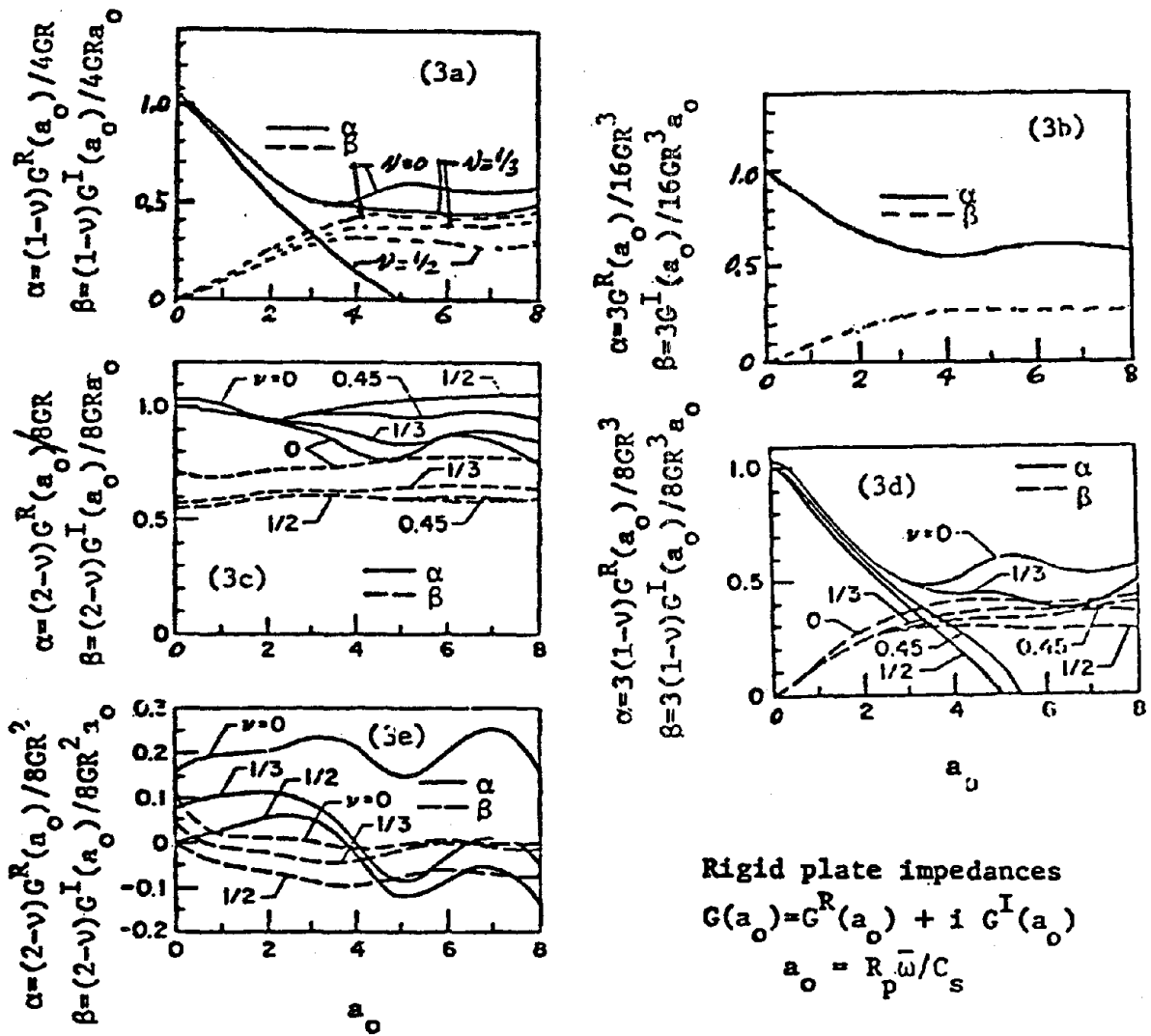


Fig.5.3 Simple SDOF Structure Supported at Points A and B with Two Independent Massless Foundation Mats



- (3a) Vertical translation
- (3b) Torsion
- (3c) Lateral translation
- (3d) Rocking
- (3e) Coupled lateral translation-rocking

Fig.5.4 Typical Impedance Values Obtained by Veletsos and Wei (1971)

CHAPTER 6 EXAMPLES

In the previous chapters, methods were presented for simulating spatially correlated multiple ground motions compatible with a prescribed response spectrum and for evaluating the structural responses to such motions. A computer program, named SSIAM, was developed for these methods and is used below to determine the response in two examples.

6.1 Description of the SSIAM Program

The program SSIAM (Soil-Structure Interaction Analysis with Multiple Inputs) was developed for the numerical methods discussed in the previous chapters. It is briefly described as follows:

1. First, the total number of nodes, the number of contact nodes for the structure and foundation, and the total number of element types in the system are read. The element types include 3D truss elements, 2D and 3D frame elements, 3 to 9 node plane stress and plane strain elements, and axisymmetric elements.
2. Then, the element properties are read, and the element stiffness matrix and lumped mass matrix are formulated.
3. The banded stiffness matrix and lumped mass matrix are formulated for the system, and then the hysteretic damping matrix according to Eq.(5.30).
4. Whether the spatially correlated multiple ground motions are simulated or given as inputs is next checked. If the ground motions are simulated, the program reads the quasi-stationary power spectral density functions, coherency functions, and shape functions. Equation (4.13) is used and all the ground motions are iterated until compatible with the given response spectrum.
5. These ground motions are interpolated to obtain the ground motions for the locations on the structure-foundation surface where the ground motions were not simulated.
6. The soil properties are read and the impedance matrix is formulated.
7. The total system is solved in the frequency domain using the interpolation technique.
8. The structural responses are transformed into the time domain.
9. The stresses and strains of the elements are calculated.

6.2 Verification of the SSIAM Program

Before the two examples were solved, the SSIAM computer program was tested using a three-story building with stiffness $k = 50.0$, mass $M = 10.0$ at each floor, and a damping ratio $\xi = 0.05$, as shown in Fig. 6.1. The responses of this building were solved by both SSIAM and the existing program CAL86 (Wilson, 1986). Figure 6.2 shows the displacement transfer function at the top floor for a unit harmonic excitation. The two results were obtained by SSIAM with and without using the interpolation technique. From the figure, one can see that both curves agree very well. Only about 5% of the effort spent to solve the equations without using the interpolation, was used if the interpolation was included. The natural frequencies obtained using SSIAM are $f_1 = 0.2197Hz$, $f_2 = 0.61035Hz$, and $f_3 = 0.952148Hz$, which are very close to the natural frequencies obtained using CAL86 and solved in the time domain; they are $f_1 = 0.22398Hz$, $f_2 = 0.62762Hz$, and $f_3 = 0.9068Hz$. The differences between the two sets of results increase as the mode increases. The largest error occurs in the third mode. It is about 4.7%.

To calculate the structural responses, two cycles of a sine wave with amplitude 1.0 and period π was chosen as the input, as shown in Fig. 6.3. The structural responses were first calculated using SSIAM with and without using the interpolation technique. The results are shown in Fig. 6.4. These results show very little differences. Figure 6.5 shows the results obtained using SSIAM and CAL86. It can be seen that both results match well. The result obtained using SSIAM does not start from rest because of the problem of a quiet zone in the frequency domain approach. It is expected that if a longer quiet zone is used, the starting value would be closer to zero.

From a close comparison of the results obtained using these two programs, it was concluded that SSIAM is reliable.

6.3 Example I, A Long Span Arch Beam

A 100m long span arch frame constructed by steel is considered; see Fig. 6.6: area $A = 1080cm^2$, moment of inertia $I = 40255000cm^4$, Young's modulus $E = 2043050kg/cm^2$, and density $\rho = 0.00783kg/cm^3$. Hysteretic type damping is used with damping ratio $\xi = 0.05$. A homogeneous half-space foundation is assumed for soil-structure interaction purposes; the soil properties used are: shear wave velocity $V_s = 130m/s$, shear modulus $G = 310kg/cm^2$, bulk density $\rho = 1.83 \times 10^{-6}kg/cm^3$, and Poisson's ratio $\nu = \frac{1}{3}$. Assume there is a massless rigid circular plate with radius $R_p = 6m$ at each support as in Fig. 6.6. These two plates are assumed to respond independently of each other. The impedances used for each plate were those obtained by previous authors, such as Veletsos and Wei (1971), which were derived for a rigid massless circular plate resting on the homogeneous half space; see Fig. 5.4.

Using SSLAM and neglecting shear and axial deformations, the structural responses under the spatially correlated multiple ground motion excitations were solved. The displacement transfer functions at Nodes 3, 6, and 9 in the horizontal direction were calculated by inputting unit excitations at both supports throughout the frequency range; see Figs. 6.7 through 6.9. The two spatially correlated ground motions were simulated using an apparent velocity $V_{app} = 3000m/s$. The coherency model described in section 3.6 was used for this purpose, i.e. Eq.(3.9). The parameters used in this model were those obtained for the NS component of Event 45; see chapter 3. Two Tajimi-Kanai power spectral density functions were used for two time windows of 0 – 9sec and 9 – 21sec to approximate the nonstationarity property of the ground motions. The two power spectral density functions were assumed to have the properties of $\xi_g = 0.63$, $\omega_g = 0.9Hz$ and $\xi_g = 0.1$, $\omega_g = 0.5Hz$, respectively. The power spectral density function for the second window was purposely chosen to have a low central frequency and a low damping ratio. This low frequency was chosen because long span structures usually have low vibration frequencies. The frequency range of the simulated ground motions was selected to cover the structural primary vibration mode. The Bogdanoff type shape function of Eq.(3.4) was used with its peak acceleration occurring at $t = 8sec$. The simulated ground motions were made response spectrum compatible using the Newmark and Hall design response spectrum of damping ratio $\xi = 0.05$ and normalized to the peak ground acceleration of $0.5g$. The two simulated ground motions are shown in Fig. 6.10.

In order to see the effects of the ground motion phase differences on the structural responses, two other sets of spatially correlated ground motions were generated using all of the above ground motion properties, except for the apparent wave velocity. The apparent wave velocities used for the three cases were $V_{app} = 3000m/s$ (Case 1), $V_{app} = 1500m/s$ (Case 2), and $V_{app} = 300m/s$ (Case 3). The simulated ground motions in these three cases were derived from the same power spectral density and the same intensity function, and were made compatible with the same Newmark and Hall design response spectrum. The only differences among these three sets of ground motions were the phase differences between the two ground motions in each set. The results calculated in both the time and frequency domains using these three sets of ground motions as spatially correlated ground motion multiple inputs, are shown in Figs. 6.11 through 6.16. From these results, it can be noted that the peaks of the structural responses are reduced due to the effect of phase differences in the input ground motion time-histories; the larger the phase differences, the smaller the structural responses. This result is consistent with the previous results obtained by Loh, Penzien and Tsai (1982), and Abrahamson and Bolt (1985). From Figs. 6.14 through 6.16, it is also seen that the phase differences in the multiple input ground motions introduce corresponding phase differences or time lags in the structural responses; the larger the phase differences of the multiple input ground motions, the larger the phase differences or time delay in the

corresponding structural responses. The time lag between the structural responses obtained by single input and multiple inputs is in the range of 0sec to the time lag of the multiple input ground motions. For example, the time lag between the two ground motion time-histories for Case 1 is $\tau = 0.03333\text{sec}$, and the time lag between the ground motion time-histories for Case 3 is $\tau = 0.3333\text{sec}$; then, the time lag between the structural responses obtained by these two input cases is in the range of 0sec to $\hat{\tau} = 0.3\text{sec}$. Another observation is that, when using the multiple inputs, the structural responses are no longer symmetrical. For example, the structural responses at Nodes 3 and 9 are the same by the symmetry property when a single rigid foundation input assumption is used, see Figs. 6.7 and 6.9. When using multiple inputs, the structural responses at these two nodes are not the same, see Figs. 6.14 and 6.16. This conclusion is obvious because of the non-symmetry of the multiple inputs.

To compare the differences between the structural responses obtained using multiple inputs and a single input, the displacement response in the horizontal direction at Node 6 is calculated using the simulated ground motions for $V_{app} = 3000\text{m/sec}$ as the multiple inputs; this case is now called Case 1. In Case 2, the structural response at the same degree of freedom is calculated using the first time-history of the two simulated ground motion time-histories as the single input. And in Case 3, the response is calculated using the second time-history as the single input. The results for these three cases are shown in Figs. 6.17 and 6.18. From these results, it can be noted that the structural response obtained in Case 1 is the average of the responses obtained in Case 2 and Case 3. This conclusion is reasonable because of the linear property in the structural response calculation. From Figs. 6.17 and 6.18, it is also noted that the phases in the responses in these three cases are different. The peak response using multiple inputs is less than those using single input. Neither of the single input cases can be used to represent the multiple input case. Another case calculated used the averaged time-history of the multiple ground motion input time-histories as the single input to calculate the structural responses and a comparison was made with the results obtained using multiple inputs. This showed again that the structural response using multiple inputs cannot be represented by that using a single input because of the phase differences.

6.4 Example II, A Long Span Continuous Beam

A three span continuous beam structure with 100m per span was considered, see Fig. 6.19. Assume the structure was constructed by steel with Young's modulus $E = 2043050\text{kg/cm}^2$; mass density $\rho = 0.00783\text{kg/cm}^3$; area of the cross section $A = 1500\text{cm}^2$; and the moment of inertia $I = 1.315 \times 10^9\text{cm}^4$. Hysteretic type damping was used with the damping ratio $\xi = 0.05$. A massless rigid circular plate with radius $R_p = 20\text{m}$ was assumed to be placed at each support. An homogeneous half space with bulk density $\rho = 1.83 \times 10^{-6}\text{kg/cm}^3$, shear modulus $G = 310.0\text{kg/cm}^2$, shear wave velocity $V_s = 130\text{m/s}$, and Poisson's ratio $\nu = \frac{1}{3}$

was assumed. It was also assumed that the soil-structure interaction effects of the rigid plates at the supports were independent of each other. The results obtained by Veletsos and Wei (1971), shown in Fig. 5.4, were again used.

SSIAM was used to solve the problem. The structural responses were calculated by neglecting all shear and axial deformations. The displacement transfer function was calculated for the midpoint of the central span in the vertical direction. The result is shown in Fig. 6.20. Two spatially correlated ground motion time-histories were simulated to serve as the multiple inputs at Nodes 1 and 31 in the vertical direction. All the specified ground motion properties used in Example I were used here. The ground motions were simulated for three different cases using three different apparent wave velocities: $V_{app} = 3000m/sec$ (Case 1), $V_{app} = 1500m/sec$ (Case 2), and $V_{app} = 300m/sec$ (Case 3). The multiple input ground motion time-histories at Nodes 11 and 21 were obtained by interpolating the two simulated ground motion time-histories. All the ground motion time-histories were iterated until compatible with the Newmark and Hall design response spectrum with 5% damping and normalized to the 0.5g PGA level. The displacement responses at midpoint of the central span in the vertical direction were calculated for the three cases. The results in both the frequency domain and time domain are shown in Figs. 6.21 and 6.22. From these results, it is noted that the conclusions made for Example I are still valid. Figures 6.23 and 6.24 show comparisons between the vertical displacement responses at the midpoint of the central span calculated using single and multiple inputs. The single input time-history used is the first time-history of the four time-histories used for multiple inputs. Again, it is noted that the displacement response calculated for multiple inputs is smaller than that calculated for the single input.

To investigate differential displacements in the structure, which can cause higher shear stresses and usually damage some kinds of structures such as pipelines, the vertical displacements at two symmetric nodes, 12 and 20, were calculated using single input and multiple inputs. The results for both single and multiple inputs at Node 12 in the frequency domain and in the time domain are shown in Figs. 6.25 and 6.26. Like the previously obtained results, they show the property that using multiple inputs reduces the structural responses. The responses obtained for the single input at Node 20 are the same as those obtained for Node 12 by symmetry property. The results at Nodes 12 and 20 in the frequency domain and in the time domain for multiple inputs are shown in Figs. 6.27 and 6.28. It can be noted that the two responses are not the same; hence, the differential displacements were produced. This observation is consistent with the results obtained by Zerva, Ang and Wen (1988) using spectral analysis, and the results obtained by Somaini (1988) using simple harmonic plane waves travelling across the structure site. Figure 6.29 shows the differential displacement between Nodes 12 and 20 calculated for multiple inputs.

6.5 Conclusions

The following conclusions are based on the results for the calculated examples and the previous discussion:

1. The results calculated in the frequency domain by the program SSIAM agree well with the results calculated in the time domain by the existing program CAL86; and they are consistent with the results obtained by various authors such as Loh, Penzien and Tsai (1982), Abrahamson and Bolt (1985), Zerva, Ang and Wen (1988), and Somaini (1988).
2. The structural responses are reduced by using multiple inputs because of the effects of phase differences in the input ground motions; the larger the phase differences, the bigger the reductions.
3. The responses obtained using multiple inputs cannot be represented by using a single input.
4. The responses produced by multiple inputs have time delays due to the phase differences in the input motions. The delay times increase as the phase differences of the input ground motions increase.
5. Dynamic responses are reduced when using multiple inputs rather than a single rigid base input; however, quasi-static responses are produced when using multiple inputs which are not produced by a single rigid base input.

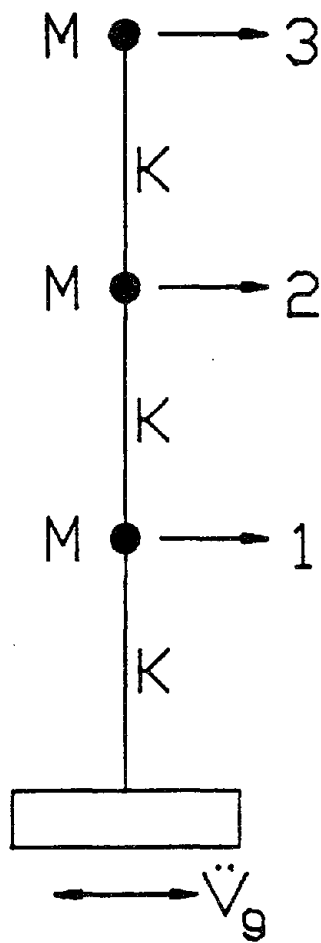


Fig.6.1 Simple Three-Story Building Models for the Program SSIAM Test

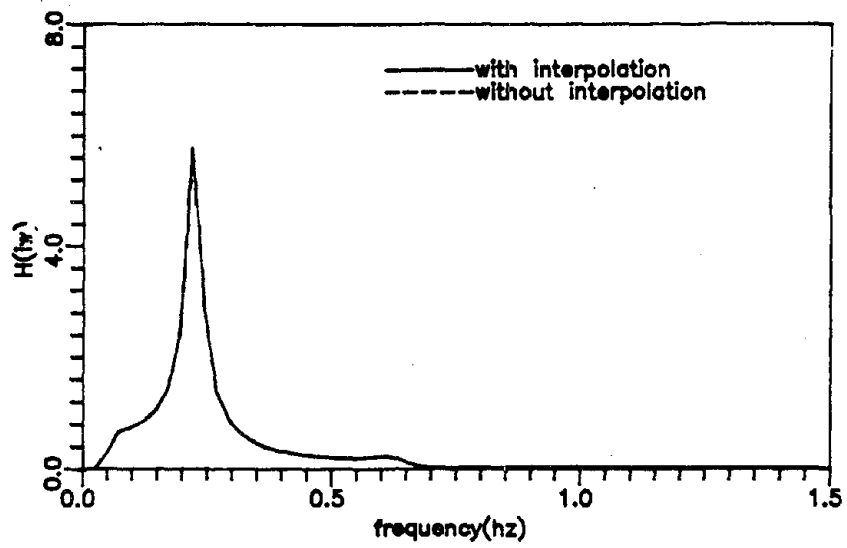


Fig.6.2 Comparison of the Transfer Functions Obtained With or Without Using the Interpolations

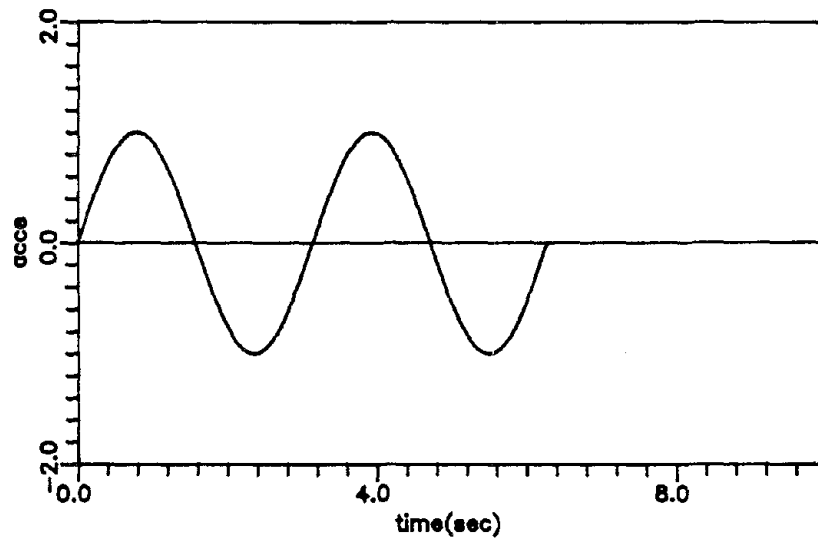


Fig.6.3 Sample Input Sine Wave for the Program SSIAM Test

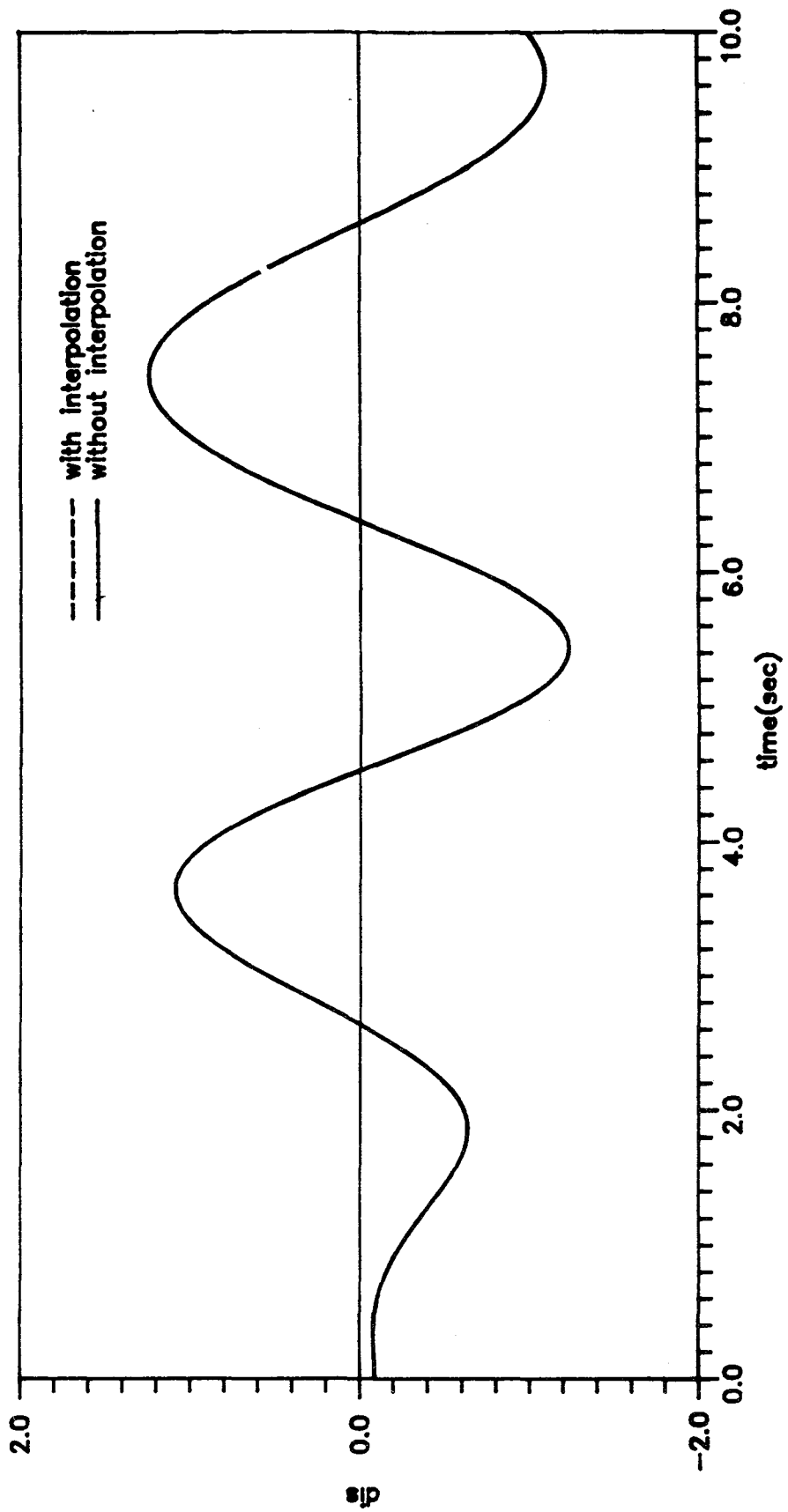


Fig.6.4 Comparison of the Displacements Calculated with or without Using Interpolations

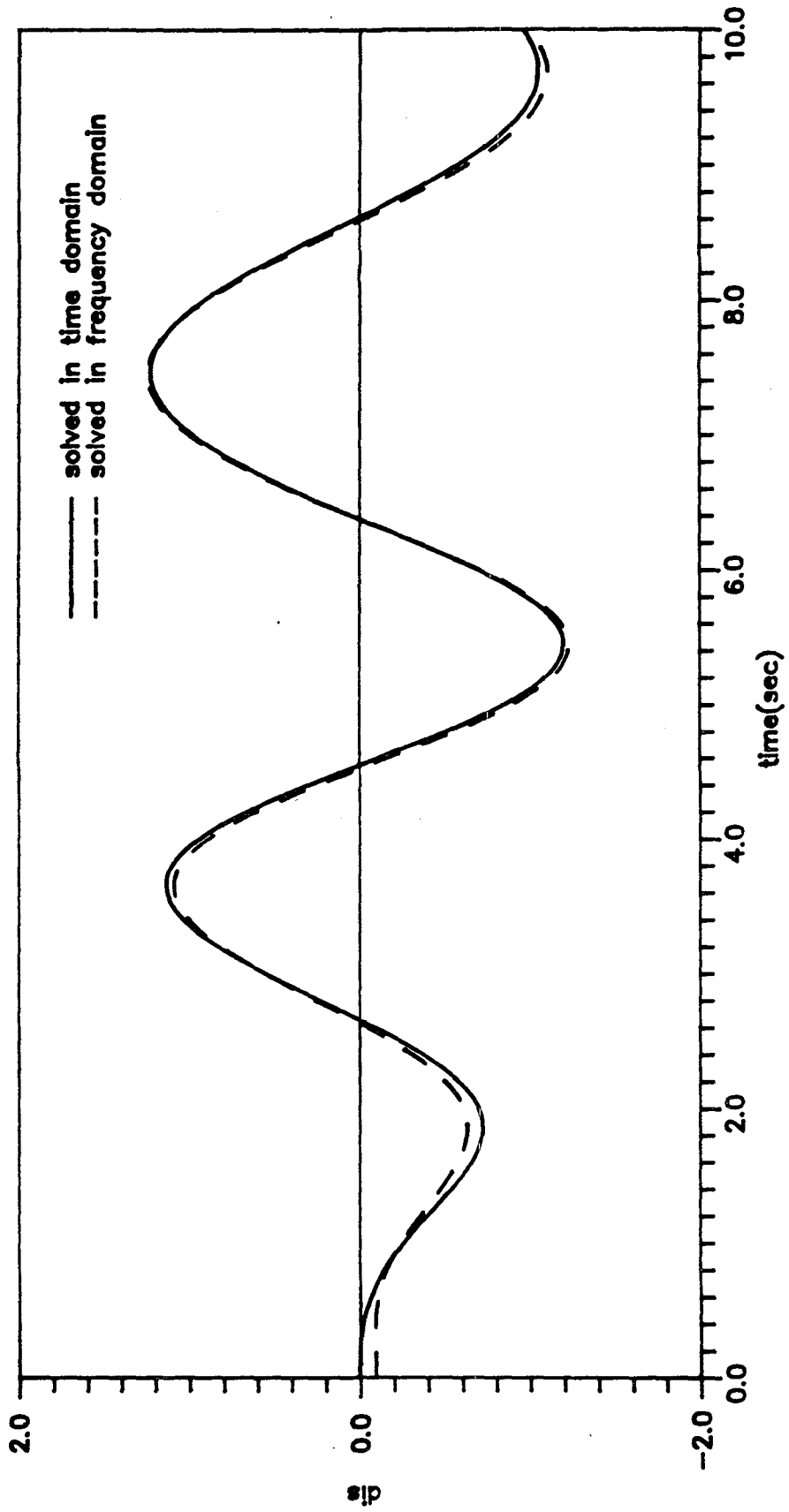


Fig.6.5 Comparison the Displacements Calculated Using Program CAL86 and SSIAM

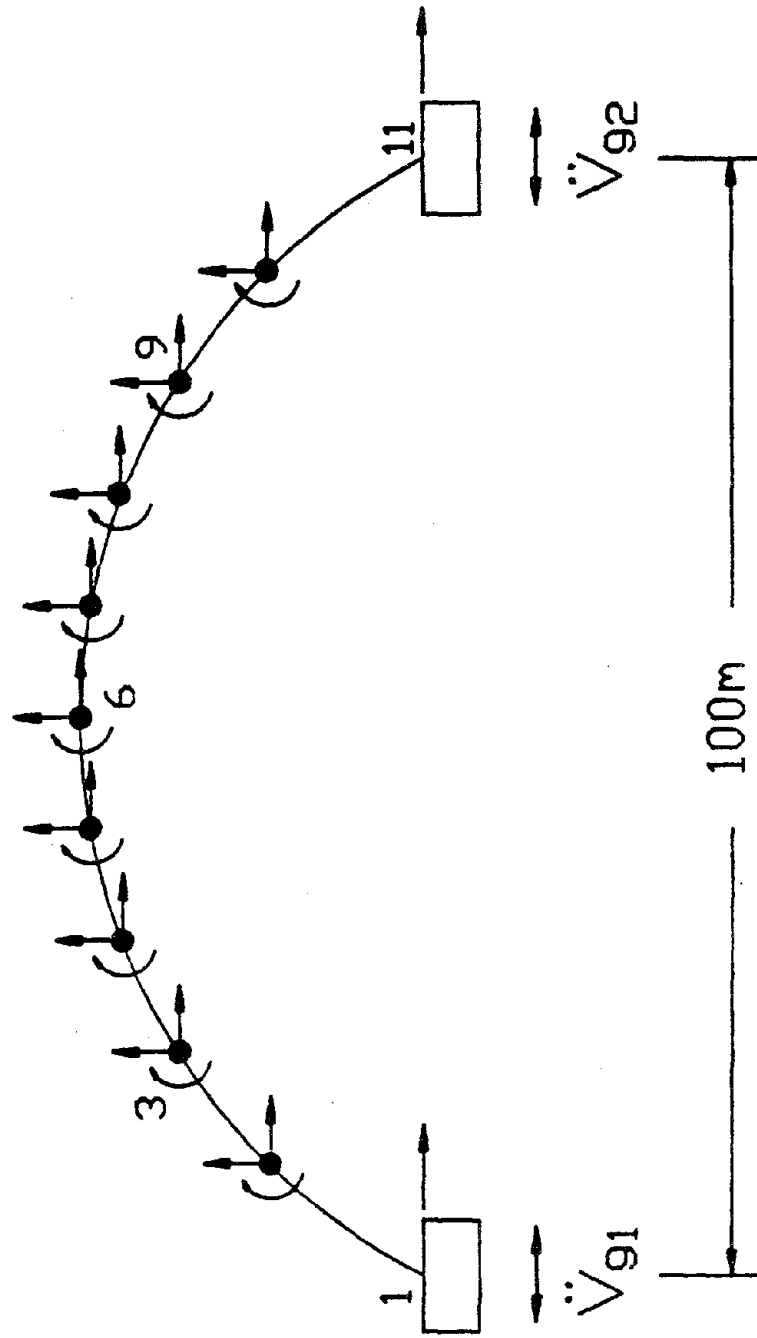


Fig 6.6 Long Span Arch Frame of the Example I

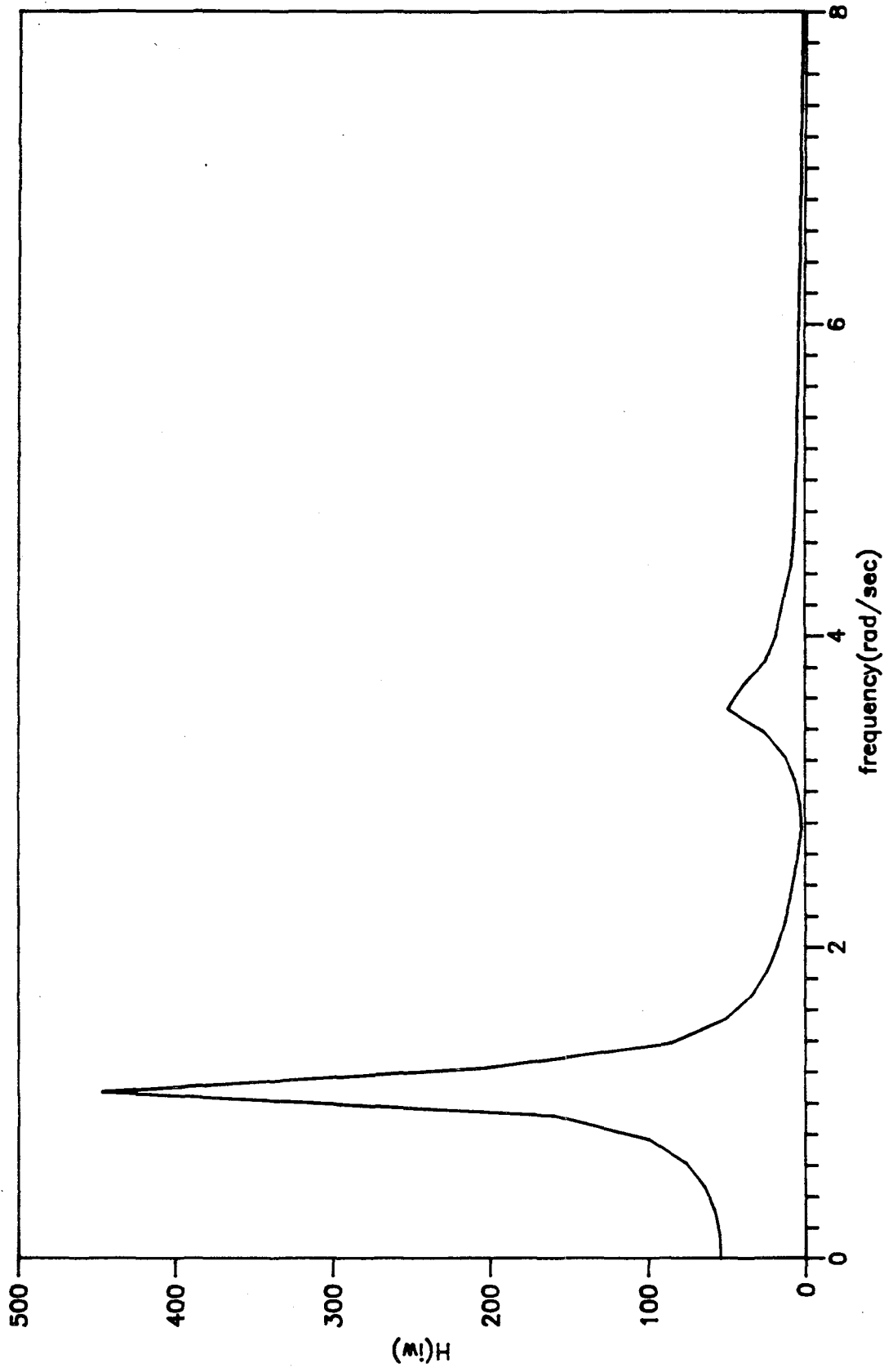


Fig.6.7 Displacement Transfer Function at Node 3 in Horizontal Direction

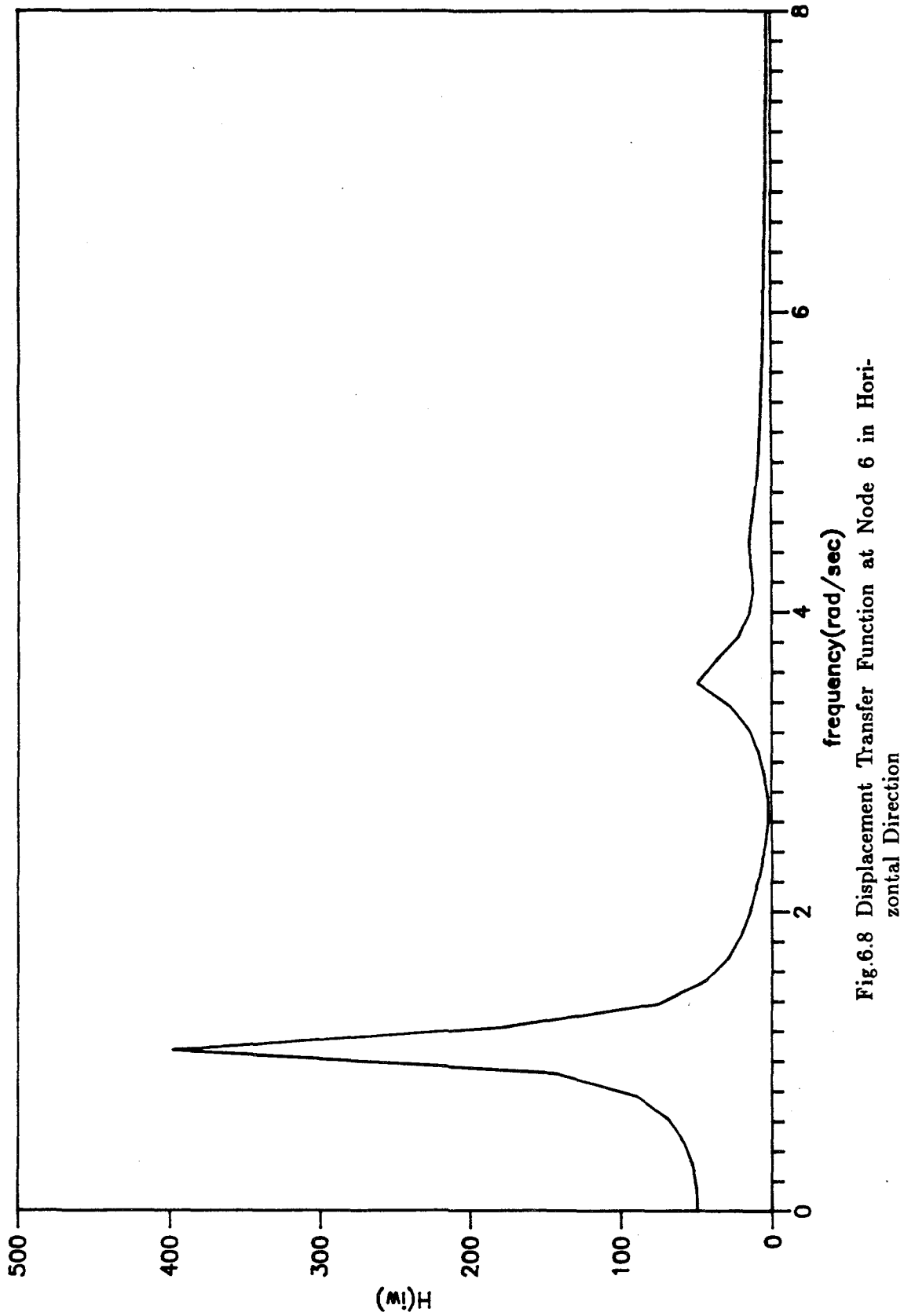


Fig.6.8 Displacement Transfer Function at Node 6 in Horizontal Direction

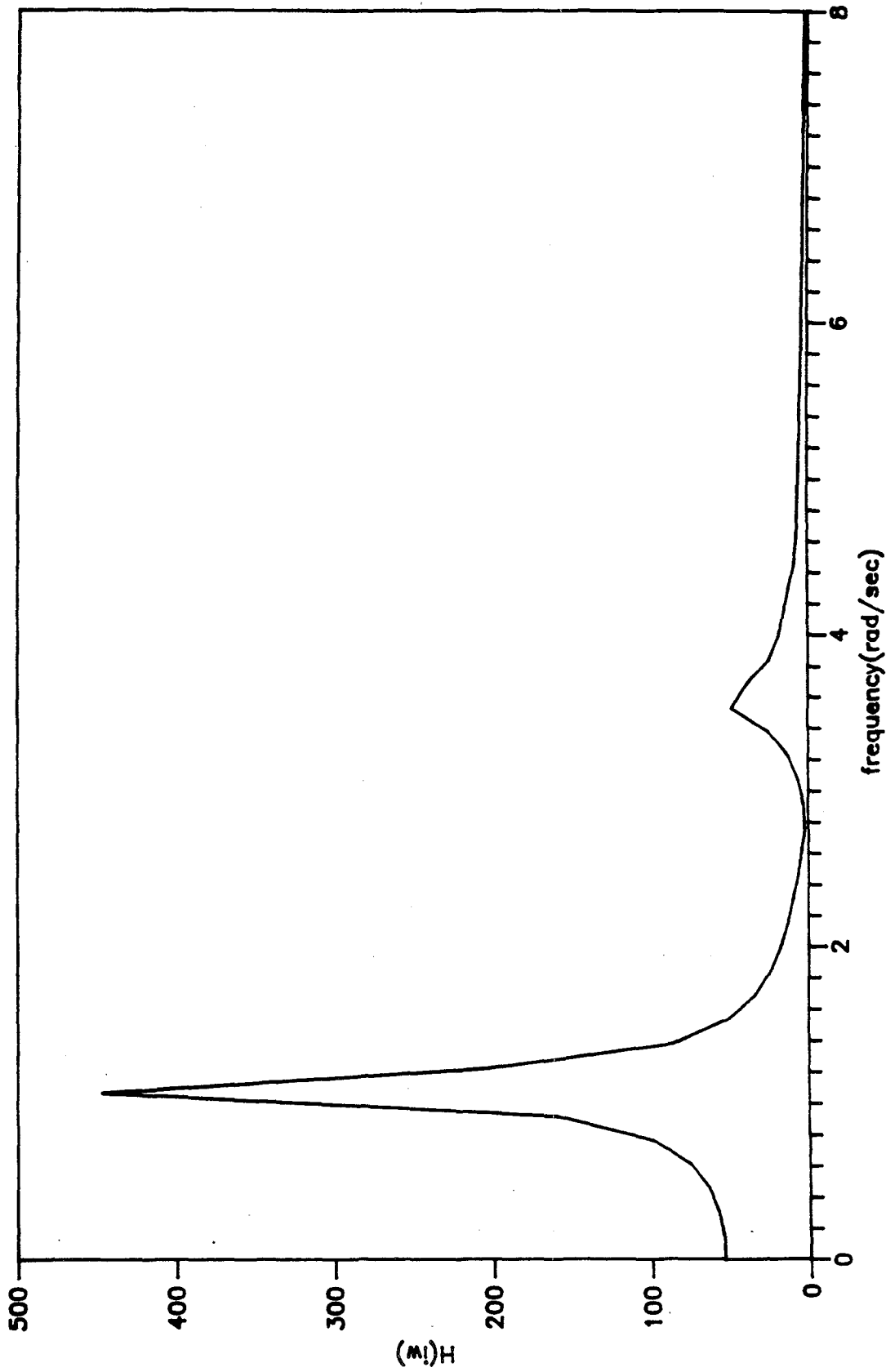


Fig.6.9 Displacement Transfer Function at Node 9 in Horizontal Direction

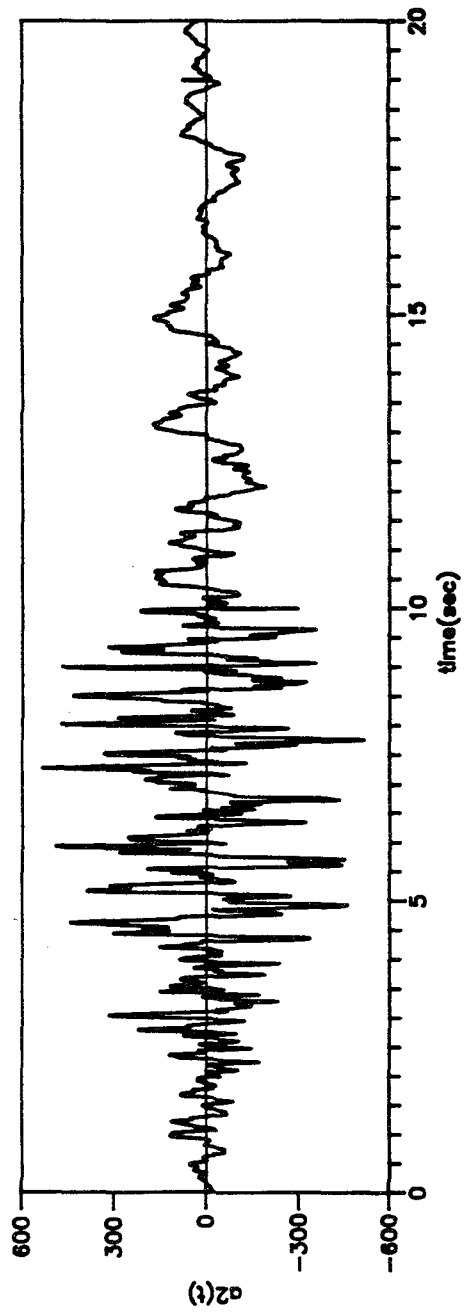
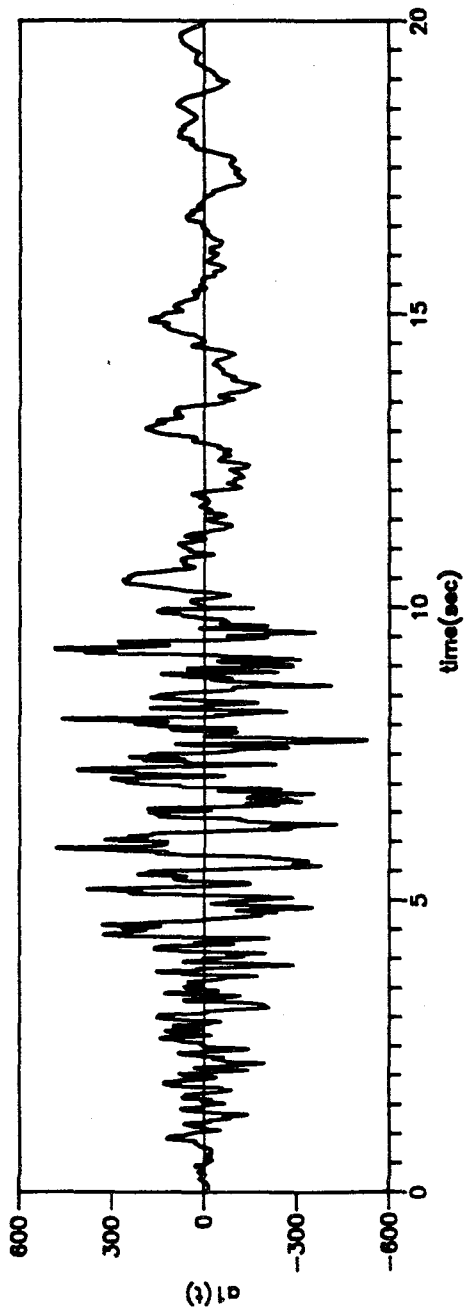


Fig.6.10 Two Simulated Quasi-Stationary Response Spectrum Compatible Ground Accelerations at the Two Supports

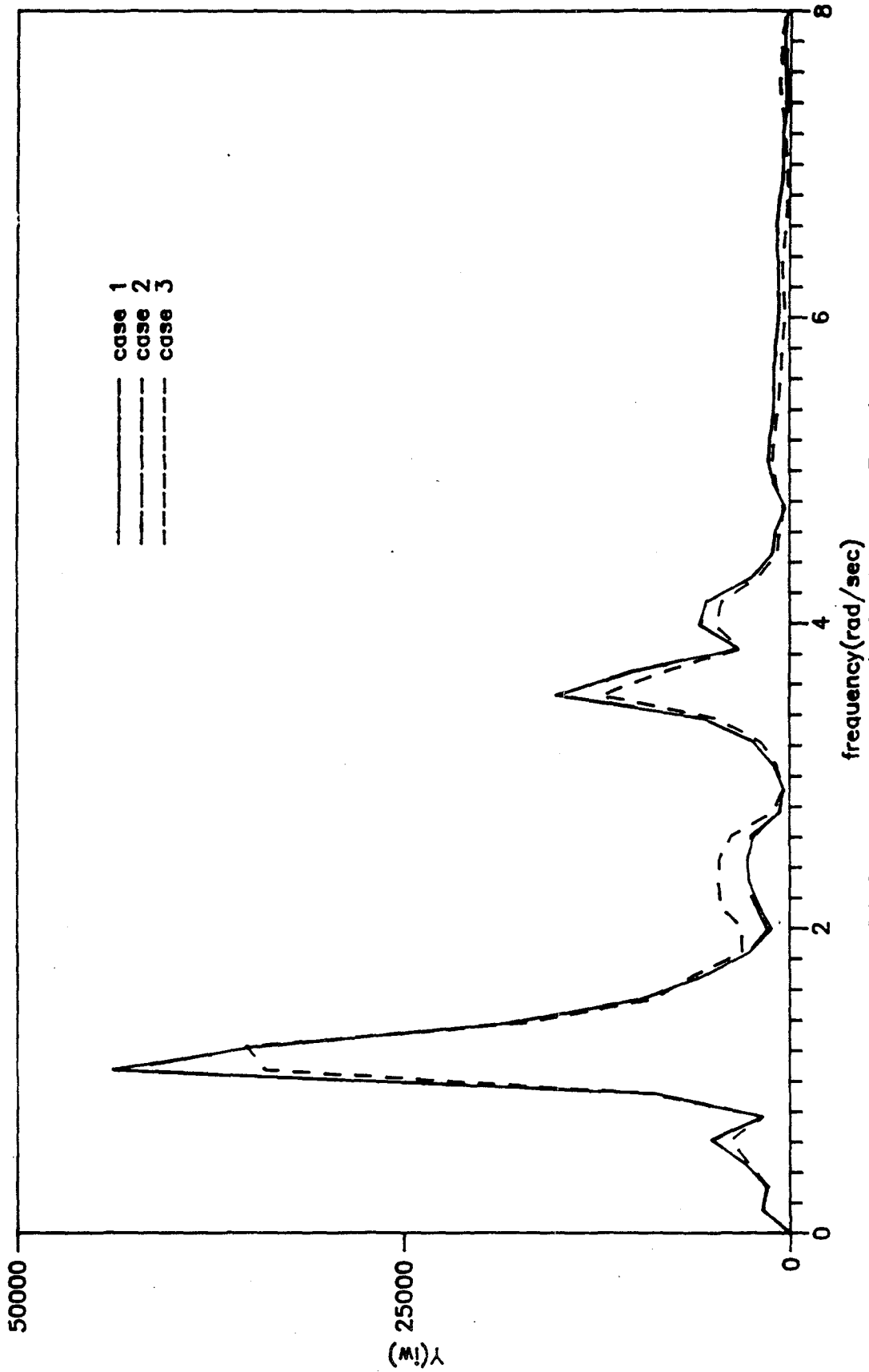


Fig.6.11 Displacement Responses in the Frequency Domain at Node 3 in Horizontal Direction Calculated for Three Different Cases

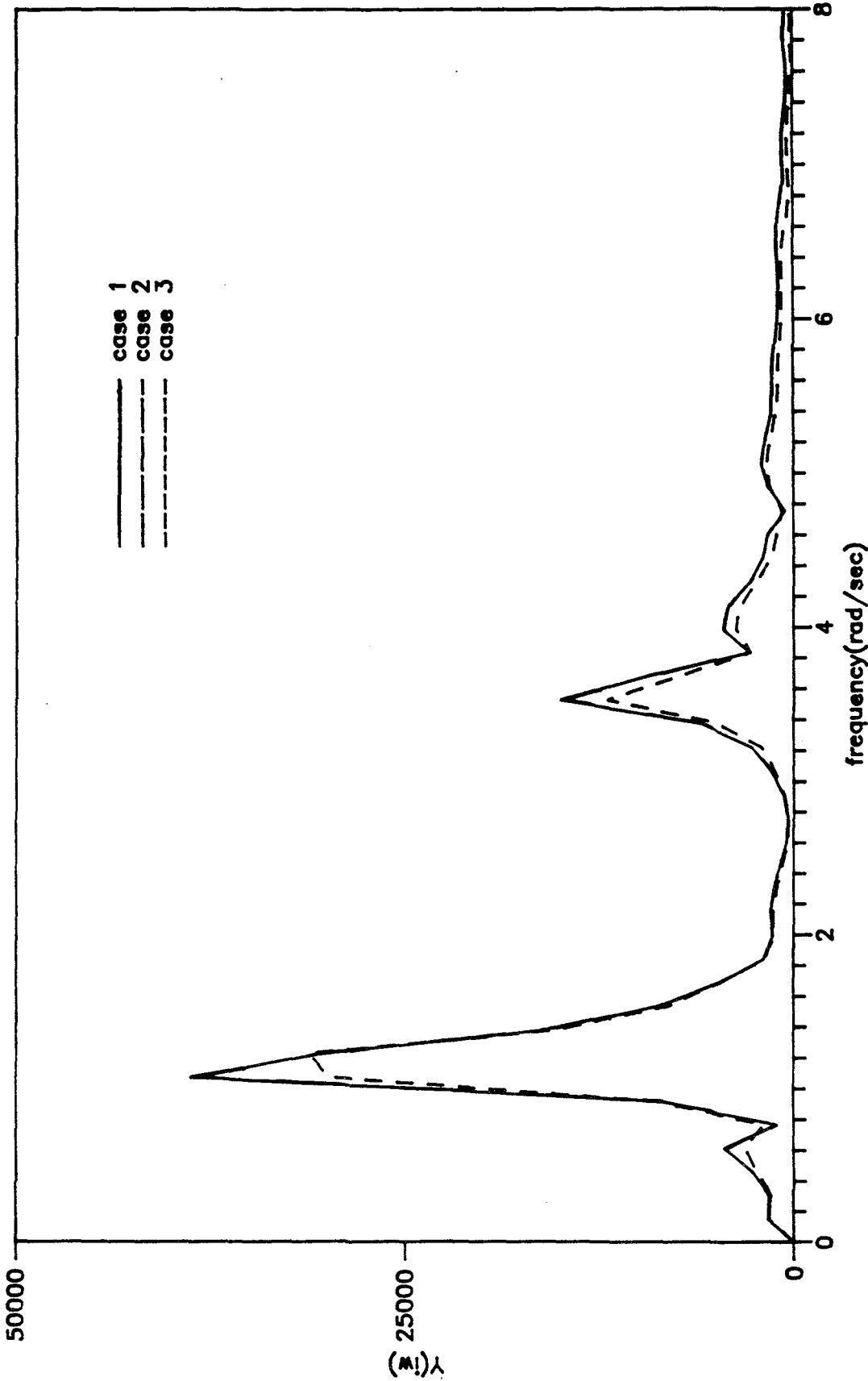


Fig.6.12 Displacement Responses in the Frequency Domain at Node 6 in Horizontal Direction Calculated for Three Different Cases

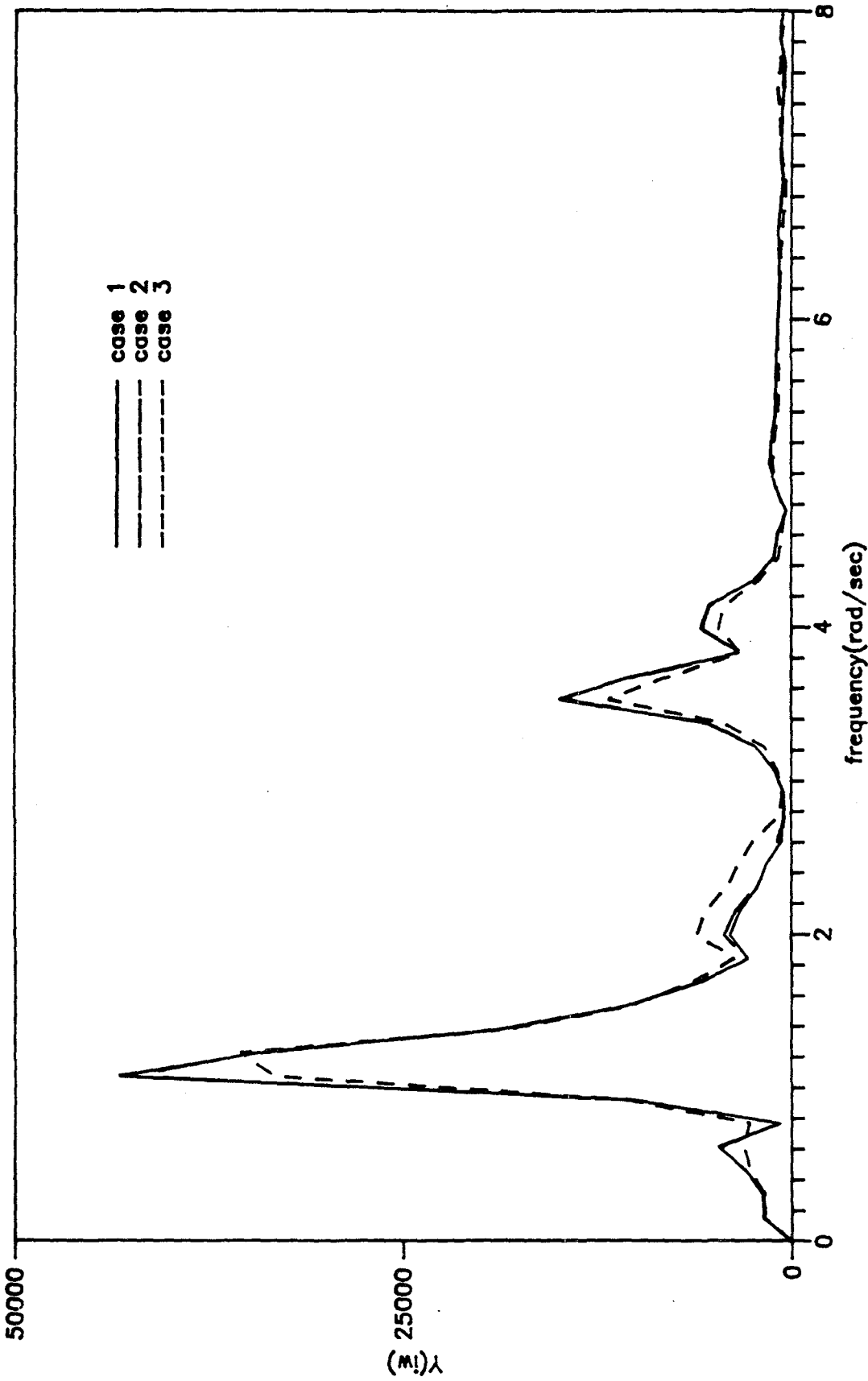


Fig.6.13 Displacement Responses in the Frequency Domain
at Node 9 in Horizontal Direction Calculated for
Three Different Cases

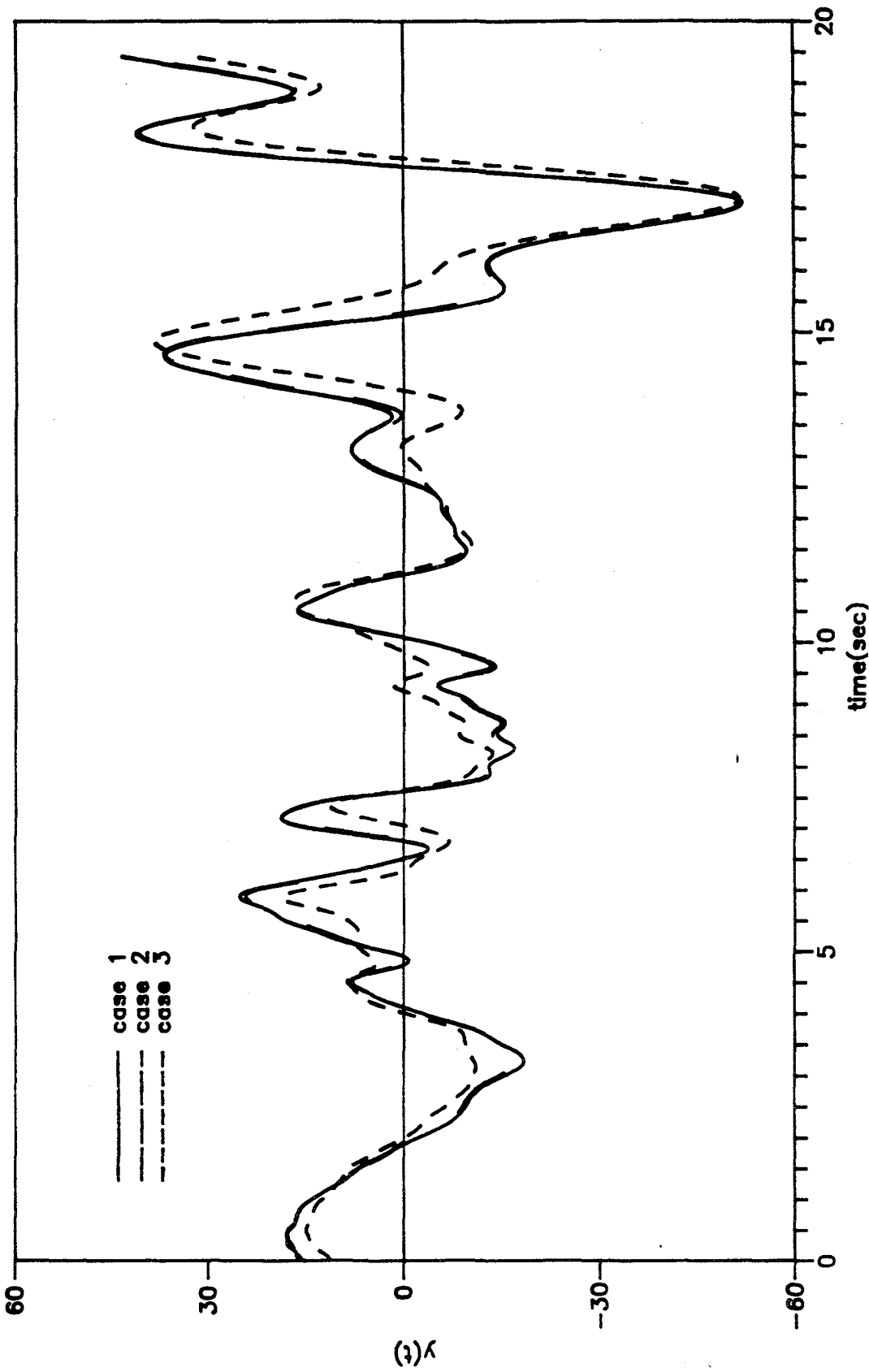


Fig.6.14 Displacement Responses in the Time Domain at Node 3 in Horizontal Direction Calculated for Three Different Cases

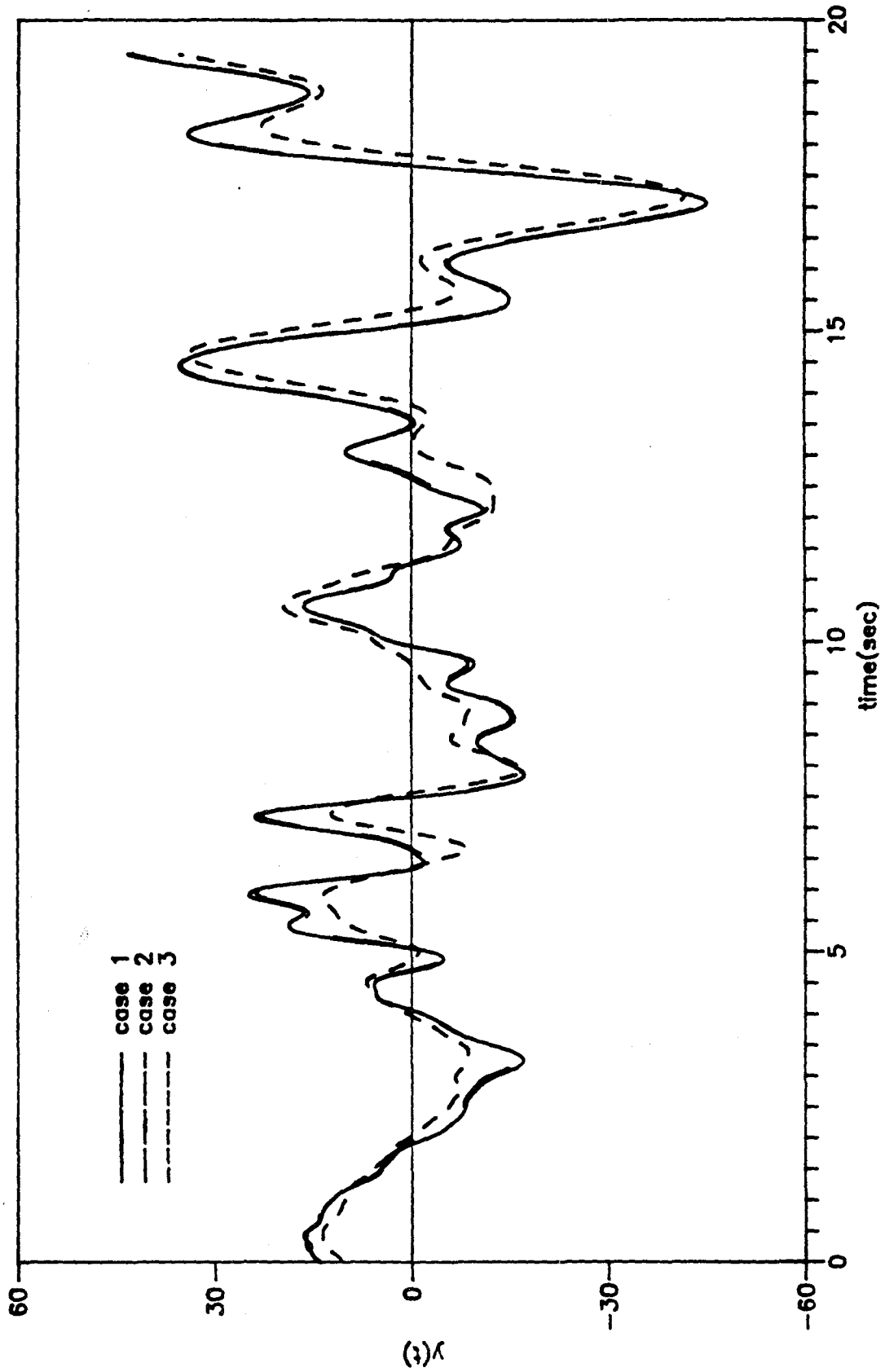


Fig.6.15 Displacement Responses in the Time Domain at Node 6 in Horizontal Direction Calculated for Three Different Cases

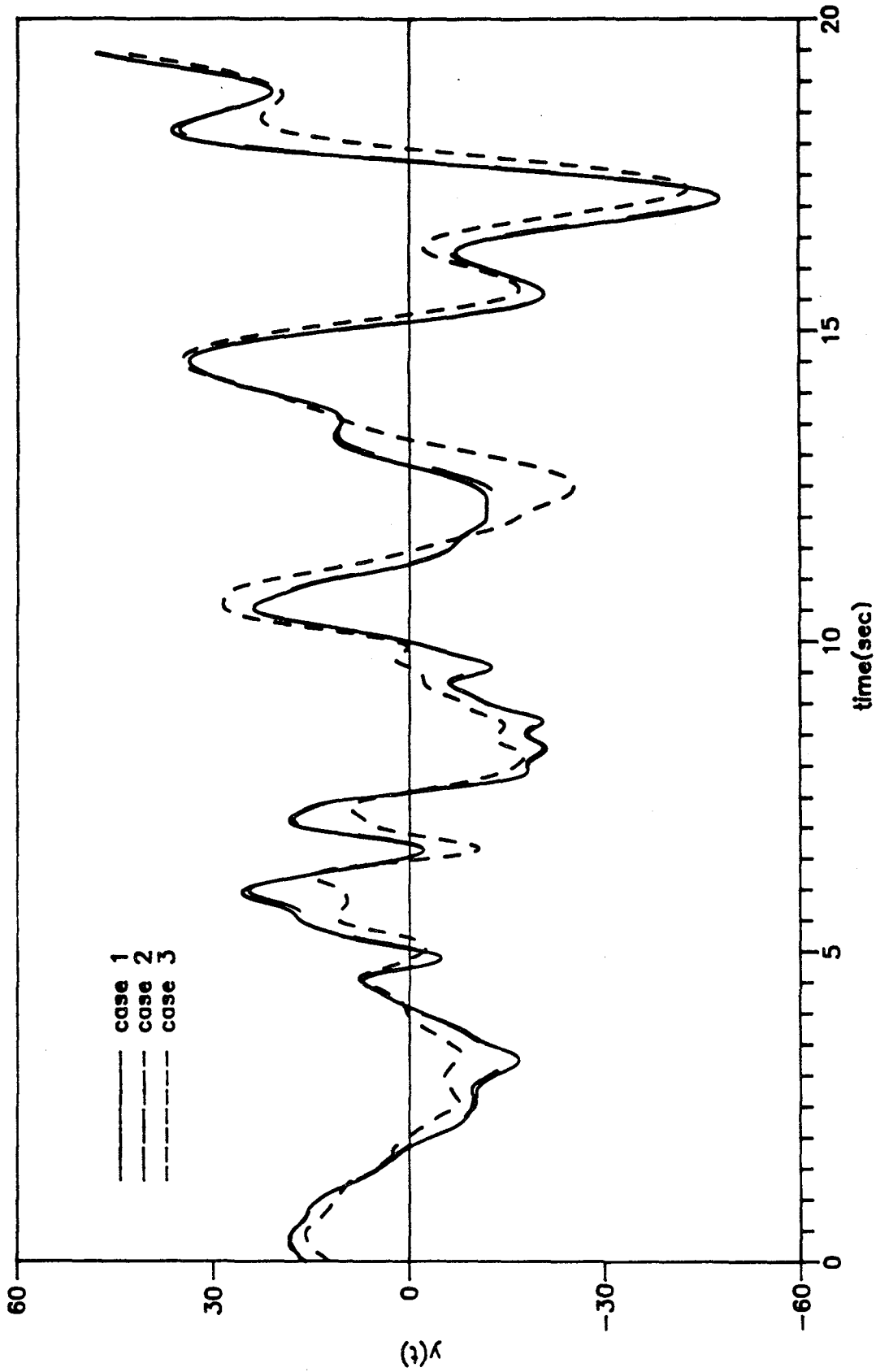


Fig.6.16 Displacement Responses in the Time Domain at Node 9 in Horizontal Direction Calculated for Three Different Cases

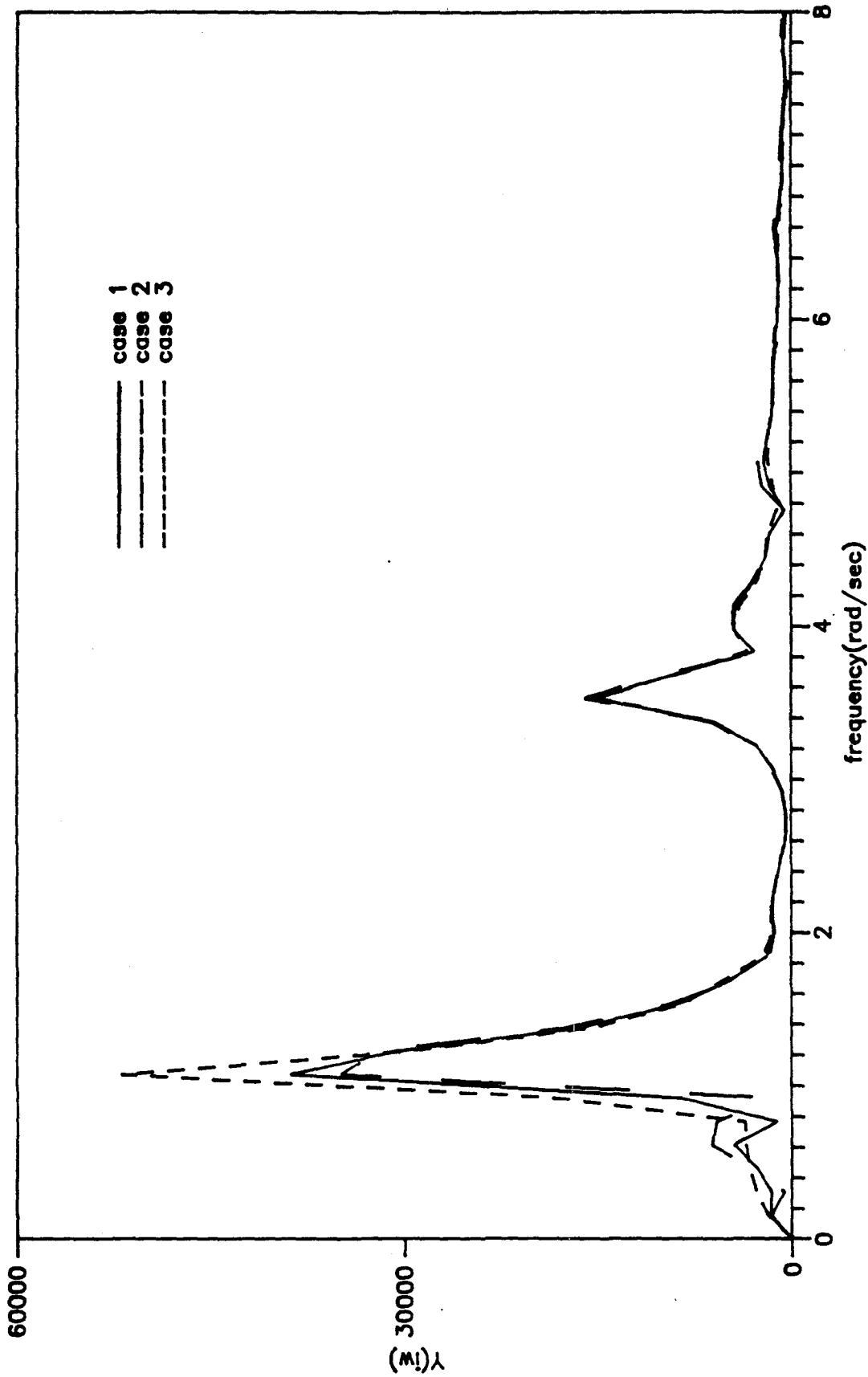


Fig.6.17 Displacement Responses in the Frequency Domain
 at Node 6 in Horizontal Direction Calculated for
 Three Different Cases of Single or Multiple Inputs

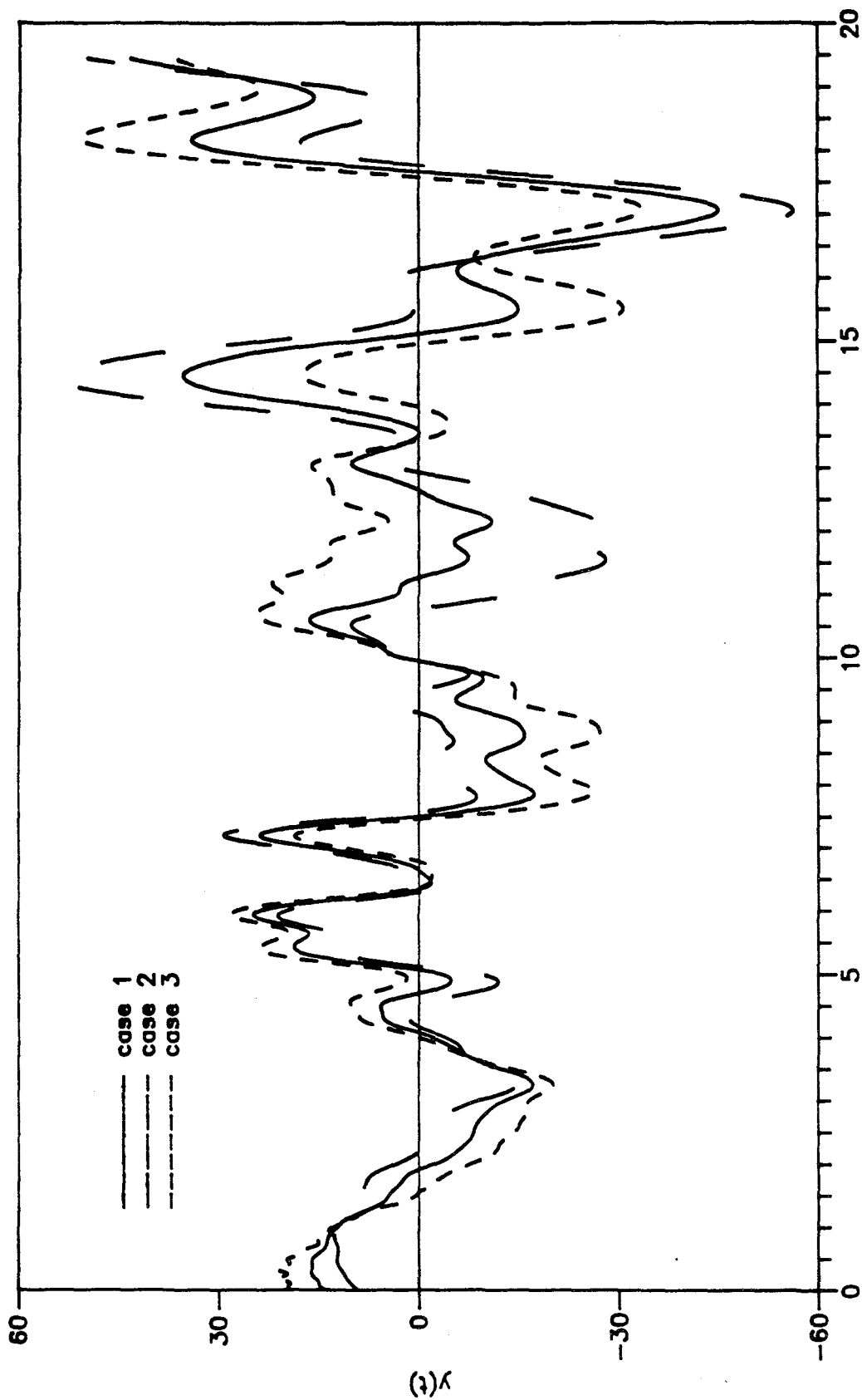


Fig.6.18 Displacement Responses in the Time Domain at Node 6 in Horizontal Direction Calculated for Three Different Cases of Single or Multiple Inputs

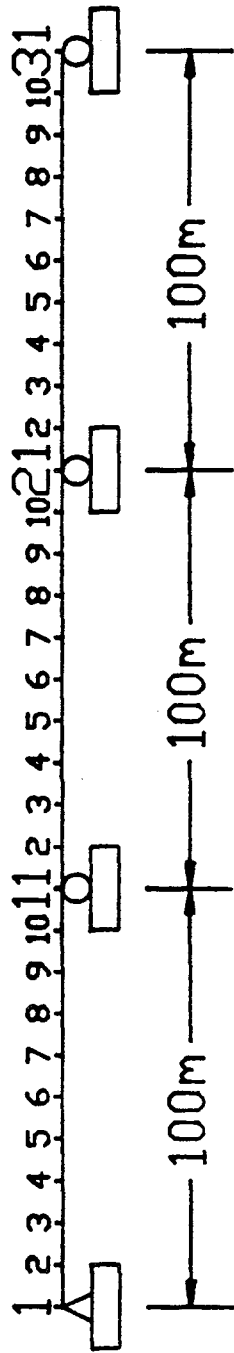


Fig.6.19 Long Span Continuous Beam Model for Example II

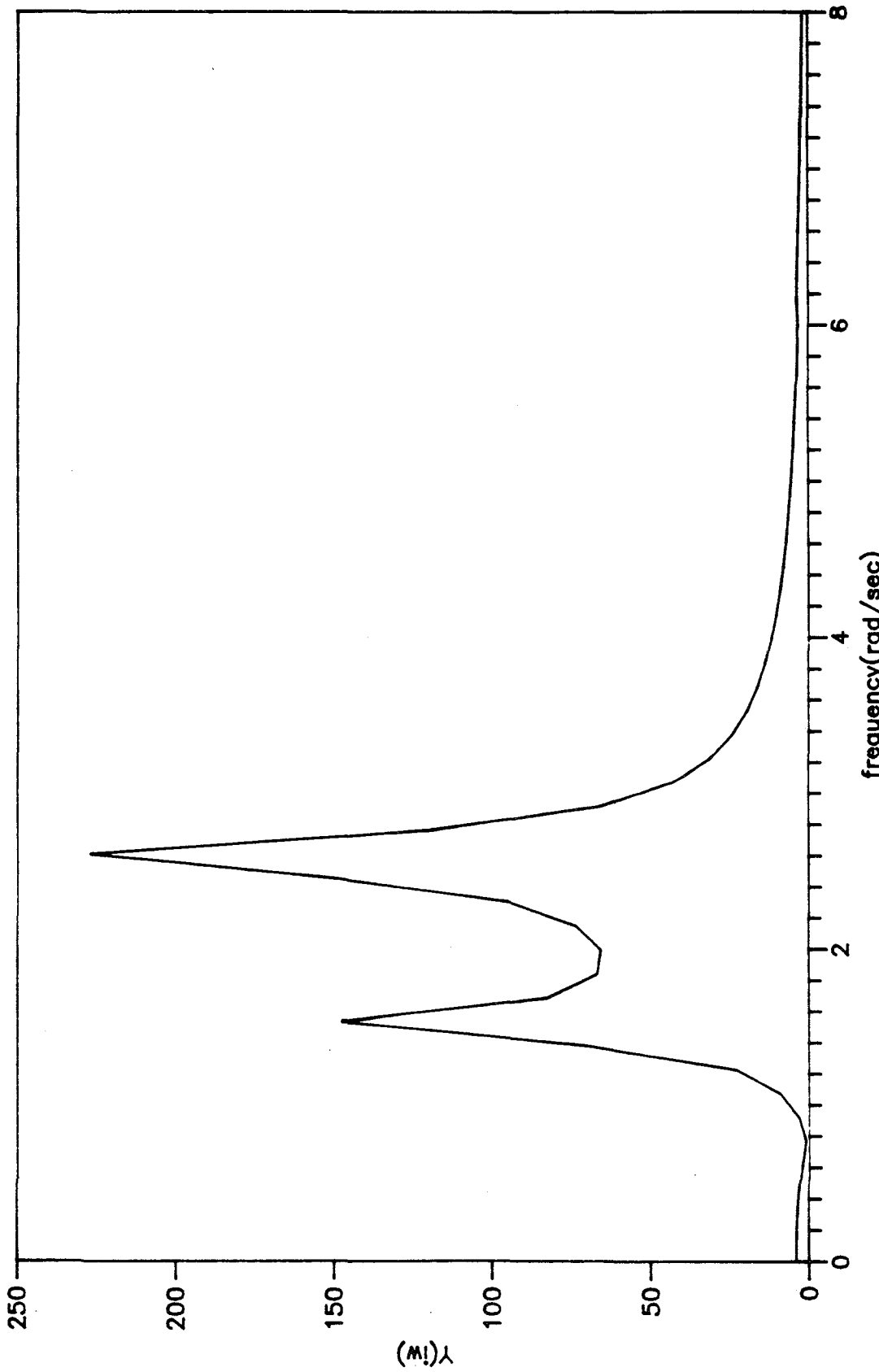


Fig.6.20 Displacement Transfer Function at Midpoint of the Central Span in Vertical Direction

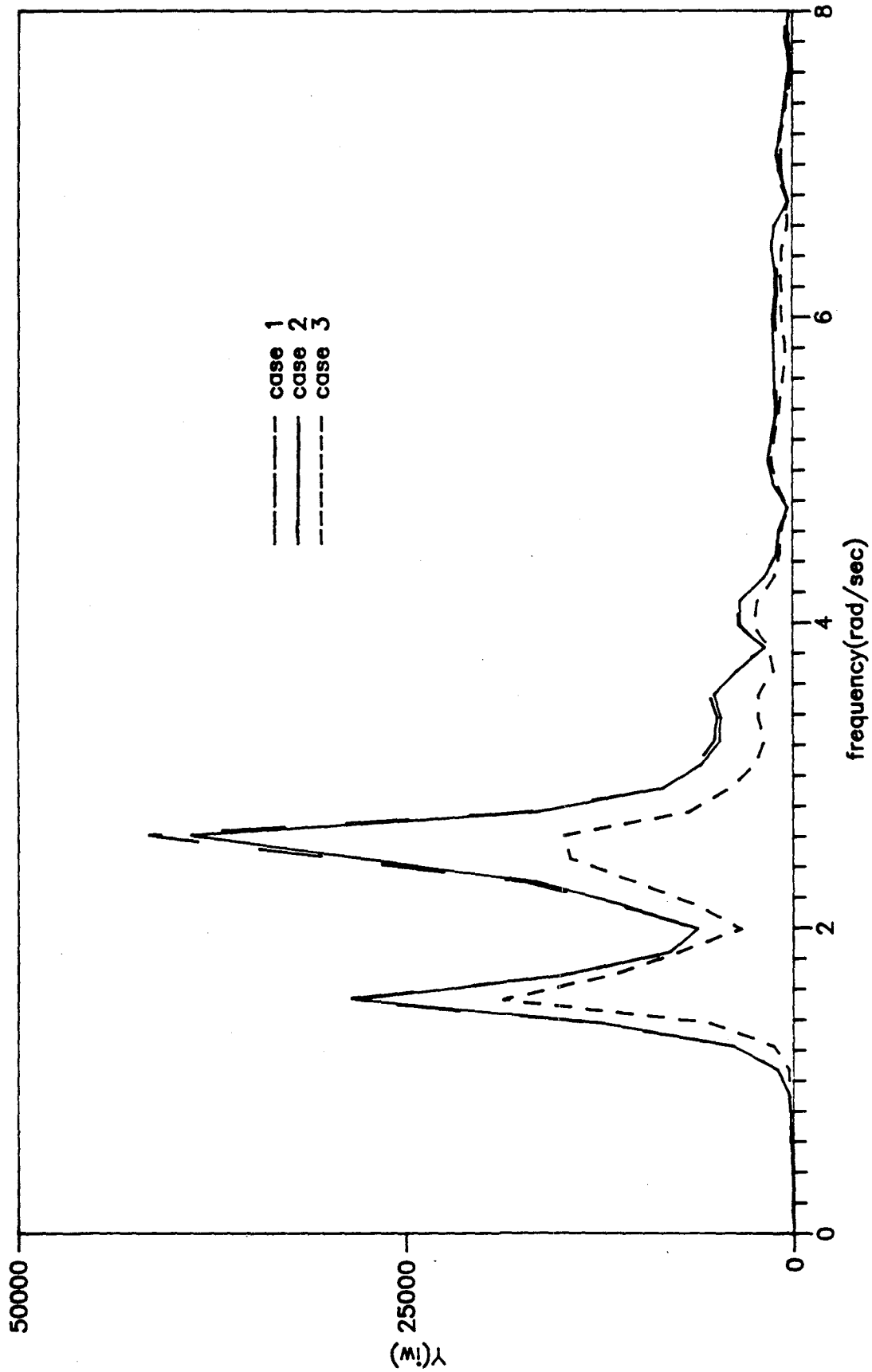


Fig.6.21 Displacement Responses in the Frequency Domain at Midpoint of the Central Span in Vertical Direction for Three Different Cases

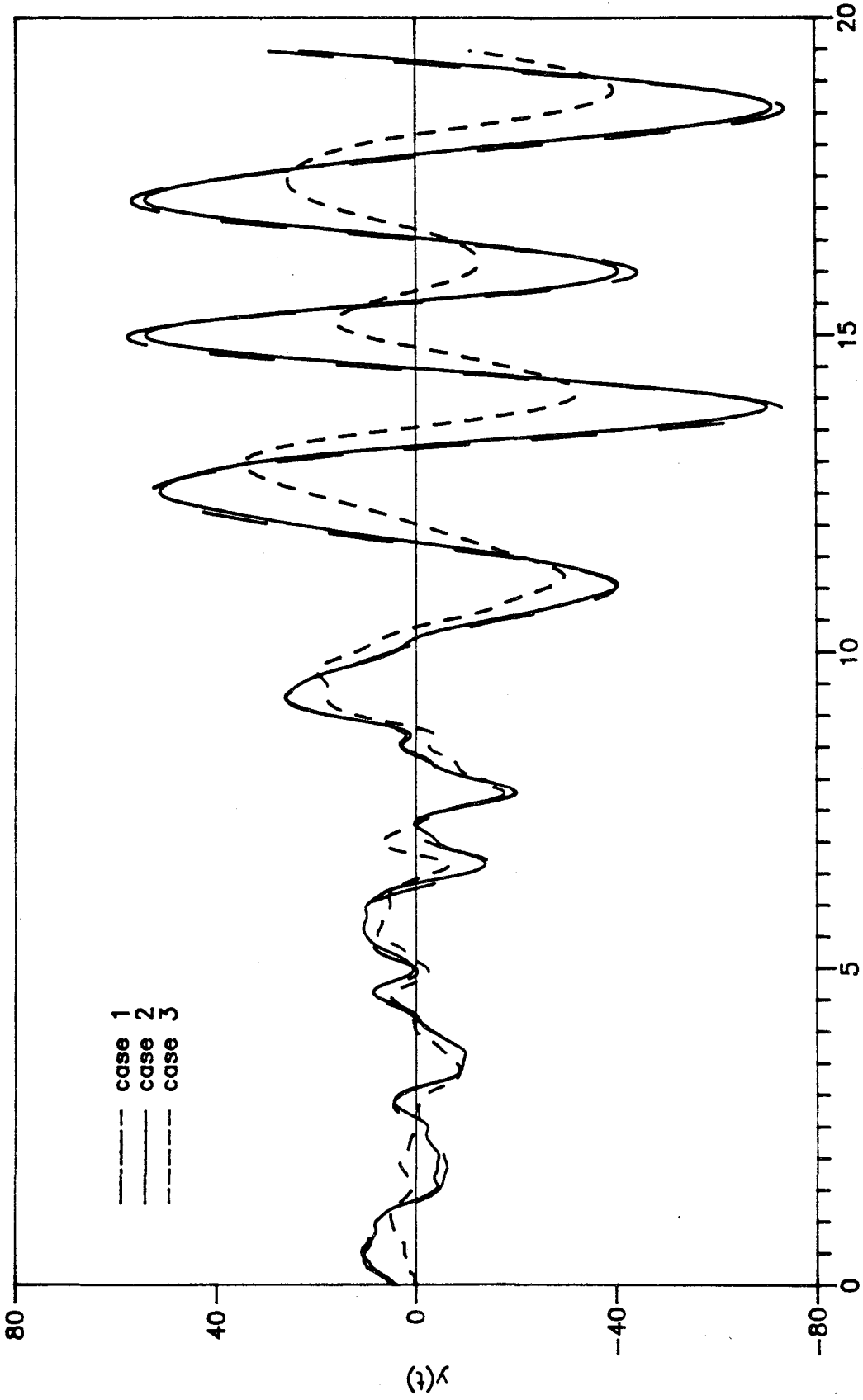


Fig.6.22 Displacement Responses in the Time Domain at Midpoint of the Central Span in Vertical Direction for Three Different Cases

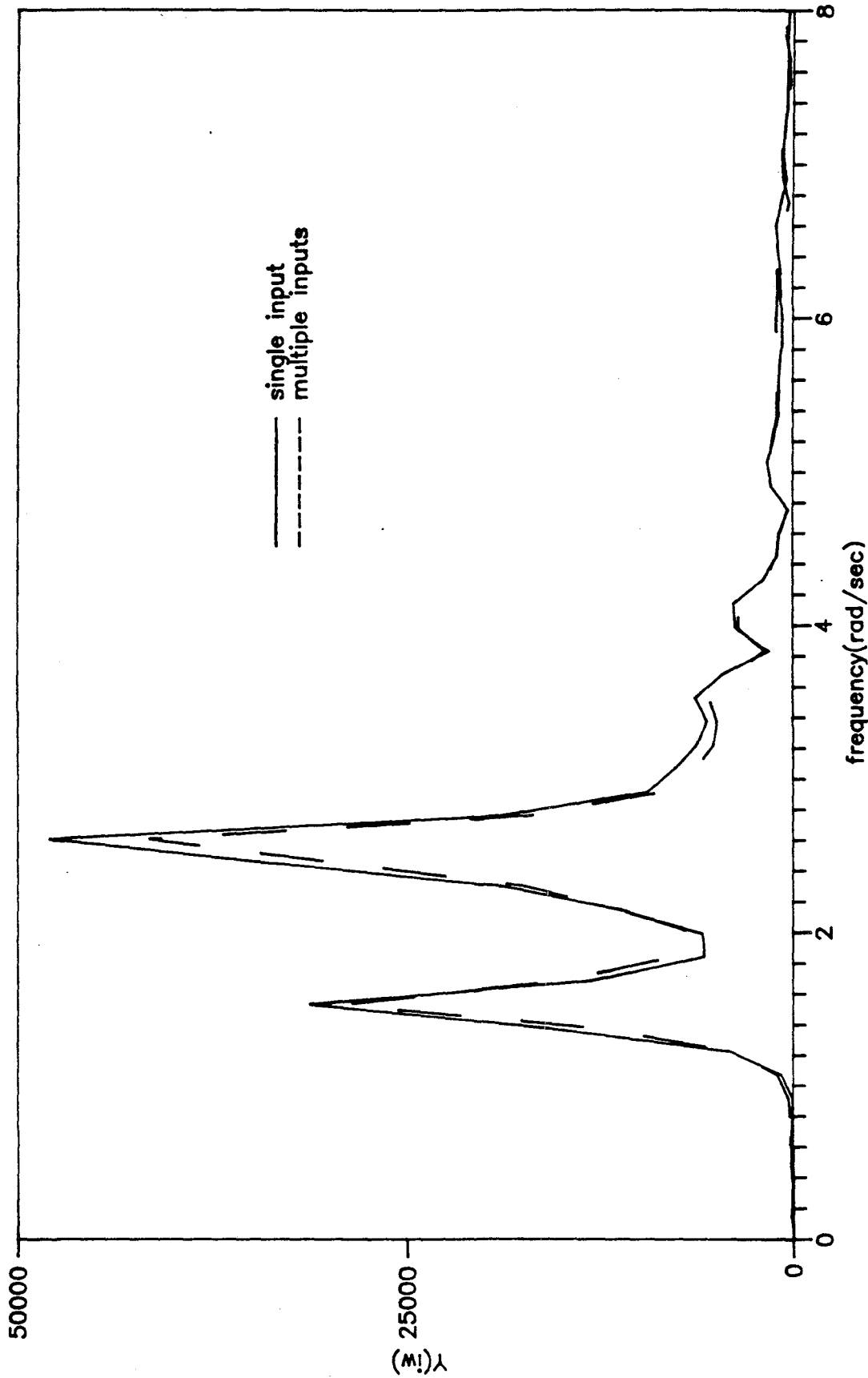


Fig.6.23 Displacement Responses in the Frequency Domain at Midpoint of the Central Span in Vertical Direction for Single or Multiple Inputs

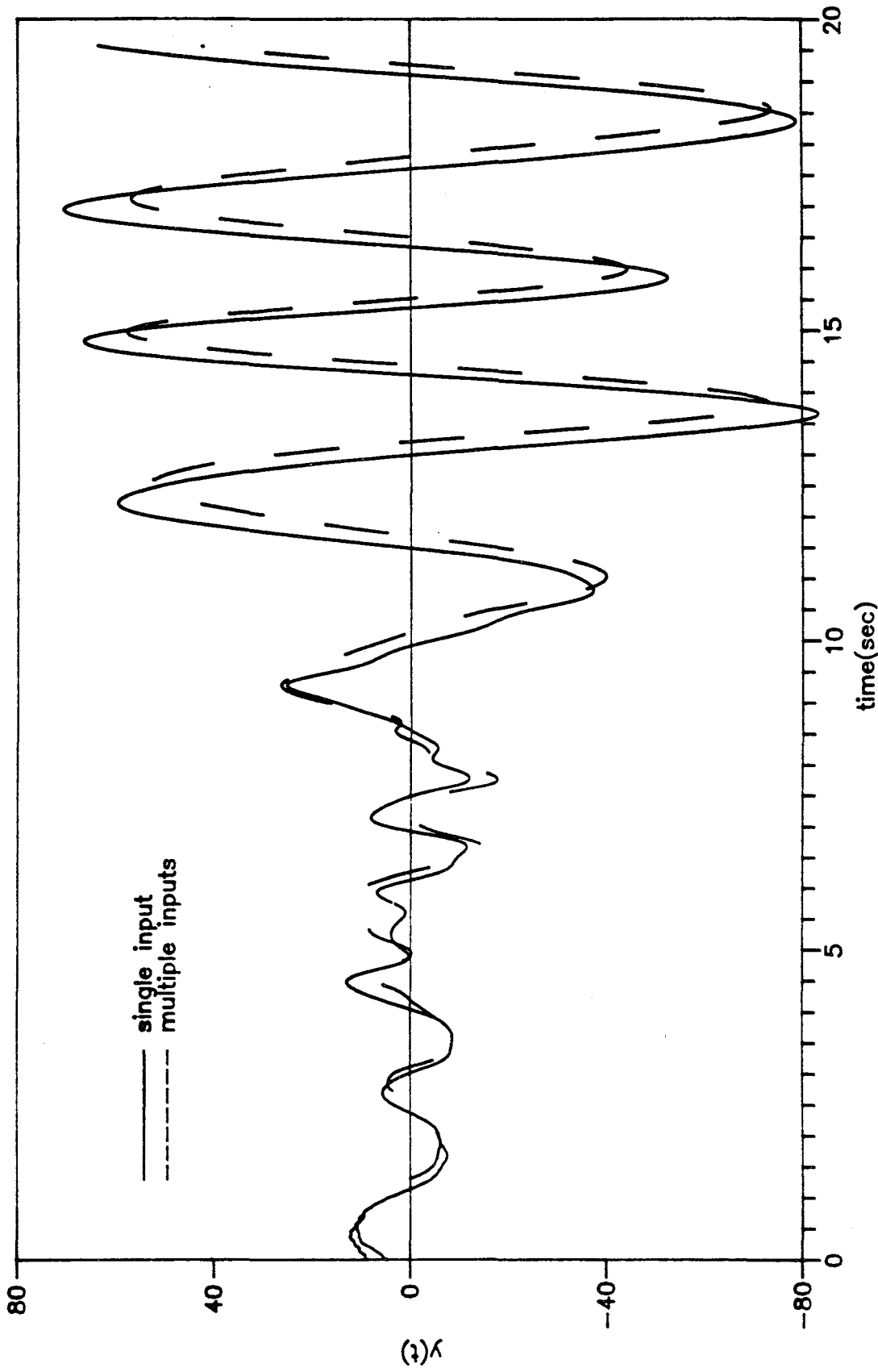


Fig.6.24 Displacement Responses in the Time Domain at Midpoint of the Central Span in Vertical Direction for Single or Multiple Inputs

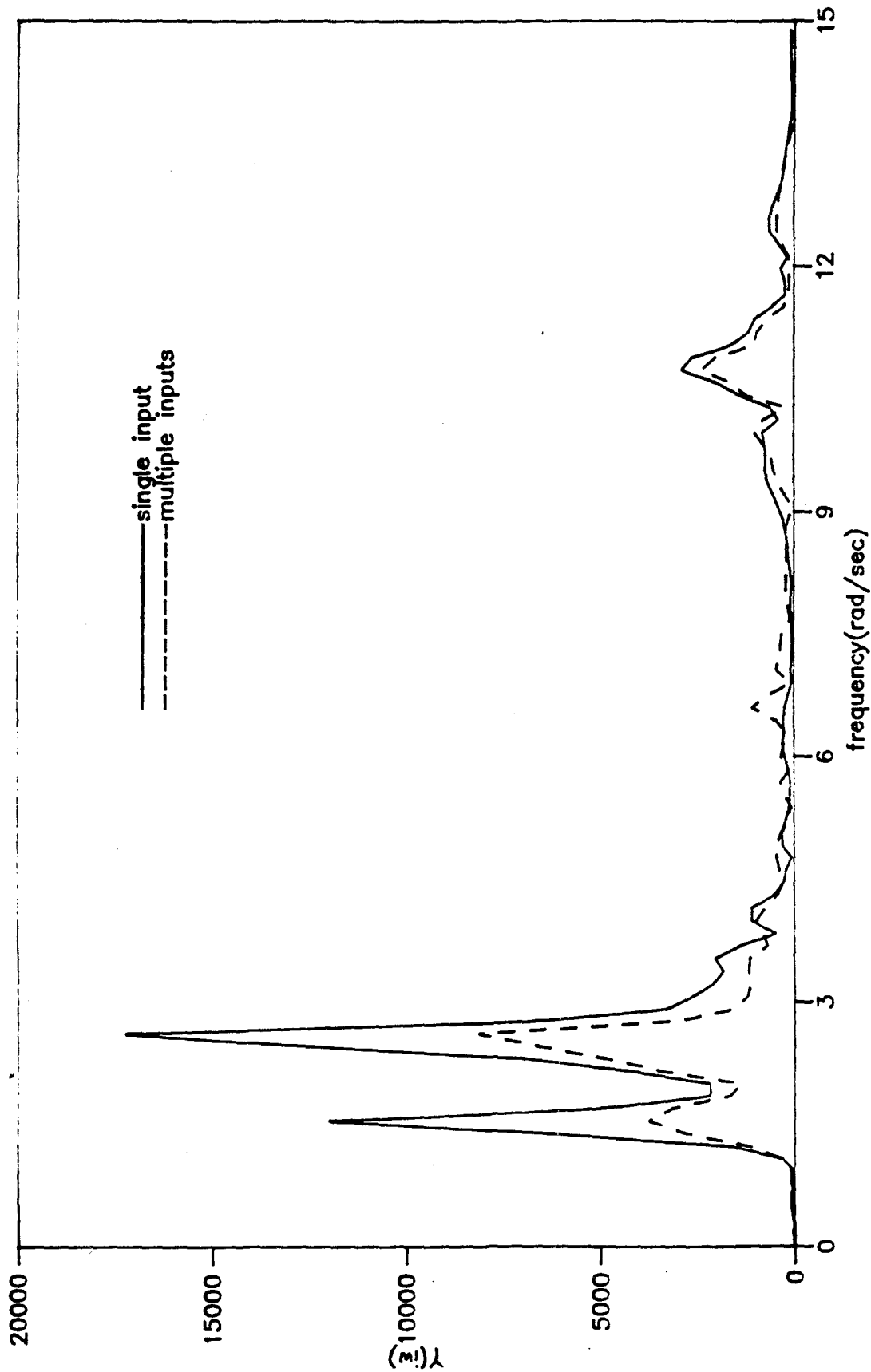


Fig.6.25 Displacement Responses in the Frequency Domain at Node 12 of the Central Span in Vertical Direction for Single or Multiple Inputs

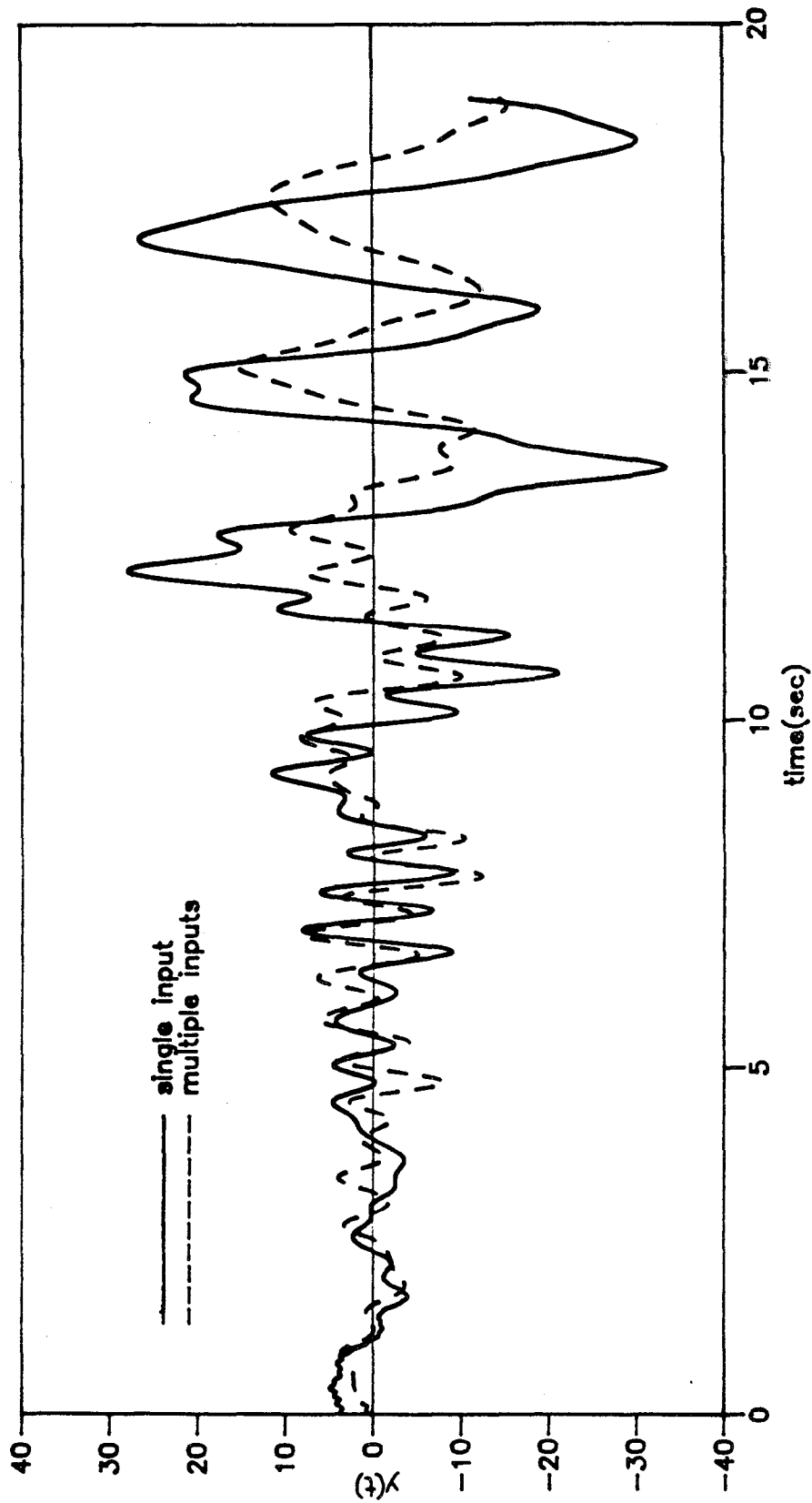


Fig.6.26 Displacement Responses in the Time Domain at Node 12 of the Central Span in Vertical Direction for Single or Multiple Inputs

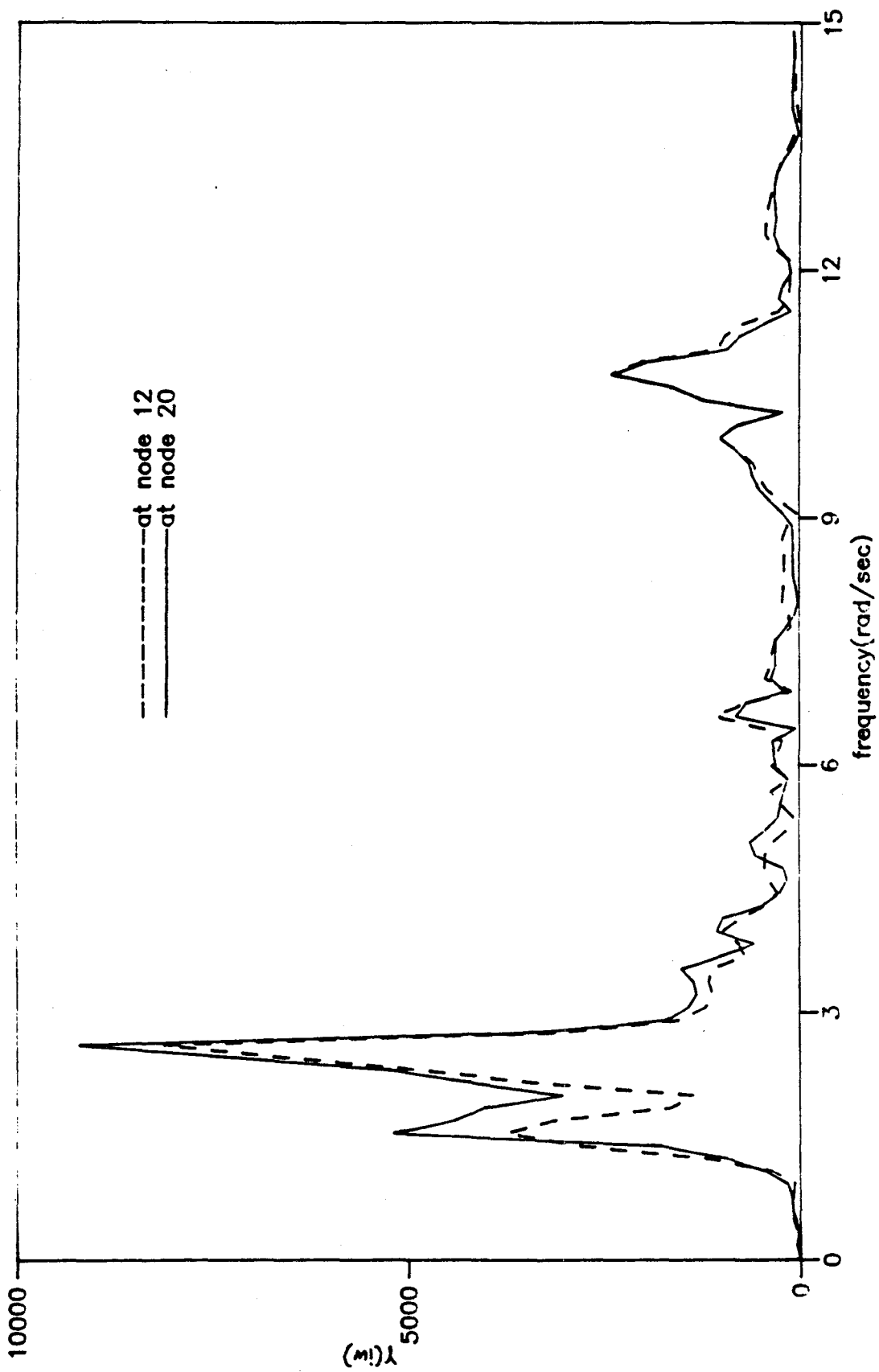


Fig.6.27 Comparison the Vertical Displacements of the Two Symmetric Nodes 12 and 20 in the Frequency Domain

CHAPTER 7 CONCLUSIONS AND RECOMMENDATIONS

Based on the results of the investigation reported herein, the following conclusions have been reached:

1. The power spectral density functions of the recorded ground motions at the SMART-1 site generally have the Tajimi-Kanai form except for the ground motions in the vertical component recorded during Event 24, which fit more closely banded white noise.
2. All the investigated time-histories have the Bogdanoff type shape function with the exception for the vertical ground motions during Event 24. These fit better the shape function proposed by Amin and Ang.
3. Apparent velocities were calculated for ground motions recorded during Events 24 and 45, but there were no clear conclusions that could be made based on those results, perhaps because of the high complexity of the seismic wave scattering.
4. A preliminary coherency model for wave propagation on the ground surface has been suggested based on the plane wave assumption. The suggested model depends on the two parameter functions $\alpha_1(f)$ and $\alpha_2(f)$, and two parameters β_1 and β_2 .
5. The two parameter functions $\alpha_1(f)$ and $\alpha_2(f)$ can be best represented by two similar nonlinear functions with different parameters.
6. The two parameters β_1 and β_2 depend on the peak ground accelerations (PGAs) of the ground motions. Higher PGAs correspond to the lower β_1 and β_2 values, and result in the higher absolute coherency values.
7. Ground motions have highest variations in the North-East direction due to the presence of mountains to the north-west of the SMART-1 site.
8. From the diverse values of the calculated parameters for $\alpha_1(f)$ and $\alpha_2(f)$ functions for the ground motions recorded during different events, coherency functions are dependent on source mechanism, path effects, and some unknown effects.
9. A method for simulation of spatially correlated, quasi-stationary multiple ground motions has been developed. All the simulated ground motions satisfy the prescribed ground motion properties and can be made compatible with the given design response spectrum.

10. The quasi-stationary method can be used to accommodate the nonstationary properties in the ground motions. Two or three time windows are chosen to represent P, S, and surface waves or just S and surface waves. An exponential type transient function can be used to combine the stationary time-histories simulated in two consecutive time windows.
11. An interpolation method has been constructed to interpolate the multiple ground motion time-histories when many ground motion time-histories are needed. The interpolated time-histories preserve the proper ground motion wave propagation properties and the response spectrum.
12. A computer program SSIAM has been developed to simulate spatially correlated multiple ground motions and the structural responses subjected to these motions, including soil-structure interaction effects.
13. The structural response is generally reduced by using multiple inputs due to the phase differences in the inputs, the larger the phase differences of the input ground motions, the larger the reductions.
14. The differential displacement in the structure is generally increased by using multiple inputs.
15. Using multiple inputs, the structural response always has a time delay due to the phase differences in the input ground motions, the larger the phase differences, the larger the delay time.
16. Multiple inputs will excite some response modes such as rotation and rocking, which sometimes will not be excited by a single input.
17. Multiple input effects cannot be represented by a single input due to the phase differences and loss of coherency values in the input ground motions. In the analysis of large dimensional structures, a multiple input technique should be used.

Further work still needs to be carried out on the effects of spatial variations of ground motion on large dimensional structures with multiple supports, a few of the possible projects are:

1. More data, either recorded at the SMART-1 site or elsewhere, need to be analyzed to check the generality of the suggested ground motion model.

2. In order to simulate more realistically the spatially correlated ground motions, the apparent wave velocity needs to be intensively studied to derive a more reliable relation between the apparent wave velocities and frequencies which would replace the constant value assumption.
3. The effects of the relation between the structural dimension and the dominant wavelength on the structural responses needs further investigation.
4. Structural types need separating according to the importance of the multiple ground motion excitations in each type.

REFERENCES

Abrahamson, N. A., (1985), "Estimation of Seismic Wave Coherency and Rupture Velocity Using the SMART-1 Strong Motion Array Recordings", Report No. UCB/EERC-85-02, Earthquake Eng. Res. Center, University of California at Berkeley.

Abrahamson, N. A., (1988), "Coherency Analysis of Strong Ground Motion", Personal Communication.

Abrahamson, N. A. and Bolt, B. A., (1985), "The Spatial Variation of the Phasing of Seismic Strong Ground Motion", Bull. Seism. Soc. of America, Vol. 75, No.5, 1247-1264.

Abrahamson, N. A. and Bolt, B. A., (1987), "Array Analysis and Synthesis Mapping of Strong Seismic Motion", in "Strong Motion Synthesis", Edited by Bolt, B. A., Academic Press, Orlando.

Abrahamson, N. A. and Darragh, R. B., (1987), "Array Estimates of Spatial Coherence of Strong Ground Motion", Personal Communication.

Amin, M. and Ang, A. H. S., (1968), "A Nonstationary Stochastic Model for Strong Motion Earthquakes", Structural Research Series, No. 306, Univ. of Illinois, Urbana, Illinois, April.

Atkinson, K. E., (1978), "An Introduction to Numerical Analysis", John Wiley and Sons, NY.

Barstein, M. F., (1960), "Application of Probability Method for Design the Effect of Seismic Forces on Engineering Structures", Proc. 2WCEE, Vol. 2, Tokyo, 1467-1481.

Berg, G. V. and Housner, G. W., (1961), "Integrated Velocity and Displacement of Strong Earthquake Ground Motion", Bull. Seism. Soc. of America, Vol. 51, 175-189.

Bogdanoff, J. L., et al., (1961), "Response of a Simple Structure to Random Earthquake Type Disturbance", Bull. of the Seismological Society of America, Vol. 51, No.2.

Bolotin, V. V., (1960), "Statistical Theory of the Aseismic Design of Structures", Proc. 2WCEE, Vol. 2, Tokyo, 1365-1374.

Bolt, B. A., (1973), "Duration of Strong Ground Motion", 5WCEE, Vol. 1, Rome, Italy.

Bolt, B. A. and Abrahamson, N. A., (1982), "New Attenuation Relations For Peak and Expected Accelerations of Strong Ground Motion", Bull. Seis. Soc. of America, Vol.72, No.6, 2307-2321.

Bolt, B. A., Loh, C. H., Penzien, J., Tsai, Y. B., and Yeh, Y. T., (1982), "Preliminary Report on the SMART-1 Strong Motion Array in Taiwan", Report No. UCB/EERC-82-13, Earthquake Eng. Res. Center, University of California at Berkeley.

Chopra, A. K. and Lopez, O. A., (1979), "Evaluation of Simulated Ground Motions for

Predicting Elastic Response of Long Period Structures and Inelastic Response of Structures", *Earthquake Engineering and Structural Dynamics*, Vol. 7, 383-402.

Darragh, R. B., (1987), "Analysis of the Near Source Wave: Separation of Wave Types Using Strong Motion Array Recordings", Ph.D. Thesis, University of California, Berkeley.

Estera, L. and Rosenblueth, E., (1964), "Espectros de Temblores A Distancias Moderadas y Grandes", *Boletin de la Sociedad Mexicana de Ingenieria*.

Fok, K. L. and Chopra, A. K., (1985), "Earthquake Analysis and Response of Concrete Arch Dams", Report No. UCB/EERC-85-07, Earthquake Eng. Res. Center, University of California at Berkeley.

Gantmacher, F. R., (1977), "The Theory of Matrices", Chelsea Publishing Company, NY.

Gupta, S., Lin, T. W., Penzien, J. and Yeh, C. S., (1980), "Hybrid Modelling of Soil-Structure Interaction", Report No. UCB/EERC-80-09, Earthquake Eng. Res. Center, University of California at Berkeley.

Gutierrez, J. A. and Chopra, A. K., (1976), "A Substructure Method for Earthquake Analysis of Structure-Soil Interaction", Report No. UCB/EERC-76-09, Earthquake Eng. Res. Center, University of California at Berkeley.

Hao, Hong, (1989), "Effects of Spatial Variation of Ground Motions on Large Multiple Supported Structures", Ph.D. Dissertation, Dept. of Civil Engineering, University of California at Berkeley, June 1989.

Harichandran, R. and Vanmarcke, E., (1984), "Space-Time Variation of Earthquake Ground Motion", Research Report R84-12, Dept. of Civil Eng. MIT.

Hoshiya, M., et al., (1976), "Nonstationary Characteristics of Earthquake Acceleration and Its Simulation", *Proc. of Japanese Society of Civil Engineering*, No. 245.

Housner, G. W., (1965), "Intensity of Earthquake Ground Shaking Near the Causative Fault", 3WCEE, New Zealand.

Iyengar, R. N. and Iyengar, K. T. S. C., (1969), "A Nonstationary Random Process Model for Earthquake Accelerations", *Bull. of the Seism. Soc. of Am.*, Vol. 59, No.3.

Jennings, P. C., Housner, G. W. and Tsai, N. C., (1968), "Simulated Earthquake Motions", EERL, 70-05, California Institute of Technology.

Joyner, W. B., Boore, D. M. and Porcella, R. C., (1981), "Peak Horizontal Acceleration and Velocity From Strong Motion Records Including Records From 1979 Imperial Valley, California Earthquake", U. S. Geological Survey, Openfile Report, 81-365.

Kanasewich, E. R., (1981), "Time Sequence Analysis in Geophysics", The University of Alberta Press, Canada.

Kausel, E., (1974), "Forced Vibrations of Circular Foundations on Layered Media", R74-11, Dept. of Civil Engineering, MIT.

Kausel, E. and Ushijima, R., (1979), "Baseline Correction of Earthquake Records in the Frequency Domain", research Report R79-34, Dept. of Civil Engineering, Constructed Facilities Division, MIT, Cambridge, Massachusetts 02139.

Kobayashi, H. and Nagahashi, S., (1977), "Response Spectra on Seismic Bedrock During Earthquake, Proc. 6WCEE, New Delhi.

Kubo, T. and Penzien, J., (1976), "Time and Frequency Domain Analysis of Three Dimensional Ground Motions, San Fernando Earthquake", Report No. UCB/EERC-76-06, Earthquake Eng. Res. Center, University of California at Berkeley.

Liou, G. S., (1988), "Analytic Solutions for Soil-Structure Interaction in Layered Media", To Be Published in Earthquake Engineering and Structural Dynamics.

Loh, C. H., (1985), "Analysis of Spatial Variation of Seismic Waves and Ground Movements for SMART-1 Array Data", Earthquake Engineering and Structural Dynamics, Vol. 13, 561-581.

Loh, C. H. and Penzien, J., (1984), "Identification of Wave Types, Directions, and Velocities Using SMART-1 Strong Motion Array Data", 8WCEE, Vol. 2, 191-198.

Loh, C. H., Penzien, J. and Tsai, Y. B., (1982), "Engineering Analysis of SMART-1 Array Accelerograms", Earthquake Engineering and Structural Dynamics, Vol. 10, 575-592.

Loh, C. H. and Yeh, Y. T., (1988), "Spatial Variation and Stochastic Modelling of Seismic Differential Ground Movement", Earthquake Engineering and Structural Dynamics, Vol. 16, 583-596.

Luco, J. E., (1976), "Vibration of a Rigid Disc on a Layered Viscoelastic Medium", Nuclear Engineering and Design, Vol. 36, 325-340

Luco, J. E., (1982), "Linear Soil-Structure Interaction: A Review", Earthquake Ground Motion and Its Effects On Structures, AMD-Vol. 53, S. K. Datta (ED), American Society of Mech. Eng., New York, 41-57.

Luco, J. E. and Westmann, R. A., (1971), "Dynamic Response of Circular Footings", Engineering Report No. 7113, School of Engineering and Applied Science, University of California at Los Angeles.

Luco, J. E. and Wong, H. L., (1986), "Response of a Rigid Foundation to a Spatially Random Ground Motion", Earthquake Engineering and Structural Dynamics, Vol. 6, 891-908.

Lysmer, J., Udaka, T., Tsai, C.-F. and Seed, H. B., (1975), "FLUSH - A Computer Program for Approximate 3-D Analysis of Soil-Structure Interaction Problems", Report No. UCB/EERC-75-30, Earthquake Eng. Res. Center, University of California at Berkeley.

Milne, W. G. and Davenport, W. G., (1969), "Distribution of Earthquake Risk in Canada", Bull. Seis. Soc. of America, Vol. 59, 729-754.

Newmark, N. M. and Hall, W. J., (1969), "Seismic Design Criteria for Nuclear Reactor Facilities", 4WCEE, Vol. 2, Santiago, Chile.

Oliveira, C. S., (1985), "Variability of Strong Ground Motion Characteristics Obtained in SMART-1 Array", Proc. 12th Regional Seminar on Earthquake Engineering, Halkidiki, Greece.

Peng, K. Z., Wu, F. T. and Song, L., (1985), "Attenuation Characteristics of Peak Horizontal Acceleration in Northeast and Southwest China", Earthquake Engineering and Structural Dynamics, Vol.13, 337-350.

Penzien, J., (1976), "Structural Dynamics of Fixed Offshore Structures", Recent Advances in Earthquake-Resistant Design of Structures, Part II, Continuing Education in Engineering, University Extension, and the College of Engineering, University of California at Berkeley, June 21-25, 1976.

Penzien, J., (1988), "Review of Seismic Design in Industry", International Workshop on Seismic Design, May 26-27, Taipei, Taiwan.

Penzien, J. and Watabe, M., (1975), "Characteristics of 3-Dimensional Earthquake Ground Motions", Earthquake Engineering and Structural Dynamics, Vol. 3, 365-373.

Ruiz, P. and Penzien, J., (1969), "Artificial Generation of Earthquake Accelerograms", Report No. UCB/EERC-69-03, Earthquake Eng. Res. Center, University of California at Berkeley.

Scanlan, R. H. and Sachs, K., (1974), "Earthquake Time Histories and Response Spectra", Journal of Engineering Mechanics, ASCE, p10703.

Shinozuka, M., Editor, (1987), "Stochastic Mechanics", Vol. 2, Dept. of Civil Engineering and Engineering Mechanics, Columbia University, New York.

Shinozuka, M. and Sato, Y., (1967), "Simulation of Nonstationary Random Process", ASCE, EM1, Feb..

Somaini, D. R., (1988), "Seismic Behavior of Girder Bridges for Horizontally Propagating Waves", Earthquake Engineering and Structural Dynamics, Vol. 15, 777-793.

Tajimi, H., (1960), "A Statistical Method of Determining the Maximum Response of a Building Structure During an Earthquake", Proc. 2WCEE, Vol. 2, Tokyo, 781-797.

Tajirian, F. F., (1981), "Impedance Matrices and Interpolation Techniques for 3D Interaction Analysis by the Flexible Volume Method", Ph.D. Dissertation, Dept. of Civil Engineering, University of California at Berkeley.

Toki, K., (1968), "Simulation of Earthquake Motion and Its Application", Bull. Disaster Prevention Res. Inst., Kyoto University, Vol. 11-A.

Trifunac, M. D., (1979), "Preliminary Empirical Model for Scaling Fourier Amplitude Spectra of Strong Ground Motion Acceleration in Terms of Modified Mercalli Intensity and Recording Site Conditions", Earthquake Engineering and Structural Dynamics, Vol. 7, 63-74.

Trifunac, M. D. and Westermo, B. D., (1976), "Dependence of the Duration of Strong Earthquake Ground Motion on Magnitude, Epicentral Distance, Geological Conditions at the

Recording Station and Frequency of Motion", Report No. CE 76-02, Dept. of Civil Engineering, Univ. of Southern California.

Tsai, Y. B., (1988), "Empirical Characterization of Free-Field Ground Motion for Soil-Structure Interaction Analysis", 2nd Workshop on Strong Motion Arrays, Taipei, Taiwan.

Veletsos, A. S. and Wei, Y. T., (1971), "Lateral and Rocking Vibrations of Footings", J. Soil Mech. Found. Div., ASCE, 97,1227-1248.

Watabe, M., (1987), "On Synthetic Earthquake Ground Motions", Canadian Earthquake Engineering Conference.

Watabe, M., (1988), "Characteristics and Synthetic Generation of Earthquake Ground Motions", Seminar, Dept. of Civil Engineering, SEMM, University of California at Berkeley.

Watabe, M. and Tohdo, M., (1982), "Research on the Design Earthquake Ground Motions", Part 2, Trans. Archi. Inst., Japan, No. 312.

Wilson, E. L., (1986), "CAL86-Computer Assisted Learning of Structural Analysis and the CAL/SAP Development System", Report No. UCB/SESM/86-05, Dept. of Civil Engineering, University of California at Berkeley.

Wong, H. L., (1975), "Dynamic Soil-Structure Interaction", Report EERL 75-01, Earthquake Engineering Research Lab., California Institute of Technology.

Wong, H. L. and Luco, J. E., (1976), "Dynamic Response of Rigid Foundations of Arbitrary Shape", Earthquake Engineering and Structural Dynamics, Vol.4, 579-587.

Wong, H. L. and Luco, J. E., (1985), "Tables of Impedance Functions for Square Foundations on Layered Media", Soil Dynamics and Earthquake Engineering, 4: 2, 64-81.

Wong, H. L. and Trifunac, M. D., (1979), "Generation of Artificial Strong Motion Accelerograms", Earthquake Engineering and Structural Dynamics, Vol. 7, 509-527.

Zerva, A., Ang, A. H. S. and Wen, Y. K., (1988), "Lifeline Response to Spatially Variable Ground Motions", Earthquake Engineering and Structural Dynamics, Vol. 16, 361-379.

EARTHQUAKE ENGINEERING RESEARCH CENTER REPORT SERIES

EERC reports are available from the National Information Service for Earthquake Engineering(NISEE) and from the National Technical Information Service(NTIS). Numbers in parentheses are Accession Numbers assigned by the National Technical Information Service; these are followed by a price code. Contact NTIS, 5285 Port Royal Road, Springfield Virginia, 22161 for more information. Reports without Accession Numbers were not available from NTIS at the time of printing. For a current complete list of EERC reports (from EERC 67-1) and availability information, please contact University of California, EERC, NISEE, 1301 South 46th Street, Richmond, California 94804.

- UCB/EERC-80/01 "Earthquake Response of Concrete Gravity Dams Including Hydrodynamic and Foundation Interaction Effects," by Chopra, A.K., Chakrabarti, P. and Gupta, S., January 1980, (AD-A087297)A10.
- UCB/EERC-80/02 "Rocking Response of Rigid Blocks to Earthquakes," by Yim, C.S., Chopra, A.K. and Penzien, J., January 1980, (PB80 166 002)A04.
- UCB/EERC-80/03 "Optimum Inelastic Design of Seismic-Resistant Reinforced Concrete Frame Structures," by Zagajski, S.W. and Bertero, V.V., January 1980, (PB80 164 635)A06.
- UCB/EERC-80/04 "Effects of Amount and Arrangement of Wall-Panel Reinforcement on Hysteretic Behavior of Reinforced Concrete Walls," by Iliya, R. and Bertero, V.V., February 1980, (PB81 122 525)A09.
- UCB/EERC-80/05 "Shaking Table Research on Concrete Dam Models," by Niwa, A. and Clough, R.W., September 1980, (PB81 122 368)A06.
- UCB/EERC-80/06 "The Design of Steel Energy-Absorbing Restrainers and their Incorporation into Nuclear Power Plants for Enhanced Safety (Vol Ia): Piping with Energy Absorbing Restrainers: Parameter Study on Small Systems," by Powell, G.H., Oughourlian, C. and Simons, J., June 1980.
- UCB/EERC-80/07 "Inelastic Torsional Response of Structures Subjected to Earthquake Ground Motions," by Yamazaki, Y., April 1980, (PB81 122 327)A08.
- UCB/EERC-80/08 "Study of X-Braced Steel Frame Structures under Earthquake Simulation," by Ghanaat, Y., April 1980, (PB81 122 335)A11.
- UCB/EERC-80/09 "Hybrid Modelling of Soil-Structure Interaction," by Gupta, S., Lin, T.W. and Penzien, J., May 1980, (PB81 122 319)A07.
- UCB/EERC-80/10 "General Applicability of a Nonlinear Model of a One Story Steel Frame," by Sveinsson, B.I. and McNiven, H.D., May 1980, (PB81 124 877)A06.
- UCB/EERC-80/11 "A Green-Function Method for Wave Interaction with a Submerged Body," by Kioka, W., April 1980, (PB81 122 269)A07.
- UCB/EERC-80/12 "Hydrodynamic Pressure and Added Mass for Axisymmetric Bodies," by Nilrat, F., May 1980, (PB81 122 343)A08.
- UCB/EERC-80/13 "Treatment of Non-Linear Drag Forces Acting on Offshore Platforms," by Dao, B.V. and Penzien, J., May 1980, (PB81 153 413)A07.
- UCB/EERC-80/14 "2D Plane/Axisymmetric Solid Element (Type 3-Elastic or Elastic-Perfectly Plastic)for the ANSR-II Program," by Mondkar, D.P. and Powell, G.H., July 1980, (PB81 122 350)A03.
- UCB/EERC-80/15 "A Response Spectrum Method for Random Vibrations," by Der Kiureghian, A., June 1981, (PB81 122 301)A03.
- UCB/EERC-80/16 "Cyclic Inelastic Buckling of Tubular Steel Braces," by Zayas, V.A., Popov, E.P. and Mahin, S.A., June 1981, (PB81 124 885)A10.
- UCB/EERC-80/17 "Dynamic Response of Simple Arch Dams Including Hydrodynamic Interaction," by Porter, C.S. and Chopra, A.K., July 1981, (PB81 124 000)A13.
- UCB/EERC-80/18 "Experimental Testing of a Friction Damped Aseismic Base Isolation System with Fail-Safe Characteristics," by Kelly, J.M., Beucke, K.E. and Skinner, M.S., July 1980, (PB81 148 595)A04.
- UCB/EERC-80/19 "The Design of Steel Energy-Absorbing Restrainers and their Incorporation into Nuclear Power Plants for Enhanced Safety (Vol.1B): Stochastic Seismic Analyses of Nuclear Power Plant Structures and Piping Systems Subjected to Multiple Supported Excitations," by Lee, M.C. and Penzien, J., June 1980, (PB82 201 872)A08.
- UCB/EERC-80/20 "The Design of Steel Energy-Absorbing Restrainers and their Incorporation into Nuclear Power Plants for Enhanced Safety (Vol 1C): Numerical Method for Dynamic Substructure Analysis," by Dickens, J.M. and Wilson, E.L., June 1980.
- UCB/EERC-80/21 "The Design of Steel Energy-Absorbing Restrainers and their Incorporation into Nuclear Power Plants for Enhanced Safety (Vol 2): Development and Testing of Restraints for Nuclear Piping Systems," by Kelly, J.M. and Skinner, M.S., June 1980.
- UCB/EERC-80/22 "3D Solid Element (Type 4-Elastic or Elastic-Perfectly-Plastic) for the ANSR-II Program," by Mondkar, D.P. and Powell, G.H., July 1980, (PB81 123 242)A03.
- UCB/EERC-80/23 "Gap-Friction Element (Type 5) for the Ansr-II Program," by Mondkar, D.P. and Powell, G.H., July 1980, (PB81 122 285)A03.
- UCB/EERC-80/24 "U-Bar Restraint Element (Type 11) for the ANSR-II Program," by Oughourlian, C. and Powell, G.H., July 1980, (PB81 122 293)A03.
- UCB/EERC-80/25 "Testing of a Natural Rubber Base Isolation System by an Explosively Simulated Earthquake," by Kelly, J.M., August 1980, (PB81 201 360)A04.
- UCB/EERC-80/26 "Input Identification from Structural Vibrational Response," by Hu, Y., August 1980, (PB81 152 308)A05.
- UCB/EERC-80/27 "Cyclic Inelastic Behavior of Steel Offshore Structures," by Zayas, V.A., Mahin, S.A. and Popov, E.P., August 1980, (PB81 196 180)A15.
- UCB/EERC-80/28 "Shaking Table Testing of a Reinforced Concrete Frame with Biaxial Response," by Oliva, M.G., October 1980, (PB81 154 304)A10.
- UCB/EERC-80/29 "Dynamic Properties of a Twelve-Story Prefabricated Panel Building," by Bouwkamp, J.G., Kollegger, J.P. and Stephen, R.M., October 1980, (PB82 138 777)A07.
- UCB/EERC-80/30 "Dynamic Properties of an Eight-Story Prefabricated Panel Building," by Bouwkamp, J.G., Kollegger, J.P. and Stephen, R.M., October 1980, (PB81 200 313)A05.
- UCB/EERC-80/31 "Predictive Dynamic Response of Panel Type Structures under Earthquakes," by Kollegger, J.P. and Bouwkamp, J.G., October 1980, (PB81 152 316)A04.
- UCB/EERC-80/32 "The Design of Steel Energy-Absorbing Restrainers and their Incorporation into Nuclear Power Plants for Enhanced Safety (Vol 3): Testing of Commercial Steels in Low-Cycle Torsional Fatigue," by Spanner, P., Parker, E.R., Jongewaard, E. and Dory, M., 1980.

- UCB/EERC-80/33 "The Design of Steel Energy-Absorbing Restrainers and their Incorporation into Nuclear Power Plants for Enhanced Safety (Vol 4): Shaking Table Tests of Piping Systems with Energy-Absorbing Restrainers," by Stierner, S.F. and Godden, W.G., September 1980, (PB82 201 880)A05.
- UCB/EERC-80/34 "The Design of Steel Energy-Absorbing Restrainers and their Incorporation into Nuclear Power Plants for Enhanced Safety (Vol 5): Summary Report," by Spencer, P., 1980.
- UCB/EERC-80/35 "Experimental Testing of an Energy-Absorbing Base Isolation System," by Kelly, J.M., Skinner, M.S. and Beucke, K.E., October 1980, (PB81 154 072)A04.
- UCB/EERC-80/36 "Simulating and Analyzing Artificial Non-Stationary Earth Ground Motions," by Nau, R.F., Oliver, R.M. and Pister, K.S., October 1980, (PB81 153 397)A04.
- UCB/EERC-80/37 "Earthquake Engineering at Berkeley - 1980," by , September 1980, (PB81 205 674)A09.
- UCB/EERC-80/38 "Inelastic Seismic Analysis of Large Panel Buildings," by Schrickler, V. and Powell, G.H., September 1980, (PB81 154 338)A13.
- UCB/EERC-80/39 "Dynamic Response of Embankment, Concrete-Gavity and Arch Dams Including Hydrodynamic Interaction," by Hall, J.F. and Chopra, A.K., October 1980, (PB81 152 324)A11.
- UCB/EERC-80/40 "Inelastic Buckling of Steel Struts under Cyclic Load Reversal," by Black, R.G., Wenger, W.A. and Popov, E.P., October 1980, (PB81 154 312)A08.
- UCB/EERC-80/41 "Influence of Site Characteristics on Buildings Damage during the October 3,1974 Lima Earthquake," by Repetto, P., Arango, I. and Seed, H.B., September 1980, (PB81 161 739)A05.
- UCB/EERC-80/42 "Evaluation of a Shaking Table Test Program on Response Behavior of a Two Story Reinforced Concrete Frame," by Blondet, J.M., Clough, R.W. and Mahin, S.A., December 1980, (PB82 196 544)A11.
- UCB/EERC-80/43 "Modelling of Soil-Structure Interaction by Finite and Infinite Elements," by Medina, F., December 1980, (PB81 229 270)A04.
- UCB/EERC-81/01 "Control of Seismic Response of Piping Systems and Other Structures by Base Isolation," by Kelly, J.M., January 1981, (PB81 200 735)A05.
- UCB/EERC-81/02 "OPTNSR- An Interactive Software System for Optimal Design of Statically and Dynamically Loaded Structures with Nonlinear Response," by Bhatti, M.A., Ciampi, V. and Pister, K.S., January 1981, (PB81 218 851)A09.
- UCB/EERC-81/03 "Analysis of Local Variations in Free Field Seismic Ground Motions," by Chen, J.-C., Lysmer, J. and Seed, H.B., January 1981, (AD-A099508)A13.
- UCB/EERC-81/04 "Inelastic Structural Modeling of Braced Offshore Platforms for Seismic Loading," by Zayas, V.A., Shing, P.-S.B., Mahin, S.A. and Popov, E.P., January 1981, (PB82 138 777)A07.
- UCB/EERC-81/05 "Dynamic Response of Light Equipment in Structures," by Der Kiureghian, A., Sackman, J.L. and Nour-Omid, B., April 1981, (PB81 218 497)A04.
- UCB/EERC-81/06 "Preliminary Experimental Investigation of a Broad Base Liquid Storage Tank," by Bouwkamp, J.G., Kollcgger, J.P. and Stephen, R.M., May 1981, (PB82 140 385)A03.
- UCB/EERC-81/07 "The Seismic Resistant Design of Reinforced Concrete Coupled Structural Walls," by Aktan, A.E. and Bertero, V.V., June 1981, (PB82 113 358)A11.
- UCB/EERC-81/08 "Unassigned," by Unassigned, 1981.
- UCB/EERC-81/09 "Experimental Behavior of a Spatial Piping System with Steel Energy Absorbers Subjected to a Simulated Differential Seismic Input," by Stierner, S.F., Godden, W.G. and Kelly, J.M., July 1981, (PB82 201 898)A04.
- UCB/EERC-81/10 "Evaluation of Seismic Design Provisions for Masonry in the United States," by Sveinsson, B.I., Mayes, R.L. and McNiven, H.D., August 1981, (PB82 166 075)A08.
- UCB/EERC-81/11 "Two-Dimensional Hybrid Modelling of Soil-Structure Interaction," by Tzong, T.-J., Gupta, S. and Penzien, J., August 1981, (PB82 142 118)A04.
- UCB/EERC-81/12 "Studies on Effects of Infills in Seismic Resistant R/C Construction," by Brokken, S. and Bertero, V.V., October 1981, (PB82 166 190)A09.
- UCB/EERC-81/13 "Linear Models to Predict the Nonlinear Seismic Behavior of a One-Story Steel Frame," by Valdimarsson, H., Shah, A.H. and McNiven, H.D., September 1981, (PB82 138 793)A07.
- UCB/EERC-81/14 "TLUSH: A Computer Program for the Three-Dimensional Dynamic Analysis of Earth Dams," by Kagawa, T., Mejia, L.H., Seed, H.B. and Lysmer, J., September 1981, (PB82 139 940)A06.
- UCB/EERC-81/15 "Three Dimensional Dynamic Response Analysis of Earth Dams," by Mejia, L.H. and Seed, H.B., September 1981, (PB82 137 274)A12.
- UCB/EERC-81/16 "Experimental Study of Lead and Elastomeric Dampers for Base Isolation Systems," by Kelly, J.M. and Hodder, S.B., October 1981, (PB82 166 182)A05.
- UCB/EERC-81/17 "The Influence of Base Isolation on the Seismic Response of Light Secondary Equipment," by Kelly, J.M., April 1981, (PB82 255 266)A04.
- UCB/EERC-81/18 "Studies on Evaluation of Shaking Table Response Analysis Procedures," by Blondet, J. M., November 1981, (PB82 197 278)A10.
- UCB/EERC-81/19 "DELIGHT.STRUCT: A Computer-Aided Design Environment for Structural Engineering," by Balling, R.J., Pister, K.S. and Polak, E., December 1981, (PB82 218 496)A07.
- UCB/EERC-81/20 "Optimal Design of Seismic-Resistant Planar Steel Frames," by Balling, R.J., Ciampi, V. and Pister, K.S., December 1981, (PB82 220 179)A07.
- UCB/EERC-82/01 "Dynamic Behavior of Ground for Seismic Analysis of Lifeline Systems," by Sato, T. and Der Kiureghian, A., January 1982, (PB82 218 926)A05.
- UCB/EERC-82/02 "Shaking Table Tests of a Tubular Steel Frame Model," by Ghanaat, Y. and Clough, R.W., January 1982, (PB82 220 161)A07.

- UCB/EERC-82/03 "Behavior of a Piping System under Seismic Excitation: Experimental Investigations of a Spatial Piping System supported by Mechanical Shock Arrestors," by Schneider, S., Lee, H.-M. and Godden, W. G., May 1982, (PB83 172 544)A09.
- UCB/EERC-82/04 "New Approaches for the Dynamic Analysis of Large Structural Systems," by Wilson, E.L., June 1982, (PB83 148 080)A05.
- UCB/EERC-82/05 "Model Study of Effects of Damage on the Vibration Properties of Steel Offshore Platforms," by Shahrivar, F. and Bouwkamp, J.G., June 1982, (PB83 148 742)A10.
- UCB/EERC-82/06 "States of the Art and Practice in the Optimum Seismic Design and Analytical Response Prediction of R/C Frame Wall Structures," by Aktan, A.E. and Bertero, V.V., July 1982, (PB83 147 736)A05.
- UCB/EERC-82/07 "Further Study of the Earthquake Response of a Broad Cylindrical Liquid-Storage Tank Model," by Manos, G.C. and Clough, R.W., July 1982, (PB83 147 744)A11.
- UCB/EERC-82/08 "An Evaluation of the Design and Analytical Seismic Response of a Seven Story Reinforced Concrete Frame," by Charney, F.A. and Bertero, V.V., July 1982, (PB83 157 628)A09.
- UCB/EERC-82/09 "Fluid-Structure Interactions: Added Mass Computations for Incompressible Fluid," by Kuo, J.S.-H., August 1982, (PB83 156 281)A07.
- UCB/EERC-82/10 "Joint-Opening Nonlinear Mechanism: Interface Smeared Crack Model," by Kuo, J.S.-H., August 1982, (PB83 149 195)A05.
- UCB/EERC-82/11 "Dynamic Response Analysis of Techii Dam," by Clough, R.W., Stephen, R.M. and Kuo, J.S.-H., August 1982, (PB83 147 496)A06.
- UCB/EERC-82/12 "Prediction of the Seismic Response of R/C Frame-Coupled Wall Structures," by Aktan, A.E., Bertero, V.V. and Piazza, M., August 1982, (PB83 149 203)A09.
- UCB/EERC-82/13 "Preliminary Report on the Smart 1 Strong Motion Array in Taiwan," by Bolt, B.A., Loh, C.H., Penzien, J. and Tsai, Y.B., August 1982, (PB83 159 400)A10.
- UCB/EERC-82/14 "Shaking-Table Studies of an Eccentrically X-Braced Steel Structure," by Yang, M.S., September 1982, (PB83 260 778)A12.
- UCB/EERC-82/15 "The Performance of Stairways in Earthquakes," by Roha, C., Axley, J.W. and Bertero, V.V., September 1982, (PB83 157 693)A07.
- UCB/EERC-82/16 "The Behavior of Submerged Multiple Bodies in Earthquakes," by Liao, W.-G., September 1982, (PB83 158 709)A07.
- UCB/EERC-82/17 "Effects of Concrete Types and Loading Conditions on Local Bond-Slip Relationships," by Cowell, A.D., Popov, E.P. and Bertero, V.V., September 1982, (PB83 153 577)A04.
- UCB/EERC-82/18 "Mechanical Behavior of Shear Wall Vertical Boundary Members: An Experimental Investigation," by Wagner, M.T. and Bertero, V.V., October 1982, (PB83 159 764)A05.
- UCB/EERC-82/19 "Experimental Studies of Multi-support Seismic Loading on Piping Systems," by Kelly, J.M. and Cowell, A.D., November 1982.
- UCB/EERC-82/20 "Generalized Plastic Hinge Concepts for 3D Beam-Column Elements," by Chen, P. F.-S. and Powell, G.H., November 1982, (PB83 247 981)A13.
- UCB/EERC-82/21 "ANSR-II: General Computer Program for Nonlinear Structural Analysis," by Oughourlian, C.V. and Powell, G.H., November 1982, (PB83 251 330)A12.
- UCB/EERC-82/22 "Solution Strategies for Statically Loaded Nonlinear Structures," by Simons, J.W. and Powell, G.H., November 1982, (PB83 197 970)A06.
- UCB/EERC-82/23 "Analytical Model of Deformed Bar Anchorages under Generalized Excitations," by Ciampi, V., Eligehausen, R., Bertero, V.V. and Popov, E.P., November 1982, (PB83 169 532)A06.
- UCB/EERC-82/24 "A Mathematical Model for the Response of Masonry Walls to Dynamic Excitations," by Sucuoglu, H., Mengi, Y. and McNiven, H.D., November 1982, (PB83 169 011)A07.
- UCB/EERC-82/25 "Earthquake Response Considerations of Broad Liquid Storage Tanks," by Cambra, F.J., November 1982, (PB83 251 215)A09.
- UCB/EERC-82/26 "Computational Models for Cyclic Plasticity, Rate Dependence and Creep," by Mosaddad, B. and Powell, G.H., November 1982, (PB83 245 829)A08.
- UCB/EERC-82/27 "Inelastic Analysis of Piping and Tubular Structures," by Mahasuverachai, M. and Powell, G.H., November 1982, (PB83 249 987)A07.
- UCB/EERC-83/01 "The Economic Feasibility of Seismic Rehabilitation of Buildings by Base Isolation," by Kelly, J.M., January 1983, (PB83 197 988)A05.
- UCB/EERC-83/02 "Seismic Moment Connections for Moment-Resisting Steel Frames," by Popov, E.P., January 1983, (PB83 195 412)A04.
- UCB/EERC-83/03 "Design of Links and Beam-to-Column Connections for Eccentrically Braced Steel Frames," by Popov, E.P. and Malley, J.O., January 1983, (PB83 194 811)A04.
- UCB/EERC-83/04 "Numerical Techniques for the Evaluation of Soil-Structure Interaction Effects in the Time Domain," by Bayo, E. and Wilson, E.L., February 1983, (PB83 245 605)A09.
- UCB/EERC-83/05 "A Transducer for Measuring the Internal Forces in the Columns of a Frame-Wall Reinforced Concrete Structure," by Sause, R. and Bertero, V.V., May 1983, (PB84 119 494)A06.
- UCB/EERC-83/06 "Dynamic Interactions Between Floating Ice and Offshore Structures," by Croteau, P., May 1983, (PB84 119 486)A16.
- UCB/EERC-83/07 "Dynamic Analysis of Multiply Tuned and Arbitrarily Supported Secondary Systems," by Igusa, T. and Der Kiureghian, A., July 1983, (PB84 118 272)A11.
- UCB/EERC-83/08 "A Laboratory Study of Submerged Multi-body Systems in Earthquakes," by Ansari, G.R., June 1983, (PB83 261 842)A17.
- UCB/EERC-83/09 "Effects of Transient Foundation Uplift on Earthquake Response of Structures," by Yim, C.-S. and Chopra, A.K., June 1983, (PB83 261 396)A07.
- UCB/EERC-83/10 "Optimal Design of Friction-Braced Frames under Seismic Loading," by Austin, M.A. and Pister, K.S., June 1983, (PB84 119 288)A06.
- UCB/EERC-83/11 "Shaking Table Study of Single-Story Masonry Houses: Dynamic Performance under Three Component Seismic Input and Recommendations," by Manos, G.C., Clough, R.W. and Mayes, R.L., July 1983, (UCB/EERC-83/11)A08.
- UCB/EERC-83/12 "Experimental Error Propagation in Pseudodynamic Testing," by Shiing, P.B. and Mahin, S.A., June 1983, (PB84 119 270)A09.
- UCB/EERC-83/13 "Experimental and Analytical Predictions of the Mechanical Characteristics of a 1/5-scale Model of a 7-story R/C Frame-Wall Building Structure," by Aktan, A.E., Bertero, V.V., Chowdhury, A.A. and Nagashima, T., June 1983, (PB84 119 213)A07.

- UCB/EERC-83/14 "Shaking Table Tests of Large-Panel Precast Concrete Building System Assemblages," by Oliva, M.G. and Clough, R.W., June 1983, (PB86 110 210/AS)A11.
- UCB/EERC-83/15 "Seismic Behavior of Active Beam Links in Eccentrically Braced Frames," by Hjelmstad, K.D. and Popov, E.P., July 1983, (PB84 119 676)A09.
- UCB/EERC-83/16 "System Identification of Structures with Joint Rotation," by Dimsdale, J.S., July 1983, (PB84 192 210)A06.
- UCB/EERC-83/17 "Construction of Inelastic Response Spectra for Single-Degree-of-Freedom Systems," by Mahin, S. and Lin, J., June 1983, (PB84 208 834)A05.
- UCB/EERC-83/18 "Interactive Computer Analysis Methods for Predicting the Inelastic Cyclic Behaviour of Structural Sections," by Kaba, S. and Mahin, S., July 1983, (PB84 192 012)A06.
- UCB/EERC-83/19 "Effects of Bond Deterioration on Hysteretic Behavior of Reinforced Concrete Joints," by Filippou, F.C., Popov, E.P. and Bertero, V.V., August 1983, (PB84 192 020)A10.
- UCB/EERC-83/20 "Correlation of Analytical and Experimental Responses of Large-Panel Precast Building Systems," by Oliva, M.G., Clough, R.W., Velkov, M. and Gavrilovic, P., May 1988.
- UCB/EERC-83/21 "Mechanical Characteristics of Materials Used in a 1/5 Scale Model of a 7-Story Reinforced Concrete Test Structure," by Bertero, V.V., Aktan, A.E., Harris, H.G. and Chowdhury, A.A., October 1983, (PB84 193 697)A05.
- UCB/EERC-83/22 "Hybrid Modelling of Soil-Structure Interaction in Layered Media," by Tzong, T.-J. and Penzien, J., October 1983, (PB84 192 178)A08.
- UCB/EERC-83/23 "Local Bond Stress-Slip Relationships of Deformed Bars under Generalized Excitations," by Elgehausen, R., Popov, E.P. and Bertero, V.V., October 1983, (PB84 192 848)A09.
- UCB/EERC-83/24 "Design Considerations for Shear Links in Eccentrically Braced Frames," by Malley, J.O. and Popov, E.P., November 1983, (PB84 192 186)A07.
- UCB/EERC-84/01 "Pseudodynamic Test Method for Seismic Performance Evaluation: Theory and Implementation," by Shing, P.-S.B. and Mahin, S.A., January 1984, (PB84 190 644)A08.
- UCB/EERC-84/02 "Dynamic Response Behavior of Kiang Hong Dian Dam," by Clough, R.W., Chang, K.-T., Chen, H.-Q. and Stephen, R.M., April 1984, (PB84 209 402)A08.
- UCB/EERC-84/03 "Refined Modelling of Reinforced Concrete Columns for Seismic Analysis," by Kaba, S.A. and Mahin, S.A., April 1984, (PB84 234 384)A06.
- UCB/EERC-84/04 "A New Floor Response Spectrum Method for Seismic Analysis of Multiply Supported Secondary Systems," by Asfura, A. and Der Kiureghian, A., June 1984, (PB84 239 417)A06.
- UCB/EERC-84/05 "Earthquake Simulation Tests and Associated Studies of a 1/5th-scale Model of a 7-Story R/C Frame-Wall Test Structure," by Bertero, V.V., Aktan, A.E., Charney, F.A. and Sause, R., June 1984, (PB84 239 409)A09.
- UCB/EERC-84/06 "R/C Structural Walls: Seismic Design for Shear," by Aktan, A.E. and Bertero, V.V., 1984.
- UCB/EERC-84/07 "Behavior of Interior and Exterior Flat-Plate Connections subjected to Inelastic Load Reversals," by Zee, H.L. and Moehle, J.P., August 1984, (PB86 117 629/AS)A07.
- UCB/EERC-84/08 "Experimental Study of the Seismic Behavior of a Two-Story Flat-Plate Structure," by Moehle, J.P. and Diebold, J.W., August 1984, (PB86 122 553/AS)A12.
- UCB/EERC-84/09 "Phenomenological Modeling of Steel Braces under Cyclic Loading," by Ikeda, K., Mahin, S.A. and Dermitzakis, S.N., May 1984, (PB86 132 198/AS)A08.
- UCB/EERC-84/10 "Earthquake Analysis and Response of Concrete Gravity Dams," by Fenves, G. and Chopra, A.K., August 1984, (PB85 193 902/AS)A11.
- UCB/EERC-84/11 "EAGD-84: A Computer Program for Earthquake Analysis of Concrete Gravity Dams," by Fenves, G. and Chopra, A.K., August 1984, (PB85 193 613/AS)A05.
- UCB/EERC-84/12 "A Refined Physical Theory Model for Predicting the Seismic Behavior of Braced Steel Frames," by Ikeda, K. and Mahin, S.A., July 1984, (PB85 191 450/AS)A09.
- UCB/EERC-84/13 "Earthquake Engineering Research at Berkeley - 1984," by , August 1984, (PB85 197 341/AS)A10.
- UCB/EERC-84/14 "Moduli and Damping Factors for Dynamic Analyses of Cohesionless Soils," by Seed, H.B., Wong, R.T., Idriss, I.M. and Tokimatsu, K., September 1984, (PB85 191 468/AS)A04.
- UCB/EERC-84/15 "The Influence of SPT Procedures in Soil Liquefaction Resistance Evaluations," by Seed, H.B., Tokimatsu, K., Harder, L.F. and Chung, R.M., October 1984, (PB85 191 732/AS)A04.
- UCB/EERC-84/16 "Simplified Procedures for the Evaluation of Settlements in Sands Due to Earthquake Shaking," by Tokimatsu, K. and Seed, H.B., October 1984, (PB85 197 887/AS)A03.
- UCB/EERC-84/17 "Evaluation of Energy Absorption Characteristics of Bridges under Seismic Conditions," by Imbsen, R.A. and Penzien, J., November 1984.
- UCB/EERC-84/18 "Structure-Foundation Interactions under Dynamic Loads," by Liu, W.D. and Penzien, J., November 1984, (PB87 124 889/AS)A11.
- UCB/EERC-84/19 "Seismic Modelling of Deep Foundations," by Chen, C.-H. and Penzien, J., November 1984, (PB87 124 798/AS)A07.
- UCB/EERC-84/20 "Dynamic Response Behavior of Quan Shui Dam," by Clough, R.W., Chang, K.-T., Chen, H.-Q., Stephen, R.M., Ghanaat, Y. and Qi, J.-H., November 1984, (PB86 115177/AS)A07.
- UCB/EERC-85/01 "Simplified Methods of Analysis for Earthquake Resistant Design of Buildings," by Cruz, E.F. and Chopra, A.K., February 1985, (PB86 112299/AS)A12.
- UCB/EERC-85/02 "Estimation of Seismic Wave Coherency and Rupture Velocity using the SMART 1 Strong-Motion Array Recordings," by Abrahamson, N.A., March 1985, (PB86 214 343)A07.

- UCB/EERC-85/03 "Dynamic Properties of a Thirty Story Condominium Tower Building," by Stephen, R.M., Wilson, E.L. and Stander, N., April 1985, (PB86 118965/AS)A06.
- UCB/EERC-85/04 "Development of Substructuring Techniques for On-Line Computer Controlled Seismic Performance Testing," by Dermitzakis, S. and Mahin, S., February 1985, (PB86 132941/AS)A08.
- UCB/EERC-85/05 "A Simple Model for Reinforcing Bar Anchorages under Cyclic Excitations," by Filippou, F.C., March 1985, (PB86 112 919/AS)A05.
- UCB/EERC-85/06 "Racking Behavior of Wood-framed Gypsum Panels under Dynamic Load," by Oliva, M.G., June 1985.
- UCB/EERC-85/07 "Earthquake Analysis and Response of Concrete Arch Dams," by Fok, K.-L. and Chopra, A.K., June 1985, (PB86 139672/AS)A10.
- UCB/EERC-85/08 "Effect of Inelastic Behavior on the Analysis and Design of Earthquake Resistant Structures," by Lin, J.P. and Mahin, S.A., June 1985, (PB86 135340/AS)A08.
- UCB/EERC-85/09 "Earthquake Simulator Testing of a Base-Isolated Bridge Deck," by Kelly, J.M., Buckle, I.G. and Tsai, H.-C., January 1986, (PB87 124 152/AS)A06.
- UCB/EERC-85/10 "Simplified Analysis for Earthquake Resistant Design of Concrete Gravity Dams," by Fenves, G. and Chopra, A.K., June 1986, (PB87 124 160/AS)A08.
- UCB/EERC-85/11 "Dynamic Interaction Effects in Arch Dams," by Clough, R.W., Chang, K.-T., Chen, H.-Q. and Ghanaat, Y., October 1985, (PB86 135027/AS)A05.
- UCB/EERC-85/12 "Dynamic Response of Long Valley Dam in the Mammoth Lake Earthquake Series of May 25-27, 1980," by Lai, S. and Seed, H.B., November 1985, (PB86 142304/AS)A05.
- UCB/EERC-85/13 "A Methodology for Computer-Aided Design of Earthquake-Resistant Steel Structures," by Austin, M.A., Pister, K.S. and Mahin, S.A., December 1985, (PB86 159480/AS)A10.
- UCB/EERC-85/14 "Response of Tension-Leg Platforms to Vertical Seismic Excitations," by Liou, G.-S., Penzien, J. and Yeung, R.W., December 1985, (PB87 124 871/AS)A08.
- UCB/EERC-85/15 "Cyclic Loading Tests of Masonry Single Piers: Volume 4 - Additional Tests with Height to Width Ratio of 1," by Sveinsson, B., McNiven, H.D. and Sucuoglu, H., December 1985.
- UCB/EERC-85/16 "An Experimental Program for Studying the Dynamic Response of a Steel Frame with a Variety of Infill Partitions," by Yanev, B. and McNiven, H.D., December 1985.
- UCB/EERC-86/01 "A Study of Seismically Resistant Eccentrically Braced Steel Frame Systems," by Kasai, K. and Popov, E.P., January 1986, (PB87 124 178/AS)A14.
- UCB/EERC-86/02 "Design Problems in Soil Liquefaction," by Seed, H.B., February 1986, (PB87 124 186/AS)A03.
- UCB/EERC-86/03 "Implications of Recent Earthquakes and Research on Earthquake-Resistant Design and Construction of Buildings," by Bertero, V.V., March 1986, (PB87 124 194/AS)A05.
- UCB/EERC-86/04 "The Use of Load Dependent Vectors for Dynamic and Earthquake Analyses," by Leger, P., Wilson, E.L. and Clough, R.W., March 1986, (PB87 124 202/AS)A12.
- UCB/EERC-86/05 "Two Beam-To-Column Web Connections," by Tsai, K.-C. and Popov, E.P., April 1986, (PB87 124 301/AS)A04.
- UCB/EERC-86/06 "Determination of Penetration Resistance for Coarse-Grained Soils using the Becker Hammer Drill," by Harder, L.F. and Seed, H.B., May 1986, (PB87 124 210/AS)A07.
- UCB/EERC-86/07 "A Mathematical Model for Predicting the Nonlinear Response of Unreinforced Masonry Walls to In-Plane Earthquake Excitations," by Mengi, Y. and McNiven, H.D., May 1986, (PB87 124 780/AS)A06.
- UCB/EERC-86/08 "The 19 September 1985 Mexico Earthquake: Building Behavior," by Bertero, V.V., July 1986.
- UCB/EERC-86/09 "EACD-3D: A Computer Program for Three-Dimensional Earthquake Analysis of Concrete Dams," by Fok, K.-L., Hall, J.F. and Chopra, A.K., July 1986, (PB87 124 228/AS)A08.
- UCB/EERC-86/10 "Earthquake Simulation Tests and Associated Studies of a 0.3-Scale Model of a Six-Story Concentrically Braced Steel Structure," by Uang, C.-M. and Bertero, V.V., December 1986, (PB87 163 564/AS)A17.
- UCB/EERC-86/11 "Mechanical Characteristics of Base Isolation Bearings for a Bridge Deck Model Test," by Kelly, J.M., Buckle, I.G. and Koh, C.-G., November 1987.
- UCB/EERC-86/12 "Effects of Axial Load on Elastomeric Isolation Bearings," by Koh, C.-G. and Kelly, J.M., November 1987.
- UCB/EERC-87/01 "The FPS Earthquake Resisting System: Experimental Report," by Zayas, V.A., Low, S.S. and Mahin, S.A., June 1987.
- UCB/EERC-87/02 "Earthquake Simulator Tests and Associated Studies of a 0.3-Scale Model of a Six-Story Eccentrically Braced Steel Structure," by Whitaker, A., Uang, C.-M. and Bertero, V.V., July 1987.
- UCB/EERC-87/03 "A Displacement Control and Uplift Restraint Device for Base-Isolated Structures," by Kelly, J.M., Griffith, M.C. and Aiken, I.D., April 1987.
- UCB/EERC-87/04 "Earthquake Simulator Testing of a Combined Sliding Bearing and Rubber Bearing Isolation System," by Kelly, J.M. and Chalhoub, M.S., 1987.
- UCB/EERC-87/05 "Three-Dimensional Inelastic Analysis of Reinforced Concrete Frame-Wall Structures," by Moazzami, S. and Bertero, V.V., May 1987.
- UCB/EERC-87/06 "Experiments on Eccentrically Braced Frames with Composite Floors," by Ricles, J. and Popov, E., June 1987.
- UCB/EERC-87/07 "Dynamic Analysis of Seismically Resistant Eccentrically Braced Frames," by Ricles, J. and Popov, E., June 1987.
- UCB/EERC-87/08 "Undrained Cyclic Triaxial Testing of Gravels-The Effect of Membrane Compliance," by Evans, M.D. and Seed, H.B., July 1987.
- UCB/EERC-87/09 "Hybrid Solution Techniques for Generalized Pseudo-Dynamic Testing," by Thewalt, C. and Mahin, S.A., July 1987.
- UCB/EERC-87/10 "Ultimate Behavior of Butt Welded Splices in Heavy Rolled Steel Sections," by Bruneau, M., Mahin, S.A. and Popov, E.P., July 1987.
- UCB/EERC-87/11 "Residual Strength of Sand from Dam Failures in the Chilean Earthquake of March 3, 1985," by De Alba, P., Seed, H.B., Retamal, E. and Seed, R.B., September 1987.

- UCB/EERC-87/12 "Inelastic Seismic Response of Structures with Mass or Stiffness Eccentricities in Plan," by Bruneau, M. and Mahin, S.A., September 1987.
- UCB/EERC-87/13 "CSTRUCT: An Interactive Computer Environment for the Design and Analysis of Earthquake Resistant Steel Structures," by Austin, M.A., Mahin, S.A. and Pister, K.S., September 1987.
- UCB/EERC-87/14 "Experimental Study of Reinforced Concrete Columns Subjected to Multi-Axial Loading," by Low, S.S. and Moehle, J.P., September 1987.
- UCB/EERC-87/15 "Relationships between Soil Conditions and Earthquake Ground Motions in Mexico City in the Earthquake of Sept. 19, 1985," by Seed, H.B., Romo, M.P., Sun, J., Jaime, A. and Lysmer, J., October 1987.
- UCB/EERC-87/16 "Experimental Study of Seismic Response of R. C. Setback Buildings," by Shahrooz, B.M. and Moehle, J.P., October 1987.
- UCB/EERC-87/17 "The Effect of Slabs on the Flexural Behavior of Beams," by Pantazopoulou, S.J. and Moehle, J.P., October 1987.
- UCB/EERC-87/18 "Design Procedure for R-FBI Bearings," by Mostaghel, N. and Kelly, J.M., November 1987.
- UCB/EERC-87/19 "Analytical Models for Predicting the Lateral Response of R C Shear Walls: Evaluation of their Reliability," by Vulcano, A. and Bertero, V.V., November 1987.
- UCB/EERC-87/20 "Earthquake Response of Torsionally-Coupled Buildings," by Hejal, R. and Chopra, A.K., December 1987.
- UCB/EERC-87/21 "Dynamic Reservoir Interaction with Monticello Dam," by Clough, R.W., Ghanaat, Y. and Qiu, X-F., December 1987.
- UCB/EERC-87/22 "Strength Evaluation of Coarse-Grained Soils," by Siddiqi, F.H., Seed, R.B., Chan, C.K., Seed, H.B. and Pyke, R.M., December 1987.
- UCB/EERC-88/01 "Seismic Behavior of Concentrically Braced Steel Frames," by Khatib, I., Mahin, S.A. and Pister, K.S., January 1988.
- UCB/EERC-88/02 "Experimental Evaluation of Seismic Isolation of Medium-Rise Structures Subject to Uplift," by Griffith, M.C., Kelly, J.M., Coveney, V.A. and Koh, C.G., January 1988.
- UCB/EERC-88/03 "Cyclic Behavior of Steel Double Angle Connections," by Astaneh-Asl, A. and Nader, M.N., January 1988.
- UCB/EERC-88/04 "Re-evaluation of the Slide in the Lower San Fernando Dam in the Earthquake of Feb. 9, 1971," by Seed, H.B., Seed, R.B., Harder, L.F. and Jong, H.-L., April 1988.
- UCB/EERC-88/05 "Experimental Evaluation of Seismic Isolation of a Nine-Story Braced Steel Frame Subject to Uplift," by Griffith, M.C., Kelly, J.M. and Aiken, I.D., May 1988.
- UCB/EERC-88/06 "DRAIN-2DX User Guide," by Allahabadi, R. and Powell, G.H., March 1988.
- UCB/EERC-88/07 "Cylindrical Fluid Containers in Base-Isolated Structures," by Chalhoub, M.S. and Kelly, J.M., April 1988.
- UCB/EERC-88/08 "Analysis of Near-Source Waves: Separation of Wave Types using Strong Motion Array Recordings," by Darragh, R.B., June 1988.
- UCB/EERC-88/09 "Alternatives to Standard Mode Superposition for Analysis of Non-Classically Damped Systems," by Kusainov, A.A. and Clough, R.W., June 1988.
- UCB/EERC-88/10 "The Landslide at the Port of Nice on October 16, 1979," by Seed, H.B., Seed, R.B., Schlosser, F., Blondeau, F. and Juran, I., June 1988.
- UCB/EERC-88/11 "Liquefaction Potential of Sand Deposits Under Low Levels of Excitation," by Carter, D.P. and Seed, H.B., August 1988.
- UCB/EERC-88/12 "Nonlinear Analysis of Reinforced Concrete Frames Under Cyclic Load Reversals," by Filippou, F.C. and Issa, A., September 1988.
- UCB/EERC-88/13 "Implications of Recorded Earthquake Ground Motions on Seismic Design of Building Structures," by Uang, C.-M. and Bertero, V.V., September 1988.
- UCB/EERC-88/14 "An Experimental Study of the Behavior of Dual Steel Systems," by Whittaker, A.S., Uang, C.-M. and Bertero, V.V., September 1988.
- UCB/EERC-88/15 "Dynamic Moduli and Damping Ratios for Cohesive Soils," by Sun, J.I., Goleorkhi, R. and Seed, H.B., August 1988.
- UCB/EERC-88/16 "Reinforced Concrete Flat Plates Under Lateral Load: An Experimental Study Including Biaxial Effects," by Pan, A. and Moehle, J., November 1988.
- UCB/EERC-88/17 "Earthquake Engineering Research at Berkeley - 1988," by EERC, November 1988.
- UCB/EERC-88/18 "Use of Energy as a Design Criterion in Earthquake-Resistant Design," by Uang, C.-M. and Bertero, V.V., November 1988.
- UCB/EERC-88/19 "Steel Beam-Column Joints in Seismic Moment Resisting Frames," by Tsai, K.-C. and Popov, E.P., September 1988.
- UCB/EERC-88/20 "Base Isolation in Japan, 1988," by Kelly, J.M., December 1988.
- UCB/EERC-89/01 "Behavior of Long Links in Eccentrically Braced Frames," by Engelhardt, M.D. and Popov, E.P., January 1989.
- UCB/EERC-89/02 "Earthquake Simulator Testing of Steel Plate Added Damping and Stiffness Elements," by Whittaker, A., Bertero, V.V., Alonso, J. and Thompson, C., January 1989.
- UCB/EERC-89/03 "Implications of Site Effects in the Mexico City Earthquake of Sept. 19, 1985 for Earthquake-Resistant Design Criteria in the San Francisco Bay Area of California," by Seed, H.B. and Sun, J.I., March 1989.
- UCB/EERC-89/04 "Earthquake Analysis and Response of Intake-Outlet Towers," by Goyal, A. and Chopra, A.K., July 1989.
- UCB/EERC-89/05 "The 1985 Chile Earthquake: An Evaluation of Structural Requirements for Bearing Wall Buildings," by Wallace, J.W. and Moehle, J.P., July 1989.
- UCB/EERC-89/06 "Effects of Spatial Variation of Ground Motions on Large Multiply-Supported Structures," by Hao, H., July 1989.